AD/A-001 064

MULTIPATH MEASUREMENTS

D. G. Armstrong, et al

Raytheon Company

Prepared for:

Defense Advanced Research Projects Agency
Army Missile Command

August 1974

DISTRIBUTED BY:

NTIS

National Technical Information Service
U. S. DEPARTMENT OF COMMERCE

Unclassified

SECURITY CLASSIFICATION OF THIS PAGE (When Data Entered)

REPORT DOCUMENTATION PAGE	READ INSTRUCTIONS BEFORE COMPLETING FORM
1 REPORT NUMBER / 2 GOVT ACCESSION NO.	3 RECIPIENT'S CATALOG NUMBER: AD/A-001064
4 TITLE (and Subtitle): MULTIPATH MEASUREMENTS	5 TYPE OF REPORT & PERIOD COVERED: Final Report 4-30-74 to 8-15-74
	6 PERFORMING ORG. REPORT NUMBER: ER74-4316
7 AUTHOR(s): D. G. Armstrong, P. E. Cornwell, A. H. Greene	8 CONTRACT OR GRANT NUMBER(s): DAAH01-74-C-0704
9 PERFORMING ORGANIZATION NAME AND ADDRESS: Raytheon Company, Advanced Development Laboratory, Wayland, Massachusetts 01778	10 PROGRAM ELEMENT, PROJECT, TASK AREA & WORK UNIT NUMBERS: ARPA Order No. 2731
11 CONTROLLING OFFICE NAME AND ADDRESS: Defense Advanced Research Projects Agency, 1400 Wilson Boulevard, Arlington, Virginia 22209	12 REPORT DATE: August 1974
	13 NUMBER OF PAGES: 264
14 MONITORING AGENCY NAME & ADDRESS(if different from Controlling Office): U. S. Army Missile Command, Redstone Arsenal, Alabama 35805	15 SECURITY CLASS. (of this report): Unclassified
	15a DECLASSIFICATION/DOWNGRADING SCHEDULE
16 DISTRIBUTION STATEMENT (of this Report)	
17 DISTRIBUTION STATEMENT (of the abstract entered in Block 20, if different from Report)	
18 SUPPLEMENTARY NOTES	

Reproduced by
NATIONAL TECHNICAL
INFORMATION SERVICE
U S Department of Commerce
Springfield VA 22151

19. KEY WORDS (Continue on reverse side if necessary and identify by block number)

Multipath Theory
Multipath Measurements
Specular Reflection
Diffuse Scattering
Multipath Simulation
Low Angle Radar Tracking Simulation

20. ABSTRACT (Continue on reverse side if necessary and identify by block number)

Reported is Phase I of a research task to refine the classical multipath theory. The study completed has culminated in the design of a measurement program which can obtain data on terrain and sea reflection phenomena. The processed data can be used to quantify existing theory to assist in improving the performance of tracking radars operating at low elevation angles.

The measurement program may be carried out in Phases I and II.

DD FORM 1 JAN 73 1473 EDITION OF 1 NOV 65 IS OBSOLETE

Unclassified

SECURITY CLASSIFICATION OF THIS PAGE (When Data Entered)

(Abstract con't.)

which include respectively, measurements and data reduction, and comprehensive reporting.

The theory of specular and diffuse reflections is discussed in considerable detail, including the most recent modifications which deal quantitatively with the interaction of specular and diffuse reflectivity over the glistening surface. A computer simulation based on the advanced theory is described. The simulation models one way reflectivity measurements and low angle radar tracking in elevation. Typical results are presented.

The experimental measurements to be performed have been considered in detail. To obtain adequate resolution of diffuse reflectivity measurements a low sited wide bandwidth receiver is to be used, sensing signals from a narrow pulse transmitter (1 nanosecond) supported aloft by a balloon, kite or helicopter. The narrow pulse provides the principal resolution over the glistening surface for obtaining the distribution of diffuse reflectivity. For regions near the receiver, additional resolution is provided by the receiving antenna, which will have a beamwidth of 0.5 degrees. Measurements are planned at a frequency of 16 GHz.

Independent measurements of the terrain and ocean surfaces to be studied will be made by aerial photography. For land areas accurate contour maps will be produced from the data. For ocean regions the Stilwell process will be employed to provide ocean spectra data. These data will be used in conjuction with the computer simulation to assist in interpretation of the diffuse multipath measurements

FINAL TECHNICAL REPORT
FOR
MULTIPATH MEASUREMENTS

ER74-4316 August 1974

This report covers the period 30 April to 15 August 1974.

Prepared by

D. G. Armstrong
P. E. Cornwell
A. H. Greene

RAYTHEON COMPANY
EQUIPMENT DEVELOPMENT LABORATORIES
ADVANCED DEVELOPMENT LABORATORY
Wayland, Massachusetts 01778

Sponsored by

Defense Advanced Research Projects Agency
ARPA Order No. 2731

This research was supported by the Defense Advanced Research Projects Agency of the Department of Defense and was monitored by the U.S. Army Missile Command under Contract Number DAAH01-74-C-0704.

The views and conclusions contained in this document are those of the authors and should not be interpreted as necessarily representing the official policies, either expressed or implied, of the Defense Advanced Research Projects Agency or the U.S. Government.

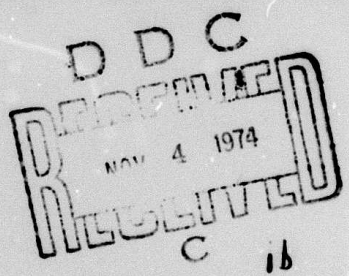

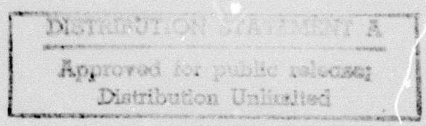

REPORT SUMMARY

Reported is Phase I of a research task to refine the classical multipath theory. The study completed has culminated in the design of a measurement program which can obtain data on terrain and sea reflection phenomena. The processed data can be used to quantify existing theory to assist in improving the performance of tracking radars operating at low elevation angles.

The measurement program may be carried out in Phases II and III which include respectively, measurements and data reduction, and comprehensive reporting.

The theory of specular and diffuse reflections is discussed in considerable detail, including the most recent modifications which deal quantitatively with the interaction of specular and diffuse reflection and which also describe the distribution of diffuse reflectivity over the glistening surface. A computer simulation based on the advanced theory is described, and typical results presented.

The experimental measurements to be performed have been considered in detail. To obtain adequate resolution of diffuse reflectivity measurements a low sited wide bandwidth receiver is to be used, sensing signals from a narrow pulse transmitter (1 nanosecond) supported aloft by a balloon, kite or helicopter. The narrow pulse provides the principal resolution over the glistening surface for obtaining the distribution of diffuse reflectivity. For regions near the receiver, additional resolution is provided by the receiving antenna, which will have a beamwidth of 0.5 degrees. Measurements are planned at a frequency of 16 GHz.

Independent measurements of the terrain and ocean surfaces to be studied will be made by aerial photography. For land areas accurate contour maps will be produced from the data. For ocean regions the Stilwell process will be employed to provide ocean spectra data. These data will be used in conjunction with the computer simulation to assist in interpretation of the diffuse multipath measurements.

Measurements and Data Reduction (Phase II)are planned for an 18 month period and Comprehensive Reporting (Phase III) for the subsequent six months. The results of the total effort will be published as a handbook of surface reflectivity information.

PREFACE

In developing the multipath theory, simulation and experiment concept discussed in this report, we have been assisted greatly by many of our colleagues at the Raytheon Company, namely:

D.K. Barton, who defined the basic theory which the experiment is to investigate.

R.B. Campbell, Jr., who convinced us and others that such an experiment is feasible.

J. DeBettencourt, E. Brookner, and D. Odom, who provided propagation information.

R. Kasevich, who tailored the Stilwell process to the needs of this investigation.

N. Freedman, S. Riceman, J. Zimmer and Neil Lacey who generated hardware information and suggested experimental approaches.

J.H. Long and S. Powers, who developed portions of the multipath computer program.

R. Lindquist, who developed the antenna mounting and mechanical designs.

R. Blanton, who performed many of the trade-off analyses.

F. Morrison, who helped develop the data analysis approach.

J. Urner and D.H. Refoy, who provided the aerial mapping approach.

In addition, we appreciate the encouragement received from

Mr. Sam Uptain, U.S. Army Missile Command, Huntsville, Ala. and

Major John Meinhardt, ARPA Headquarters, Washington, D.C.

TABLE OF CONTENTS

TABLE OF CONTENTS (Cont)

TABLE OF CONTENTS (Cont)

LIST OF ILLUSTRATIONS

LIST OF ILLUSTRATIONS (Cont)

LIST OF ILLUSTRATIONS (Cont)

LIST OF SYMBOLS

		Page
A_r	Receiver antenna aperture	35
A_r	Free space field strength of the source at this image antenna	10
A_t	Free space field strength of the source at the antenna	10
A_1	Amplitude of incident field, E_1 (equation 2.3.5)	18
a	Effective earth's radius to account for atmospheric refraction	12
C	Resolution cell center	37 ff
C	Correlation coefficient (equation 2.3.24)	24
c	Velocity of light	34
D	Ground distance between Transmitter and Receiver	37 ff
D	Divergence factor to account for the effect of the earth's curvature on the Fresnel reflection coefficient (equation 2.2.4)	12
D_1	Ground distance between receiver and resolution cell center	37 ff
d_c	Correlation distance of the surface heights (used in the calculation of rms surface slope - equation 2.2.8)	13
E	Voltage field on surface element, S_1 (equation 2.3.8)	19, 20
E	Total signal received by the antenna (equation 2.2.1)	10
E_1	Incident field signal	18
E_2	Scattered field signal (equation 2.3.21)	18, 23
F_d	Scaling factor for the diffuse power contribution for varying surface roughness (equation 2.3.17)	22
F_n	Receiver noise figure	35
f	Frequency	34
$f(\theta)$	Antenna voltage gain pattern	10
G_o	Bistatic reflectivity coefficient (equation 3.4.6)	96
G_r	Gain of receive antenna	34
G_t	Gain of transmitting antenna	34
g	Roughness parameter (equation 2.3.10)	20
g_1	Gain of the transmitter antenna in direction of patch	21
g_2	Gain of the receiver antenna in direction of patch	21
g_{10}	Gain of the transmitter antenna in the direction of the receiver	21
g_{20}	Gain of the receiver antenna in the direction of the transmitter	21

LIST OF SYMBOLS (cont.)

		Page
h_r	Height of receiving antenna	37
h_t	Height of transmitting antenna	40
$\mathcal{I}$	Angle between local surface normal and incident ray (Figure 8)	19
K	Boltzman's Constant (1.38×10^{-23} watts/Hz/°K)	35
K_i	Asymmetry factor for ith patch in a resolution cell (equation 2.3.36)	27, 28
$k=2\pi/\lambda$		
$\hat{k}_1$	Unit vector in the direction of the incident wave (equation 2.3.5 and Figure 7)	18, 19
$\hat{k}_2$	Unit vector in the direction of the reflected wave (Figure 7)	19
L_r	Losses in receiving system	35
$\hat{n}$	Local (unit) normal to surface-rough earth	20
$\hat{n}_s$	Local (unit) normal to surface-smooth earth	114
P	Point of observation when determing the scattered field, E_2 (equation 2.3.8)	19
P	Diffuse power return, power reflected from the glistening surface in a non-specular direction (equation 2.2.9)	15
P_r	Direct power from the source (equation 2.3.15)	21
P_t	Peak transmitter power	20
P_2	Total mean scattered power received from the glistening surface (equation 2.3.11)	20, 21
R_e	4/3 times geometric earth radius	37
R_o	Magnitude of the Fresnel reflection coefficient (equation 2.3.7)	10, 18
R_1	Transmitter distance from patch as defined in theory sections (Figure 3)	11
R_2	Receiver distance from patch as defined in theory sections (Figure 3)	11
R_3	Transmitter-receiver direct path separation as defined in theory sections (Figure 3)	11
r_D	Transmitter-receiver direct path separation as defined in measurements sections (Figure 13)	35, 38
r_1	Receiver distance from patch as defined in measurements sections (Figure 13)	38
r_2	Transmitter distance from patch as defined in measurements sections (Figure 13)	38

LIST OF SYMBOLS (cont.)

		Page
r	Distance from receiver to intersection point on resolution contour	40
$\vec{r}$	Surface patch geometry radius vector (Figure 6)	17, 18
S	Surface element of incremental area δ_s	17
s_1	Standard deviation of the real part of the reflected field distribution	24
s_2	Standard deviation of the imaginary part of the reflected field distribution	24
T_o	Standard receiver reference temperature (290°K)	35
U, V	Random numbers chosen from a normal distribution used in calculating the random vector field, E_2 (equation 2.3.27)	26
α	Total phase shift between direct and indirect path signals	10
β	Angle between local rough earth normal and local smooth earth normal	13
β_o	rms slope of surface irregularities if Gaussian distribution of surface slopes is assumed. (equation 2.2.8)	13
	Maximum slope of surface irregularities if uniform distribution of surface slopes is assumed.	13
δ	Depression angle of receiving antenna beam axis	40
δA	Area of a rectangular surface patch (equation 2.3.4)	17
δ_o	Path difference between reflected and direct signal transmissions ($R_1 + R_2 - R_3$)	10
δ_s	Incremental area of a surface element S	17
δ_u	Normalized mean square scattered field (equation 2.3.13)	21
ϵ_c	Complex dielectric constant of terrain (equation 2.3.7)	18, 19
ζ	Height of normally distributed surface (rough in two dimensions)	17
η_a	Receiver antenna aperture efficiency	35
θ	Receiving antenna half beamwidth	40
θ_r	Elevation angle between the receiver antenna and the image source as viewed from the receiver and measured with respect to the local horizontal at the receiver antenna (Figure 3)	10, 11

LIST OF SYMBOLS (cont.)

		Page
θ_t	Elevation angle between the receiver antenna and source as viewed from the receiver and measured with respect to the local horizontal at the receiver antenna (figure 3)	10, 11
θ_1	Angle from the receiver to an arbitrary reflection point measured from the local vertical at the receiver (figure 13)	37, 38
θ_2	Angle from the transmitter to an arbitrary reflection point measured from the local vertical at the transmitter (figure 13)	38, 39
θ_1	Angle between incident ray and smooth earth local normal	19
θ_2	Angle between reflected ray and smooth earth local normal	19
θ_3	Out of incident plane reflection angle	19
λ	Wavelength	10
ρ_s	rms specular scattering factor for a perfectly conducting round earth	12
ρ_d	rms diffuse scattering factor	15
σ_h	rms surface height variation of surface irregularities	12
τ	Pulsewidth	34
τ_d	Time delay measured with respect to the direct path	39
Φ	Fundamental solution of the three dimensional wave equation	19
ψ	Specular reflection angle (equation 2.2.3)	12
ψ_1, ψ_2	Local grazing angles (figure 7)	19, 22
φ	Phase of the Fresnel reflection coefficient (equation 2.3.38)	10, 28

FINAL TECHNICAL REPORT
MULTIPATH MEASUREMENTS

SECTION 1. INTRODUCTION

1.1 Total Program Objectives

The studies reported represent Phase I of a research task to refine the classical multipath theory. Central to the activity is a measurements program to obtain data on terrain and sea reflection phenomena. These data will be used to quantify existing theory and provide a means for accurately predicting and improving performance of tracking radars at low elevation angles.

Three phases were initially planned as follows:

- Phase I - Measurements Program Design
- Phase II - Measurements Program
- Phase III - Data Reduction and Reporting

Phase I has been performed to define requirements for the multipath measurements and recommend the best design configuration for the experiment. As a result of this planning effort, it has become evident that Phases II and III should be redefined to insure a closer relation between measurement activity and data reduction. Hence, objectives for each are now the following:

- Phase II - Measurements and Data Reduction
- Phase III - Comprehensive Reporting

Phase II will involve developing the configuration and techniques designed in Phase I so that measurements may be taken at a variety of sites at different times of the year. Alternate or overlapping measurement and data reduction efforts, gradually building in complexity, will be performed over land and sea areas.

Phase III will begin once a significant body of reduced data has been accumulated for a comprehensive collection of sites. The reduced data will be correlated and compared with existing information from other sources, and a handbook of surface reflectivity information will be published for future use in multipath and other studies.

1.2 Phase I Objectives

The objectives of the current phase have been to develop a comprehensive computer model, to define the measurement concept to be used in Phase II, and to develop specifications and plans for implementing the measurements and associated data analyses.

The multipath computer model is based upon the theory discussed below in Section 2, and the simulation itself is described in detail in Section 4. The model can simulate the measurement experiment quite accurately, including the effects of specific terrain/ocean characteristics. In addition, it can operate in a radar tracking mode.

Development of the measurement concept has been guided by the principle that complexity should be avoided in favor of obtaining repeatable reliable data. Thus, fundamental one-way reflected power measurements are to be made and involved applications such as closed loop radar tracking in the presence of multipath are to be avoided. Sites chosen for initial measurement activities are likewise to be uncomplicated, e.g. flat or gently rolling terrain or ocean at moderate sea states. Measurement of more complicated surfaces will be deferred until the initial information is processed and understood. The concept selected is summarized in the following subsection and is described in detail in Section 3.

The specifications and plans comprise an Equipment Specification, an Equipment Implementation Plan, a Measurements Plan, and a Data Analysis Plan. They will be submitted separately as part of a proposal for the Phase II effort, although the basic material is to be found in this report (see Section 3.0).

1.3 Summary of Experimental Concept

The experimental measurements are intended to gather data which will quantitatively define the magntiude and spatial distribution of diffuse reflections. The classical theory treats specular reflections in a satisfactory way, but precise measurement data are needed to confirm and refine the models that treat diffuse reflections.

Consider a low sited receiver and an elevated transmitter as in Figure 1. The transmitted energy will arrive at the receiver on a direct path and any number of indirect paths. If the surface appears smooth at the propagation

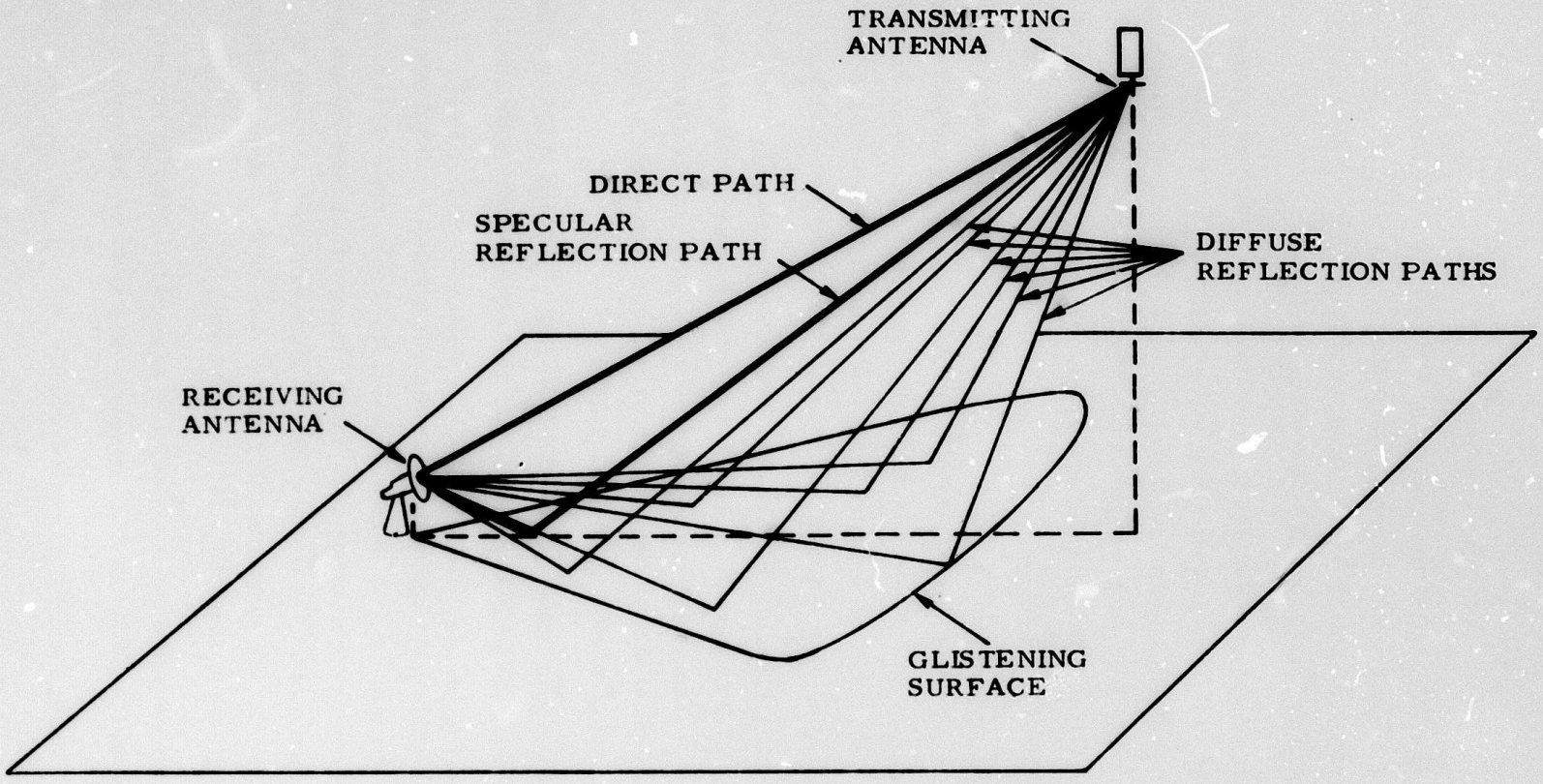

Figure 1. Multipath Propagation

frequency and target elevation angle chosen, the only significant indirect path is the specular one. For rough surfaces, there are many indirect paths, each characterized by a different diffuse reflection factor. The region over which these reflections occur is called the glistening surface.

The purpose of the experiment is to examine the received power and from this determine the relative diffuse power reflected from each point (or small sub region) of the glistening surface. If the power arriving via the direct path is used as a reference, the power received via each other path can be used to determine the diffuse reflection coefficients, provided the geometry and equipment characteristics are accurately known.

The key requirement is to achieve sufficient resolution over the glistening surface so that an adequate number of sub regions can be identified. Because of the shallow sight lines to the surface from the low sited receiver, good resolution in the down range direction cannot be achieved from the receiving antenna pattern alone for any practical size antenna at transmission frequencies of interest.

To remove this difficulty and obtain fine down range resolution, a transmitter generating a very narrow pulse ($\approx$ 1 ns) will be used with a receiver having a 1 GHz bandwidth. The resulting resolution will approximate that shown in Figure 2. In the receiver, a time reference is provided via a small auxiliary antenna which receives the direct signal pulse.

Figure 2 is a plan view of the glistening surface for a transmitter-receiver ground distance of about 6 km. To show the narrow glistening surface adequately, the scale has been greatly expanded in the cross range direction. The entire glistening surface for the example shown is included within approximately 0.5 degrees in azimuth. A 0.5 degree beamwidth is planned. If the frequency is high enough, the receiving antenna size can be kept within reasonable bounds. At the planned frequency of 16 GHz, the antenna diameter will be about 2.5 meters. For rougher surfaces, the glistening surface will be wider, thus permitting the beam azimuth resolution capability to be effective.

The transmitted pulse moves along the ground toward the receiver providing a broadening resolution as it moves. Several examples of the apparent pulsewidth

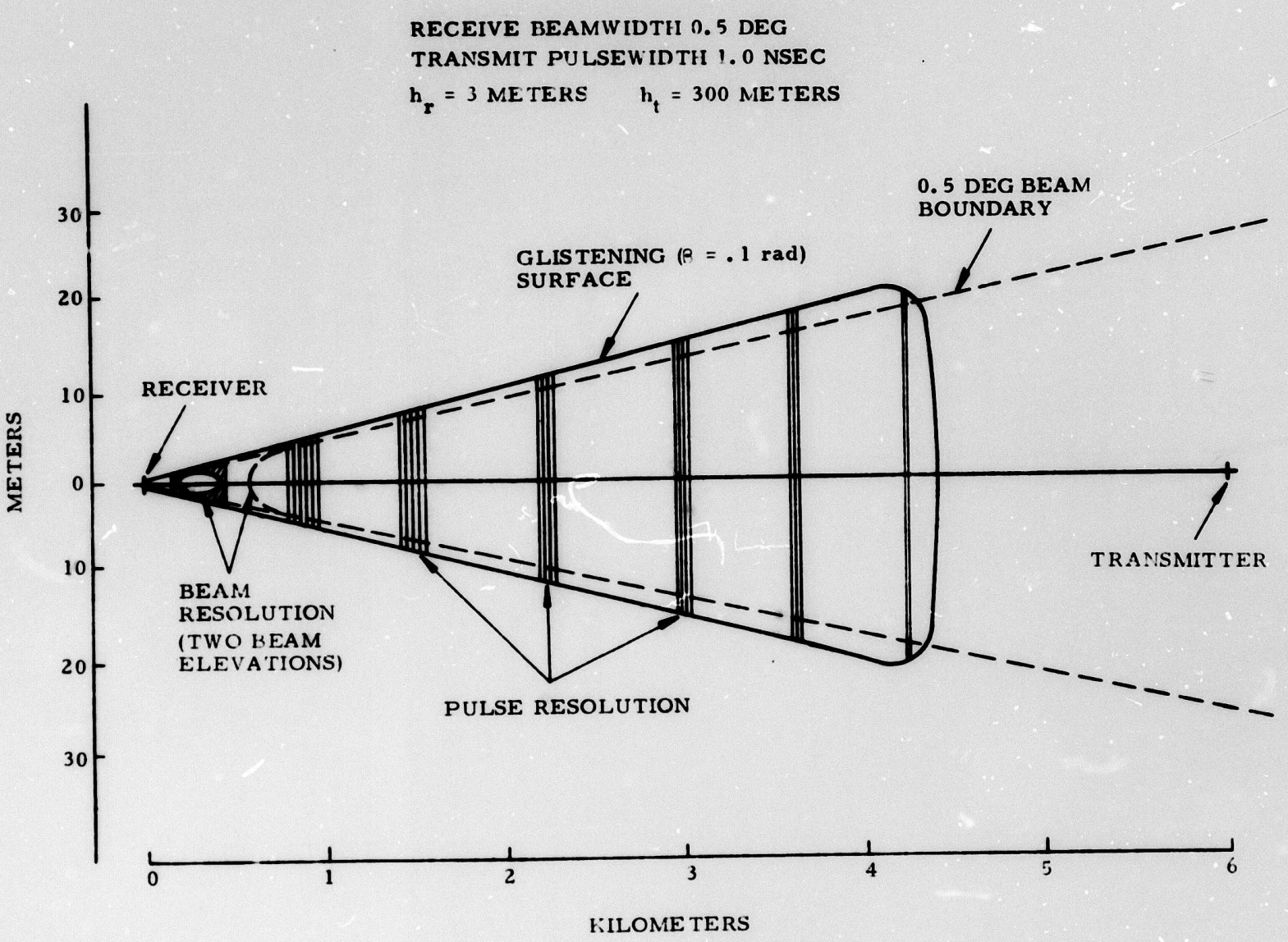

Figure 2. Plan View Multipath Measurements

(resolution) at various down range locations are illustrated in Figure 2. Although the resolution cells are shown with straight line boundaries, they are actually somewhat curved concave toward the receiver. The resolution cell is never greater than 240 meters up to about 300 meters from the receiver. For shorter ranges, the 0.5 degree receiving beam provides finer resolution as the receiving beam is directed towards steeper negative elevation angles.

For maximum flexibility, the receiving equipment will be mounted on a truck or transportable trailer. The transmitter (a solid state low power unit weighing less than 2 pounds) will be suspended either by a tethered aerodynamic device or by a helicopter, depending on constraints imposed by the site environment.

Typical system parameters are listed in Table I. It is believed that reasonable extrapolation of results from 16 GHz can be accomplished to predict effects at X-Band and at lower bands commonly used for radar. It is also possible to make measurements directly at X-Band. Azimuth resolution would be degraded somewhat at X-Band, but down range resolution would not be affected.

Table I

Typical Experiment System Parameters

Frequency	16 GHz
Receiving Antenna Diameter	2.5 meters
Transmitter PRF	40 - 80 kHz
Receiving Antenna Height	4 meters
Transmitter Height	50 - 600 meters
Transmitter Peak Power	100 watts
Pulsewidth	1 nsec
Transmitter-Receiver Ground Distance	3 - 10 km

1.4 Data Collection and Analysis

A number of potential data collection sites have been investigated. It is believed that initial activity should take place relatively near Raytheon facilities to minimize operational burdens. Initial measurements should occur over simple terrain or over water at an accessible location. Accordingly, three sites

within Massachusetts have been tentatively selected for measurements next spring. They are listed with prospective measurement dates in Table II.

Table II.

Measurement Sites

Date	Site
March 15-April 7	Otis Air Force Base, Cape Cod (near Falmouth, Massachusetts)
April 23-May 15	Race Point Coast Guard Station, Cape Cod (near Provincetown, Massachusetts)
June 1-15	Westover Air Force Base (near Springfield, Massachusetts)

The Air Force bases are now operated by the Massachusetts Air National Guard and traffic is relatively light. Westover can provide clear coverage over flat grassy and paved terrain up to 4.6 km (15,000 ft.). Otis is similar although the clear distance is shorter; but because of its location, Otis loses its snow early in the season. Consequently, Otis has been selected for initial equipment shake-down measurements in March. Later, terrain measurements at Westover will be performed to examine longer distances.

To insure accurate correlation of measurements with theory, a 3-dimensional map of the terrain will be made by Raytheon's Autometric facility from aerial photographs.

Diffuse reflection measurements of the ocean surface will be taken at Race Point. Ocean statistics will be simultaneously gathered photographically and reduced via the Stilwell process (see Appendix F).

In all cases, theodolites, tracking telescopes and/or lasers will be used as required to accurately locate the transmitter while measurements are taking place. In addition, power measurements will be referenced against the direct path by pointing the receiving antenna at the transmitter occasionally for calibration.

All data will be stored on tape at the site. Data reduction will utilize the multipath computer program described in Section 4 to determine the accuracy to

which the theory would predict the power vs. reflection location, given detailed knowlege of the terrain or ocean surface and the geometry. Deviations between prediction and measurements will be examined to improve the theory and/or computer mode. A comprehensive discussion of the measurements and data analysis is given in Section 3. Note that no phase measurements are contemplated, since the basic difficulty in prediction concerns power amplitude, not phase.

Once the basic measurements have been successfully completed, sites with more complex terrain will be visited and measurements made and analyzed. More details on plans and schedules may be found in Section 5.

1.5 Notation

In preparing this report consistency in the use of notation has been emphasized. However, some range and angle terms used in the section covering theory, differ from those of equivalent meaning used in the sections covering measurements. To avoid confusion, all terms are clearly defined in the sections in which they appear, and are further defined in the glossary included at the beginning of this report.

SECTION 2. MULTIPATH THEORY

2.1 Introduction

The multipath problem is due to contamination of the direct signal return from a source by the indirect return from the same source which arrives by a reflected path. Multipath can cause errors in all three of the radar tracking coordinates, and the errors may become quite large when, for example, the main beam of the antenna intersects the ground plane and the surface reflectivity is such that the reflected signal is of magnitude comparable to that of the direct signal.

The first step in studying the multipath phenomenon has been the development of a specular multipath model. In such a model, all of the reflected energy is assumed to arrive at the radar from an image source at a well defined position below the real source. It is clear that for such a model to be valid, the reflecting surface must be relatively smooth. Since the earth's surface consists, in general, of small scale surface irregularities superimposed on hills, mountains, etc., it is not surprising that past proposals for the elimination of multipath error, based on this specular reflection model, have for the most part proved disappointing.

The need for a multipath model that may be applied over general terrain with varying degrees of roughness has led to the development of a theory which describes the effects of diffuse scattering from the terrain between the source and receiver. In this theory, the power per unit area scattered via diffuse scattering is considerably less than the power reflected per unit area in the specular direction. Nevertheless, the diffuse scattering is important and often dominant in low angle tracking because the area producing the diffuse scattering (Glistening Surface) includes virtually all of the terrain between the source and receiver. The onset of dominance of diffuse over specular returns is determined in the theory by surface roughness. The rougher the surface, the lower the elevation angles at which diffuse scattering dominates.

The purpose of this section is threefold. First, a brief description will be given of a simplified specular/diffuse multipath model which is based on the classical multipath theory (Refs. 1 and 2) and which has been used over the past few years in lieu of a more detailed treatment of the same classical theory.

Secondly, to provide understanding of the restrictions on the use of the simplified model and the characteristics of the detailed multipath model developed under this contract (see Section 4), a brief description of the classical theory will be given with a more detailed discussion appearing in Appendix C. Finally, the latest theoretical modifications (also included in the detailed multipath simulation) leading to the refined multipath theory proposed by D. K. Barton (Ref. 3) will be described.

2.2 Simplified Specular/Diffuse Multipath Model

Specular Reflection

Consider the smooth flat earth geometry depicted in Figure 3. Here it is assumed that the source radiates or reflects signals uniformly in all directions and that the antenna receives a direct signal from an elevation angle θ_t and a reflected signal from an image source at an elevation θ_r, where both angles are measured with respect to the antenna axis. In accordance with the laws of geometric optics, the total signal received by the antenna is

$$E = A_t f(\theta_t) + A_r R_o f(-\theta_r) e^{-i\alpha} \qquad (2.2.1)$$

where

A_t = free-space field strength of the source at the antenna
A_r = free-space field strength of the source at the image antenna
$f(\theta)$ = antenna voltage gain pattern
R_o = magnitude of the Fresnel reflection coefficient $R = R_o e^{-i\varphi}$
α = total phase shift = $\frac{2\pi\delta_o}{\lambda} + \varphi$
λ = wavelength
δ_o = path difference = $R_1 + R_2 - R_3$ (see Figure 3)

As the planar surface becomes rough - that is, when surface irregularities are superimposed on the planar surface - theoretical considerations suggest that the amplitude of the specular component of the surface reflections (second term in (2.2.1)) is reduced by an amount dependent upon the roughness of the surface. To be specific, a more precise evaluation of the amplitude of the specular reflection component is obtained by replacing R_o in (2.2.1) by the product

$$\rho = R_o \rho_s \qquad (2.2.2)$$

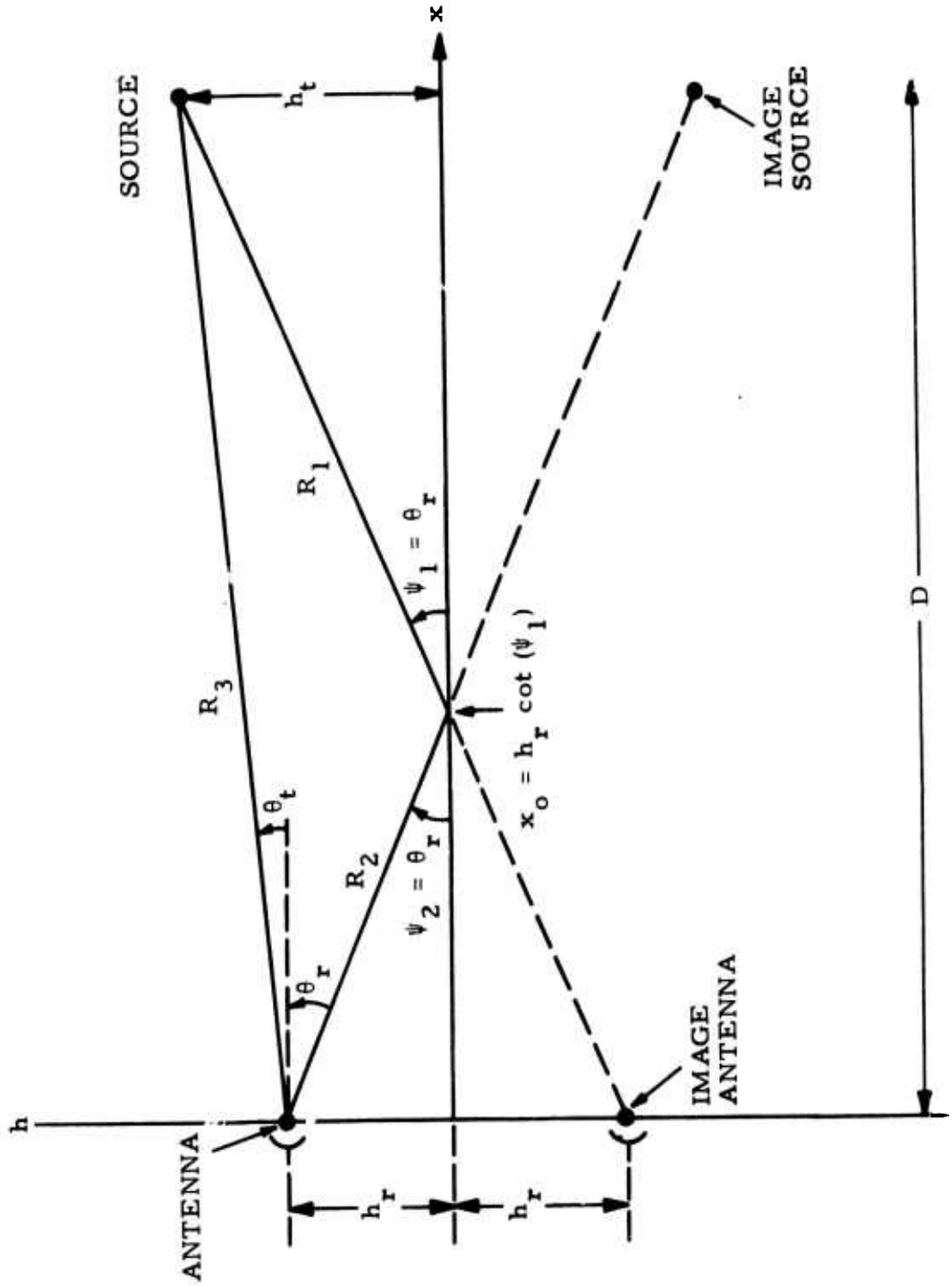

Figure 3. Specular Reflection Geometry

where ρ_s is the rms specular scattering coefficient[1] for a perfectly conducting rough-earth and is given by

$$\rho_s^2 = \exp\left[-\left(\frac{4\pi\sigma_h \sin\psi}{\lambda}\right)^2\right] \qquad (2.2.3)$$

with σ_h denoting the rms surface height variation of the surface irregularities (assumed normally distributed) and ψ is the specular reflection angle.

In order to account for the effect of the earth's curvature on the Fresnel reflection coefficient, which is usually derived for a flat earth, an additional factor (divergence factor)

$$D = \left[1 + \frac{2R_1 R_2}{a(R_1 + R_2)\sin\psi}\right]^{-1/2} \qquad (2.2.4)$$

is introduced as a multiplier of R_o. The "a" in (2.2.4) is an effective earth's radius derived in theory to account for atmospheric refraction.

The total signal received by the antenna is now given in this specular reflection theory by

$$E = A_t f(\theta_t) + A_r(DR_o)\rho_s f(-\theta_r)e^{-i\sigma} \qquad (2.2.5)$$

The second term in the above expression should be considered as the signal received by the antenna that is reflected in the specular direction only, by a curved earth with small scale surface irregularities.

Since Equation (2.2.5) is valid only for surfaces that are relatively smooth, an agreement has to be made as to when a surface can be considered smooth for the proper application of the above specular theory.

Specular reflection theory may be considered to apply when

---

[1] This scattering coefficient may be regarded as the rms field intensity at the antenna for a perfectly conducting rough earth that is due to a point source located at the image source and normalized to the smooth plane earth return for the same geometry.

$$\frac{\sigma_h}{\lambda} \sin \psi < .065 \quad \text{(Ref 1, 2).} \tag{2.2.6}$$

This inequality should be interpreted as the condition for which specular reflection will dominate, or equivalently, the condition for defining a smooth surface. Conversely, a surface is considered "rough" when the sense of the inequality in (2.2.6) is reversed. Again, from (2.2.6) surface roughness is a function of both σ_h/λ and the angle of incidence ψ (or equivalently, source position) and cannot be expressed solely in terms of terrain characteristics for a given wavelength λ. That is, a surface may be considered smooth when either

$$\frac{\sigma_h}{\lambda} \to 0 \quad \text{or} \quad \psi \to 0 . \tag{2.2.7}$$

Diffuse Scattering

In general, as a surface becomes rough, diffusely scattered energy arrives at the antenna from an extended region about the specular point, and the specular reflection theory will, in itself, no longer be valid. This scattering region, known as the glistening surface, may extend over virtually all of the terrain between the antenna and the source. More specifically, the glistening surface may be considered as the region from which power can be reflected to the radar by facets having slopes, β, less than or equal to

$$\beta_o = 2\sigma_h/d_c \tag{2.2.8}$$

the rms surface slope. Here d_c denotes the correlation distance of the surface heights. Figure 4 illustrates the extent of various glistening surfaces in the azimuth and elevation coordinates for targets at different elevations over terrain with constant β_o (or equivalently, in view of (2.2.6), for different degrees of surface roughness). These glistening surfaces were calculated using flat earth geometry and the approximation $\theta_t \approx \theta_r$ (see Figure 3).

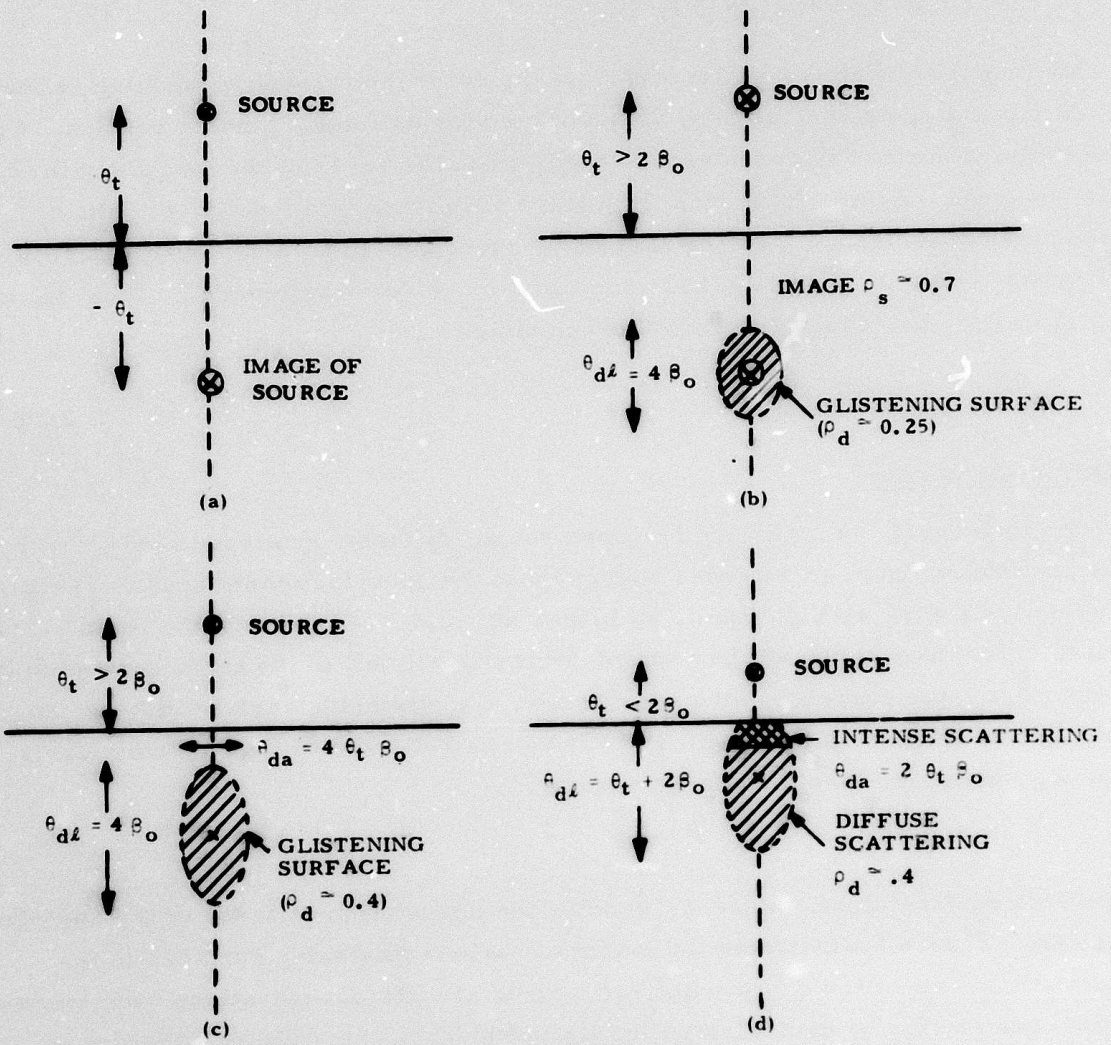

Figure 4. Specular and Diffuse Multipath - Variation in Source of Reflection with Elevation Angle and Roughness:

(a) Specular reflection, $\rho_s \simeq 1$, $\rho \simeq \rho_o$,

(b) Slight roughness, $\sigma_h/\lambda \sin \theta_t \simeq .06$

(c) Rough surface

(d) Low elevation, curved earth

The diffuse power return may be regarded as that power reflected from the glistening surface in a non-specular direction and is given by

$$P_D = (R_o \rho_d)^2 P_r \qquad (2.2.9)$$

where

R_o is again the magnitude of the Fresnel reflection coefficient

ρ_d is an rms diffuse scattering factor

P_r is the direct power from the source

The problem in (2.2.9) is in the determination of ρ_d. Figure 5 is an attempt to express ρ_d as a simple function of $(\sigma_h/\lambda \sin \psi)$, and is at best a compromise (the validity of which is questionable) between theory and a few sets of experimental data. In general ρ_d is a complicated function of ψ, σ_h, λ, and the receiver/source geometry.

Theoretical derivations with source elevation angles and specular angles of incidence that are small compared to the rms surface slope β_o, indicate that the sources of significant diffuse power are concentrated near the two ends of the glistening surface. In view of this, a simplified diffuse model has sometimes been used in which the diffuse power is equally divided between the foreground component immediately in front of the antenna and a horizon component below and in front of the target. In addition, the power is apportioned in this model between the specular and diffuse components in accordance with Figure 5.

This simplified model, when applied to radar tracking problems, can lead to overly optimistic results. This, together with the questionable estimates of ρ_d from Figure 5 suggests the need for the development of a more detailed and more accurate multipath model.

A brief treatment of the classical theory, together with the latest modifications to this theory (Ref. 3) will follow. The treatment is intended to provide a theoretical background for the understanding of the detailed multipath model developed under this contract (Section 4). In addition, it will provide a better understanding of the spatial distribution of diffuse power and the limitations to the use of the simplified multipath model. A more complete discussion of the theory is given in Appendix C.

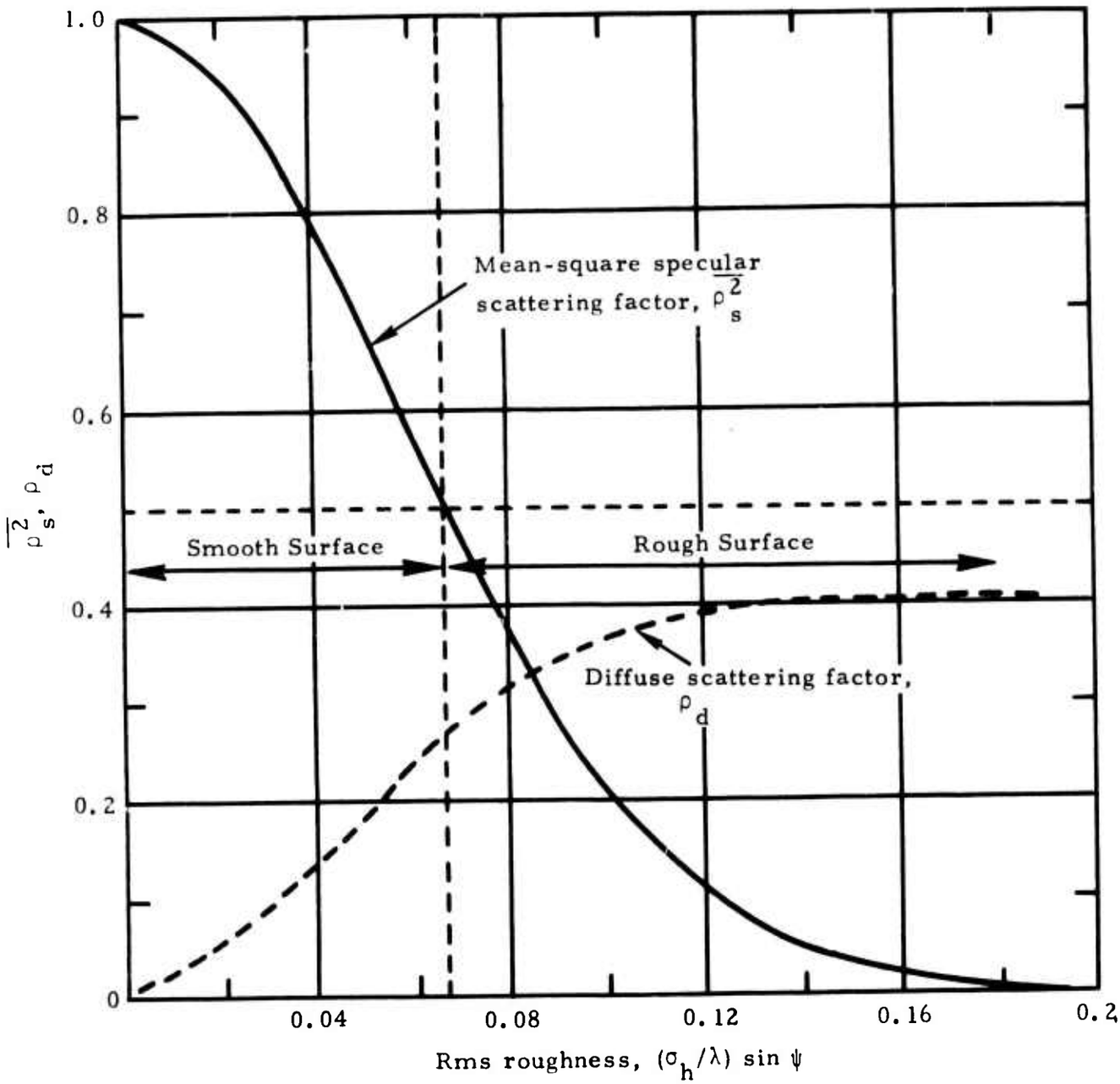

Figure 5. Reflection Coefficients

2.3 Specular/Diffuse Multipath Theory

Notation

In the following discussion, unless stated to the contrary,

$$\zeta = \zeta(x, y) \tag{2.3.1}$$

denotes the height of a normally distributed surface (rough in two dimensions) with mean and variance

$$\langle \zeta \rangle = 0 \tag{2.3.2}$$

$$D\{\zeta\} = \sigma_h^2 \tag{2.3.3}$$

respectively[1]. Figure 6 shows a surface element S of incremental area δ_S, together with an associated coordinate system. Without loss of generality, the projection of S onto the xy-plane is assumed to be rectangular with area

$$\delta A = 4 \Delta X \Delta Y \tag{2.3.4}$$

and the mean level of the surface element is taken to be the plane z = 0.

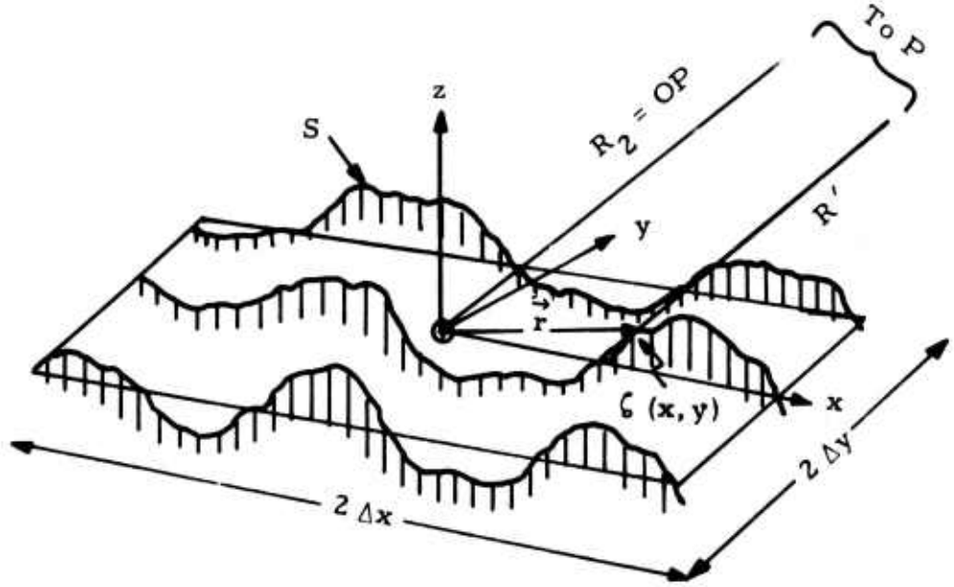

Figure 6. Surface Patch Geometry

[1] Notation used in this section is consistent with that used throughout Reference 1. A list of symbols and definitions is provided at the beinning of this report.

All quantities associated with the incident field will be denoted by the subscript 1 and those associated with the scattered field by the subscript 2. Accordingly, the incident field is denoted $\vec{E}_1$ and the scattered field $\vec{E}_2$. In what follows, $\vec{E}_1$ is either vertically or horizontally polarized (although the results may be generalized for arbitrary polarization). It is therefore necessary here to consider only the scalar value $E_1 (\equiv |\vec{E}_1|)$ of the vector $\vec{E}_1$. Also, E_1 is assumed to be the harmonic plane wave

$$E_1 = A_1 e^{i(\vec{k}_1 \cdot \vec{r} - \omega t)} \tag{2.3.5}$$

where

$$\left.\begin{aligned} \vec{k}_1 &= k\hat{k}_1 = \frac{2\pi}{\lambda}\hat{k}_1 \\ \hat{k}_1 &= \text{unit vector in the direction of the incident wave} \end{aligned}\right\}^1 \tag{2.3.6}$$

$\vec{r}$ is the radius vector $x\hat{x}_o + y\hat{y}_o + z\hat{z}$ (see Figure 6.)

$e^{-i\omega t}$ is a time factor which will henceforth be suppressed

A_1 (assumed constant) is the amplitude of E_1

Further notation connected with the scattering geometry is shown in Figures 7 & 8.

Finally, the Fresnel reflection coefficients for a smooth plane are

$$R^+ = \frac{\epsilon_c \sin\psi_1 - \sqrt{\epsilon_c - \cos^2\psi_1}}{\epsilon_c \sin\psi_1 + \sqrt{\epsilon_c - \cos^2\psi_1}} \tag{2.3.7}$$

$$R^- = \frac{\sin\psi_1 - \sqrt{\epsilon_c - \cos^2\psi_1}}{\sin\psi_1 + \sqrt{\epsilon_c - \cos^2\psi_1}}$$

---

[1] Similarly, $\vec{k}_2 = k\hat{k}_2 = \frac{2\pi}{\lambda}\hat{k}_2$ where $\hat{k}_2$ is a unit vector in the direction of the reflected wave.

where the "+" and "-" denote vertical and horizontal polarizations, respectively, and ϵ_c is the complex dielectric constant of the terrain.

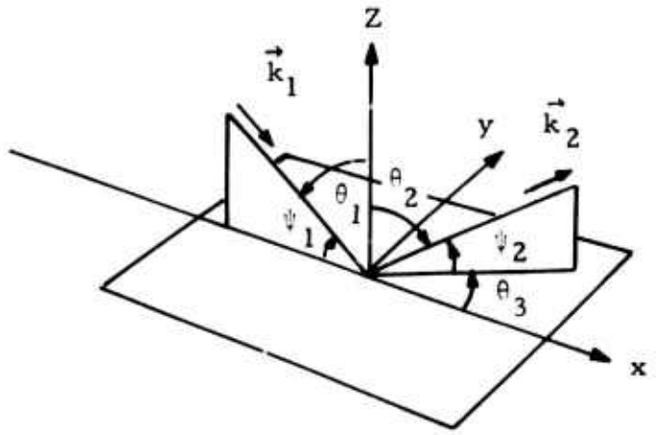

Figure 7. Scattering Geometry

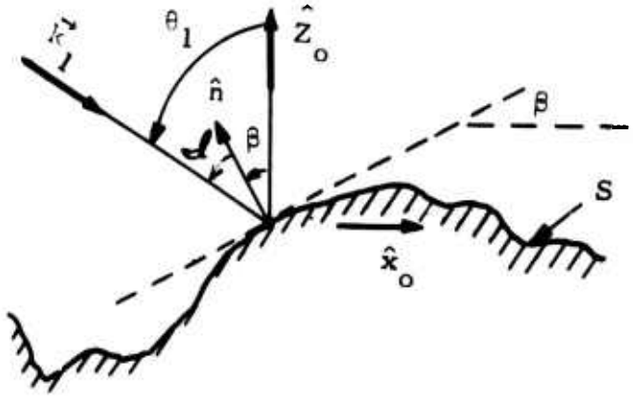

Figure 8. Local Scattering Geometry

Mean Patch Power Determination

A general expression for the scattered field E_2 at a point of observation P is given in the theory by the Helmholtz integral

$$E_2(P) = \frac{1}{4\pi}\iint_S \left(E \frac{\delta \Psi}{\delta n} - \Psi \frac{\delta E}{\delta n}\right) dS \qquad (2.3.8)$$

where Ψ is an appropriate fundamental solution of the three-dimensional wave equation, E is the voltage field on S and $\frac{\delta E}{\delta n}$ is its normal derivative. It is assumed here that the radii of curvature of the surface irregularities are large in comparison to the wavelength λ so that E and $\frac{\delta E}{\delta n}$ may be approximated on S by

$$\left.\begin{aligned} (E)_S &= (1 + R^{\pm} E_1) \\ \left(\frac{\delta E}{\delta n}\right)_S &= i(1 - R^{\pm}) E_1 (\vec{k}_1 \cdot \hat{n}) \end{aligned}\right\} \qquad (2.3.9)$$

where $\hat{n}$ denotes the unit normal to S (see Figure 8). The derivation of the mean scattered field from S using (2.3.8) and (2.3.9) is heavily dependent upon the roughness of the patch, that is on the value of the roughness parameter g, where

$$\sqrt{g} = \frac{2\pi\sigma_h}{\lambda} (\cos\theta_1 + \cos\theta_2) \qquad (2.3.10)$$

With the surface assumed very rough ($g >> 1$) (2.3.8) and (2.3.9) lead to the approximation

$$\langle \delta P_2 \rangle = \frac{1}{2} Y_o \langle E_2 E_2^* \rangle \qquad (2.3.11)$$

for the mean scattered power from the surface patch S. The asterisk (*) in this expression denotes the complex conjugate and Y_o is the admittance of free space. Also $\langle E_2 E_2^* \rangle$ is given as

$$\langle E_2 E_2^* \rangle = \frac{2 P_t g_1 g_2 \lambda^2 |R(\psi_1)|^2 \cot^2 \rho_o}{Y_o (4\pi)^3 (R_1 R_2)^2} \exp\left(-\frac{\tan^2\beta}{\tan^2\beta_o}\right) \delta A \qquad (2.3.12)$$

Here P_t is the peak transmitter power; g_1 and g_2 are the power gains of the transmitter and receiver, respectively, in the direction of the patch; R_1 and R_2 are the transmitter and receiver distances from the patch; and all other quantities have previously been defined. If (2.3.11) is normalized by the direct power return at the receiver, the normalized mean squared scattered field is

$$\langle \delta_u \rangle = |R(\psi_1)|^2 \Delta\rho_d^2 \tag{2.3.13}$$

where

$$\Delta\rho_d^2 = \frac{1}{4\pi} \frac{g_1 g_2}{g_{10} g_{20}} \left(\frac{R_3}{R_1 R_2}\right)^2 \cot^2 \varepsilon_o \exp\left(\frac{-\tan^2 \varepsilon}{\tan^2 \varepsilon_o}\right) \delta A \tag{2.3.14}$$

and g_{10} and g_{20} are the power gains of the transmitter in the direction of the receiver and of the receiver in the direction of the transmitter, respectively, and R_3 is the transmitter-receiver separation.

For a very rough surface the scattered field is completely incoherent, that is, the phases of the elementary fields are independent and uniformly distributed over a basic interval of length 2π. Accordingly, powers add and the total mean power from the glistening surface is given in this classical theory by

$$\langle P_2 \rangle = P_r \sum \langle \delta u \rangle \tag{2.3.15}$$

or equivalently

$$\langle P_2 \rangle = P_r \sum |R(\psi_1)|^2 \Delta\rho_d^2 \tag{2.3.16}$$

The notation P_r appearing in (2.3.15) and (2.3.16) is used to denote the direct power at the receiver from the source.

Unfortunately, the above expression for $\langle P_2 \rangle$ is valid only for glistening surfaces that can be classified as rough ($g >> 1$) at all points. In practice, portions of the glistening surface are rough and portions are not. This is true even if the surface is uniform with respect to the roughness parameters ε_o and σ_h, because the roughness parameter g is also a function of the reflection angles to the elementary patches and may vary considerably from patch to patch along the glistening surface. As surface patches become smooth,

the diffusely scattered power given by (2.3.11) or (2.3.13) must be scaled appropriately and the specularly reflected power determined. The mean scattered patch power is then the sum of the resulting diffuse power and the specularly reflected power.

The most recent development in the multipath theory (Ref 3) suggests a method of scaling the diffuse power contribution for varying surface roughness. The procedure used is to apply separate scaling factors to each surface patch on the glistening surface, so that in effect each $\Delta\rho_d^2$ is multiplied by a factor depending on the local angles of incidence and the rms height of the surface irregularities over the patch. Because the effect applies separately to the two paths R_1 and R_2, a geometric mean of the two grazing angles ψ_1 and ψ_2 is used:

$$F_d^2 = \sqrt{\left(1 - \rho_{s_1}^2\right)\left(1 - \rho_{s_2}^2\right)} \tag{2.3.17}$$

where

$$\rho_{s_i}^2 = \exp\left[-\left(\frac{4\pi\sigma_h \sin\psi_i}{\lambda}\right)\right]^2 \quad i = 1,2 \tag{2.3.18}$$

It should be noted that the above choice for the scaling of the diffuse power contribution includes the horizon effect for a curved earth and also accounts for the energy reflected specularly at low angles of incidence from the tops of rounded irregularities.

With the introduction of F_d^2, a general expression for the mean scattered patch power is given by

$$\langle \delta P_2 \rangle = P_r |R(\psi_1)|^2 D^2 \left[\frac{g_1 g_2}{g_{10} g_{20}}\left(\frac{R_3}{R_1 + R_2}\right)^2 \frac{\rho_s^2}{4\pi} + F_d^2 \Delta\rho_d^2\right] \tag{2.3.19}$$

where ρ_s^2 is the specular contribution from the patch and $F_d^2 \Delta\rho_d^2$ the appropriately scaled diffuse contribution. In practice ρ_s^2 is taken to be

$$\rho_s^2 = \begin{cases} \exp\left[-\left(\frac{4\pi\sigma_h \sin\psi_1}{\lambda}\right)^2\right] & \text{if the specular point is on the patch} \\ 0 & \text{otherwise} \end{cases} \qquad (2.3.20)$$

and is defined as the mean square specular reflection coefficient. Refer to Appendix C for a detailed derivation and discussion of ρ_s^2.

The D^2 in (2.3.19) is the divergence factor introduced in section 2.2 (equation 2.2.4).

The equation (2.3.19) should be considered as an improvement to (2.3.11) where $\langle E_2 E_2^* \rangle$ is defined by (2.3.12). With regard to its use in determining the total reflected power from the glistening surface, the incoherence of the scattered field is still necessary if the elementary powers are simply to be added together. In theory it is known that a continuous transition from incoherence to coherence (constant phase) exists as the surface becomes smooth, but there is as yet no established method of measuring this transition for the purpose of accurately defining the criteria for adding the elementary powers in the determination of the total scattered power.

One alternative to adding elementary powers is to establish the scattered field distribution. Random fields for each patch can then be chosen and vectorially added for each member of a Monte Carlo process to determine the sample voltage field from the glistening surface and an associated power. The mean scattered power from the glistening surface is then found by averaging the sample powers over all Monte Carlo samples.

It follows from the derivations in Appendix C that the mean and variance of the scattered field distribution for a patch are given respectively by

$$\langle E_2 \rangle = \begin{cases} -\frac{D\, g_1 g_2 \lambda\, R(\psi_1)}{(R_1 + R_2)} \left(\frac{P_t}{2\pi Y_o}\right)^{1/2} \exp\left[ik(R_1 + R_2) - \frac{1}{2}\left(\frac{4\pi\sigma_h \cos\theta_1}{\lambda}\right)^2\right] & \text{if the specular point is on the patch} \\ 0 & \text{otherwise} \end{cases}$$

(2.3.21)

$$D\{E_2\} = \frac{2\ P_t D^2 (g_1 g_2\ \lambda)^2\ |R(\psi_1)|^2 \cot^2 \beta_o\ F_d^2\ \exp\left(-\frac{\tan^2\beta}{\tan^2\beta_o}\right)\delta A}{Y_o\ (4\pi)^3\ (R_1 R_2)^2} \qquad (2.3.22)$$

Where g_1 and g_2 now denote voltage gains in the source-patch, and receiver-patch directions, respectively.

The random vector field from S can be represented as the sum of a constant vector and a fluctuating Hoyt vector with components chosen from normal distributions with mean zero and appropriate variances. To be specific, introduce the notation.

$$\left.\begin{aligned} E_2 &= x + jy \\ s_1 &= D\{x\} \\ s_2 &= D\{y\} \end{aligned}\right\} \qquad [1] \qquad (2.3.23)$$

for the scattered field E_2 and the variances of its real and imaginary parts, and let x', y' denote new coordinate axes turned through an angle φ_o with respect to the axes x, y so that x' and y' are independent (see Figure 9). This rotation transformation is well known in probability theory and the required angle φ_o is found from

$$\tan 2\varphi_o = \frac{2C\sqrt{s_1 s_2}}{s_1 - s_2} \qquad (2.3.24)$$

where C is a correlation coefficient. Let

$$\left.\begin{aligned} E_2' &= x' + jy' \\ \text{where} \\ x' &= x\cos\varphi_o + y\sin\varphi_o \\ y' &= y\cos\varphi_o - x\sin\varphi_o \end{aligned}\right\} \qquad (2.3.25)$$

Here E_2' is merely the scattered field E_2 expressed in the x', y' system.

[1] The j is now being used to denote $\sqrt{-1}$ in place of the i used previously to eliminate confusion on the following few pages.

In this $x'y'$ system

$$\left.\begin{aligned} \langle x' \rangle &= \langle x \rangle \cos \varphi_o + \langle y \rangle \sin \varphi_o \\ \langle y' \rangle &= \langle y \rangle \cos \varphi_o - \langle x \rangle \sin \varphi_o \\ s_1' = D\{x'\} &= s_1 \cos^2 \varphi_o + s_2 \sin^2 \varphi_o \\ s_2' = D\{y'\} &= s_2 \cos^2 \varphi_o + s_1 \sin^2 \varphi_o \end{aligned}\right\} \qquad (2.3.26)$$

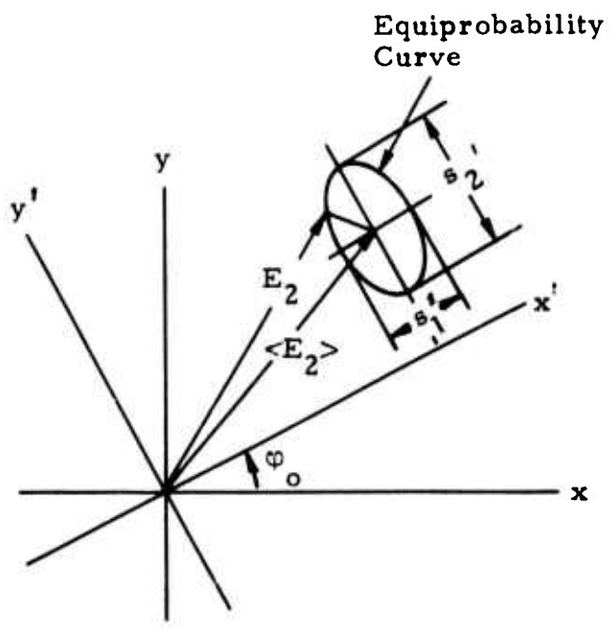

Figure 9. Random Scattered Field

Now the random (vector) field E_2 from the patch S can be represented in the $x'y'$ coordinate system as the sum of the constant vector $\langle E_2' \rangle$ and a fluctuating Hoyt vector with x' and y' components chosen from normal distributions with mean zero and variances s_1', s_2'. That is

$$E_2' = \langle E_2' \rangle + [s_1' U + j s_2' V] \tag{2.3.27}$$

where U and V are random numbers chosen from a normal distribution with zero mean and unit standard deviation. Rewriting (2.3.27) as

$$E_2' = \xi + j\eta \tag{2.3.28}$$

where

$$\left.\begin{aligned} \xi &= \langle x' \rangle + s_1' U \\ \eta &= \langle y' \rangle + s_2' V \end{aligned}\right\} \tag{2.3.29}$$

the random field E_2' can be rotated back to the xy coordinate system with the result

$$\left.\begin{aligned} E_2 &= x + jy \\ x &= \xi \cos\varphi_o - \eta \sin\varphi_o \\ y &= \xi \sin\varphi_o + \eta \cos\varphi_o \end{aligned}\right\} \tag{2.3.30}$$

Now introducing the subscript i to denote the ith patch on the glistening surface and the superscript n to denote the nth sample of a Monte Carlo process, the random scattered field from the ith patch and for the nth sample is given as

$$E_{2_i}^{\,n} = x_i^{\,n} + jy_i^{\,n} \tag{2.3.31}$$

where

$$\left.\begin{aligned}
x_i^n &= \xi_i^n \cos\varphi_{o_i} - \eta_i^n \sin\varphi_{o_i} \\
y_i^n &= \xi_i^n \sin\varphi_{o_i} - \eta_i^n \cos\varphi_{o_i} \\
\xi_i^n &= \langle x\rangle_i \cos\varphi_{o_i} + \langle y\rangle_i \sin\varphi_{o_i} + s_{1_i}{}' U_i^n \\
\eta_i^n &= \langle y\rangle_i \cos\varphi_{o_i} - \langle x\rangle_i \sin\varphi_{o_i} + s_{2_i}{}' V_i^n \\
s_{1_i}{}' &= s_{1_i} \cos^2\varphi_{o_i} + s_{2_i} \sin^2\varphi_{o_i} \\
s_{2_i}{}' &= s_{2_i} \cos^2\varphi_{o_i} + s_{1_i} \sin^2\varphi_{o_i}
\end{aligned}\right\} \qquad (2.3.32)$$

Accordingly, the total field from the glistening surface for the nth sample is

$$E_2^n = \sum_{i=1}^{M} [x_i^n + jy_i^n] \qquad (2.3.33)$$

where M is the number of patches and x_i^n and y_i^n are defined by (2.3.32). Expressing the total reflected power (at the receiver) for the nth sample in terms of E_2^n,

$$P_2^n = \frac{1}{2} Y_o \left\langle E_2^n E_2^{n*} \right\rangle, \qquad (2.3.34)$$

and hence the total mean scattered power received from the glistening surface is

$$\langle P_2 \rangle = \frac{1}{N} \sum_{n=1}^{N} P_2^n \qquad (2.3.35)$$

where N is the number of samples.

It remains only to determine s_{1_i} and s_{2_i} and the correlation coefficient C appearing in (2.3.24). To do this, the asymmetry factor

$$K_i = \sqrt{\frac{s_{2_i}}{s_{1_i}}} \tag{2.3.36}$$

is introduced. It may be shown that

$$K_i^2 = \begin{cases} \dfrac{(1 - \chi^2(v_z)) + (\chi^2(v_z) - \chi(2v_z))\cos\beta}{(1 - \chi^2(v_z)) - (\chi^2(v_z) - \chi(2v_z))\cos\beta} & \text{if specular point is on patch} \\ 1 & \text{otherwise} \end{cases} \tag{2.3.37}$$

is a reasonable approximation, where

$$\left.\begin{aligned} v_z &= -\frac{2\pi}{\lambda}(\cos\theta_1 + \cos\theta_2) \\ \chi(x) &= \exp\left(-\frac{1}{2}\sigma_h^2 x^2\right)^2 \\ \beta &= 2(kR_2 + \varphi) \\ \varphi &= \text{Phase of the Fresnel reflection coefficient.} \end{aligned}\right\} \tag{2.3.38}$$

Since

$$D\{E_2\}_i = s_{1_i} + s_{2_i} \tag{2.3.39}$$

is known, s_{1_i} and s_{2_i} can be determined (using (2.3.36) - (2.3.39) with the result

$$s_{1_i} = \frac{D\{E_2\}_i}{K_i^2 + 1}, \qquad s_{2_i} = K_i^2 s_{1_i} \tag{2.3.40}$$

With regard to the correlation coefficient C, it can be shown that if the distribution of surface heights is symmetric about zero and normally distributed (as has been assumed throughout this discussion)

$$C = \begin{cases} \dfrac{(\chi^2(v_z) - \chi(2v_z))\sin\beta}{\sqrt{(1 - \chi^2(v_z))^2 - (\chi^2(v_z) - \chi(2v_z))^2\cos^2\beta}} & \text{if specular point is in patch} \\ 0 & \text{otherwise} \end{cases} \tag{2.3.41}$$

is an appropriate approximation to C.

In the event experimental data indicates that an asymmetrical distribution for $\zeta(x, y)$ is more appropriate, only minor coding changes to the simulation will be required.

Final Remarks

Consider a receiver at an altitude of five meters and a source at a distance of 10 km from the receiver and at an altitude of 105 m. In addition, assume $\sigma_h/\lambda = 5$ and $\beta_o = .1$. Equation (2.3.16), with $|R(\psi_1)|^2$ set equal to 1 and with $\Delta\rho_d^2$ defined by (2.3.14) leads to the graph in Figure 10 (Reference 3) for the distribution of diffusely scattered power in down-range increments of 500 m. In this case the source elevation angle and the specular angle of incidence are small compared to the rms surface slope β_o, and the graphs shows that the major contributions to the diffuse power come from the ends of the glistening surface in agreement with the simplified multipath model discussed in section 2.2. However, equation (2.3.14) is valid only for a very rough surface, and since, in general, surface roughness is a function of receiver-source geometry and surface patch location in addition to terrain characteristics, the graph in Figure 10 may be misleading. Indeed, if each term on the right-hand side of (2.5.2) is multipled by the roughness factor F_d^2, which scales surface roughness according to patch location as well as surface characteristics, Figure 11 (Reference 3) is obtained. In this figure it is seen that the diffuse contribution directly below and in front of the transmitter is substantially reduced over that indicated in Figure 10. This does not suggest that the simplified model is totally incorrect, but it does indicate that care should be taken in the application of the simplified model to certain receiver-source configurations. In the geometry leading to Figure 11, the source (transmitter) is near the horizon where the earth appears relatively smooth to the receiver. This horizon effect is included in the roughness factor F_d^2 and accounts for the reduction of the diffuse contributions in this region.

The multipath model described in Section 4 gives a precise treatment of the refined multipath theory presented in Reference 3 and supports the preliminary computations made in this reference that lead to Figures 10 and 11.

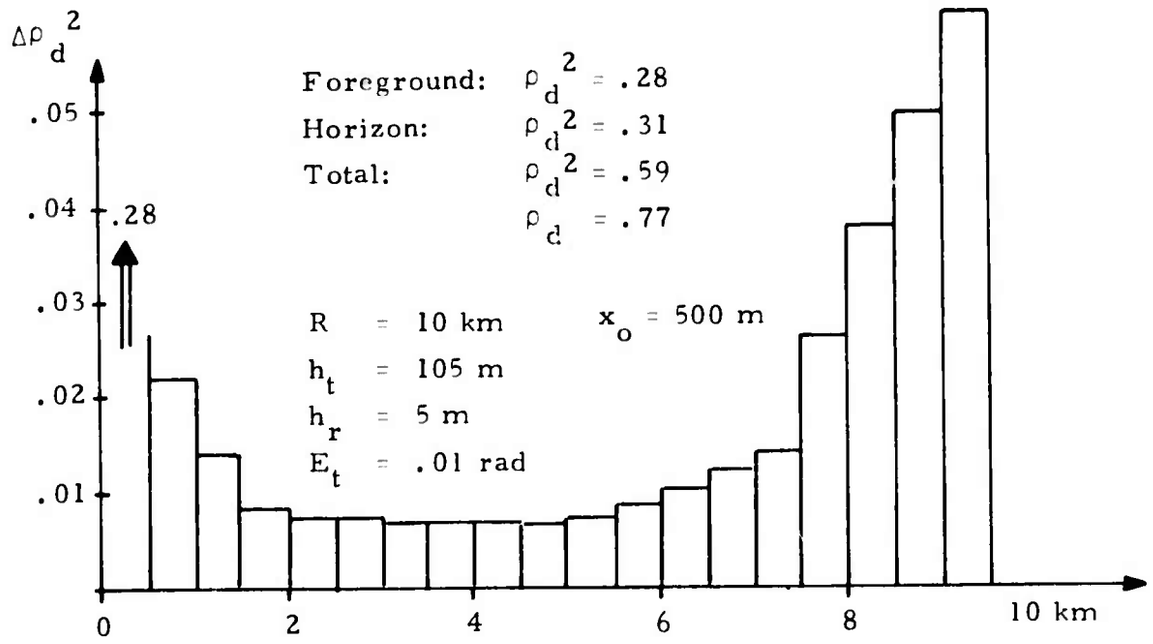

Figure 10. Distribution of Scattered Power in Ground Range (Classical Theory)

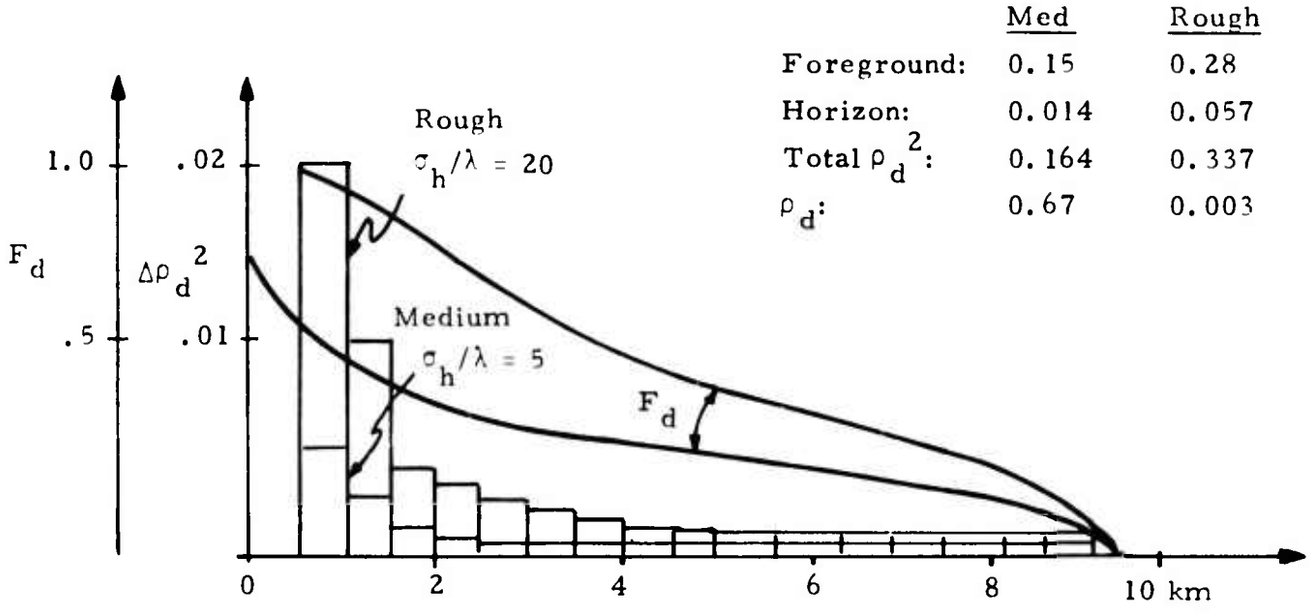

Figure 11. Distribution of Scattered Power in Ground Range (Modified Theory)

SECTION 3. EXPERIMENTAL MEASUREMENTS

The measurement approach is intended to provide accurate and reliable data for refining and quantifying the theory discussed in section 2. To this end an uncomplicated concept has been selected and an effort made to minimize equipment complexity.

This section discusses (1) trade-off studies performed to establish basic parameters for the experiment, (2) the equipment configuration selected, (3) the measurement approach, including site selection and auxiliary measurement requirements, and (4) data analyses needed to make best use of the measurements.

3.1 Trade-Off Studies

3.1.1 General

In order to proceed with design of the experiment certain ground rules were established early in the study. Major emphasis is to be placed upon determining how diffuse power is distributed along the glistening surface. Key factors which have been considered to achieve this goal in the most straightforward way are the following:

1. Radar vs one way measurement
2. Path orientation and length
3. Desirability of measuring phase
4. Techniques for achieving sufficient ground resolution
5. Choice of frequency
6. Choice of polarization
7. Signal strength

Radar vs. One Way Measurement

A major area of application for the refined theory will relate to radar tracking, which involves consideration of two-way paths. All basic information needed to determine the multipath effects of diffuse reflection may be obtained, however, from one-way measurements. Therefore, even though a tracking radar is modeled in the computer simulation (see Section 4), the measurement system needs to employ one way measurements. As a result, only a separate receiver and transmitter are needed rather than a complete tracking radar and a beacon target.

Path Orientation and Length

The geometry of greatest interest to the radar designer and user involves tracking targets close to the horizon from a radar site close to the ground. For the measurements, it was decided to let the receiver be located on the ground with the processing and recording equipment. The transmitter, a light weight, low power device, could then be in the target position, slightly elevated in angle above the horizon, supported by a balloon, parafoil, or helicopter. Maximum distance between transmitter and receiver should be the horizon distance as viewed from the ground sited equipment. The height of the phase center of the receiving antenna was selected to be 3 to 5 meters above the ground. Corresponding horizon distances are as given in Table III

Table III

Distances to Horizon

Antenna Height (m)	Horizon Distance (km)
3	7100
4	8200
5	9200

Since significant reflections may be expected at least up to the horizon, measurements should be made with transmitter-receiver distances at least this great.

Desirability of Measuring Phase

The complete description of the reflectivity of any patch on the ground requires that both amplitude and phase be given. Phase observed at the receiver, however, will vary rapidly with small changes in geometric placement of transmitter, patch and receiver. For wavelengths at microwave frequencies, practical geometric measurements will not be accurate enough to correlate with measured phase. In addition because the phase will vary rapidly in a real application, the precise phase bias indicated by the reflection is relatively unimportant.

Knowledge of the amplitude of the diffuse return, on the other hand, is of great importance if the theory is to be refined, and it is also easily measured.

It has been decided, therefore, to obtain data on the diffuse power from each patch without attempting to extract the phase information. This leads to an equipment simplification since CW signals need not travel simultaneously over both direct and indirect paths.

Techniques for Achieving Sufficient Ground Resolution

Because of the oblique geometry, it is very difficult to divide the glistening surface into small enough patches using angular resolution alone. The narrow angular resolution must be carried out either by the elevated transmitter or by the low sited receiver.

As an example, consider a receiver antenna 4 meters above ground level, and a transmitter located at horizon distance (8200 meters) at an elevation of 2.6 degrees above the horizon (372 meters high). If a ground patch resolution of 300 meters is to be provided by the transmitter in the receiver-transmitter direction, an elevation angular resolution of 0.107 degrees is needed. This would call for an antenna elevation dimension of 11.6 meters at Ku band and larger at lower frequencies.

To achieve this resolution along the glistening surface with the low sited receiver instead would call for a far larger antenna because of the extremely oblique geometry.

Although the geometry allows for a reasonable solution in azimuth, the range dimension must be treated differently. Use of a narrow pulse to provide downrange resolution appears to be feasible. A 1 nsec pulse generated at the transmitter will keep the resolution below 300 meters at all points on the glistening surface for geometries of interest. As indicated in Section 3.2 a very light weight transmitter can provide this capability.

It is intended to meet the resolution requirements with the narrow pulse transmitter and a directional receiving beam of about 0.5 degree beamwidth. The receiver will have a broad bandwidth (1 GHz) and the airborne transmitter antenna will be nearly omnidirectional to minimize angular control requirements.

Details of resolution studies for variation in test geometry parameters are covered in Section 3.1.2 below.

Choice of Frequency

Refinement of the diffuse reflection theory is desired over a broad range of frequencies. On the other hand the frequency should be high to achieve desired resolution, both keep antenna sizes within bounds for the azimuth dimension and to achieve the very wide bandwidth needed for the down range resolution. A Ku band (≈ 16 GHz) frequency has been chosen because it meets these requirements, because much radar and communication activity currently exists at Ku band, and also because it is believed that much of the diffuse reflection data gathered can be successfully extrapolated to lower bands such as X, C, S and L.

Choice of Polarization

As discussed in Section 3.2, it may be feasible to perform experiments with either vertical or horizontal polarization. If not, the equipment will be configured for horizontal polarization only, since the least complicated correlation of measurements and theory can be developed at this polarization. For this case the Brewster angle reduced return does not occur, so that uncertainties in expected smooth earth return, due to angle of incidence and reflection, will be minimized.

Signal Strength

For reliable measurements, adequate signal-to-noise ratio, S/N, must exist at the receiver. For the geometry of Figure 13, (see page 38) the direct path S/N per pulse is given by

$$S/N = \frac{P_t G_r G_t c^2 \tau}{(4\pi)^2 f^2 r_D^2 K T_o F_n L_r}$$

where

P_t = transmitter pulse power
G_r = gain of receiving antenna
G_t = gain of transmitting antenna
c = velocity of light
τ = pulsewidth
f = frequency

r_D = direct path distance between transmitter and receiver
K = Boltzmans Constant (1.38×10^{-23} watts/Hz/^oK)
T_o = standard receiver reference temperature (290^oK)
F_n = receiver noise figure
L_r = losses in receiving system

The transmitter losses are not explicitly called out because P_t is defined as the power radiated from the transmitting antenna when its gain is unity. Since the transmitter may be moving about quite freely, the antenna will be as omnidirectional as possible, and a gain (G_r) of 0 dB is therefore assumed.

The receiver gain is given by

$$G_r = \frac{4\pi A_r}{\lambda^2} \eta_a$$

where A_r is aperture and
η_a aperture efficiency

In terms of antenna diameter (d) and rf frequency, the gain can be expressed as

$$G_r = \frac{\pi^2 d^2 f^2}{c^2} \eta_a$$

For f = 16 GHz, d = 2.5 meters, and η_a = .6, the gain is 50.2 dB. For calculations, a gain of 50.0 dB has been assumed.

It is expected that a solid state light weight transmitter with a peak output power of 100 watts and a pulsewidth of 1 nanosecond can be obtained (a potential source is discussed in paragraphs 3.2.1.). Assuming these values and the following

r_D = 6 km
F_n = 8 dB
L_r = 2 dB

The direct path, single pulse S/N becomes

S/N = 41.9 dB

For the indirect paths relative attenuations of 30 dB may typically be expected, resulting in a S/N of 11.9 dB.

Should this level of signal prove inadequate, the pulses may be integrated incoherently to achieve desired signal strength. For most situations, an integration of 10 pulses (adding about 8 dB) should be adequate although integration of larger numbers would not be difficult. See Table IV, where S/N is given for various measurement ranges.

In the table

$(S/N)_D$ = Single Pulse Direct Path S/N

S/N = Single Pulse Indirect Path, Minimum S/N

$(S/N)_{10}$ = Ten pulse Integrated Minimum S/N for Indirect Path

Table IV

S/N at Various Ranges for 30 dB Indirect Path Attenuation

Range (r_D) km	$(S/N)_D$	S/N	$(S/N)_{10}$
3	47.9	17.9	25.9
5	43.5	13.5	21.5
6	41.9	11.9	19.9
7	40.6	10.6	18.6
10	37.5	7.5	15.5

The simulation computer program developed under the current study has been run to predict some typical results (see Section 4.0, Figures 49 through 60). Depending on conditions in these examples, indirect path returns exhibit attenuations of 17.8 dB and greater. Diffuse attenuation is particularly large when the

terrain is very smooth. On the other hand for moderately rough terrain the diffuse return from a significant portion of the glistening surface will produce acceptable S/N levels. In developing the experiment, it must be recognized that for a given beam position only a portion of the predicted signal level can be observed because of equipment limitations.

However, for a reasonably rough surface most portions of the glistening surface can be examined by using various beam positions to illuminate each region of interest. If in these regions, the observed power matches theoretical predictions, confidence in the theory can be increased and theoretical extrapolation beyond observations can be justified. The transmitter power level planned for the experiment is therefore expected to be adequate.

Detailed Parameter Trade-offs

The above considerations have led to the choice of the experimental configuration outlined in Section 1.3. Detailed parameter trade-offs which were used in selecting configuration parameters and determining some of the requirements for auxiliary equipment follow. Discussed are resolution, shape of the glistening surface, and accuracy with which transmitter location must be determined.

3.1.2 Resolution

The critical resolution direction is along the ground projection of the direct transmitter-receiver path. The geometry is treated briefly below and trade-off curves presented for typical cases which show the relationships which govern resolution among receiving antenna beamwidth, transmitter pulsewidth and geometric placement. Next are shown the contours of receiving beam intersection with the ground so that the cross range resolution attributable to receiving beam shape may be understood.

Resolution Along Transmitter-Receiver Ground Path Projection

Relationships governing angular resolution have been developed using the geometry of Figure 12, for a spherical Earth, where

R_e = 4/3 times geometric Earth Radius

h_r = height of receiving antenna (R)

D_1 = Ground Distance to resolution cell center (C)

ϕ_1 = Look angle to C with respect to vertical

The relationships are:

$$\phi_1 = \frac{D_1}{R_e}$$

$$\theta_1 = \arctan\left[\frac{R_e \sin \phi_1}{R_e + h_r - R_e \cos \phi_1}\right]$$

The required beamwidth $\Delta\theta$, for given resolution distance ΔD_1 can be obtained by solving these equations for values of D_1 at each end of the desired resolution interval.

Figure 13 represents the corresponding situation for time delay range resolution. In the figure, h_t is the height of the transmitter (T). D is the receiver transmitter projected ground distance.

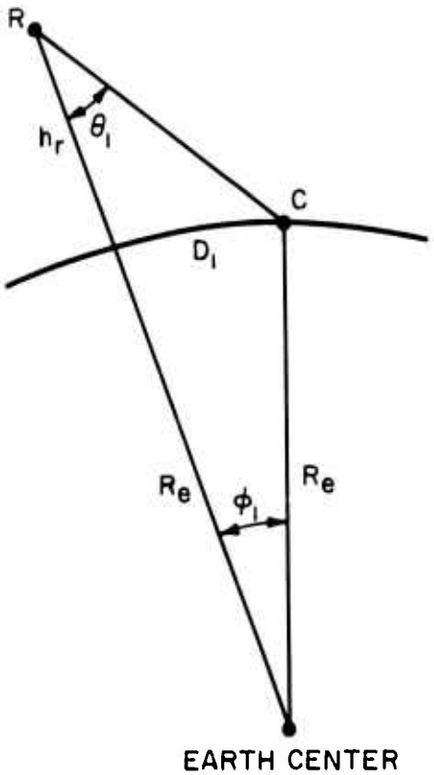

Figure 12.
Angular Resolution Geometry

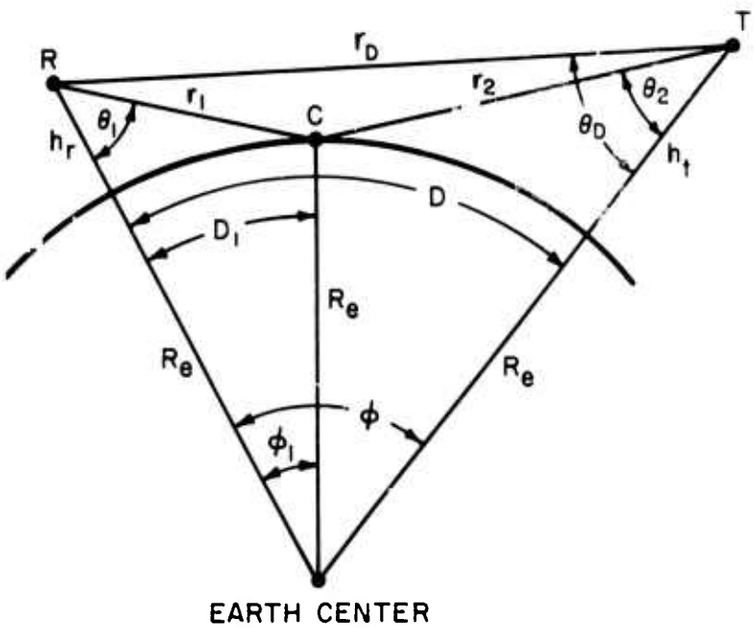

Figure 13.
Range Resolution Geometry

The total path length (r) is given by

$$r = r_1 + r_2$$

and

$$r_1 = R_e \frac{\sin \phi_1}{\sin \theta_1}$$

where

$$\phi_1 = \frac{D_1}{R_e} \quad \text{and} \quad \theta_1 = \arctan \frac{R_e \sin \phi_1}{R_e + h_r - R_e \cos \phi_1}$$

and

$$r_2 = R_e \frac{\sin (\phi - \phi_1)}{\sin \theta_2}$$

where

$$\phi - \phi_1 = (D - D_1)/R_e$$

$$\theta_2 = \arctan \left[\frac{R_e \sin (\phi - \phi_1)}{R_e + h_t - R_e \cos (\phi - \phi_1)} \right]$$

The direct path distance (r_D) is given by

$$r_D = (R_e + h_r) \frac{\sin \phi}{\sin \theta_D}$$

where

$$\theta_D = \arctan \left[\frac{(R_e + h_r) \sin \phi}{R_e + h_t - (R_e + h_r) \cos \phi} \right]$$

Resolution may be expressed in terms of the change in D_1, i.e. ΔD_1, as the differential time between direct and indirect paths is varied. Thus in the measurement equipment a pulse received over the direct path is used as the reference for signals received from points C over indirect paths.

Time delay (τ_d) is

$$\tau_d = (r - r_D)/c$$

where c = velocity of light

Since r_D is constant during a set of measurements the change in time delay, $\Delta \tau_d$, is

$$\Delta \tau_d = \Delta r / c$$

This may be interpreted as the pulsewidth. The resolution, ΔD_1, is directly related through the above equations to $\Delta \tau_d$ as a function of the location of point C.

Angular and range ground resolutions have been computed for geometries of interest and are presented in Figures 14 through 20. Results assume a receiving elevation beamwidth of 0.5 degree and a transmitter pulsewidth of 1 nanosecond, since these appear to be reasonable values for the measurement program. For other values linear scaling may be applied.

Displayed are receiver-transmitter distances of 3, 5, 7 and 10 km for a receiver height (h_r) of 3 meters and distances of 5, 10 and 15 km for h_r of 5 meters. Resolution is shown as a function of ground distance (D_1) for a range of transmitter heights (h_t). Maximum values of h_t are great enough to insure a resolution of 300 meters or less at all points. The maximum resolution occurs when the angular resolution and pulse resolution curves cross. This occurs fairly close to the receiver. The slight kink in the angular resolution curve represents an approximation to the cross over between far and near field patterns for the receiving antenna. It was assumed that the beamwidth is 3 meters at the cross over point.

There is little difference due to change in receiver height. Furthermore all curves seem to indicate that if 300 meters resolution is to be met at all ground points the elevation angle of the transmitter as viewed from the receiver must be no less than about 2.5 degrees.

Receiving Beam Contours

The shape of the receiving beam intersection with the ground at its 3 dB contours has been calculated for a flat earth. This provides the beam shape contribution to resolution boundaries. Figure 21 illustrates the geometry.

Resolution contours are traced out as ϕ is rotated through 360 degrees. Parametric equations for the contours are

$$x = r(\cos\theta\cos\delta + \sin\theta\sin\delta\cos\phi)$$

$$y = r\sin\theta\sin\phi$$

$$r = h_r/(\cos\theta\sin\delta - \sin\theta\cos\delta\cos\phi)$$

where

h_r = receiver height

r = distance from receiver to intersection point on resolution contour

θ = half beamwidth (conical beam)

δ = depression angle of beam axis

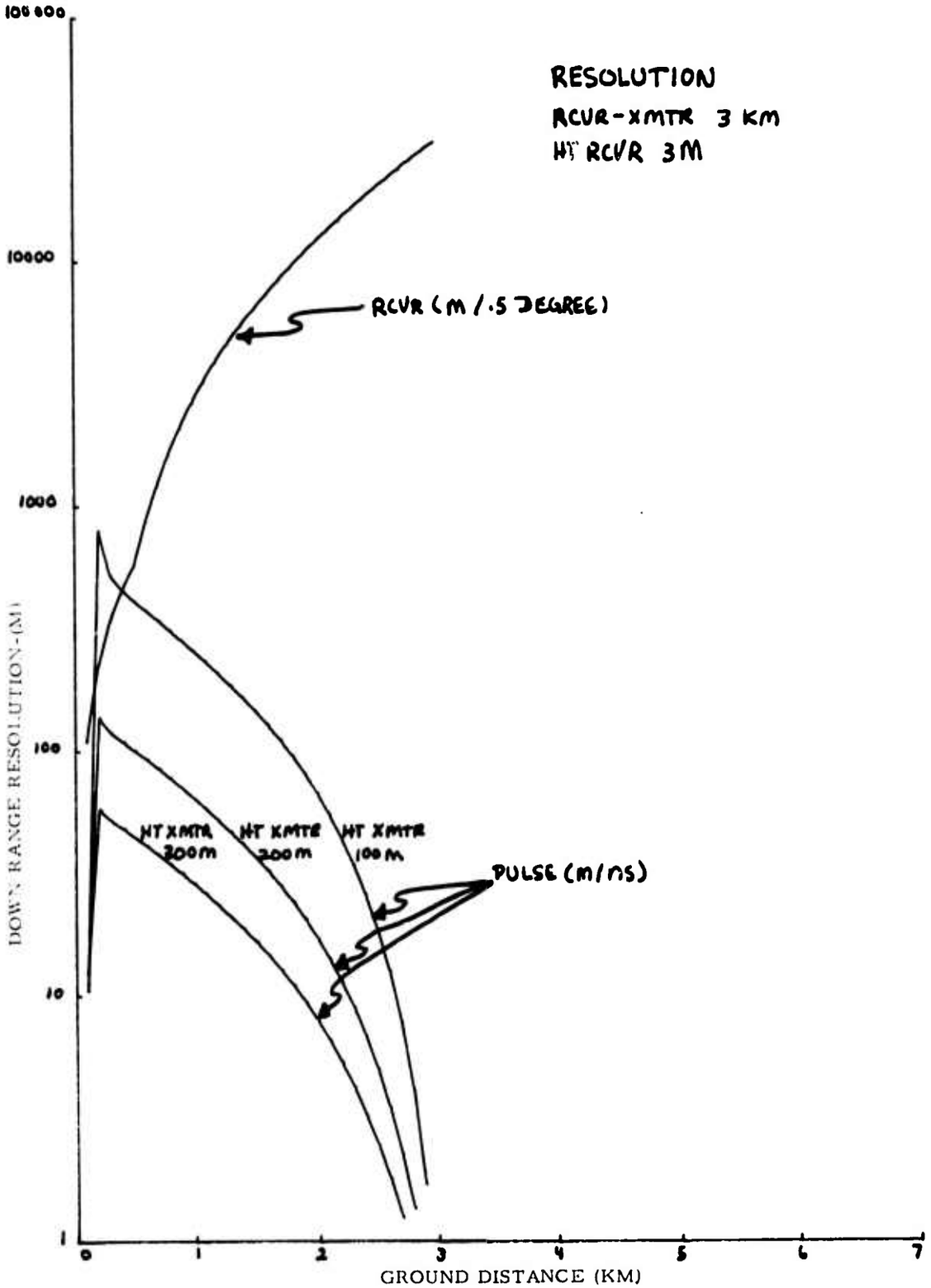

Figure 14. Down Range Resolution
(D = 3 km, h_r = 3 m)

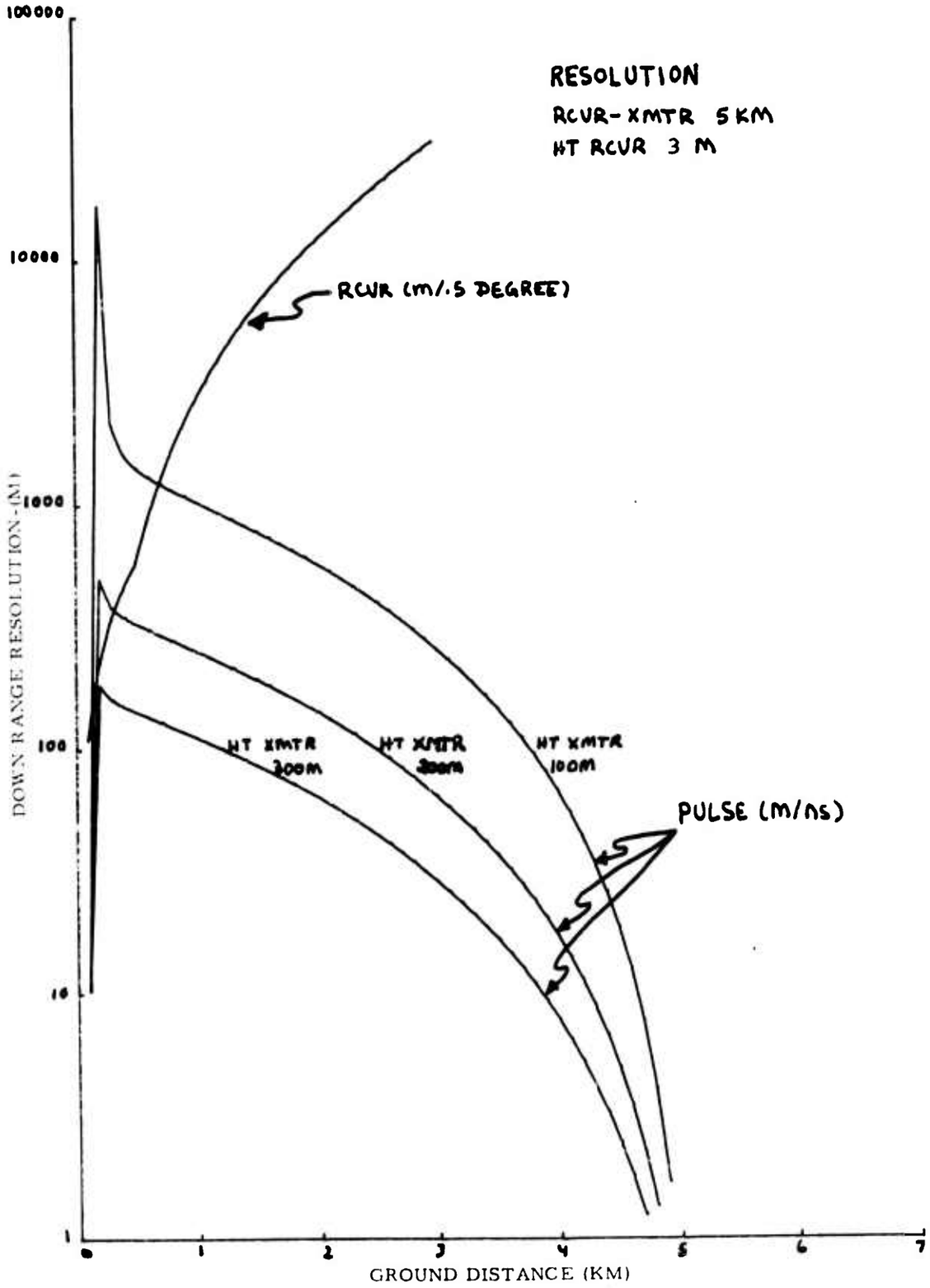

Figure 15. Down Range Resolution
(D = 5 km, h_r = 3 m)

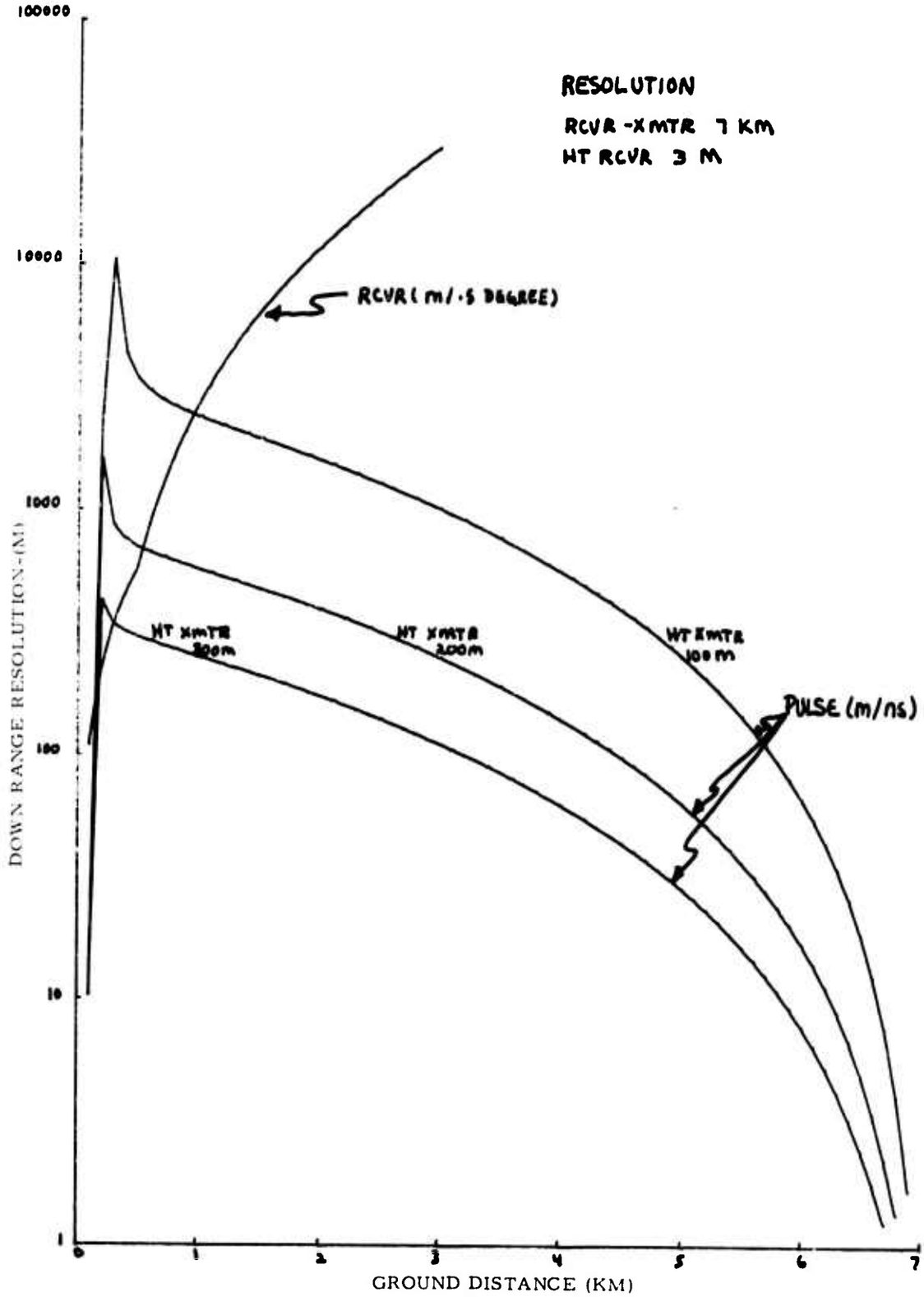

Figure 16. Down Range Resolution
(D = 7 km, h_r = 3 m)

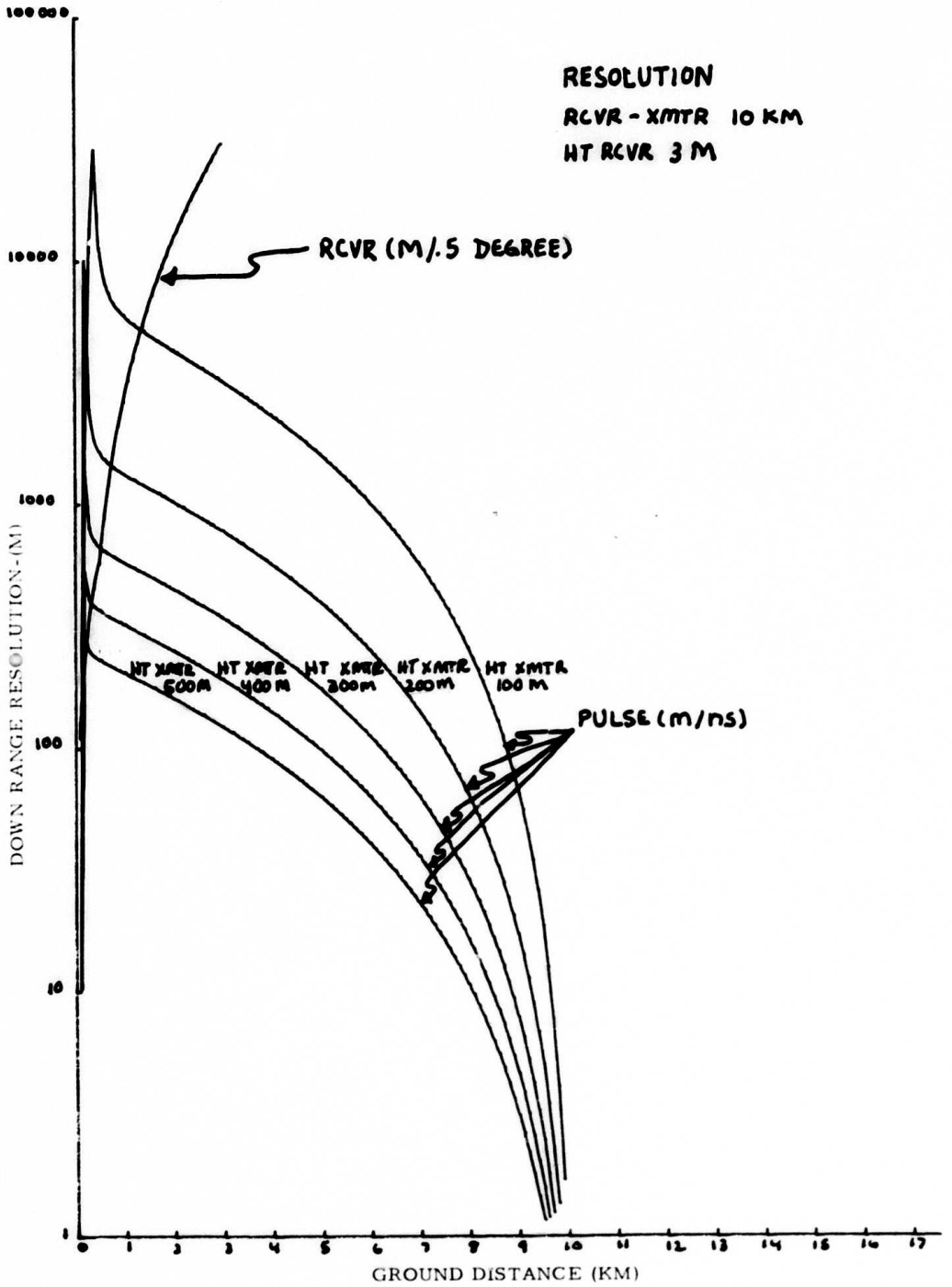

Figure 17. Down Range Resolution
(D = 10 km, h_r = 3 m)

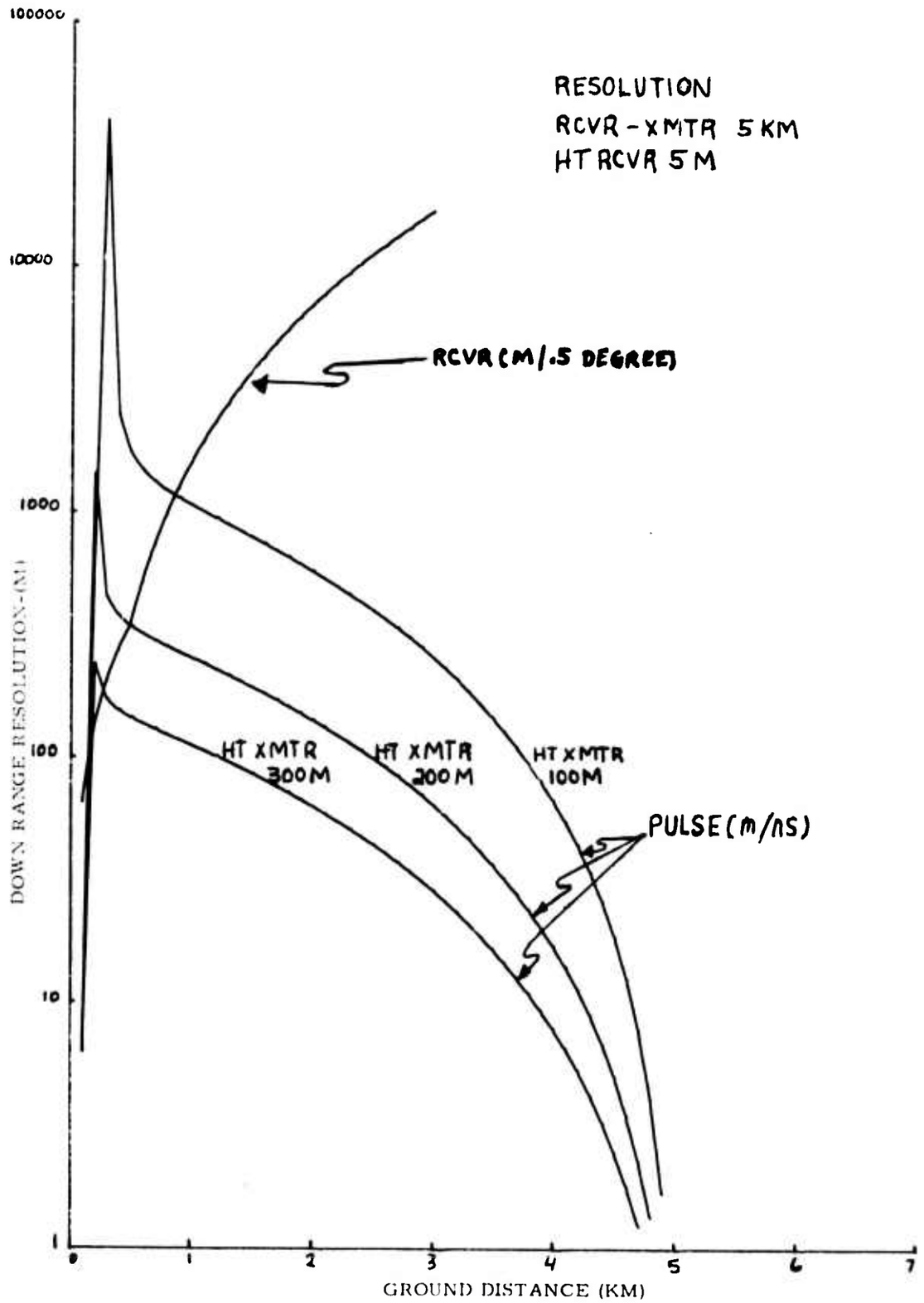

Figure 18. Down Range Resolution
(D = 5 km, h_r = 5 m)

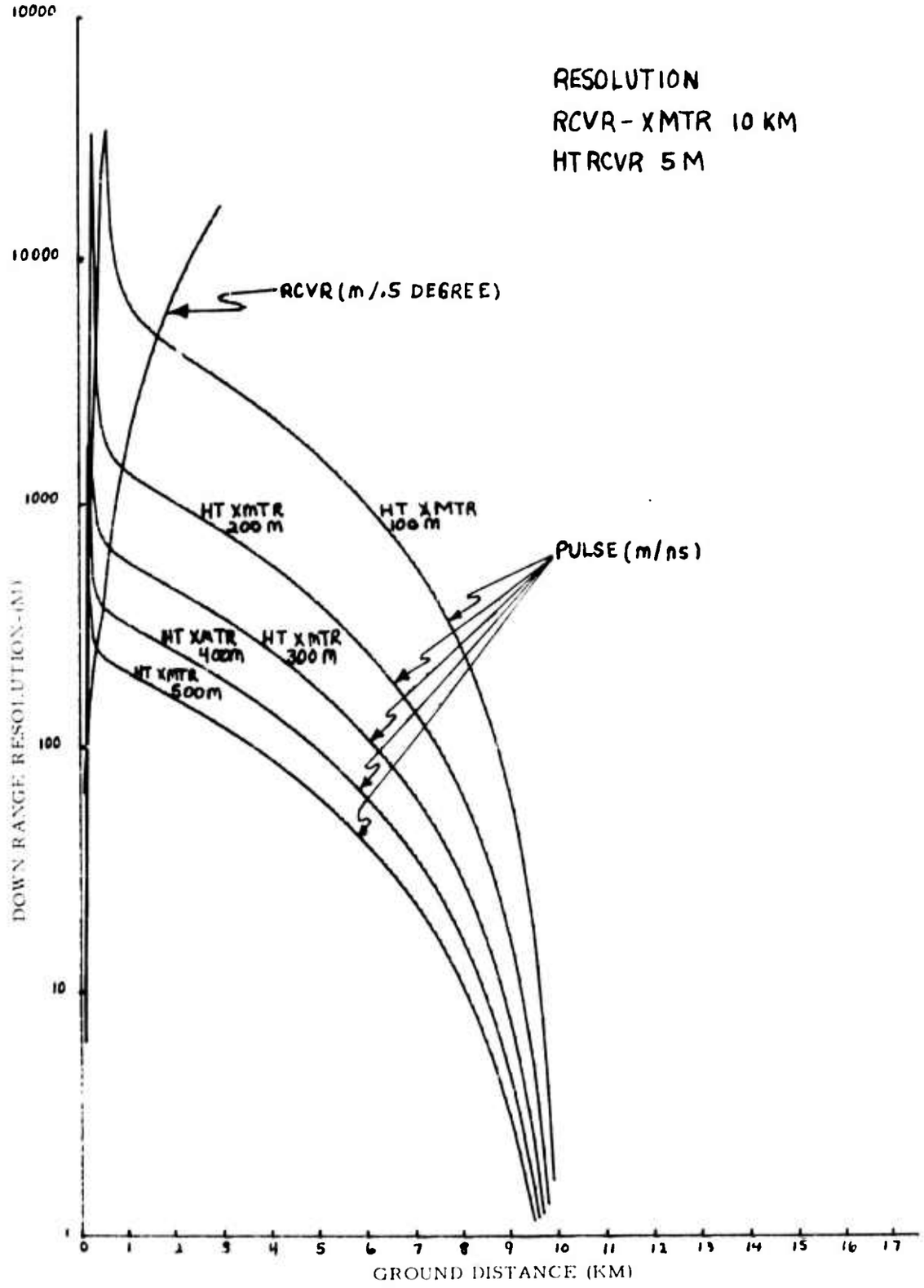

Figure 19. Down Range Resolution
(D = 10 km, h_r = 5 m)

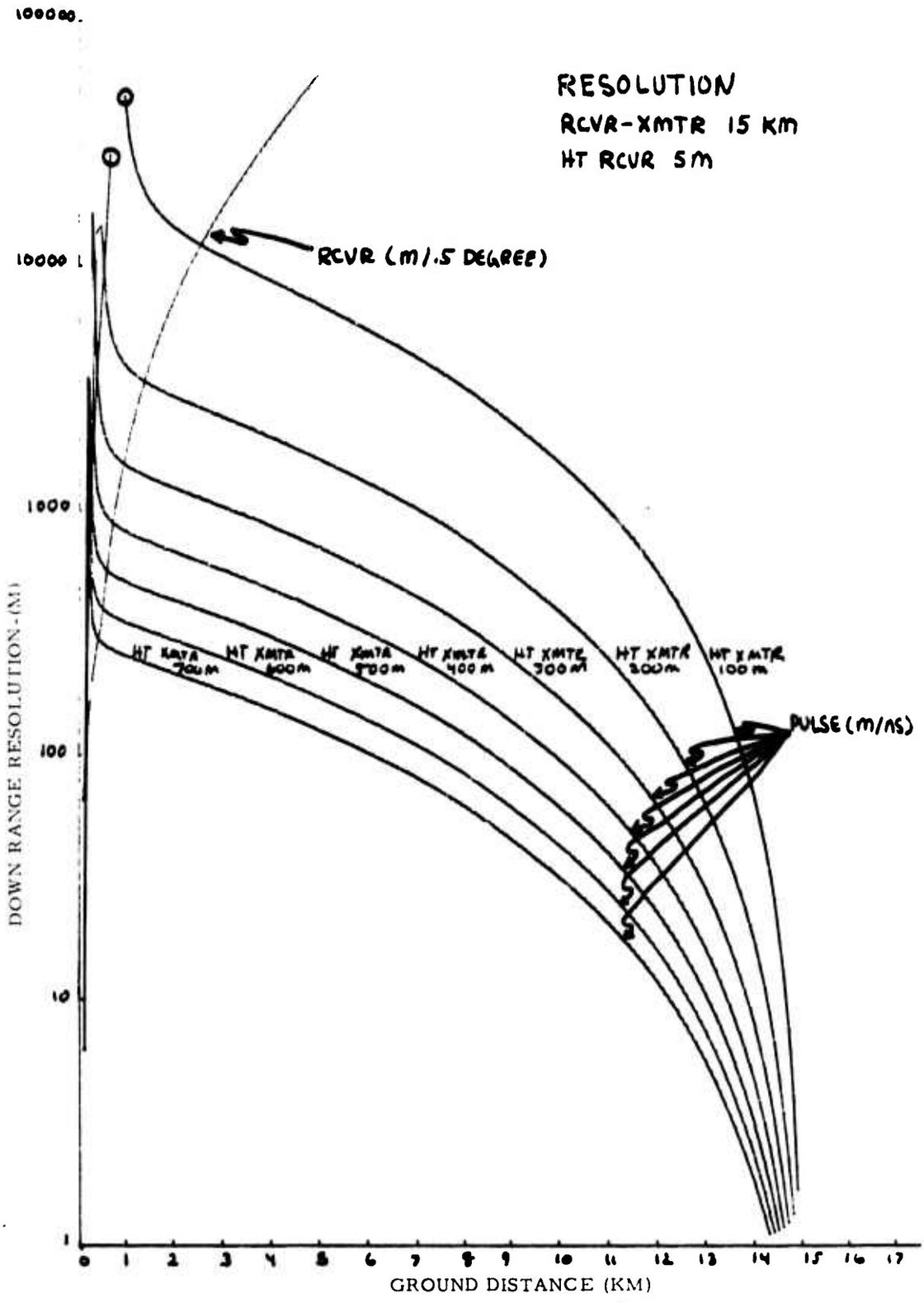

Figure 20. Down Range Resolution
(D = 15 km, h_r = 5 m)

Contours developed for a 5 meter receiver height are presented in Figure 22. The black dots on the down range axis represent position of the beam axis for each contour. These contours assume a 0.5 degree beamwidth at all ranges. Actually, close to the receiver the near field pattern exhibits a larger angular beamwidth. Hence for ranges less than about 400 meters the resolution contours will be somewhat longer than illustrated. Nevertheless it is clear that good two dimensional resolution can be obtained with the receiving antenna at short distances.

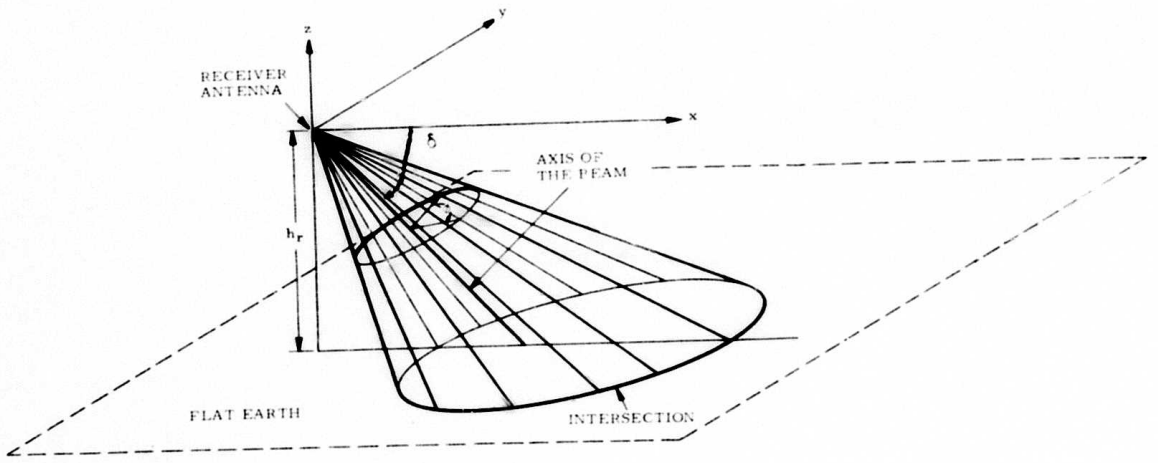

Figure 21. Receiving Beam Geometry

3.1.3 Glistening Surface Shape

The shape of the glistening surface is of interest because it represents the region over which diffuse returns may be expected. The boundary of the surface for a flat earth is given by (Ref. 1):

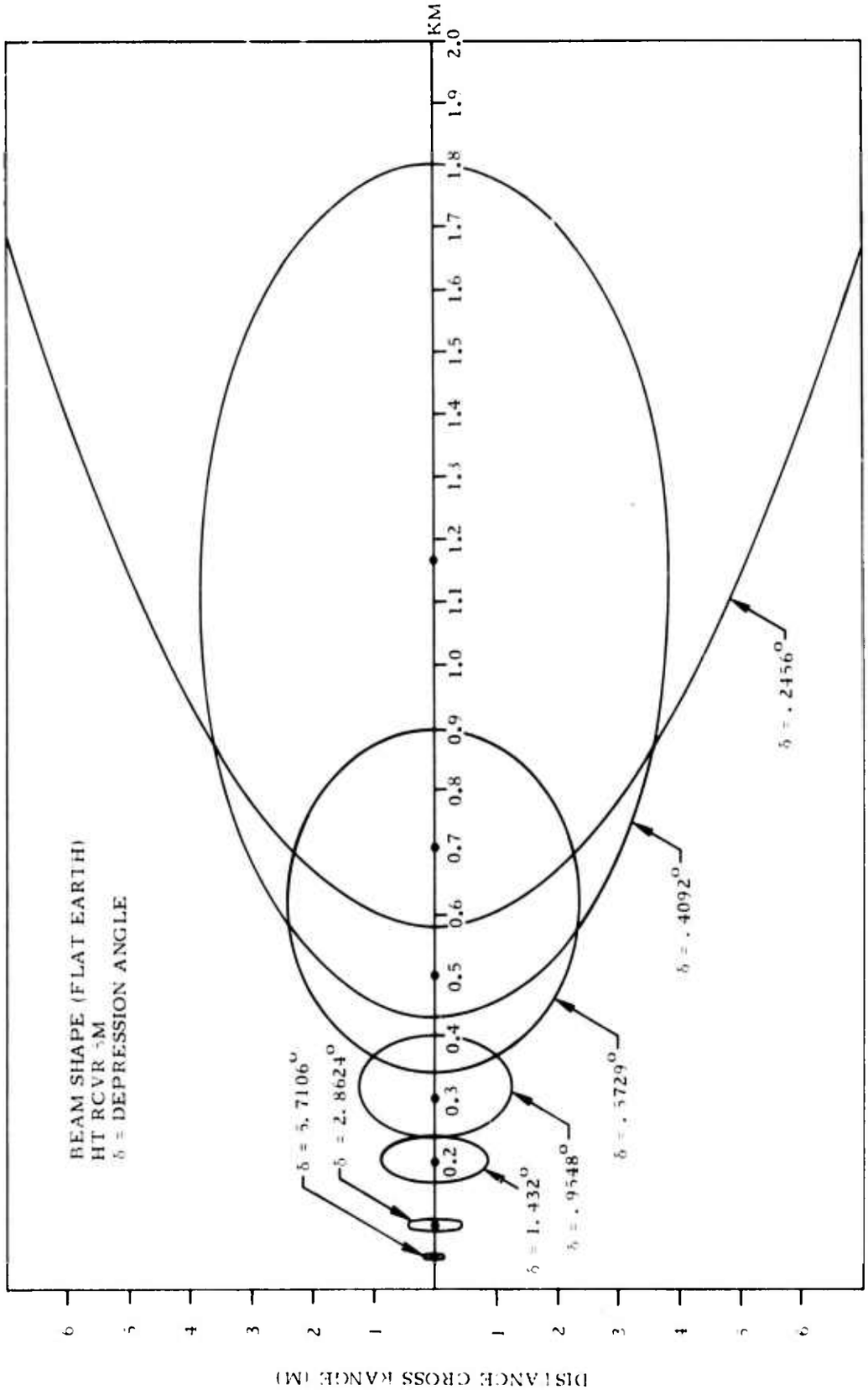

Figure 22. Receiving Beam Contours

$$y = \pm \frac{D_1 D_2}{D} \left(\frac{h_r}{D_1} + \frac{h_t}{D_2} \right) \sqrt{\tan^2 \beta_o - \frac{1}{4} \left(\frac{h_r}{D_1} - \frac{h_t}{D_2} \right)^2}$$

This equation defines a boundary line in terms of an ordinate y (cross range) and an abscissa, D_1, (down range distance), measured with respect to an origin beneath the receiver and a line projected on the earth below the receiver-transmitter direct path.

In this equation

D = ground distance between receiver and transmitter
$D_2 = D - D_1$ = down range distance measured from transmitter ground projection
h_r = height of receiver
h_t = height of transmitter
β_o = slope of terrain

If the slope, β_o, is distributed such that β_o is maximum magnitude, then all diffuse reflections will arrive from some location within the boundary. If, instead, β_o is the rms slope then most diffuse reflections originate within the boundary, but some returns will come from outside.

All the geometric conditions of Section 3.1.1 have been examined for glistening surface shape. In each case plots have been made for β_o values of .1, .25, .5 and 1.0 radians. Representative examples are shown in Figures 23 through 28. In each contour, bounding increments of 0.5 degree receiver beamwidth are superimposed to show conditions under which azimuth resolution will provide useful information.

A listing of parameters selected for each figure is given in Table V

Table V.

Glistening Surface Parameters

Fig. No.	D(km)	h_r (m)	h_t (m)
23	3	3	200
24	5	3	200
25	7	3	100
26	7	3	300
27	10	3	400
28	10	5	400

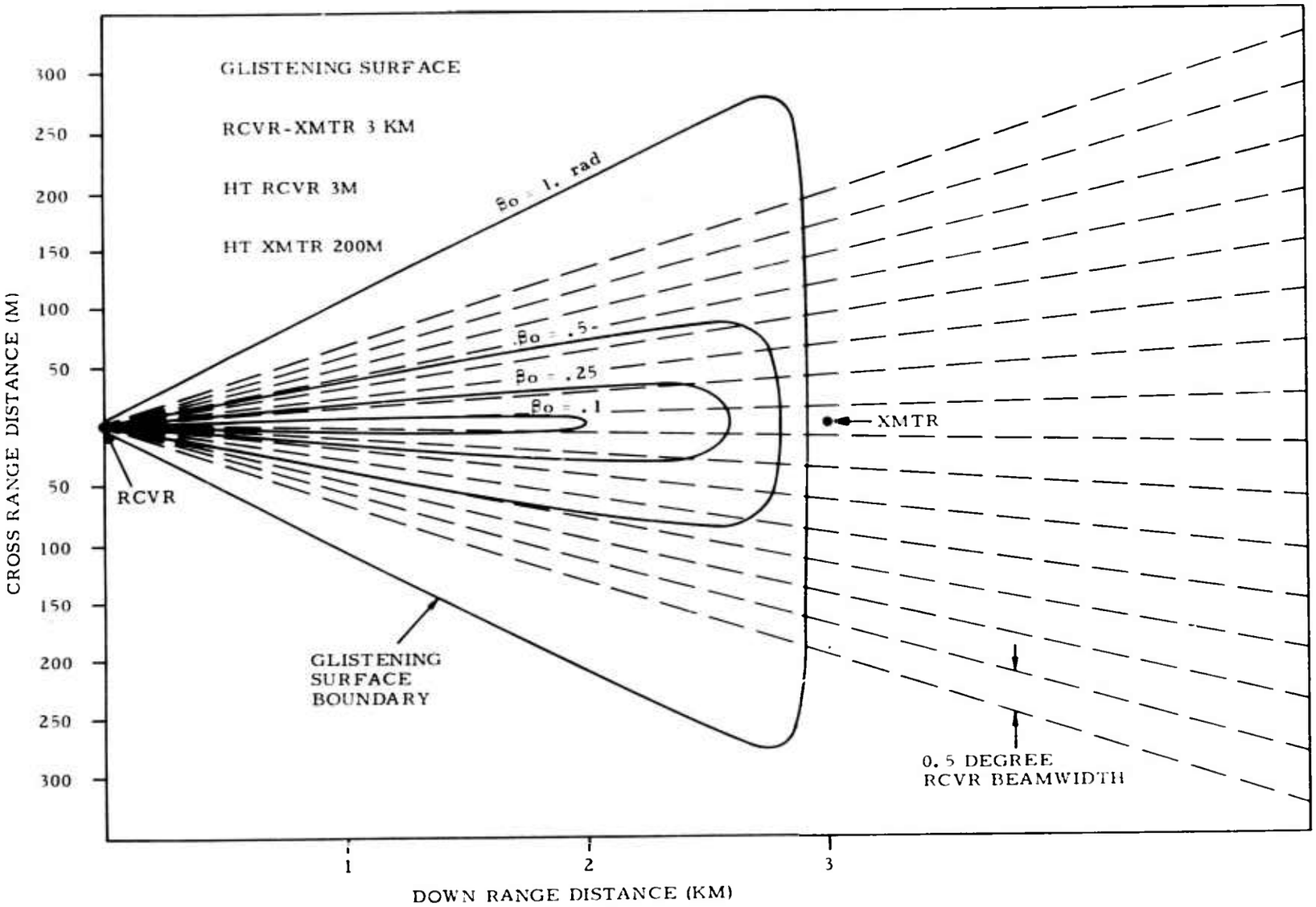

Figure 23. Glistening Surface Boundaries
(D = 3 km, h_r = 3 m, h_t = 200 m)

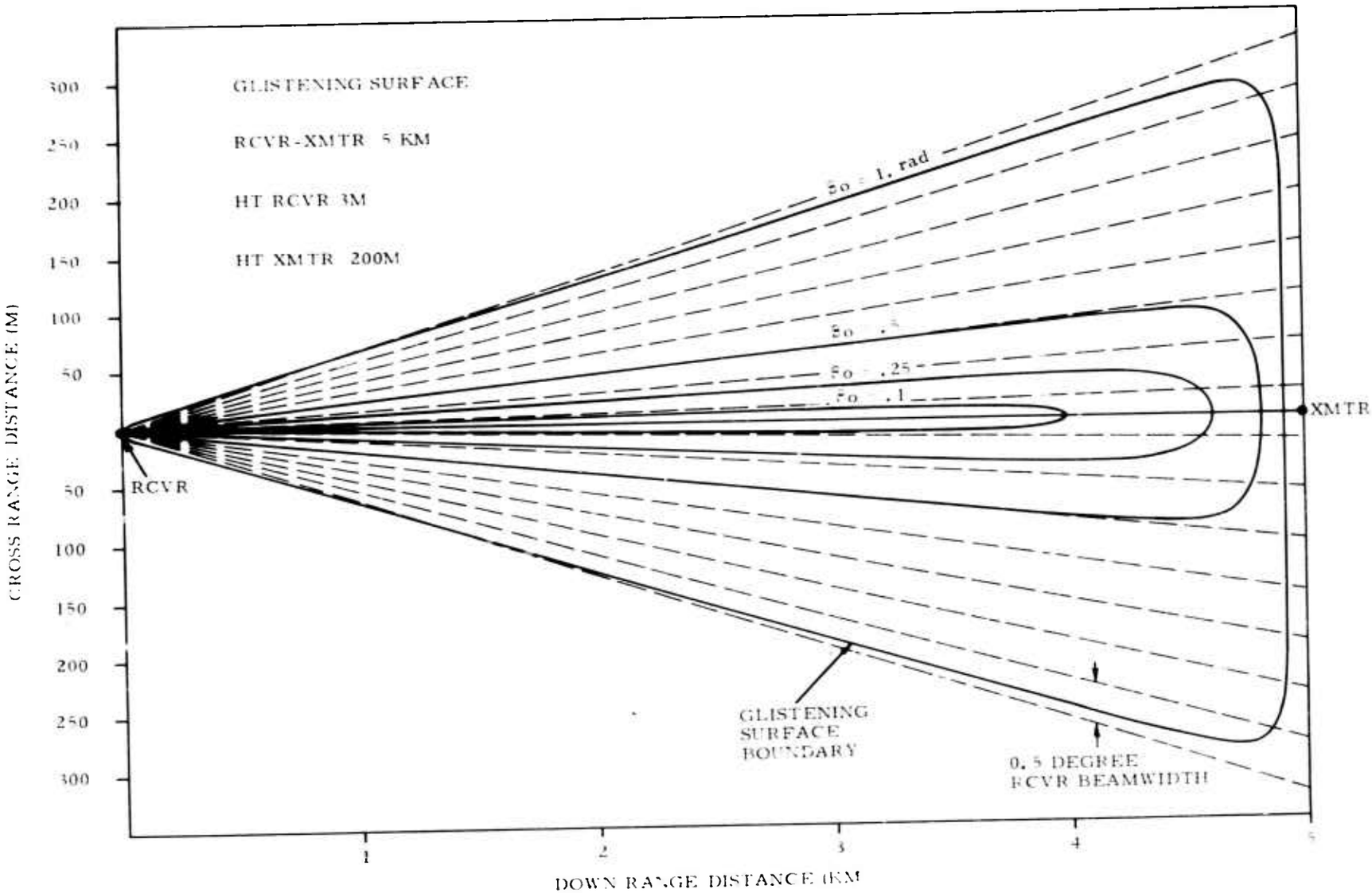

Figure 24. Glistening Surface Boundari
(D = 5 km, h_r = 3 m, h_t = 200 m)

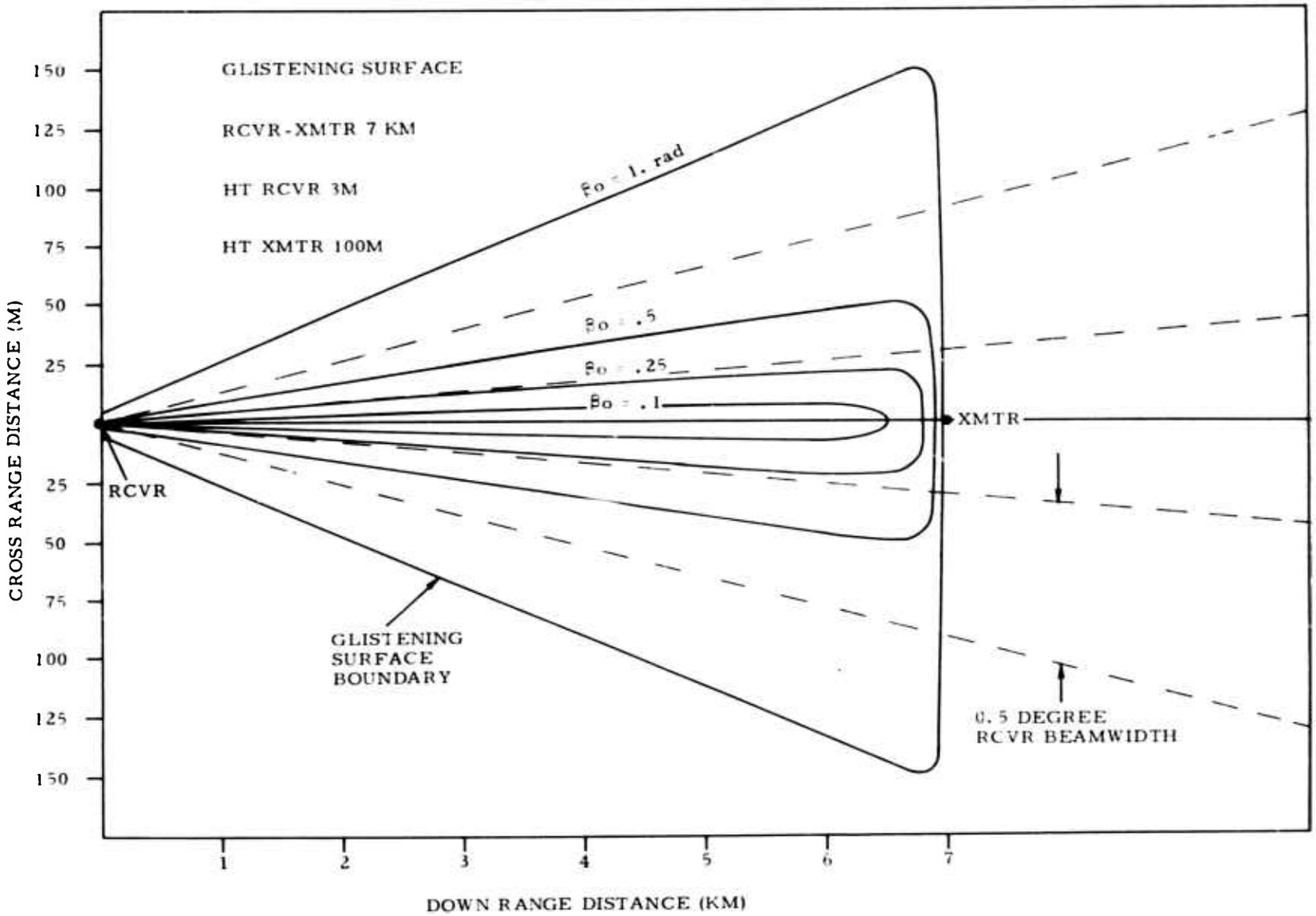

Figure 25. Glistening Surface Boundaries
(D = 7 km, h_r = 3 m, h_t = 100 m)

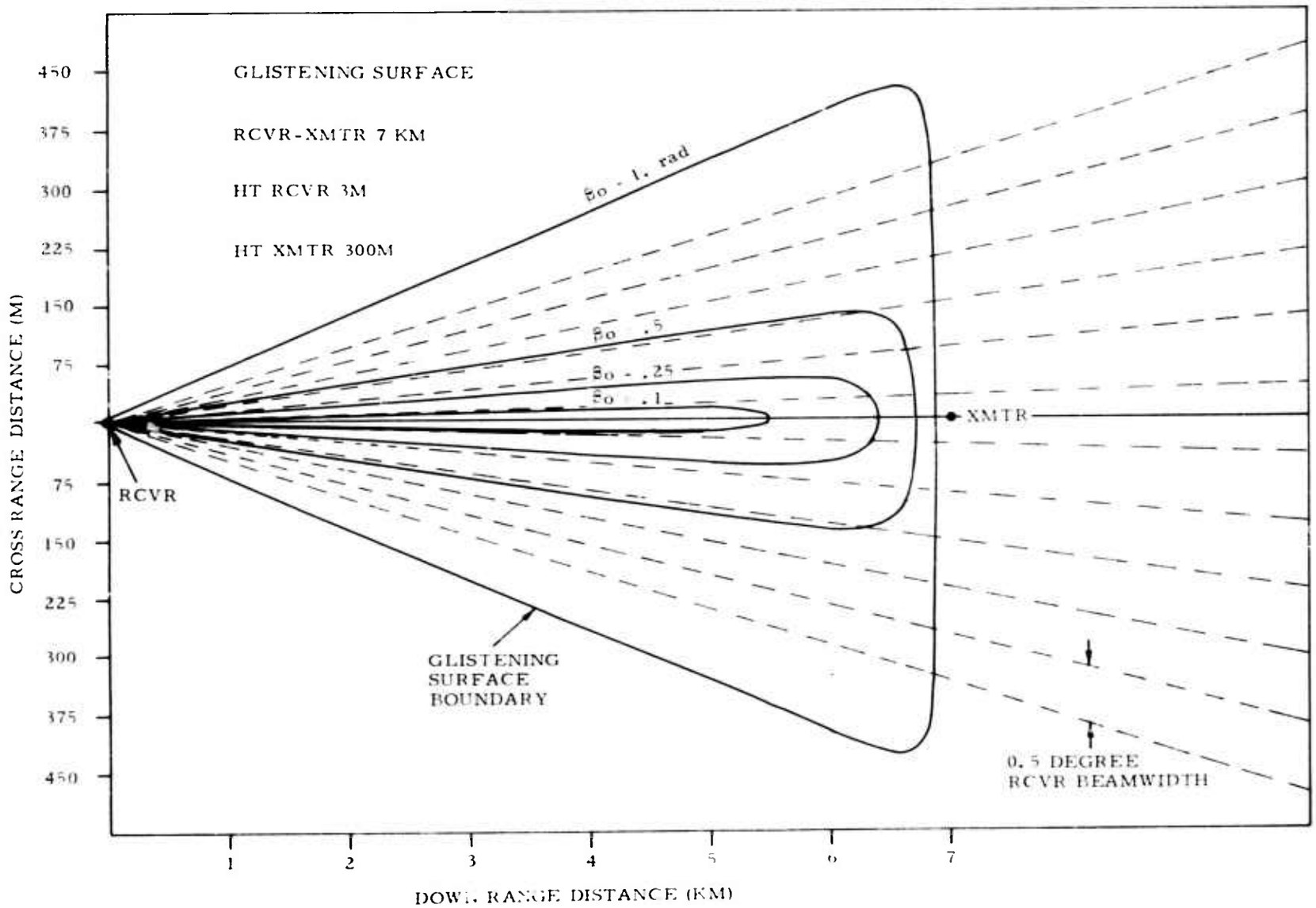

Figure 26. Glistening Surface Boundaries
(D = 7 km, h_r = 3 m, h_t = 300 m)

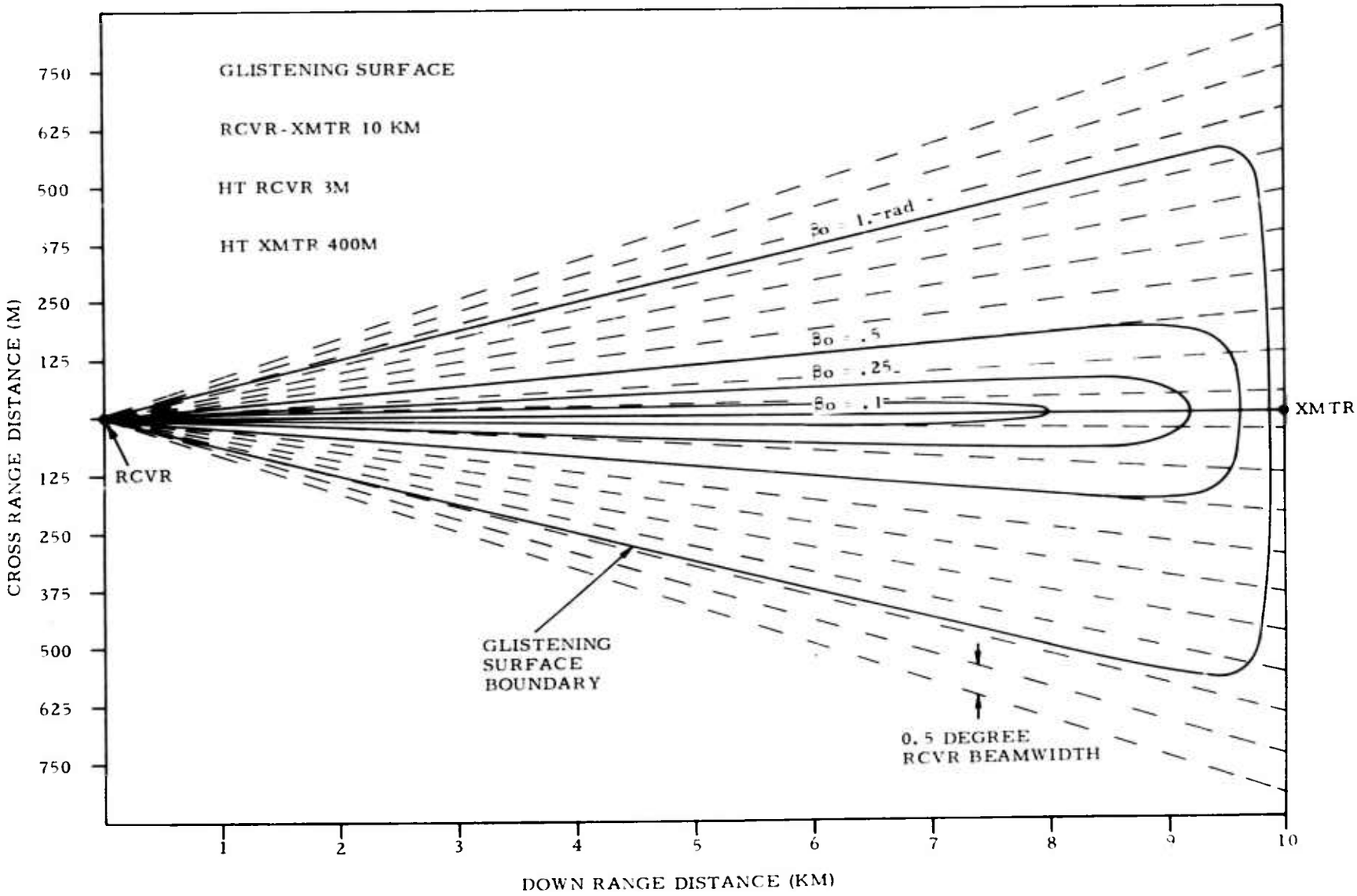

Figure 27. Glistening Surface Boundaries
(D = 10 km, h_r = 3 m, h_t = 400 m)

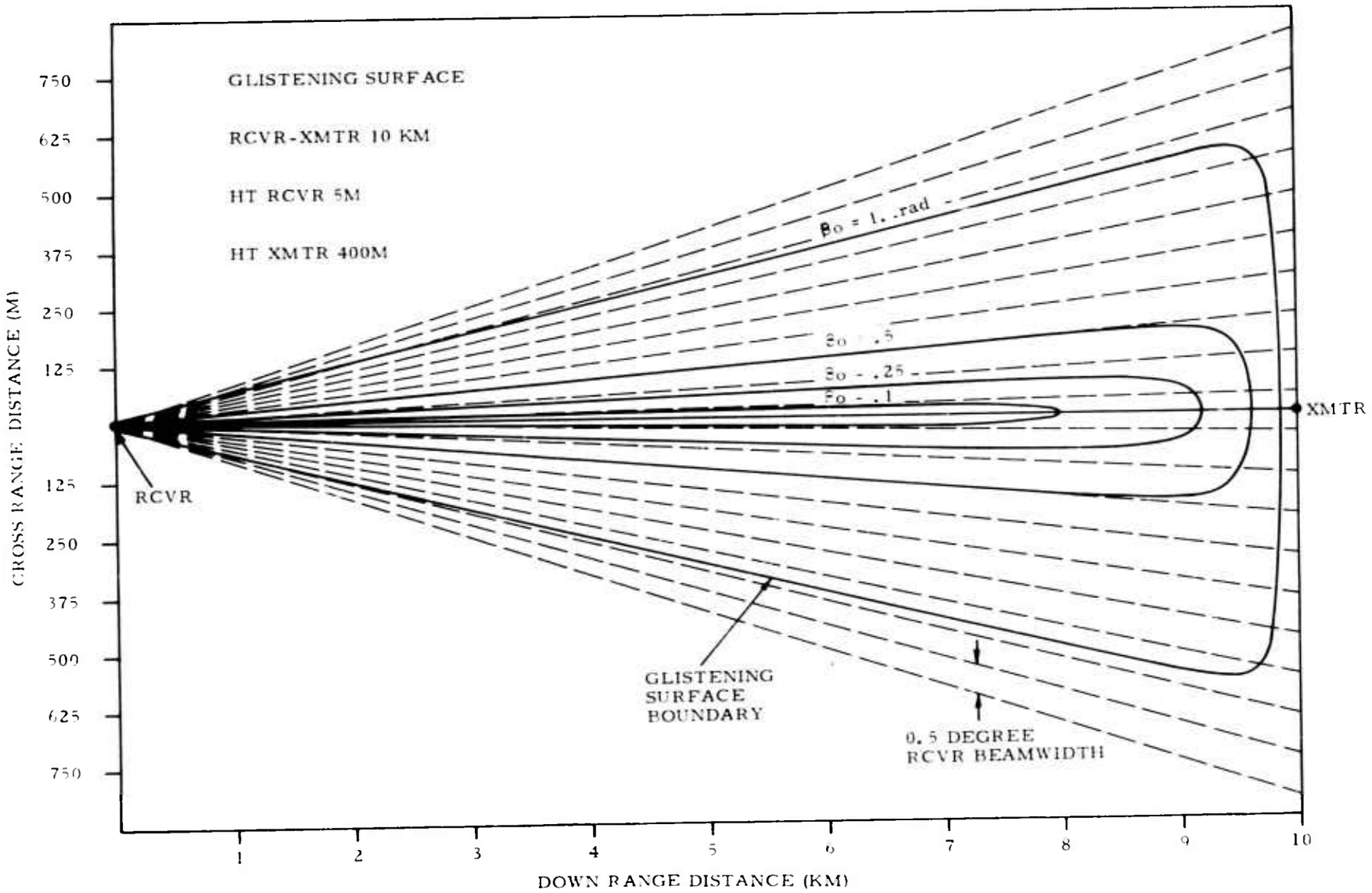

Figure 28. Glistening Surface Boundaries
(D = 10 km, h_r = 5m, h_t = 400 m)

Although the earth is actually curved these plots may be expected to be accurate except when the horizon distance from the receiver is exceeded (refer to Table III). For these cases the glistening surface terminates at the horizon.

To achieve the desired resolution of 300 meters maximum, the transmitter elevation angle should be at least 2.5 degrees as viewed from the receiver. For these cases the $\beta_0 = 0.1$ radian boundary is enclosed within a single 0.5 degree beamwidth. For greater values of surface roughness beamwidth azimuth resolution becomes important. For example, if $\beta_0 = 0.5$, five angular beamwidths are enclosed within the glistening surface boundary.

The shape of the boundaries (for flat earth) is little affected by receiver height changes, as long as the height is relatively quite low. Thus Figures 27 and 28 appear identical even though receiver heights are 3 and 5 meters respectively.

3.1.4 Transmitter Location Accuracy Requirement

Since the transmitter is to be held aloft by a non-rigid support (e.g. balloon or helicopter) the effect of inaccurate knowledge of its position with respect to the receiver must be evaluated. This information will determine the specifications needed for auxiliary tracking equipment. Accordingly the unobservable change in reflection point due to an unknown change in transmitter height (elevation error) or in receiver-transmitter ground distance (down range error) has been examined.

Figure 29 shows the "flat" earth receiver-transmitter configuration. Check calculations with a curved earth have confirmed that this approximation gives a very accurate result for the error relationship. Symbols used have equivalent meaning to those used in Figure 13.

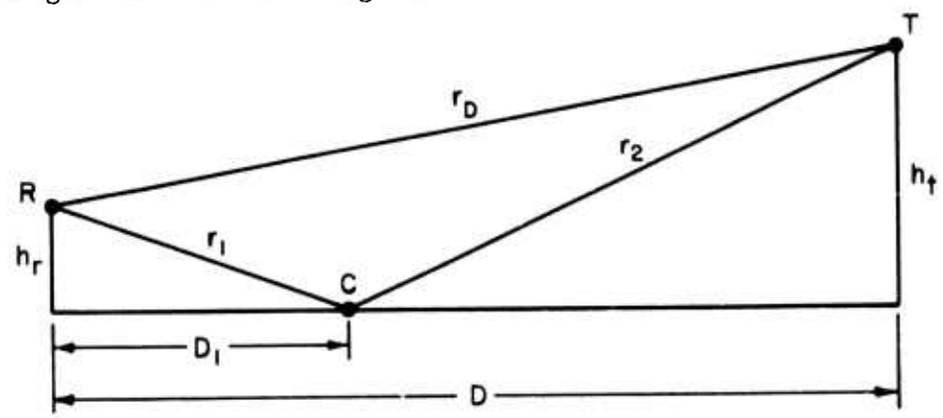

Figure 29. Geometry for Error Analysis

Elevation Error

This is defined as the change of ground distance to the reflection point, C, given a change in transmitter height under the constraint that the net path length, r, be constant. Net path length is

$$r \equiv r_1 + r_2 - r_D$$

This is the quantity directly measured by the timing circuits in the receiver. Changes in D_1 with net path length constant will be undetectable by the measuring equipment.

The elevation error, $\frac{\partial D_1}{\partial h_t}$, has been derived from the geometry of the figure with the above constraint, namely

$$\frac{\partial r}{\partial h_t} = \frac{\partial r_1}{\partial h_t} + \frac{\partial r_2}{\partial h_t} - \frac{\partial r_D}{\partial h_t} = 0$$

The result is

$$\frac{\partial D_1}{\partial h_t} = \frac{r_1 \left[r_2 (h_t - h_r) - r_D h_t \right]}{r_D \left[r_2 D_1 - r_1 (D - D_1) \right]}$$

Down Range Error

This is defined as the change of ground distance to the reflection point, C, given a change in receiver-transmitter ground distance under the same constraint as above.

The down range error is

$$\frac{\partial D_1}{\partial D} = \frac{r_1 \left[r_2 D - r_D (D - D_1) \right]}{r_D \left[r_2 D_1 - r_1 (D - D_1) \right]}$$

Numerical Results

The errors have been evaluated for all cases examined in Section 3.1.2. Representative results for $\frac{\partial D_1}{\partial h_t}$ are given in Figures 30 through 33, which cover values of D from 3 to 10 km, with h_r = 3 m Results for h_t = 5 m are substantially the same.

The error reaches its maximum near the center of the reflective region and its value is a function of the elevation angle to the transmitter. For the nominal value (2.5 deg) selected in Section 3.1.2 for resolution purposes, the elevation error has a magnitude of about 12, i.e., a 1 meter change in transmitter height requires a 12 meter change in reflection point to keep the time difference constant.

There is as well some anomalous behavior close to the receiver, but resolution in this region will be handled by the receiving beam pattern so that timing effects will not be important.

The error of value 12 implies that an elevation tracker located at the receiver and having an accuracy of 0.5 mr will introduce an error of 60 meters at midrange if the transmitter is 10 km distant. This is less than the 90 meters resolution expected at that point and considerably lower than the desired resolution of about 300 meters. Azimuth tracking errors will be less severe since no geometric dilution exists.

Figure 34 shows a representative case for down range error, hr = 3 m, D = 7 km. No geometric dilution exists here except for an anomalous behavior close to the receiver.

The above results indicate that requirements for tracking the transmitter are not severe, and place relatively mild demands on auxiliary equipment.

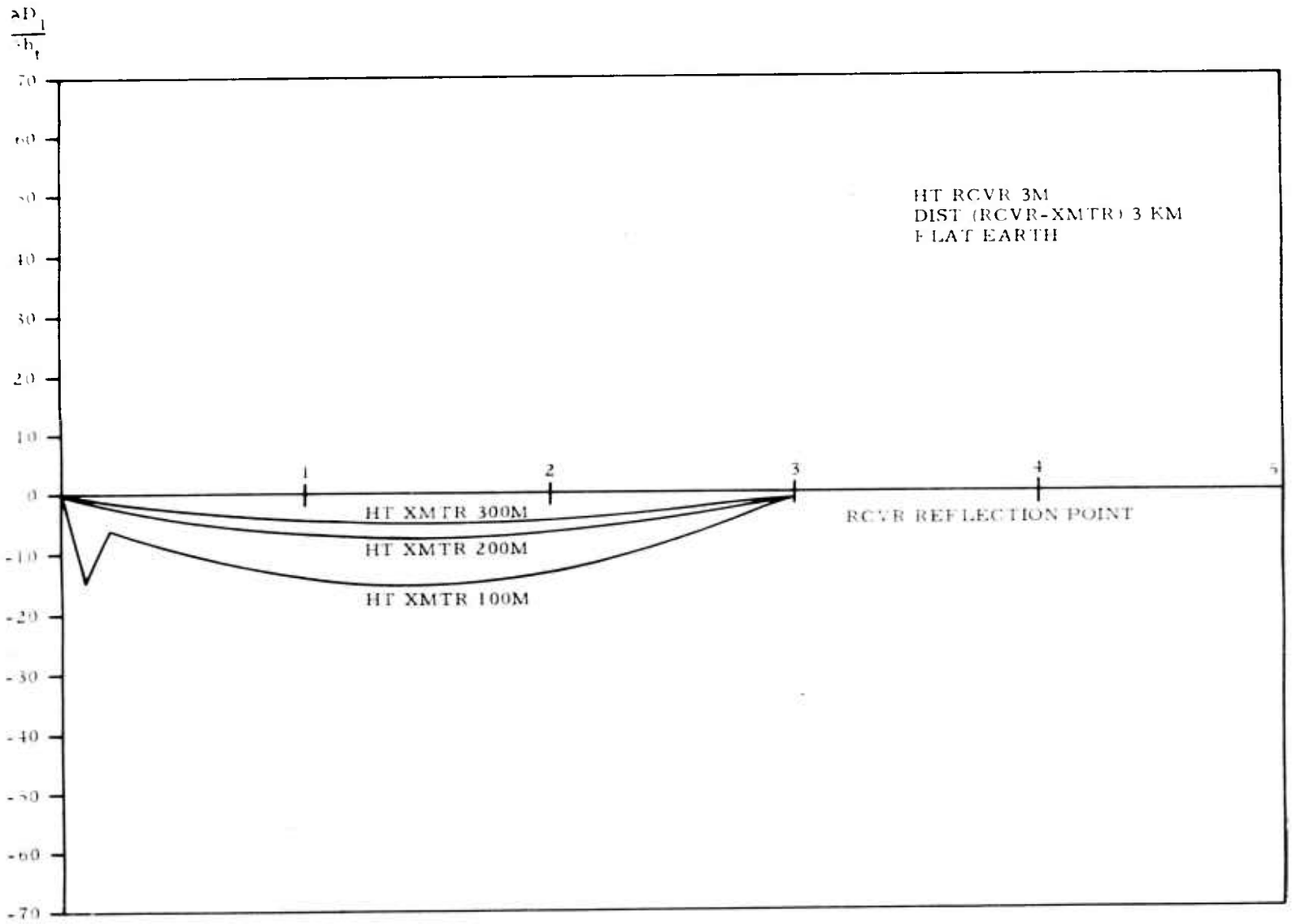

Figure 30. Elevation Error
(D = 3 km, h_r = 3m)

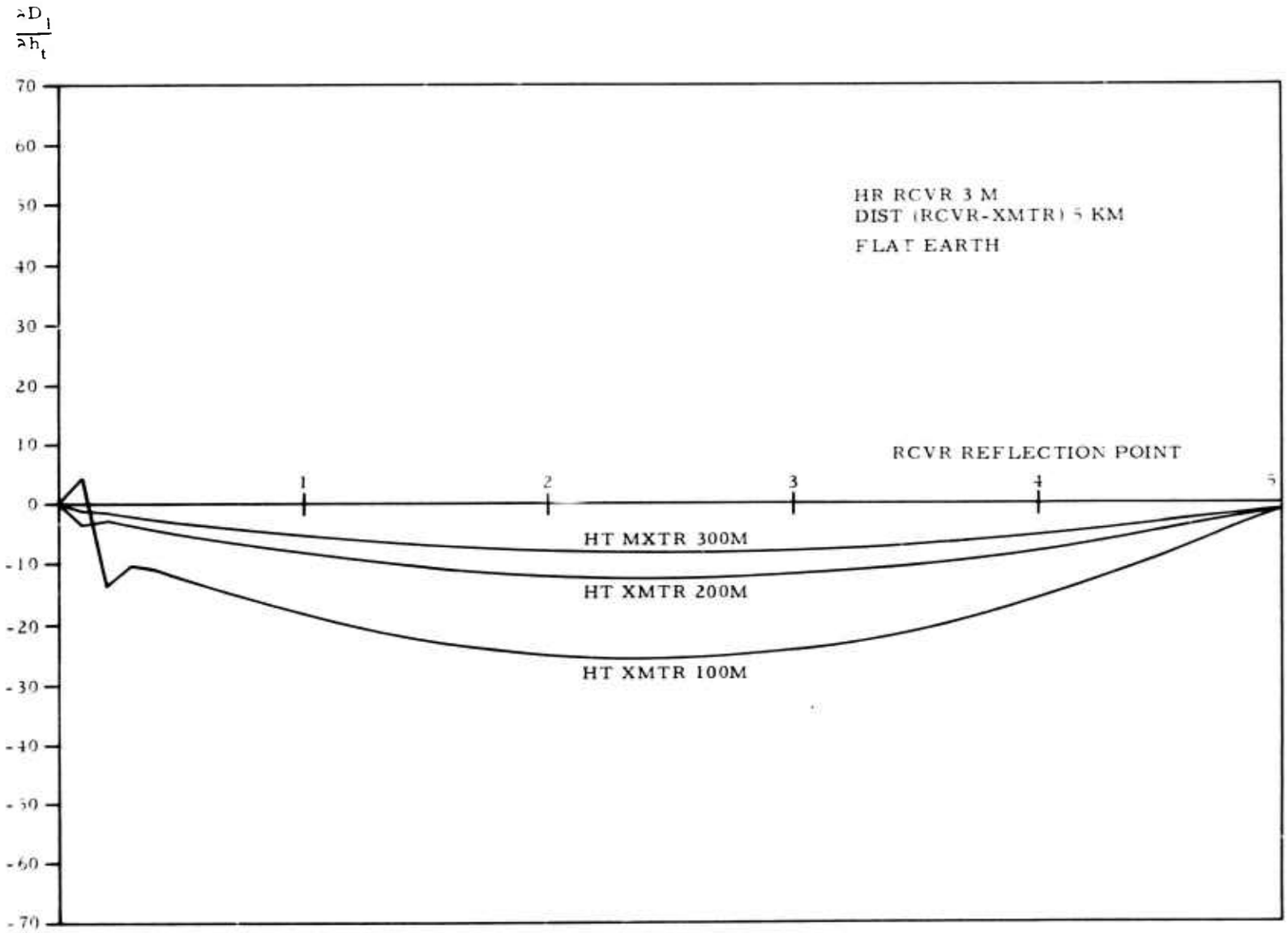

Figure 31. Elevation Error
($D = 5$ km, $h_r = 3$m)

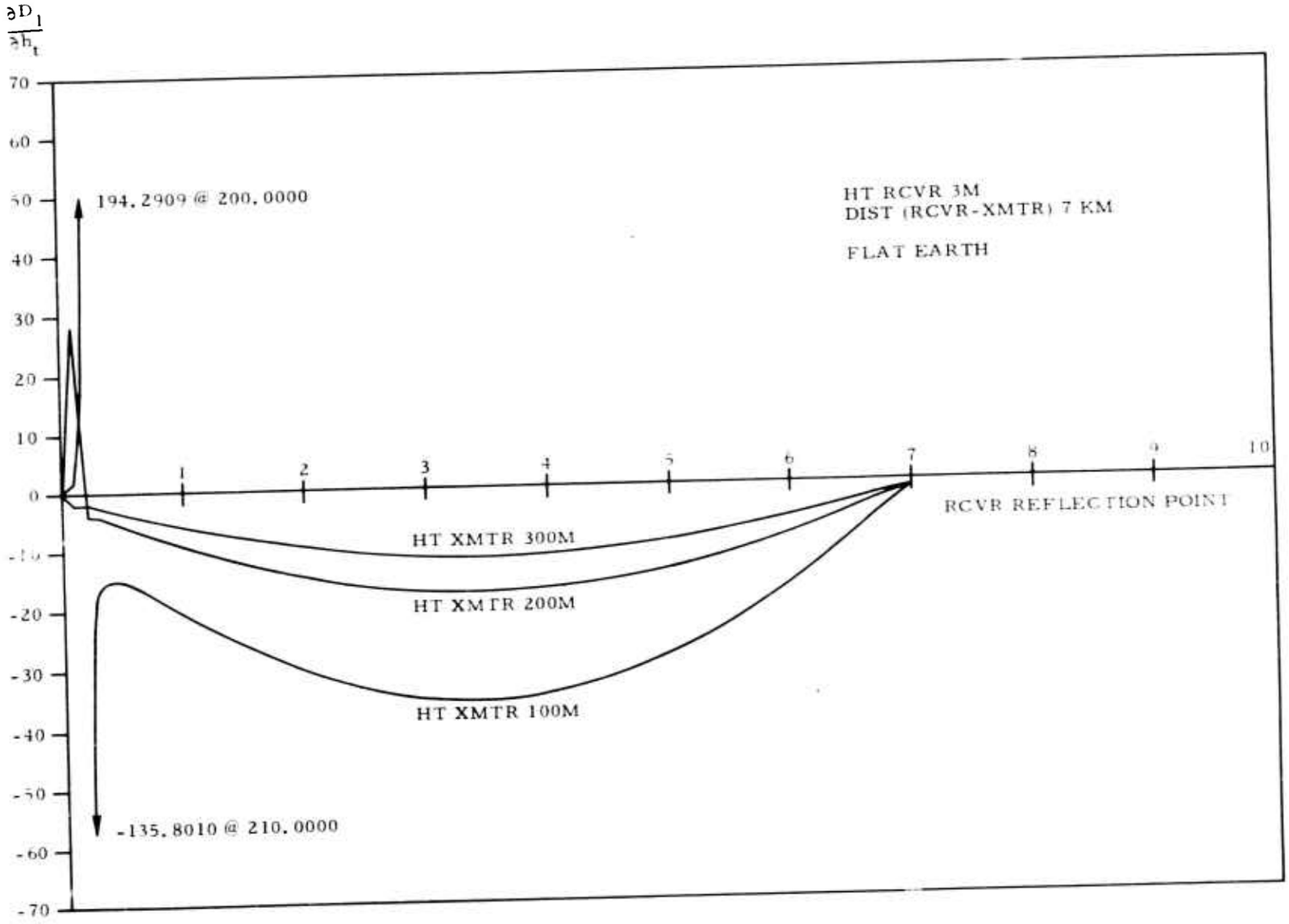

Figure 32. Elevation Error
($D = 7$ km, $h_r = 3$ m)

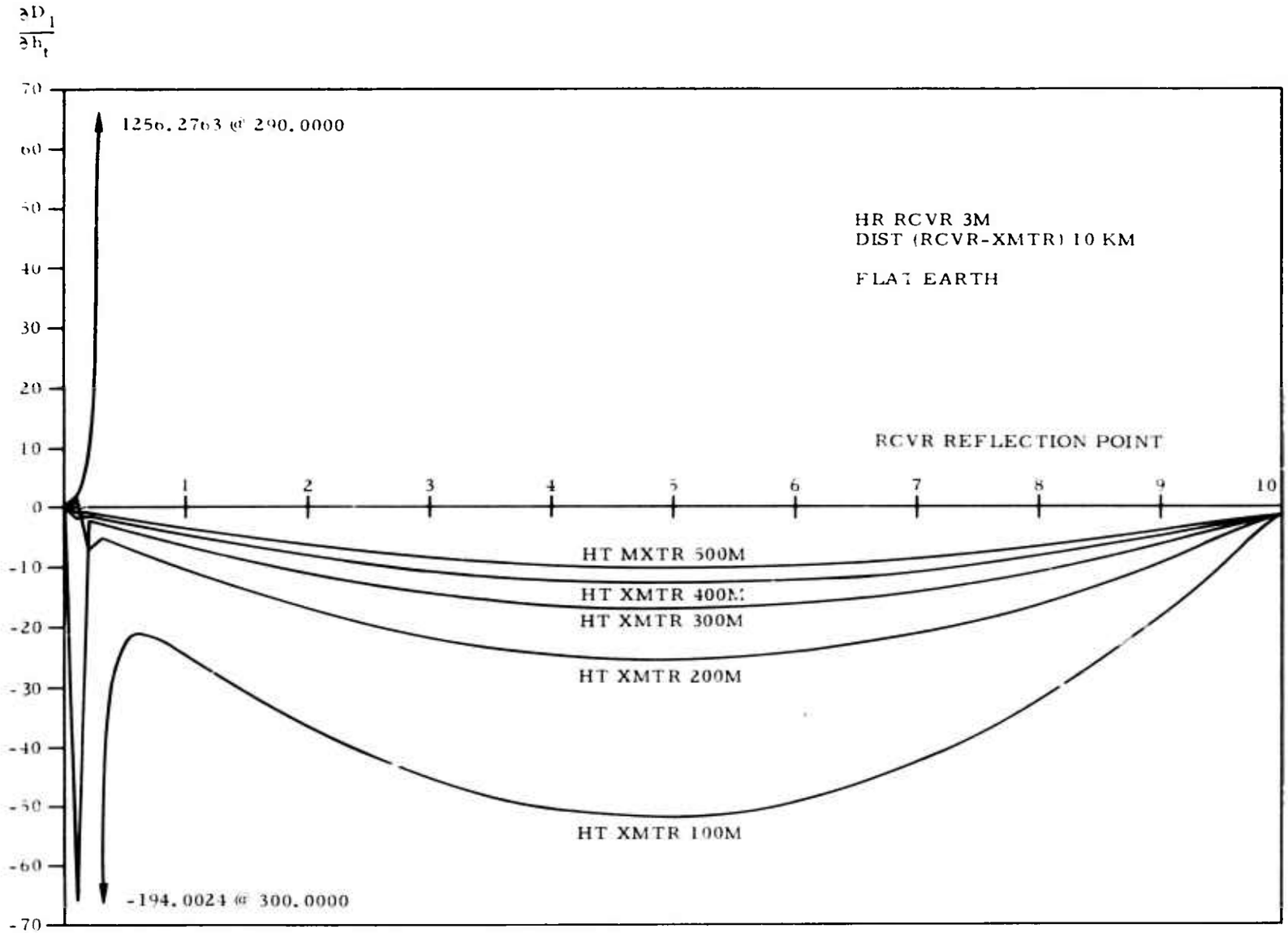

Figure 33. Elevation Error
(D = 10 km, h_r = 3 m)

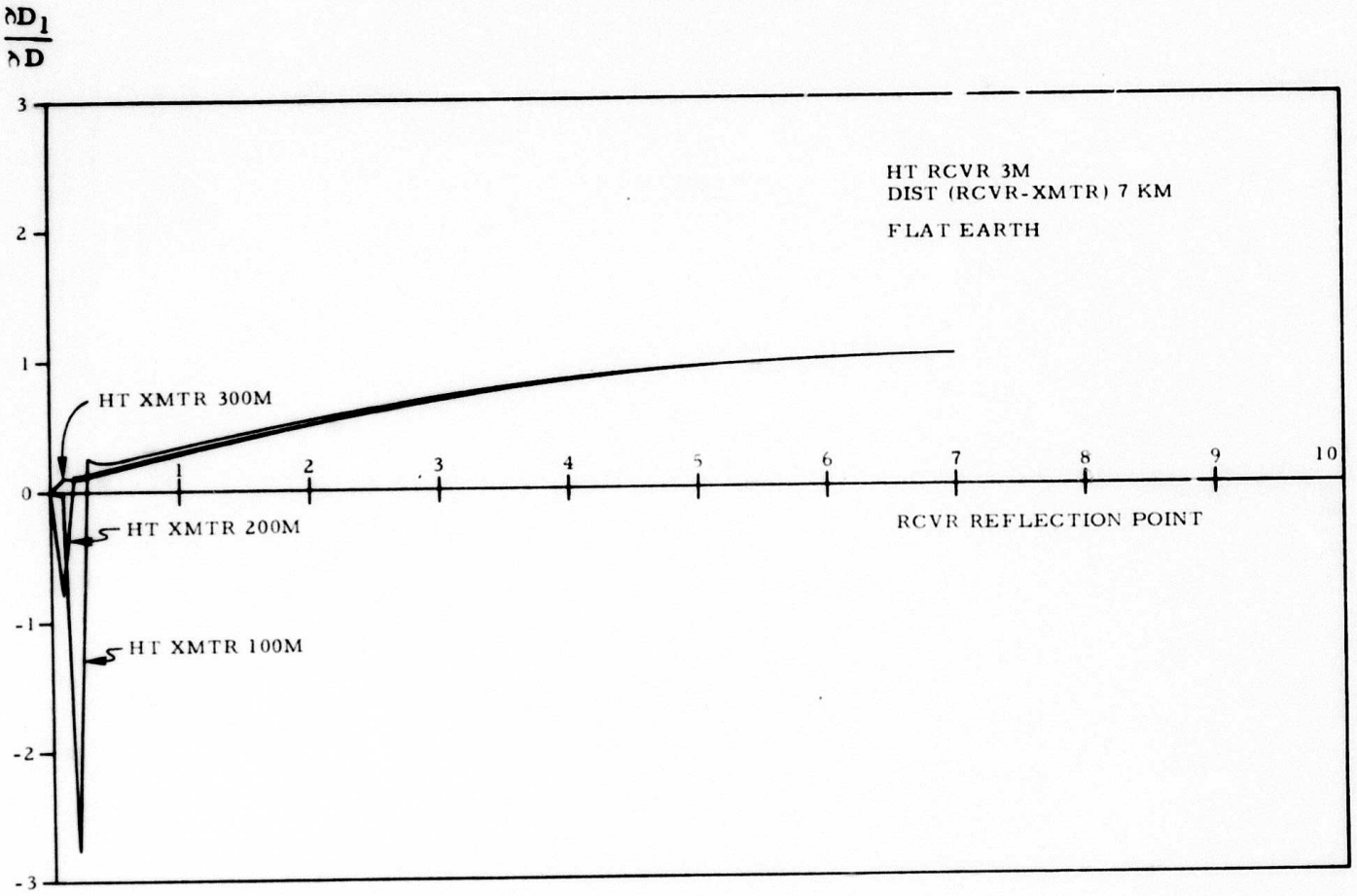

Figure 34. Down Range Error
(D = 7 km, h_r = 3 m)

3.2 Equipment

Measurements to provide an experimental basis for validating multipath theory will require a transmitter to be suspended at a height of from 50 to 600 meters above the earth, with an antenna having a beamwidth broad enough to illuminate an area which will include substantially all of the glistening surface, and a receiver with an antenna mounted three or four meters above the earth and having a narrow beam which can be directed to various parts of the glistening surface (see Figure 35). The received information will be processed for display, to permit immediate local monitoring, and will be converted to digital form and recorded for subsequent detailed analysis. (The transmitter and receiver could, of course, be interchanged, but this would entail airborne telemetry to return the received information to earth. Since the necessary transmitter power level (see Section 3.1) can be obtained from an LSI diode oscillator which, complete with modulator, power supply and battery, will weigh less than two pounds, the arrangement shown in Figure 35 is more practical.)

Means for suspending the transmitter are discussed in Section 3.2.4, below. A helicopter will be required in some situations; in others, a tethered balloon or kite may be used. The receiving antenna and its pedestal will be mounted on a vehicle which will be capable of traversing the various kinds of terrain to be measured, and which will have space inside for the receiving, processing, display, antenna control and accessory equipment, and for people to operate and observe the equipment. A separate small antenna will be provided for receiving the direct signal from the transmitter; this antenna may be mounted on the vehicle or on a tripod nearby.

3.2.1 Transmitter

Figure 36 is a block diagram of the transmitter. The power supply, modulator, and diode oscillator (shown enclosed in dotted lines) will be bought as a package, probably from Cayuga Associates.

Cayuga has developed LSA (Limited Space-charge Accumulation) solid-state diode oscillators capable of considerably higher peak power output than can be obtained from other solid-state microwave sources. They can presently provide, as a catalog item (CA-8000), an X-band source which has a peak power of 100 watts

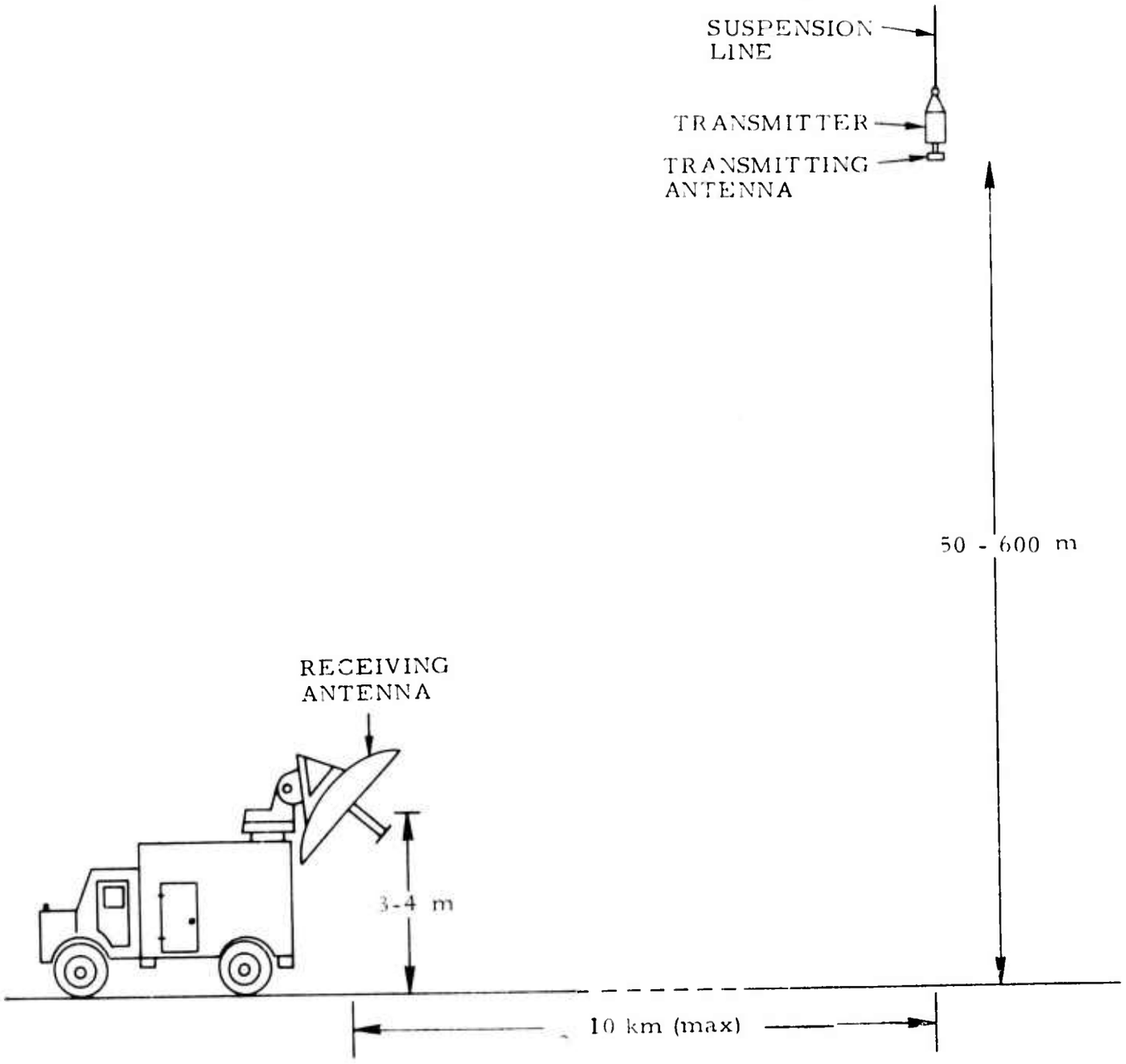

Figure 35. Measurement Configuration

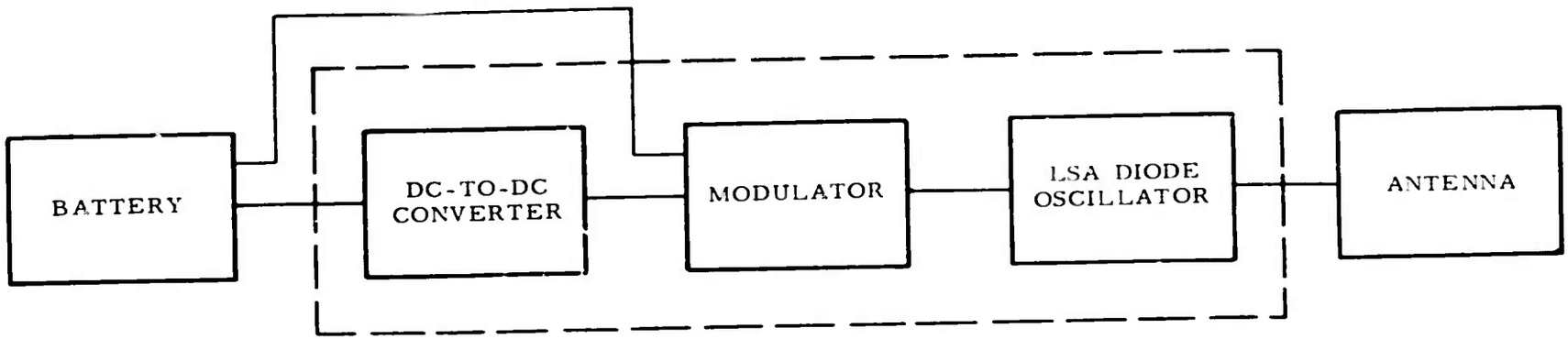

6 volts

6V to 150 V

40,000 PPS

Freq: 16 GHz
Pulse width: 1 ns
Peak power: 100 W
Rep. rate: 40 kHz

Total power consumption: 100 milliwatts

Weight (excluding battery and antenna): 12 ounces

Figure 36. Airborne (Transmitter) Electronics

and a pulse width of 2 nsec. They have made a short-pulse source at 14 GHz with 190 watts of peak power. They are confident that they can produce 100 watts at 16 GHz, with a pulsewidth at, or very close to, one nsec. They will provide, in a 12-ounce package, a Ku-band LSA oscillator, a solid-state modulator, and a DC-to-DC converter to supply 150 volts to the LSA diode. The input voltage can be 6 to 30 volts, at our option. We will probably choose 6 volts and use four alkaline "D" cells or two lithium cells for primary power.

3.2.2 Transmitting Antenna

It is desirable for the transmitting antenna to be omnidirectional horizontally so that the transmitter/antenna can be hung by a single line and permitted to rotate freely about a vertical axis. This necessarily entails having a vertical null in the radiation pattern; hence the ground directly below the antenna will not be illuminated. No special care in antenna design will be required, however, to keep the vertical null adequately narrow. In the first place, the diffuse reflection to the distant receiver from near-vertical incidence is expected to be too low to be detected even with full illumination. In the second place, since the transmitter height will be five to ten percent of the horizontal transmitter-to-receiver baseline distance, the null could have a half-width of 45° and ninety to ninety-five percent of the baseline would still be illuminated. Patterns for two simple antennas (Figures 38 and 39) show nulls with half-widths of 20° and 35° at the -3 dB points.

It may be of interest to run tests with both vertical and horizontal polarization. Figure 37 shows two suitable lightweight low cost printed-circuit antennas, which have been designed for S-band and can readily be scaled to Ku-band. Their vertical patterns are shown in Figures 38 and 39 . For illumination near the receiver, the elevation angle is about -1° to -5°, depending on transmitter height and distance. If the distance away from the receiver is limited to correspond to an elevation angle at the transmitter of -45°, as discussed above, then the total variation for the horizontal polarization pattern is less than 2 dB. The vertical polarization pattern is even better; it puts its maximum power near -45°, where the diffuse reflectivity should be weakest, and lets the power decrease for areas closer to the receiver. Similar patterns can probably be achieved for the triple dipole by putting a reflecting plane a quarter wavelength above it.

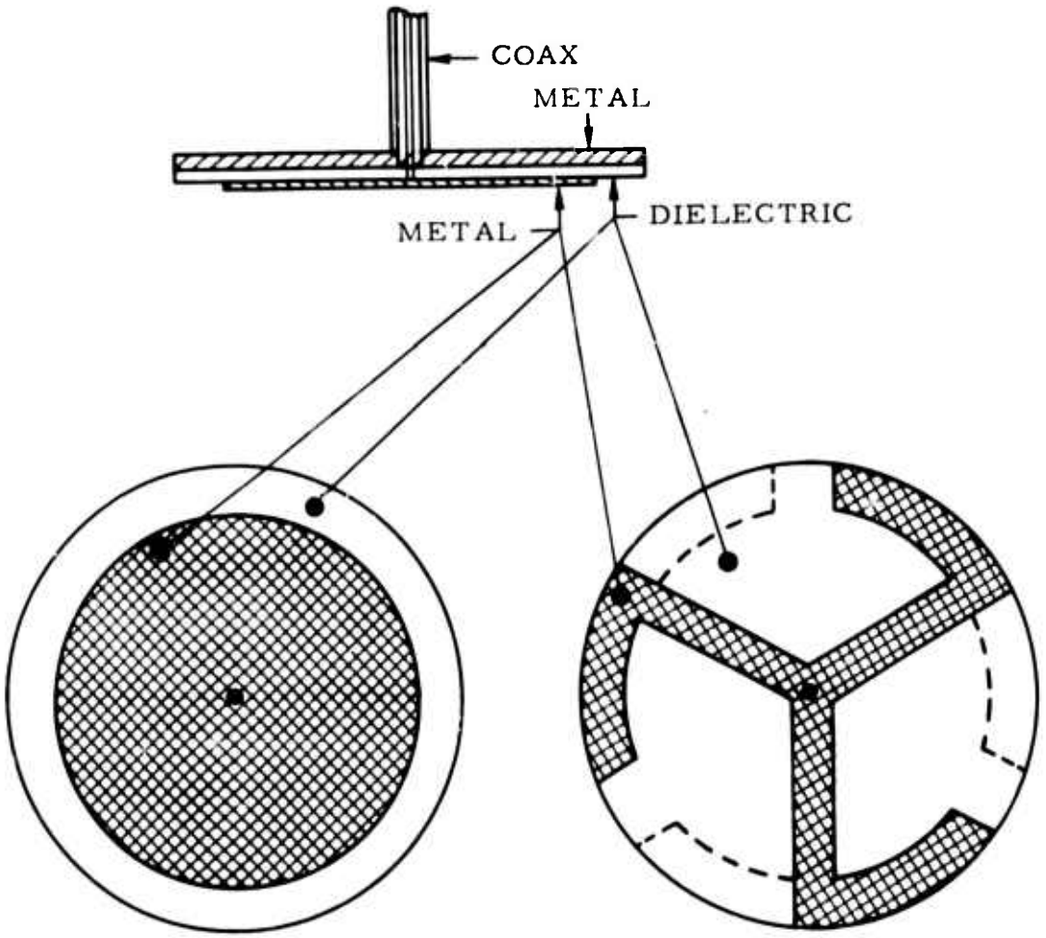

Figure 37. Printed Circuit Antennas

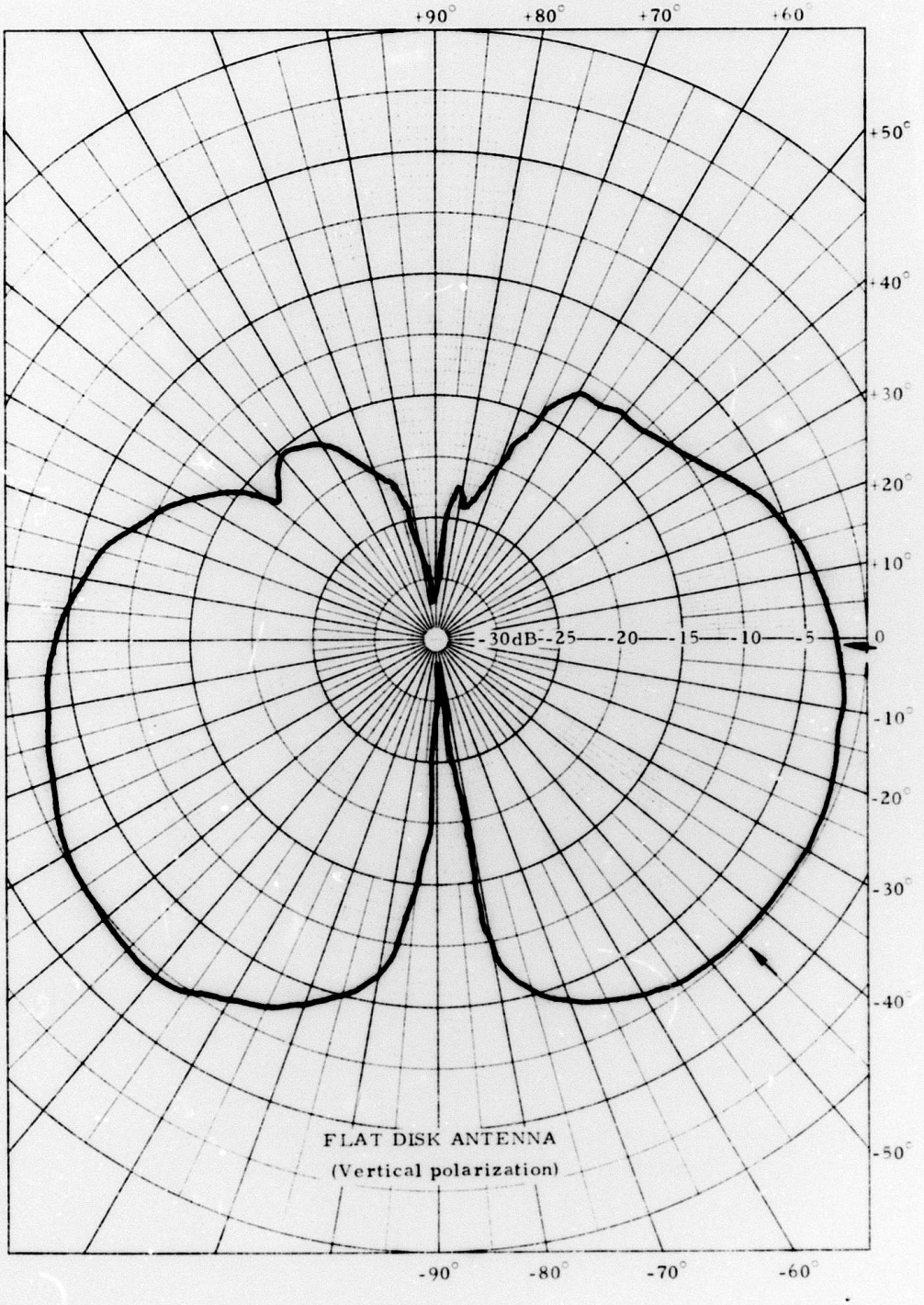

Figure 38. Flat Disk Antenna Pattern (Vertical Polarization)

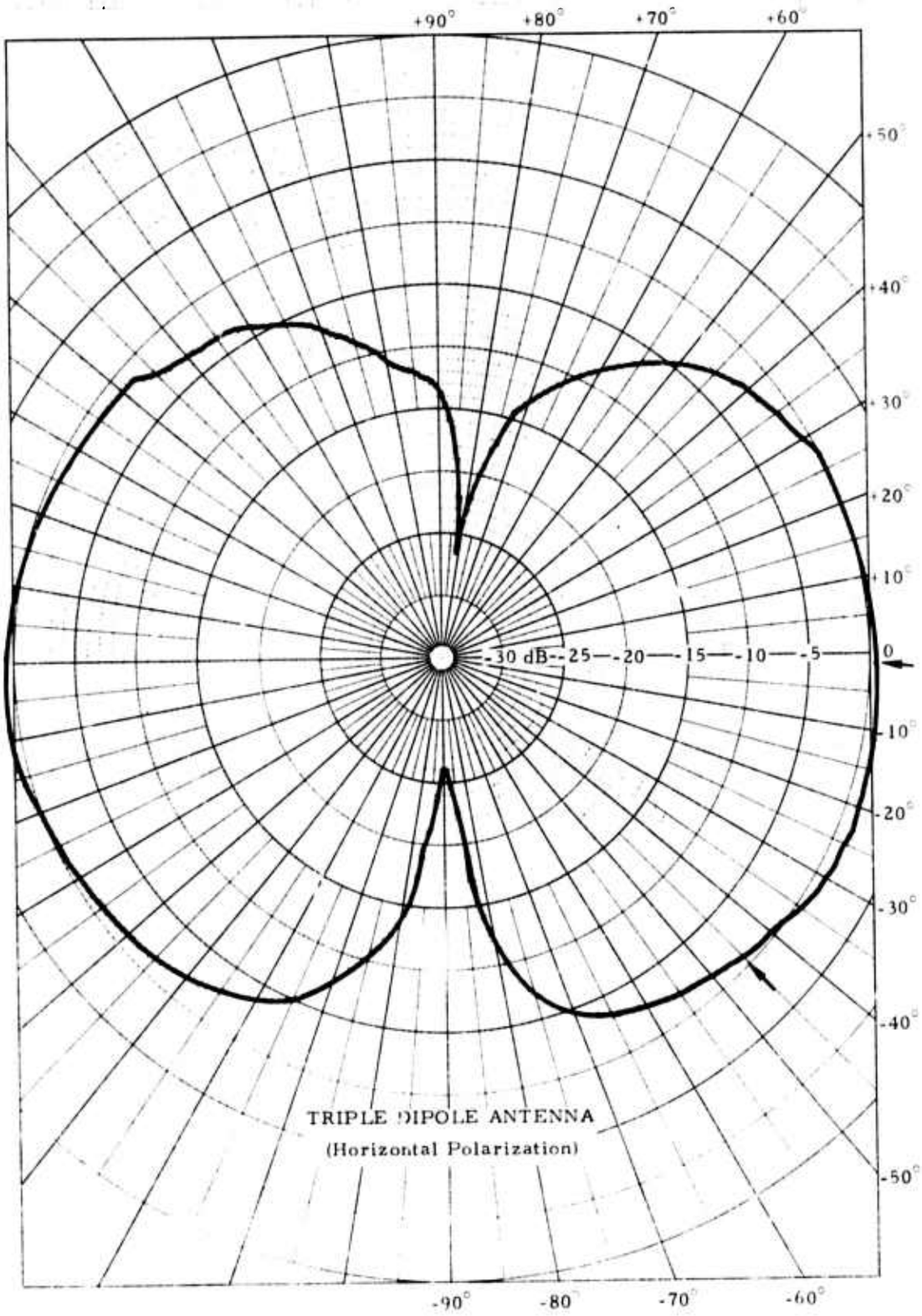

Figure 39. Triple Dipole Antenna Pattern
(Horizontal Polarization)

The transmitter/antenna assembly will be designed to hang vertically in the absence of wind. However, if it should sway in the wind so as to deviate from the vertical, the null would scan about the landscape accordingly. This can be minimized by attaching a long rod to the bottom of the assembly, extending downward for perhaps 50 to 100 cm. This rod may be made of a rigid plastic foam to minimize its effect on the antenna pattern. A lightweight line, twenty meters long or so, will be attached to the bottom of the rod, with a lead weight at the bottom end of the line. This will not only tend to keep the transmitter/antenna assembly vertical but will also be very useful when the assembly is being brought down at the end of a run of measurements. Whether the means of suspension is a helicopter, a balloon, or a parafoil or other kite, it is possible if there are uneven winds near the ground that the rate of descent will be erratic and at times perhaps faster than might be desired. The lead weight can thump against the ground without being damaged, and the line attached to it can then be used to guide the transmitter/antenna down and prevent it from striking the ground.

3.2.3 Ground Receiving Equipment

Figure 40 is a block diagram of the ground receiving equipment. Most of this equipment will be mounted inside a mobile vehicle. The main antenna and its pedestal will be mounted on the vehicle on the outside or possibly on a separate trailer or on a modified forklift. The auxiliary antenna will probably be mounted on a tripod which will be set up near the vehicle with the associated TWT amplifier and detector located close by, to minimize transmission line losses.

Main Receiving Antenna

The main receiving antenna, for receiving signals reflected from the terrain or ocean, will use a parabolic reflector about two and a half meters in diameter with a 133 cm focal length. It will have a half-power beamwidth at Ku-band of about half a degree. The reflector will probably be spun from quarter-inch thick aluminum and then machined to a tolerance of $\pm$ .25 mm rms. This is expected to weigh considerably less than a fiberglass panel reflector would, permitting the use of a smaller pedestal and making it easier to mount the entire assembly on a vehicle of reasonable size.

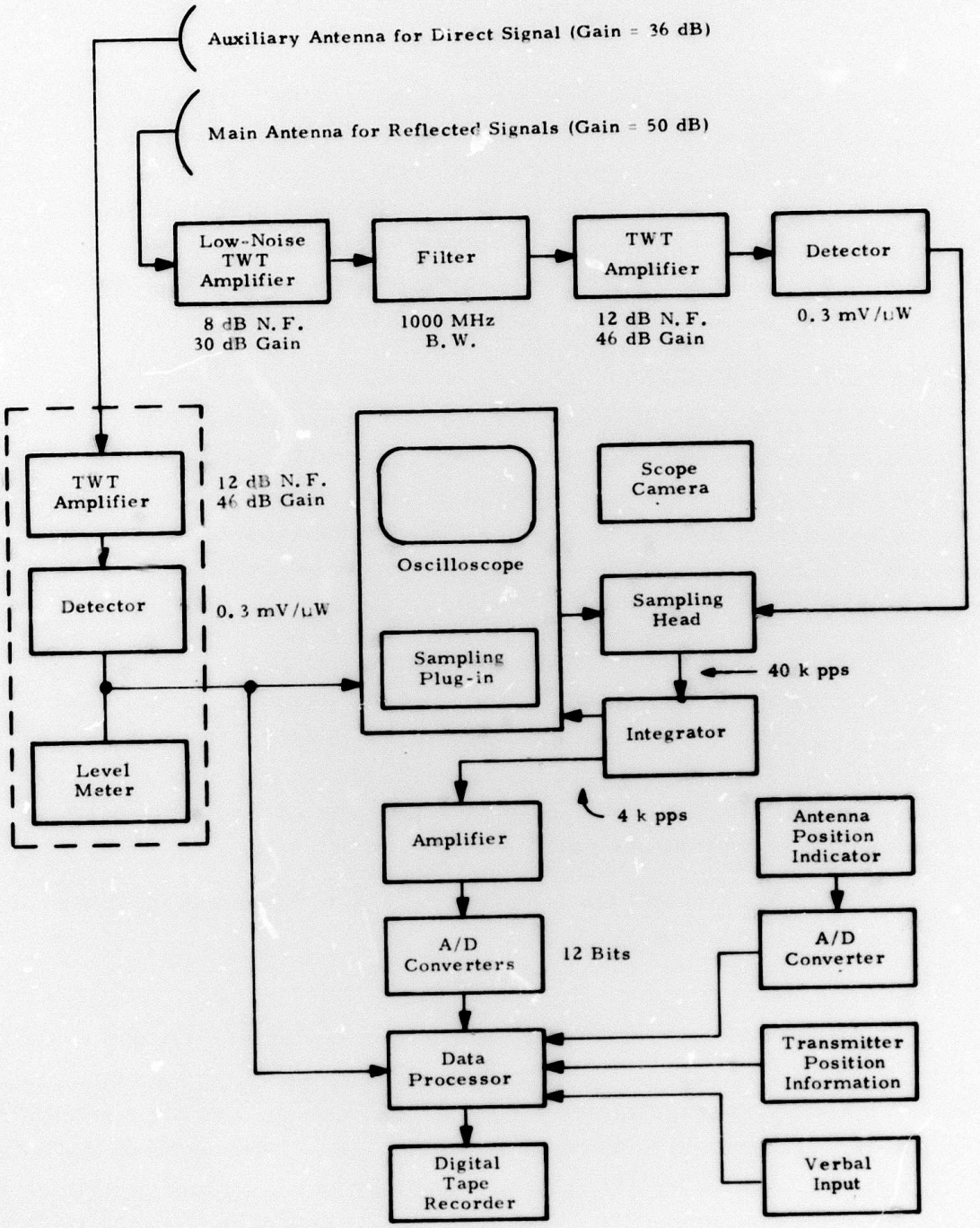

Figure 40. Ground Receiving Equipment

During the measurement of reflections from an entire glistening surface, the antenna will be required to move only a few degrees in azimuth and no more than 45^{o} in elevation. However, we will allow for 180^{o} or more of azimuth rotation so as to avoid having to align the vehicle with the transmitter/receiver baseline. We will probably avoid the use of rotary joints, either by using a length of flexible waveguide or by mounting the TWT preamplifier on the back of the reflector and using a length of flexible coax at the output of the preamplifier.

Ku-band Microwave Receiver

All of the gain required in the receiver will be provided directly at rf, rather than using a superheterodyne receiver. This will permit realization of the bandwidth necessary to take advantage of the resolution provided by the one nanosecond pulsewidth, with no difficulty. A bandpass filter in the reflected signal amplifier channel will restrict the bandwidth to match the pulse bandwidth, so as to maintain an acceptable noise figure.

Low-noise TWT preamplifiers and amplifiers having the characteristics indicated in Figure 40 are available from more than one source; the particular specifications given are for Watkins-Johnson tubes (the WJ-371 and the WJ-425-16, respectively, the former being optimized or selected for low noise at 16 GHz). The same high gain amplifier tube will be used in both the direct and reflected signal channels, permitting one spare tube to serve for both.

The filter, and probably the detectors, will be designed and fabricated at Raytheon's Wayland Laboratory.

Direct Signal Channel

The channel for receiving direct signals from the transmitter will consist of an auxiliary receiving antenna, a TWT amplifier, a detector, and a meter to indicate the relative level of the received signals. The antenna will use a small center-fed parabolic reflector, 40 to 45 cm in diameter. It may be mounted on the vehicle, with the other equipment inside, but it will probably be more convenient to mount it on a tripod outside the vehicle. The other equipment will be placed nearby, to minimize the length of transmission line between the antenna and the amplifier and to make the level meter conveniently usable as an aid in aiming the antenna. Since the antenna will have a beamwidth of about three degrees, there will be no difficulty in aiming it manually toward the transmitter.

Signal Reception

Figures affecting the signal-to-noise ratios and signal levels in the direct path and reflected path signal channels are tabulated below. The signal levels given are minimum levels, under the assumptions discussed in Section 3.1, above, for a transmitter-to-receiver distance of six kilometers.

	DIRECT PATH	REFLECTED PATH
Antenna diameter	45 cm	250 cm
Antenna gain	36 dB	50 dB
Assumed reflection loss	none	30 dB
Signal level at antenna	-46 dbm	-62 dbm
Transmission line loss	negligible	2 dB
Signal level at receiver	-46 dbm	-64 dbm
Bandwidth	1 GHz	1 GHz
KTB	-84 dbm	-84 dbm
Noise figure of receiver	12 dB	8 dB
Noise level	-72 dbm	-76 dbm
Signal-to-noise ratio	26 dB	12 dB
Total TWT amplifier gain	46 dB	76 dB
Filter loss	n/a	2 dB
Net gain	46 dB	74 dB
Signal level at detector	0 dbm	+10 dbm

If the detector in the direct path signal channel has a sensitivity of 0.3 mV/μW, the minimum trigger output will be 0.3 volt.

In the reflected path signal channel, video integration may be used to enhance the signal-to-noise ratio, particularly if interest develops in reflection losses greater than 30 dB or baseline distances greater than six kilometers.

The signal levels given above assume normal propagation through the atmosphere. Abnormal propagation conditions are discussed in Section 3.3.7.

Data Display and Recording

The direct signal from the transmitter will trigger the display oscilloscope and will serve as a zero time reference for the data processor, as shown in Figure 40. The signals reflected from the ground, delayed for various amounts of time according to the distance along the glistening surface, will appear as vertical deflections on the display. The receiver path geometry is shown in Figure 41: for a six kilometer baseline, a 300 meter transmitter height, and a 3 meter receiver height, the time difference between the direct and reflected signals varies from one nanosecond to one microsecond. A sketch of the corresponding display is shown at the bottom of Figure 41. Since the receiving antenna height is not very great, the specular reflection point (minimum time difference) is close to the receiver, well within the region where the receiving antenna elevation angle rather than the time difference is used for range resolution. For reflection points further from the receiver than the specular point, the time difference is a monotonically increasing, but highly non-linear function of distance. If the horizontal axis of the display is linear with time, the four tic marks shown on the display baseline in Figure 41 correspond to horizontal distances from the receiver of 1/2, 3/4, 7/8, and .95 of the total receiver-to-transmitter distance. Distances beyond the .95 point begin to fall into the illumination null of the transmitting antenna (see Section 3.2.2), so in practice, the region of the display to the right of the .95 mark will usually be eliminated and the rest expanded to fill the display. The display circuitry will be designed to give the operator the choice of making the horizontal axis linear with time or with distance.

A sampling system will be used, in order to permit the waveform out of the detector to be analyzed with one nanosecond resolution, with reasonable bandwidth requirements for the display and for the data digitizing and recording circuitry. A commercial oscilloscope, sampling plug-in, and sampling head will be bought, but the sampling plug-in will be modified to permit considerable flexibility in the sequence of sampling delay times and to allow a number of returns to be integrated, if desired, for improved signal-to-noise ratio.

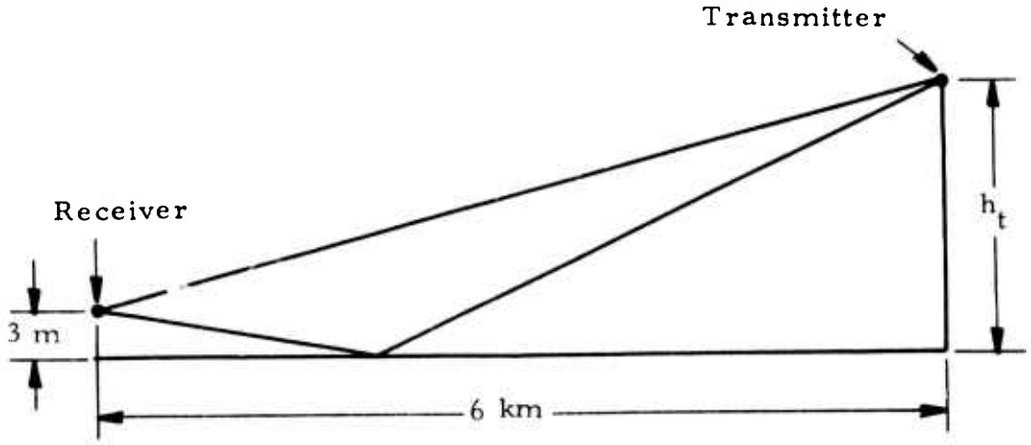

	METERS	
Transmitter Height (h_t)	300	600
Direct Path	6007.34625	6029.62760
Shortest (Specular) Reflected Path	6007.64589	6030.22462
Longest Reflected Path	6300.00075	6600.00075

1 nanosecond → 0.3 m (for one-way path)

RECEIVER PATH GEOMETRY

(Flat Earth)

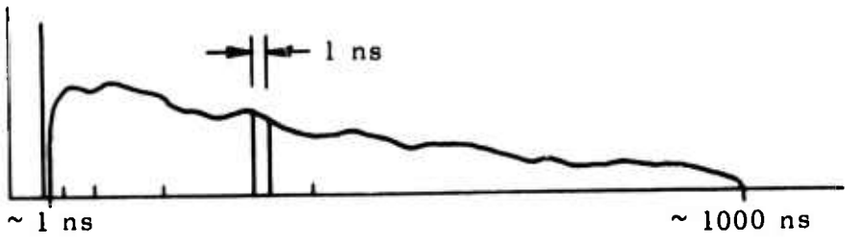

DISPLAY (h_t = 300 m)

Figure 41. Delay Geometry and Display

The amplifier, A/D converters, and digital tape recorder will be standard commercial items. The antenna azimuth and elevation position information may be generated in digital form directly, rather than using servos and A/D converters as indicated in Figure 40. Transmitter position information will be put in digitally or verbally (see Section 3.3.6), and a track will be provided for any verbal comments that may be useful during the subsequent analysis of the data. We will design a data processor to accept the various inputs and put them into suitable form for the tape recorder.

A more detailed discussion of the proposed data display and recording equipment is given in Appendix G.

3.2.4 Support for Transmitter

A number of means of supporting the transmitter at the required altitudes have been considered and investigated:

1. Towers, tall buildings
2. Helicopter
3. Tethered balloon
4. Kytoon
5. Kite
6. Tethered helicopter

Towers and Buildings

Towers and tall buildings could provide a very low cost support for the transmitter (assuming that appropriate arrangements could be made with the owners of suitable buildings) and the transmitter's position in space could be more firmly fixed and more readily determined than with any other kind of support. Measurements could be made day or night and in any reasonable conditions of wind or weather. However, the restriction on kinds of terrain to be measured to those in the vicinity of suitable buildings is so severe a limitation that little if any use will likely be made of this approach. (There is also the possibility that reflections from the building structure or from nearby buildings could cause unplanned multipath.)

Helicopter

A helicopter can be taken almost anywhere and can operate at any altitude we may require. Unlike balloons or kites, it requires no tether. This makes its use virtually mandatory when measurements are being taken at or near an airport, since it can respond quickly to a command from the control tower to clear the area; any tethered device at 600 meters would require several minutes to be brought down. When measurements of the ocean as a glistening surface are being made, the Stilwell process may be used to determine the state of the surface at the time (see Appendix F). Since this would require the use of a helicopter for taking aerial photographs, it may well prove feasible to use the same helicopter to support the transmitter.

The chief disadvantage of the use of a helicopter is its high cost - approximately $125 per hour over land and $200 per hour over water. Also, it is difficult for a helicopter to hover in one spot in space, though it can be done for a short time if the wind is steady and not too strong or too weak. It is possible, in theory, for a helicopter with a load hung at some distance below it to fly in a small circle at a constant speed in such a way that the load will remain near the vertex of a cone swept out by the line supporting it and will move in a much smaller circle than the helicopter. This maneuver is sensitive to the weight of the load, the length of the supporting line, the speed of the helicopter and the radius of the circle it flies, as well as ambient wind effects. There is little practical experience to indicate what success might be expected. If it turns out not to be practical to hold the transmitter fixed in space, an acceptable alternative is to fly it along slowly over a fixed visible reference point on the ground (or a boat at sea) keeping a constant altitude. Either the pilot or a ground observer at the reference point will communicate with the receiver site when the transmitter is directly above the reference point and a data run will be recorded at that time.

Use of a helicopter requires reliable two-way ground-to-air communications. Operation is not practical at night or during conditions of severe wind or weather, but these are probably not important limitations.

Tethered Balloon

A tethered balloon which depends on buoyancy alone for lift would have to be very large in order not to blow down in the winds that generally prevail at one or two thousand feet. Such a balloon would be expensive; it would require a crew of several people to handle it, and it would consume a large quantity of helium each time it was flown. FAA requirements for banners on the tether lines in daylight and lights at night would have to be observed. This approach can be considered to be ruled out unless some new considerations justify reconsidering it.

Kytoon

This is Dewey and Almy's company tradename for a small tethered balloon with an aerodynamic shape which depends on wind as well as buoyancy for developing lift. It is a low cost device and should be comparatively easy to store, inflate, launch and maneuver. It is just about small enough to be exempt from FAA requirements. It is launched with no payload; when it is up a few hundred feet and in a steady wind which gives it sufficient lift, the payload is attached to the tether and it is sent up until the payload is at the required height.

The "Kytoon" may be considered for possible use when there is a strong steady wind aloft but too little wind at ground level to launch a kite.

Kite

There are kites of advanced design, such as the Jalbert "Parafoil", which are capable of supporting loads considerably heavier than our transmitter/antenna, when there is a suitable wind. This is generally true at the altitudes at which we wish to operate. Enough wind at ground level to permit launching is required; a kite would be launched with no load and the load would be attached to the flying line when the kite was at a sufficient height to assure reliable lift. This is a very low cost device and might well be brought along for use in place of more expensive means, when conditions are right for it.

Tethered Helicopter

A small unmanned tethered helicopter should be able to provide a great deal more lift than a non-aerodynamic balloon, for a given horizontal cross-sectional

area, with considerably less bulk and presenting a much smaller profile to horizontal winds. In the winds that prevail aloft, it should be able to keep its tether line more nearly vertical than any balloon or kite can, possibly making it feasible to establish the location of the transmitter in space with sufficient accuracy merely by running the tether out through a footage counter from a known location on the ground. Presumably, the tether would comprise two insulated conductors to permit the rotor and the counter-rotation propeller to be electrically powered. Alternatively, it might prove feasible to use a liquid fuel motor, with the helicopter carrying enough fuel for an hour or so of operation, after which it would be brought down for refueling.

So far, insufficient information relative to this approach has been obtained to permit an evaluation of its practicality. It seems likely that there would be severe problems with aerodynamic and rotational stability.

Summary

A helicopter (with a pilot) will almost certainly be chosen to support the transmitter when measurements are being taken at airports. It will probably be used for ocean surface measurements as well. For making measurements over land and away from airports - particularly in remote areas - a parafoil or a Kytoon or even, in some cases, a parafoil hauled aloft by a Kytoon and then set free, would appear to offer a rather attractive, convenient and economical alternative to a helicopter as a means of flying the transmitter. It might turn out to be practical to use such a tethered device, flown from a boat, for ocean measurements as well.

3.2.5 Receiving Equipment Vehicle(s)

The vehicle(s) for housing and transporting the receiving equipment should be capable of being driven over many kinds of terrain. A particular problem is operation on a sandy beach for low-sited ocean surface measurements. During measurements the main receiving antenna (2 1/2 meters in diameter) must be supported with its center three or four meters above the ground. In transit it should be possible to negotiate any underpass that is likely to be encountered. A rather expensive solution to these difficult problems was found some years ago when the AN/MPS-34 was designed and built. This is a semi-trailer van with top panels near the rear which fold back and a pedestal on an elevator mechanism to which a

CPS-9 weather radar antenna was mounted, so that it could be raised for operation and lowered for transit. Three of these vans were built and equipped. They are government property and are presently at White Sands; although it appears that one of them might readily be made available for use in the multipath program, it is much larger than would actually be needed and it is doubtful that it could be satisfactorily adapted for this project. Other possibilities are a military six-by-six (GFE) with a suitable body added, or a large commercial van or truck, probably with four-wheel drive. Adding an antenna erection mechanism to such a vehicle appears to pose a number of problems, particularly in relation to stability on the road and during operation.

An alternative to a single vehicle is the use of separate vehicles for housing and operating the equipment and for transporting and erecting the antenna. The latter could be a low trailer - perhaps a modified large boat trailer - with a mast upon which the antenna and its pedestal would be swung up and down about a horizontal pivot, or it could be a large forklift, with a bracket for the antenna pedestal replacing the fork, which would move the antenna up and down along a straight vertical line of motion. The forklift would be mechanically independent of the equipment vehicle, permitting the latter to be a lightweight van or four-wheel drive station wagon. For long distance highway transit, the forklift would have to be hauled on a low trailer, but once at a selected site, it would permit moving the antenna about with maximum mobility and minimum risk from one location to another, to take advantage of the varieties of terrain and sighting angles which might be available in the vicinity. Because of its weight, the forklift would minimize the need for sway braces or guying cables. For operation on a beach, however, it would probably require that mats be laid down for it to run on.

The various possibilities will be evaluated in detail early in Phase II to permit timely specification and procurement of suitable vehicles.

3.2.6 Miscellaneous Accessory Equipment

A number of pieces of accessory equipment will be required. These include:

1. Equipment for communication among the receiving site, a reference point below the transmitter, a helicopter, an airport control tower, and a horizon check point, as required.

2. Equipment for establishing the location in space of the transmitter. (See Section 3.3.6)

3. Equipment for checking the refractive index of the air. (See Section 3.3.7)

4. Helium tanks, pressure regulator, valves, etc., if a lighter-than-air device is used.

5. Motor-generator set for operation away from public power.

3.3 Measurement Approach

Ideally, initial measurements would be made over a section of terrain three to eight kilometers long and smooth within a quarter wavelength. (At Ku-band this corresponds to a surface roughness not exceeding about half a centimeter. Cement or asphalt probably qualify but it is doubtful that anything in nature does*; large bodies of water, for instance, have waves.) Following that, measurements would be made over similar uniform expanses having graded degrees of roughness, for which accurate theoretical predictions could be made. If analysis of this experimental data gave results which generally conformed to theory (e.g., the width of the glistening surface increasing with increasing roughness as predicted, etc.) this would provide a basis for confidence that subsequent measurements of more complicated terrain could provide new information not readily derived from existing theory. The theory might then be refined and extended, and new predictions made, to be tested by further measurements. Thus a body of knowledge would be built up for use by designers and users of future radar systems.

In practice, such a range of ideal terrain may not be available. For the initial measurement, however, airport runways approach the ideal for smoothness and for overall flatness. Our measurements could hardly be carried out at a busy airport because of intolerable mutual interference between our activities and the activities incident to normal airport operation. There are, however, two former Air Force bases, Otis Field and Westover Field, which are within a two hour drive of Raytheon's Wayland Laboratory and where the current level of activity (Air National Guard, Coast Guard, etc.) is such as to permit considerable periods of time in which measurements can be taken.

*For a possible exception, see Section 3.3.5.

We have visited both of these bases, to assess the suitability of the runways and of the adjacent terrain for our measurements and to make initial contacts with the officers in charge of flight activities. We also visited the Race Point Coast Guard Station, near Provincetown, Mass., with a view to using the adjacent beach for an ocean surface measurement with a low sited receiver and then going to a nearby cliff at Highland Light in North Truro for an ocean measurement with a high sited receiver. Our reception, on all of these visits, was cordial and cooperative. Considerable interest was shown in our proposed experiments, particularly as they ultimately relate to air safety (GCA, etc.).

3.3.1 Power Level Calibration

For all measurements regardless of terrain complexity or sea conditions, accurate calibration of received power level is very important. Measured power level will be referenced to the direct path signal by pointing the receiving antenna at the source before the start of the measurement series and periodically between sequences.

To obtain a calibration power level measurement, the antenna will be pointed at the source and manually adjusted in elevation and azimuth until maximum pulse power is received. The received power level will be recorded or an attenuator will be set so that the receiver output is at a predetermined reference value.

Next the antenna will be positioned to the elevation desired for the measurement sequences and reflected pulse amplitude levels recorded as a function of time as discussed in Section 3.2 .

Since several factors can change the calibration level, such as variations in transmitter output power, drift of transmitter position, and changes in transmitting antenna orientation due to wind, frequent calibration checks may be necessary. Therefore, at the first measurement site, particular attention will be paid to evaluating the frequency of calibration checks needed. It may be that conditions will normally be stable enough to require only infrequent calibration. Should the opposite be true, however, the equipment will be capable of performing power calibration before each measurement series. Since each series will require only a few seconds to complete, maintenance of adequate calibration over such a sequence should be easy to guarantee.

3.3.2 Terrain Measurements

The longest stretches of pavement at the air bases (including the working runways themselves and the paved overrun areas at either end) are about 2.9 km at Otis and about 4.1 km at Westover. Adjacent to the runways at both Otis and Westover, there are areas of mowed field grass which are nearly as flat (though not as smooth) as the runways themselves and which extend over a somewhat greater clear distance -- about 3.7 km at Otis and about 4.8 km at Westover. With proper scheduling, it should be possible to make measurements of a grassy area before and after mowing, to show the effect of varying the vegetation factor.

We expect to start measurements in the Spring of 1975, as soon as the snow is gone. Hence, although Westover offers the possibility of longer maximum baseline distances, the first measurements will probably be made at Otis where, because of its proximity to the ocean, it will likely be free of snow long before Westover is. The generally milder weather at Otis will be helpful during the time when we are becoming accustomed to using the equipment in the field and are developing the skills required for rapid and effective deployment and operation. After Otis, we will make measurements at Westover, and then at a number of other locations, offering terrain of increasing complexity.

If it is feasible to plan return visits to Westover during the winter of 1975-76 on a flexible, fast-response basis, it might be possible to obtain measurements of a long flat expanse of new-fallen snow of various depths, before the plows arrive.

3.3.3 Physical Description of Terrain

In order to correlate the Ku-band measurements with the actual physical features of any terrain over which measurements are taken, it will be necessary to acquire independent information on the physical configuration of the terrain. Information on existing maps is inadequate (e.g., elevation contours at ten foot intervals) and, in some cases, out of date. We will rely, for the most part, on aerial photogrammetric surveys, which can be produced by Raytheon Equipment Division's Autometric Operation -- conveniently located at our Wayland Laboratory. The output of such a survey will be a set of photomaps,

rectified for accurate location of details horizontally with superimposed elevation contours at one foot intervals. This information may be supplemented, in some cases, by information acquired at ground level (e.g., inclinometer readings at certain locations, verbal descriptions of vegetation, etc). A description of the photogrammetric survey process is given in Appendix D.

3.3.4 Ocean Surface Measurements

Measurements of reflectivity from the surface of the ocean under conditions ranging from calm to stormy will be of interest. These will be taken in much the same way as terrestrial measurements, with the transmitter taken aloft by a helicoptor or a tethered lifting device at a suitable baseline distance out over the ocean and the receiver set up on the beach or, for a high sited measurement, on a cliff overlooking the ocean. If a tethered device is used to fly the transmitter, a boat will be required; if a helicopter is used, a boat may still be needed to give the helicopter pilot a visible point of reference to fly or hover over, and perhaps to serve as an observation post for transmitter location measurements (see Section 3.3.6).

3.3.5 Physical Description of Ocean Surface

Independent information on the physical configuration of the ocean surface when the reflectivity measurement is being taken can be obtained in a number of ways. The Joint North Sea Wave Project (JONSWAP) in which Raytheon Equipment Division's Advanced Development Laboratory is participating, has brought to bear on this problem a number of diverse techniques (four-frequency radar, laser profilometer, aerial photographs analyzed by the Stilwell process[1], aerial stereo photographs, underwater laser sensors, waverider buoys, pitch and roll buoys, underwater pressure sensors, wave staff arrays, white cap density analysis[2] etc.)[3]. A joint JPL/Univ. of Miami/Raytheon air-sea interaction experiment, planned for this fall, and a third JONSWAP effort, to be

---

1 See References 6 and 8, Appendix F

2 See Reference 7

3 Brief summary treatments of several of these techniques are given in Reference 5

mounted in the Summer of 1975, may provide further information of interest to us; meanwhile, we have concluded on the basis of information presently available that the Stilwell process can provide more useful information more economically than any other approach.

The Stilwell process is the only means by which information for the entire glistening surface can be obtained instantaneously (by taking a single photograph from a height of 20,000-30,000 feet). Since most of the Ku-band data (for a single azimuth position) can be taken in less than a millisecond, this permits a direct comparison, assuming that a radio link can provide suitable synchronization and that an independent means of flying the transmitter is available. Only the low-frequency (gravity) waves can be analyzed from such a long range photograph. A statistical evaluation of the fine structure of the high-frequency (capillary) waves can be obtained from a series of overlapping photographs taken at a much lower altitude and this will permit comparison with a statistical analysis of a number of runs of Ku-band data.

Our Advanced Development Laboratory's Electro-optics Department can make available the laser and optical bench equipment and the engineering assistance needed to make Fourier transform transparencies from the sea surface photographs, as required for the Stilwell process. Autometrics can scan the transparencies, using a microdensitometer, and store the digitized output on magnetic tape for subsequent data analysis. For selected cases, the original sea photo transparencies can be similarly scanned and the resulting digital output processed through an FFT (fast Fourier transform) computer code for direct comparison with the optical transform results.

For best results with the Stilwell process, photographs should be made early in the morning looking toward the west or late in the afternoon looking toward the east. Near the tip of Cape Cod in Massachusetts, it is possible to find beaches in close proximity which provide views over long uninterrupted expanses of ocean looking either east or west. Hence, this is an ideal area for initial ocean measurements.

When the ocean surface is too rough for effective use of the Stilwell process, other, less accurate, means of describing it will have to be used, such as white-cap density, wave height estimates by experienced observers, etc.

3.3.6 Saltmarsh Measurements

Located conveniently close to the sites selected for ocean surface measurements (e.g., between Herring Cove and Race Point in Provincetown) broad expanses of saltmarsh may be found. Such an area provides unique measurement possibilities. At high tide, it may be rather like open water, with very little vegetation protruding above the surface. The marsh grass below the surface, however, suppresses waves and makes the surface smoother than a similar expanse of open water would be. At low tide, it may look rather like a field of grass, but with the mud beneath providing a wide range of moisture content over a relatively short period of time. On solid land, measurements of a given area with a full range of vegetation heights may require repeated visits over a period of several months; in a tidal marsh the full range of effective vegetation heights recurs in twelve and half hours cycles.

3.3.7 Transmitter Location Measurements

Transmitter location accuracy requirements are discussed in Section 3.1.4. The errors in locating a ground reflection point which result from errors in measuring the transmitter location vertically or horizontally (longitudinally toward or away from the receiver or transversely) are a function of the range of the reflection point from the receiver. For a reflection point directly below the transmitter, the ratio between the error in reflection point location (longitudinally or transversely) and the corresponding horizontal error in transmitter location is unity; for reflection points closer to the receiver, the error in reflection point decreases--linearly for transverse errors and in accordance with the curve shown in Figure 34 for longitudinal errors.

However, for vertical errors in transmitter location, there is a longitudinal error in reflection point which is quite small directly below the transmitter and increases to a maximum near the midpoint of the baseline, as shown in Figures 30 through 33. If the elevation angle of the transmitter as seen from the receiver site is limited to no less than one degree, then the ratio of longitudinal reflection point error to vertical transmitter location error will not exceed about 30.

It follows that horizontal errors in transmitter location of 50 or even 100 meters are quite tolerable, but the vertical location should be correct within three or four meters. If the transmitter is suspended from a helicopter, the pilot can determine his altitude with a surveying altimeter (set to zero at ground level) to within about one meter and the length of the line between the helicopter and the transmitter can be accurately known. If a balloon or kite is used, it may prove practical to release the tether through a mechanical measuring device (footage counter) and correct for tether angle as seen by an observer looking transverse to the wind direction.

Commercial theodolites have more than adequate angular accuracy to determine the azimuth angle and the height (given the distance) of the transmitter from the receiver site. Two theodolites with a suitable separation could determine the transmitter location completely, if independent distance information were lacking. Raytheon's Special Microwave Devices Operation can supply a laser distance measuring device on a mount with digital distance and angular axis position readouts, which permit the location of the transmitter to be completely determined from a single location with a single instrument. Much less expensively, a theodolite and an electronic distance measuring device can be used alternately on the same mount to give complete information from a single location.

Although the angular accuracy of available devices is adequate to permit them to determine the transmitter's location by manually tracking it from the receiver site, it may be difficult, at the maximum ranges contemplated, to initially locate the transmitter in the field of view. The procedure then would be to establish observation stations at one or two locations on the baseline fairly close to the transmitter. Position data would be given to an operator at the receiver site by radio and he would digitize it manually, using thumbswitches, for processing and recording.

3.3.8 Propagation Anomalies

Under normal undisturbed conditions, there is a single unique direct signal path and each reflected signal path involves a single reflection from the ground or ocean surface (or, at least, no multiple reflections from widely separated areas). These signal paths deviate from straight lines only by the slight curvature which results from the normal vertical gradient of the atmospheric index of refraction. This curvature has the effect of extending the microwave horizon beyond the geometric horizon as if the effective radius of the earth were greater than its actual radius; a commonly used model assumes a four/thirds earth radius, and that was the model used in the calculations in Section 3.1.

However, there are known to be propagation anomalies (fading, ducting, scintillation, etc.) under conditions associated with irregular tropospheric gradients of index of refraction.* Such disturbances are more likely to occur near the ocean than far inland. Under extreme conditions, they could result in fading of the direct or reflected signals, in more than one "direct" signal, or in spurious multiple reflected signals. Under less extreme conditions, they could still change the curvature of the propagation paths sufficiently to markedly modify the position of the microwave horizon and to cause errors in the reflection points associated with the measured time differences between direct and reflected signal paths. An example is given in Appendix E, in which it appears that a disturbance, sufficient to affect the microwave horizon drastically, produced reflection point range errors of less than 50 meters.

For the relatively short signal paths and low altitudes involved in the proposed reflectivity measurements, disturbances which might cause serious reflection point errors are not expected to occur often. Three things will be done to detect such conditions if and when they do occur:

1. When the main antenna is pointed directly at the transmitter to establish a reference signal level, it will be held in that position long enough to permit observation of any fluctuations which might indicate shifting tropospheric disturbances. When it is pointed down to receive reflected signals, the level of the direct signal received by the auxiliary antenna will be similarly monitored.
2. Equipment (e.g., similar to that used in a radiosonde) for determining the approximate index of refraction of the air at ground level

* For further discussion of these anomalies, see References 9, 10, 11, and 12.

will be used to check for fluctuations. So long as there is any wind at ground level, variations of refractive index in space are likely to appear as variations with time at a fixed location.

3. Before measurements are taken, where the terrain permits, the transmitter will be carried away from the receiver in a vehicle or boat to determine the distance to the microwave horizon.* Deviations from the normal distance will indicate abnormal refractive index gradients.

If severely abnormal conditions are observed, measurements will not be taken. Moderate disturbances will be noted and taken into consideration when interpreting the data. Disturbances not detected by the techniques described above will be an undifferentiated part of the statistical variation which will characterize all of the measured data.

* If the transmitter were at ground or sea level, there would be too much sensitivity to terrain irregularities or nearby waves. Actually, the transmitter will be taken well beyond the horizon and then raised and lowered through a range of a few meters to determine the height at which the signal at the receiver appears and disappears. Given the receiver antenna height and the receiver-to-transmitter distance, the effective horizon distance can then be determined.

3.4 Data Analysis

Introduction

The experimental data taken at each site will ultimately yield mean power curves in decibels below the direct return as a function of delay time, also measured with respect to the direct path. At each site these power curves will be generated for different receive beam positions, and mean scattered power will be measured from the resolution cells formed by the intersections along the ground of the narrow ($\sim .5^{o}$) beam (for azimuth resolution) and the narrow ($\sim$1 ns) pulse (for range resolution, except at very close ranges, where the $.5^{o}$ beam provides better range resolution). Typical beam depression angles and main beam coverage diagrams are shown in Figure 42 for a receiver height of 4 meters. As seen from this figure, poor range resolution is obtained from beam positioning alone for depression angles less than about $.5^{o}$ since, for such angles, the narrow beam illuminates a sizeable portion of the terrain between the source and the receiver. A 1-ns pulse transmitter on the other hand, if used as the source, will, in conjunction with the narrow receive beam, provide the necessary resolution within the ground coverage of the beam.

The computer simulation (Section 4) has a measurement mode which was designed to simulate the experiment and calculates mean power curves (also in decibels below the direct return) as a function of delay time, using the most recent developments in the multipath theory (Section 2 and Appendix C). Efficient data analysis techniques will be needed to compare the calculated data (curves) with the measured data for the purpose of:

1. Refining and validating the existing multipath theory
2. Measuring the spatial distributions of scattered power from glistening surfaces with different terrain characteristics
3. Measuring reflectivity coefficients associated with different types of terrain.

Two data analysis techniques are outlined in this section, one for rough terrain ($\sigma_{h/\lambda} >> 0$), and one for terrain of moderate to slight roughness. For a rough surface, elementary patch powers will add, and a deterministic approach is used in the computer program to simulate the experimental results. For moderate to slight roughness, however, an option is available to monte carlo the powers within a resolution cell by appropriately defining the scattered field distribution over the cell. The deterministic and Monte Carlo modes require

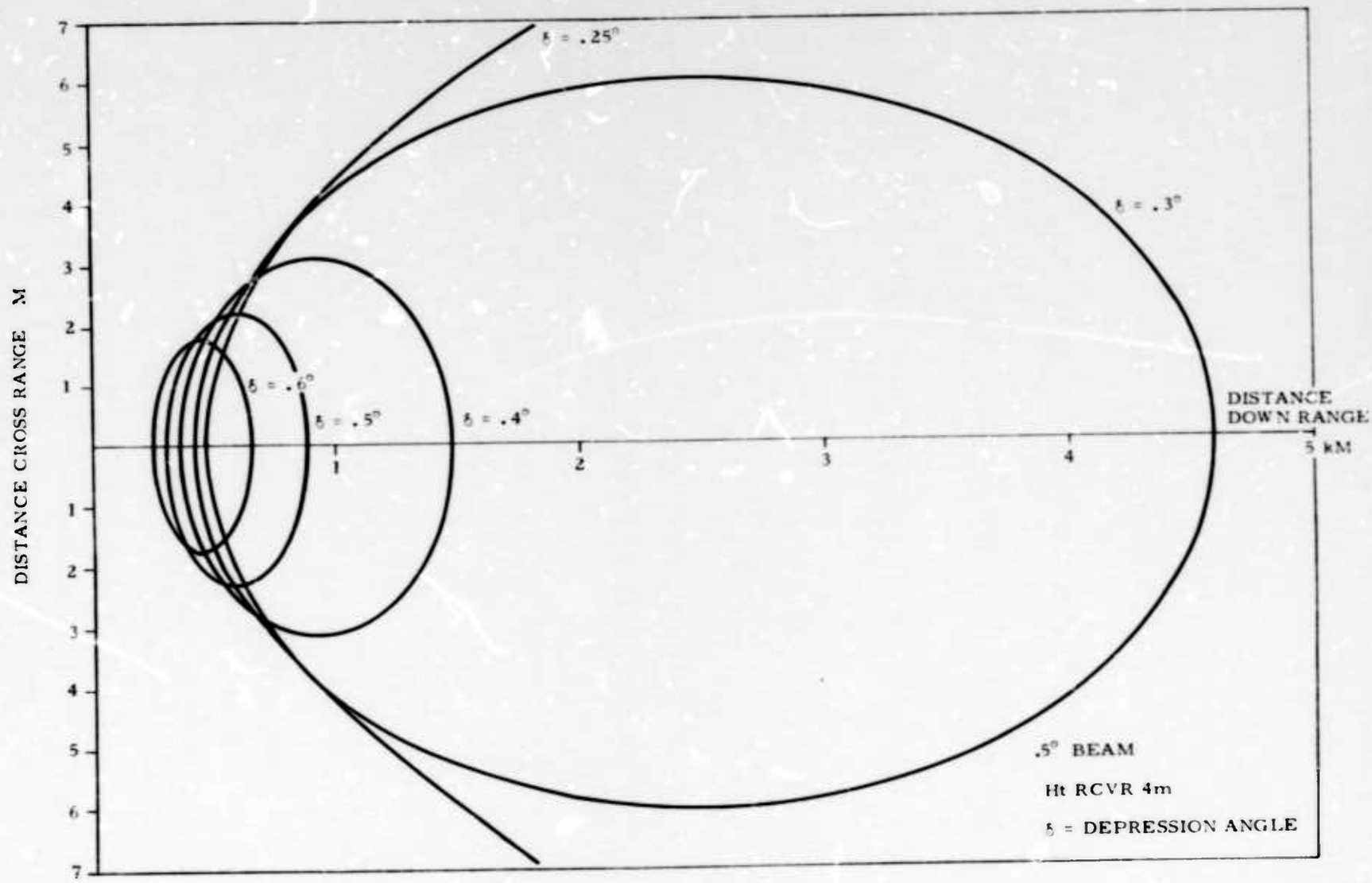

Figure 42. Main Beam Coverage Diagram

the definition of different data analysis techniques. Both techniques should be applied to each set of measured data in an effort to more accurately define the criteria for the use of the deterministic approach in lieu of the Monte Carlo process.

Data Analysis - Rough Surface

Let $\langle \delta P_2 \rangle_i$ denote the scattered power received from the ith patch within a particular resolution cell. This power is given by

$$\langle \delta P_2 \rangle_i = P_r D_i^2 \, |R(\psi_1)|_i^2 \left[\left(\frac{g_1 g_2}{g_{10} g_{20}} \right)_i \left(\frac{R_3}{R_1 + R_2} \right)_i^2 \rho_{s_i}^2 + F_{d_i}^2 \, \Delta \rho_{d_i}^2 \right]^1 \quad (3.4.1)$$

where

P_r is the direct power return from the source

D_i is the divergence factor for the ith patch

$|R(\psi_1)|_i^2$ is the rms Fresnel reflection coefficient for the ith patch at an angle of incidence ψ_i

$\rho_{s_i}^2$ is the rms specular reflection coefficient for the patch

$F_{d_i}^2$ is the diffuse roughness factor

$\Delta_{\rho_{d_i}}^2$ is the rms patch contribution to the normalized, diffusely scattered power

g_1 is the source power gain in the direction of the patch

g_2 is the receiver power gain in the direction of the patch

g_{10} is the source power gain in the direction of the receiver

g_{20} is the receiver power gain in the direction of the source

R_1, R_2, R_3 are defined in Figure 3

[1] All equations in this section, if not derived here, are discussed in Section 2 or Appendix C. For the most part they are merely repititions of equations previously derived but are repeated here for convenience to the reader.

The first step in correlating theory with data is to select terrain (see Section 3.3) that is relatively uniform with respect to the small scale roughness parameters σ_h and β_o (rms surface height and slope, respectively), and which is free from hills and other large scale ground irregularities. For such a site, the receive beam can be directed away from the specular point to eliminate any specular contribution to the reflected power from the beam/pulse resolution cell. In this case, the first term inside the brackets in (3.4.1) may be dropped and

$$\langle \delta P_2 \rangle_i = P_r \left[D_i^2 \; |R(\psi_1)|_i^2 \; F_{d_i}^2 \; \Delta\rho_{d_i}^2 \right] \tag{3.4.2}$$

Since $\Delta\rho_{d_i}^2$ is rigorously derived in the theory for a rough surface and since no theoretical verification for the choice of $F_{d_i}^2$ (see Section 2.3 and Appendix C) is given, it is more appropriate to consider $F_{d_i}^2$ (as opposed to $\Delta\rho_{d_i}^2$) as the unknown in this analysis. Also, $F_{d_i}^2$ is introduced in the theory to scale the diffuse contribution $\Delta\rho_{d_i}^2$ according to patch roughness, and leads to a reduction in the diffusely scattered power as the surface becomes smooth. Within the roughness restrictions the theoretical model, (that is, accepting the hypothesis that surface roughness can indeed be defined in terms of the small scale roughness parameters β_o, σ_h, wavelength λ, and the reflection angles ψ_1 and ψ_2) $F_{d_i}^2$ may be considered constant within the resolution cell since the terrain in the cell is chosen uniformly in the parameters β_o and σ_n, and since the glisterning surface is quite narrow, suggesting little variation in ψ_1, and ψ_2 over the resolution cell. Accordingly the subscript i on the $F_{d_i}^2$ term in (3.4.2) is dropped with the result:

$$\langle \delta P_2 \rangle_i = P_r \; D_i^2 \; |R(\psi_i)|_i^2 \; \Delta\rho_{d_i}^2 \; F_d^2 \tag{3.4.3}$$

In view of equation (3.4.3), the total mean scattered power from a resolution cell is given as

$$\langle P_2 \rangle = F_d^2 P_r \sum \left[D_i^2 \, | R(\psi_1) |_i^2 \, \Delta\sigma_{d_i}^2 \right] \tag{3.4.4}$$

from which the expression

$$F_d^2 = \frac{\langle P_2 \rangle}{P_r \sum \left[D_i^2 \, | R(\psi_1) |_i^2 \, \Delta\sigma_{d_i}^2 \right]} \tag{3.4.5}$$

is obtained for the roughness factor F_d^2 and a given resolution cell.

The measured power from the resolution cell, when substituted into (3.4.5) will yield a measured roughness factor as a function of the dimensions of the subpatches within a resolution cell. Reducing the sizes of these subpatches until the summation in the denominator of (3.4.5) is constant defines the patch sizes needed for the determination of the measured roughness factor F_d^2 associated with the resolution cell in question[1].

Consider a ground patch (the larger the better) between the transmitter and the receiver that does not contain the specular point and over which β_o and σ_h may be considered constant. Let the "roughness" parameter g be defined by

$$\sqrt{g} = \frac{2\pi \sigma_h}{\lambda} (\sin \psi_1 + \sin \psi_2)^1$$

and again assume ψ_1 and ψ_2 are constant over a given resolution cell. Consideration of many cells within the ground patch will yield the following measured curves for fixed σ_n and β_o:

1. F_d^2 vs roughness
2. G_o vs roughness

where G_o is the bistatic reflectivity coefficient given by

$$G_o = F_d^2 \cot^2 \beta_o \sum_{\text{cell}} \exp\left(- \frac{\tan^2 \beta_i}{\tan^2 \beta_o} \right) \tag{3.4.6}$$

for a Gaussian surface.

---

[1] This expression is consistent with that given in Section 2.

For the same resolution cells and roughness parameters σ_h and β_o, theoretical curves for F_d^2 and hence also G_o will be calculated and compared with the measured curves. A fitting process which cannot be defined until data are available will then be used to generate a refined empirical expression for F_d^2 in terms of the roughness parameter g and for fixed σ_h and β_o.

The theoretical F_d^2 given in Reference 3 is a function of σ_n, λ, ψ_1 and ψ_2. It may be that these parameters are not sufficient in themselves to express F_d^2 empirically. In fact, it is expected that at least the rms slope β_o should be added to this list of parameters. As a result, the above procedure will be repeated many times for different β_o, σ_h using the refined F_d^2 each time and a fitting process yet to be defined which will generate refinements in F_d^2 in terms of the necessary parameters. Ultimately then, emperical expressions for both F_d^2 and G_o will be determined which will best fit the measured data.

Next, data from the same set of experiments that were performed for the determination of F_d^2 will be analyzed for resolution cells containing the specular point. Measured specular reflection coefficients can be determined from the measured power by subtracting the diffuse contributions determined by the above procedures. These measured coefficients will then be compared with the theoretical values and appropriate modifications to the specular theory will be made.

Finally, with the theory and computer model refined to give the best fit to all data, the computer simulation will be re-run for each set of experiment geometries and parameters to generate updated estimates for the spatial distributions of diffuse power from the glistening surfaces.

Data Analysis - Moderate to Slight Roughness

It is known in the theory that for a very rough surface the phases of the individual scattered waves are uniformly distributed over the interval $[-\pi, \pi]$, that is, the scattered field is incoherent and it can be shown that the field intensities are Rayleigh-distributed. In general the scattered field can be expressed as the sum of a constant, coherent (with constant phase) component and a random, Hoyt-distributed component, that is, a vector with components chosen from normal distribution with zero means and appropriate variances (see Section 2 and Figure 9). As the surface becomes smooth the Hoyt-distribution continuously shrinks to zero

and the scattered field becomes coherent. As this continuous transition between incoherence and coherence takes place summing powers within a resolution cell may not give an accurate representation of the total reflected power from the cell. Rather, it may be necessary to establish the Hoyt-distribution mentioned above and follow a Monte Carlo process in order to obtain reliable estimates of the power contributions from given cells. For this reason and for the purpose of defining more accurate roughness criteria for the summing of powers, a Monte Carlo option has been included in the computer simulation in addition to the power option in which the cell contribution to the scattered power is found by summing powers from elementary patches within the cell. It is expected that this option will contribute significantly in understanding and refining the multipath theory as experimental data becomes available.

Let $E_{2_i}^n$ denote the random scattered field for the ith patch in a resolution cell and the nth sample in a Monte Carlo Process If the resolution cell is again chosen to exclude the specular point, the discussions in Section 2.3 imply that

$$E_2^n = F_d^2 \sum_{i=1}^{M} \eta_i^n \tag{3.4.8}$$

where η_i^n is a complex number depending on the patch location and the sample under consideration, and M is the number of patches in the cell[1]. Accordingly,

$$P_2^n = 1/2\, Y_o\, F_d^4 \sum_{i=1}^{M} \eta_i^n \sum_{k=1}^{M} (\eta_k^n)^* \tag{3.4.9}$$

and the meanpower from the resolution cell is

$$\langle P_2 \rangle = 1/2\, Y_o F_d^4 \frac{1}{N} \sum_{n=1}^{N} \sum_{i=1}^{M} \eta_i^n \sum_{k=1}^{M} (\eta_k^n)^* \tag{3.4.10}$$

where N is the number of Monte Carlo samples.

Equation (3.4.10) should replace (3.4.5) for the determination of the measured roughness factor when this Monte Carlo option is used. Other than this replacement, the data reduction procedures will be the same as those described for rough surfaces.

---

[1] η_i^n can be derived from equations (2.3.21) to (2.3.33). Its specific value is not important here.

SECTION 4. COMPUTER SIMULATION

4.1 Introduction

The multipath computer program represents an accurate treatment of the classical multipath theory (Ref. 1) with refinements (Ref. 3). A review of this theory is given in Section 2 and Appendix C of this report. The program is unique in its detailed treatment of this theory and is designed to validate and further refine the theory as experimental data are generated from the measurements program.

Two major options are available to the user, a multipath measurements option and a closed loop tracking option. The former closely simulates the measurements program design and at the same time remains flexible by allowing the choice of any of the following equipment configurations:

- Passive Receiver - Pulse Beacon
- Passive Receiver - CW Beacon
- Pulse Radar - Passive Target

The first two configurations are of specific interest here, and will be used in conjunction with the measurements program to

- Determine spatial distributions of diffuse/specular surface reflections for different receiver-beacon geometries and terrain characteristics,
- Aid in the generation of a handbook of surface reflectivity information.

The second two configurations will be used more in future multipath measurement programs once the multipath theory has been refined and validated and will at that time provide a means for accurately evaluating and quantifying the multipath effect on tracking radar at low elevation angles. It is for this purpose that the tracking option has been included in the computer

model. In this option closed loop tracking in the elevation coordinate with GHK filtering (3rd order digital filter) is possible. The same detailed multipatch theory used in the measurements mode is also used in the tracking mode to quantify the tracking errors introduced by surface reflections from virtually all of the terrain between the radar and the target.

Curved earth geometry is used in both the measurement and the tracking modes of the simulation. In addition, the program is coded to allow the user to insert gross terrain features as a function of down range distance between the receiver and beacon/target. Small scale roughness variations, vegetation variations, and variations in the electrical properties of the terrain at different down range distances are also available.

4.2 Program Inputs

All data card input is handled via namelist statements. There are a total of three namelists:

Namelist/INP0/	Tracking Information
Namelist/INP1/	Tracking/Measurement Mode Decision
Namelist/INP2/	Receiver/Source Geometry Scan Beam Depression Angles Antenna Parameters Source Parameters Surface Statistics

The input parameters are given below in table form according to Namelist.

Namelist/INP0/

Symbol	Definition	Default Value
PRF	Pulse Repetition Frequency (Pulses/sec)	0.0
TIMEOUT	Time Increment Between Flight Path Milestones (sec)	0.0
RTRMIN	Minimum Receiver-to-Target Slant Range (meters)	0.0
RTRMAX	Maximum Receiver-to-Target Slant Range (meters)	0.0

Namelist/INP1/

Symbol	Definition	Default Value
TRACK	T ≡ Tracking Option F ≡ Measurement Option	F

Namelist/INP2/

Symbol	Definition	Default Value
DGBALL	Maximum allowed change in Diffuse Gain across patch in Down Range Direction. (Controls patch subdivisions in Down Range Direction)	.01
DGBALL1	Maximum allowed change in Diffuse Gain across patch in Cross-Range Direction. (Controls patch subdivisions in Cross-Range Direction)	.01
DX	Down-Range Patch Dimension (meters)	100.0
DY	Cross-Range Patch Dimension (meters)	10.0
GR	Peak Receiver Gain	1.0
GR0	Initial Receiver-to-Source Ground Range (meters)	10000.00
GRMAX	Maximum Receiver-to-Source Ground Range (meters)	10000.00
GT	Peak Source Gain	1.0
HR	Receiver Altitude (meters)	4.0
HT	Source Altitude (meters)	200.0
ICALC	≡ 0 If Delay, Delay Min., and Delay Max are to be Calculated	0
MAXDEL	Maximum Delay (meters)	2000.0

Symbol	Definition	Default Value
MINDEL	Minimum Delay (meters)	0.0
NBEAMS	Number of Beams	10
NOUT	Number of Delay Bins (may be modified by program during execution)	20
NP	Number of Points in Pulse	5
NR	Number of Runs	1
NSAMPLE	Number of Monte Carlo Samples	1
NSLOPE	Number of Down-Range Patches over which Different Surface Statistics are specified	2
NYMAX	Maximum Number of Cross-Range Patches	10
DBBDIR	≡ T If Relative Power in dB is to be Determined.	
	≡ F If Absolute Power is to be Determined.	F
NXSDMX	Maximum Number of Subdivisions in Down-Range Direction for each Patch	10
NYSDMX	Maximum Number of Subdivisions in Cross-Range Direction for each Patch	10
PT	Peak Source Power	1.0
PWIDTH	Pulse Width (sec)	1.0×10^{-9}
SIGZ0	Radar Cross Section of Target ($meters^2$)	1.0
XLAM	Wavelength (meters)	.0164592
XV	X-Coordinate of Target Velocity (Reference Coordinate System) (meters/sec)	-1000.0
YV	Y-Coordinate of Target Velocity (Reference Coordinate System) (meters/sec)	0.0

Symbol	Definition	Default Value
ZV	Z-Coordinate of Target Velocity (Reference Coordinate System) (meters/sec)	0.0
GRAPH	≡ T for Graphing	F
NEWBEAM	≡ T for 1st Run	T
	≡ F for Additional Runs if no New Scan Beams are Introduced.	
NEWSLOP	≡ T for First Run	T
	≡ F for Additional Runs if no New Surface Statistics are Introduced.	
OUTPUT	≡ T if Printed Output is Desired	T
PASSTGT	≡ T if Passive Target is used	F
	≡ F for Beacon	
PULSE	≡ T if Pulse Source	T
	≡ F if CW Source	
SQPULSE	≡ T if Square Pulse	T
	≡ F if Cosine Pulse	
UNIFORM	≡ T if Distribution of Surface Slopes is Uniform.	F
	≡ F if Distribution of Surface Slopes is Gaussian	
VOLT	≡ T for Voltage Option	F
	≡ F for Power Option	
VPOL	≡ T for Vertical Polarization	F
	≡ F for Horizontal Polarization	
SPEC	≡ T If Specular Returns are Accumulated	T
	≡ F Otherwise	
DIFFUSE	≡ T If Diffuse Returns are Accumulated	T
	≡ F Otherwise	

Symbol	Definition	Default Value
PRINTI	≡ F on All Runs	F
PRINT 2	≡ F on All Runs	F
PRINT3	≡ F on All Runs	F
PRINT4	≡ F on All Runs	F
PRINT5	≡ F on All Runs	F
PENPLOT	≡ T Cards are Punched containing Data for Graphing ≡ F Cards are not Punched	
SANGLE (I, 1)	Ith Scan Beam Azimuth Angle (Deg)	0.0
SANGLE (I, 2)	Ith Scan Beam Depression Angle (Deg)	0.0
SLOPE (I, 1)	Maximum Ground Range for Ith set of Surface Statistics (meters)	0.0
SLOPE (I, 2)	RMS Surface Slope (β_o) (radians) for Ith set of Surface Statistics.	0.0
SLOPE (I, 3)	Mean Slope of Gross Terrain Feature in Down-Range Direction for Ith set of Surface Statistics (rad)	0.0
SLOPE (I, 4)	Mean Slope of Gross Terrain Feature in Cross-Range Direction for Ith set of Surface Statistics (rad)	0.0
SLOPE (I, 5)	Surface Permittivity for Ith set of Surface Statistics.	0.0
SLOPE (I, 6)	Surface Conductivity for Ith Set of Surface Statistics (mho-m/sqm)	0.0
SLOPE (I, 7)	Vegetation Factor	0.0
SLOPE (I, 8)	RMS Surface Height (meters)	0.0
SLOPE (I, 9)	Height of Gross Terrain Feature for Ith set of Surface Statistics (meters)	0.0
NPN	Initial Number of Points in Pulse	5

It should be noted that the logical variables PRINT1, PRINT2, PRINT3, PRINT4, PRINT5 in Namelist/INP2/are included and held in common between subroutines for the purpose of providing switches for the output of variables defined by and of specific interest to the user. However, unless additional output is defined by the user these variables should be set equal to F.

4.3 Program Outputs

A detailed flow diagram showing the program output that is currently available is given in Figure 43. Basically, the outputs may be divided into two main types, those from the measurements mode and those from the tracking mode.

If the measurements mode is selected, output is written on tape 12 and will vary in content depending on whether the source is pulse or CW (see Flow Diagram). The same information stored on tape 12 is also printed if OUTPUT = T. Also in the case of printed output, all specular points; associated delays measured with respect to the direct path; specular reflection coefficients (ρ_s^2); and specular patch gains $\rho_s^2/(R_1 + R_2)^2$ are printed. Finally, printer plots, and card output of the data arrays necessary for pen plots (e.g., for the Zeta plotter) are available in the measurements mode independent of whether or not printed output is specified.

In the tracking mode printer plots of elevation error vs slant range as well as the coordinates of each data point are printed. Also, card output for pen plots is available (as in the measurements mode) by setting PEN Plot = T.

4.4 Program Description

Coordinate Systems

Two coordinate systems are employed in both the measurements and the tracking modes of the computer model. They are a Reference (x, y, z) coordinate system and a Receiver (x', y', z') coordinate system. The reference coordinate system is fixed with its origin at the center of the earth with the z-axis passing through the receiver site. The receiver coordinate system on the other hand, with its origin also at the center of the earth and the z'axis coincident with the z-axis, is allowed to rotate in the event the source (target) is moving (tracking mode). It amounts to a counter-clockwise rotation of the

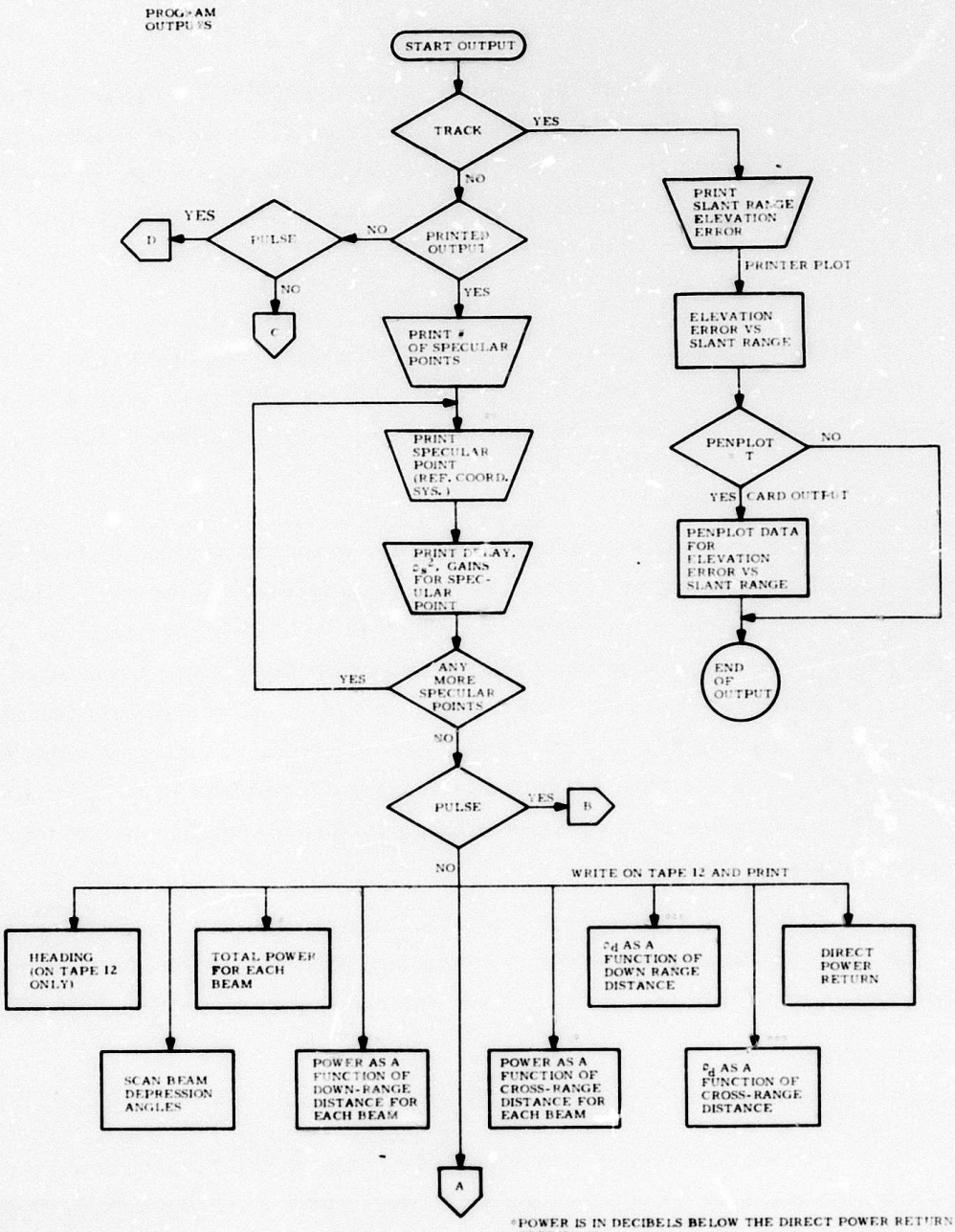

*POWER IS IN DECIBELS BELOW THE DIRECT POWER RETURN IF DBBDIR = T.

**TWO COORDINATE SYSTEMS, A REFERENCE COORDINATE SYSTEM AND A RECEIVER COORDINATE SYSTEM, ARE USED BY THE PROGRAM. FOR THEIR DEFINITIONS, SEE SECTION 4.4.

***ZEROES ARE STORED FOR σ_d UNLESS VOLT = F

Figure 43a. Program Flowchart

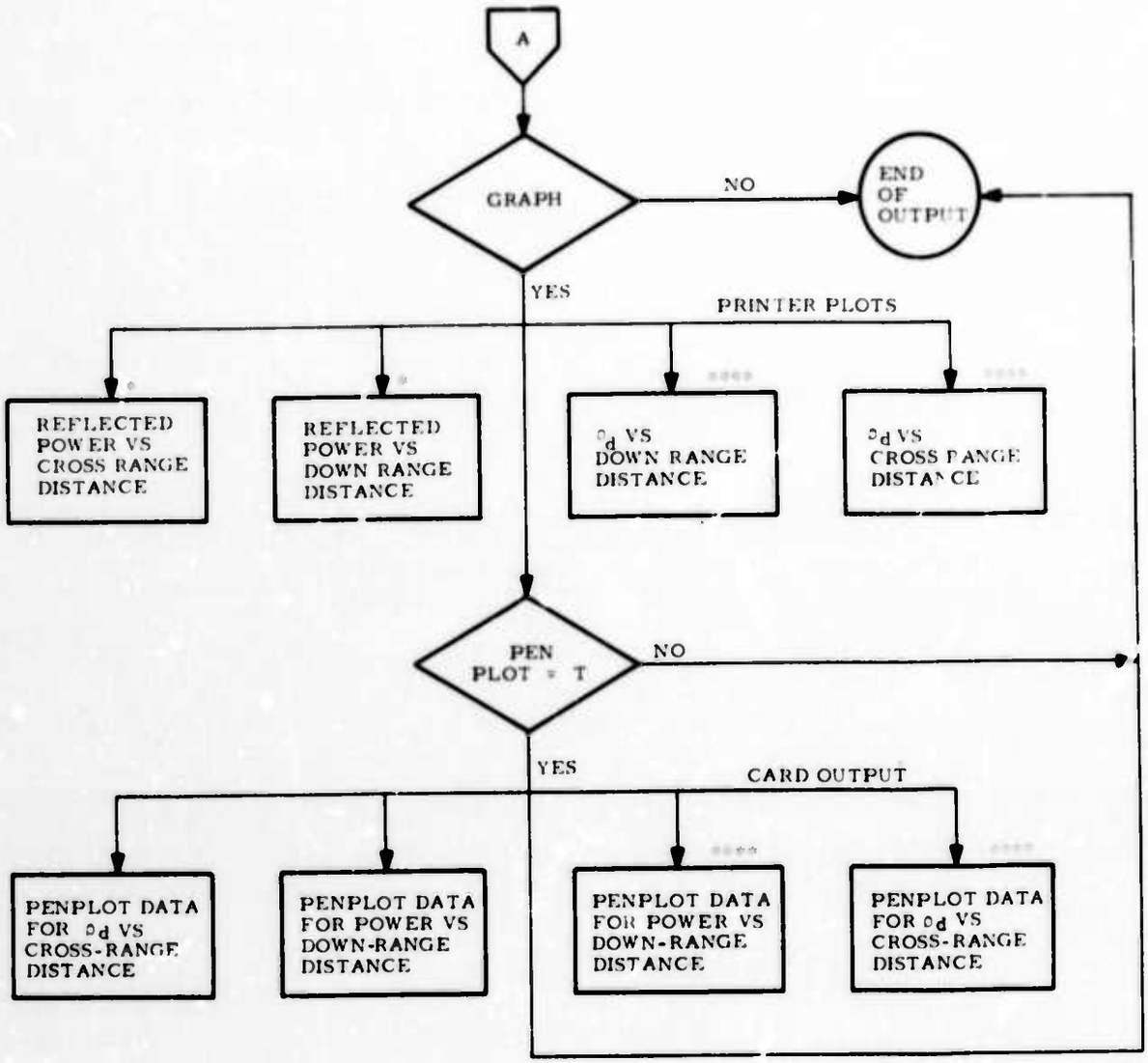

*POWER IS IN DECIBELS BELOW THE DIRECT POWER RETURN IF DBBDIR = T.

****TRUE ONLY FOR VOLT = F

Figure 43b. Program Flowchart (Cont)

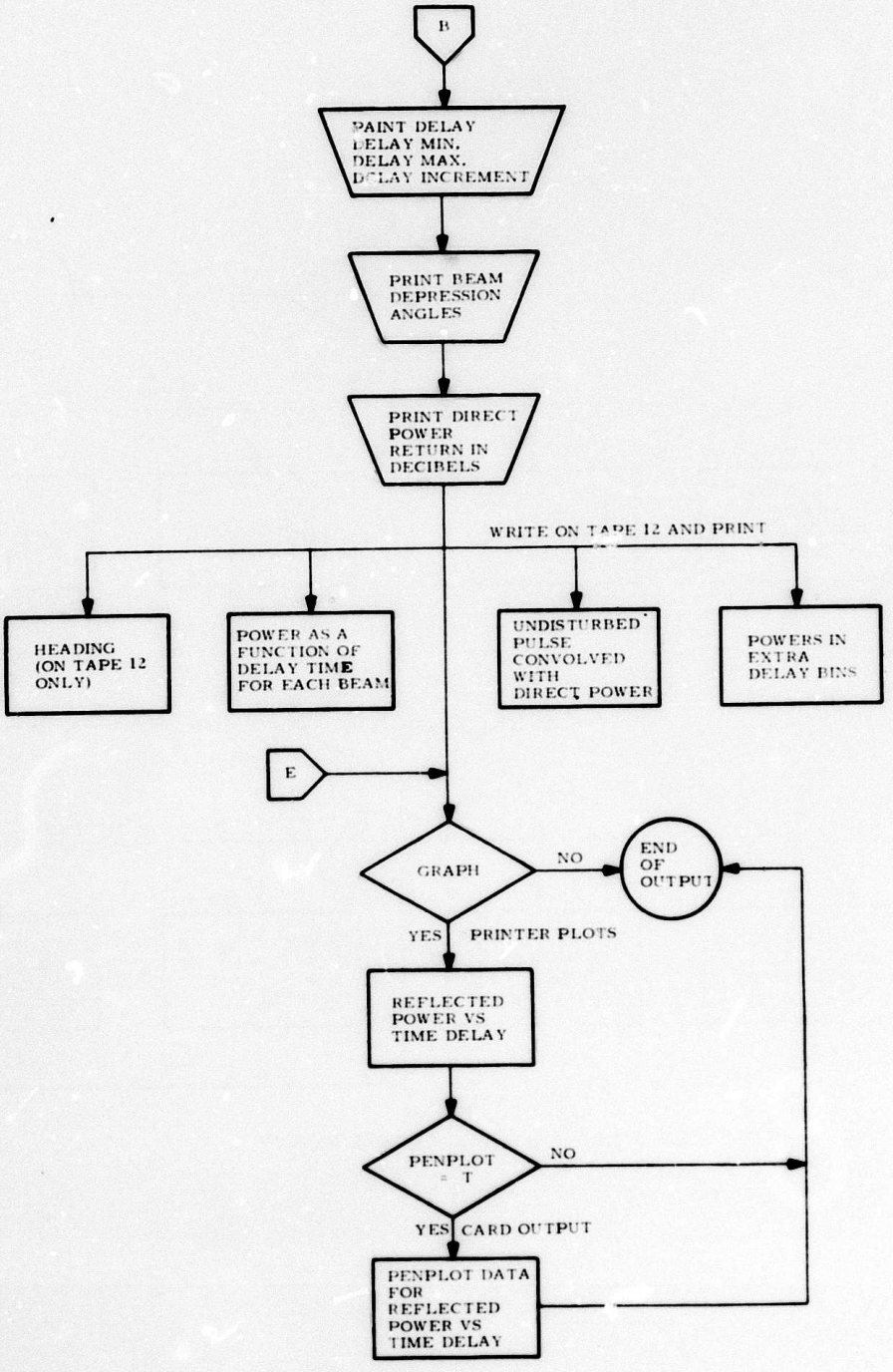

Figure 43c. Program Flowchart (Cont)

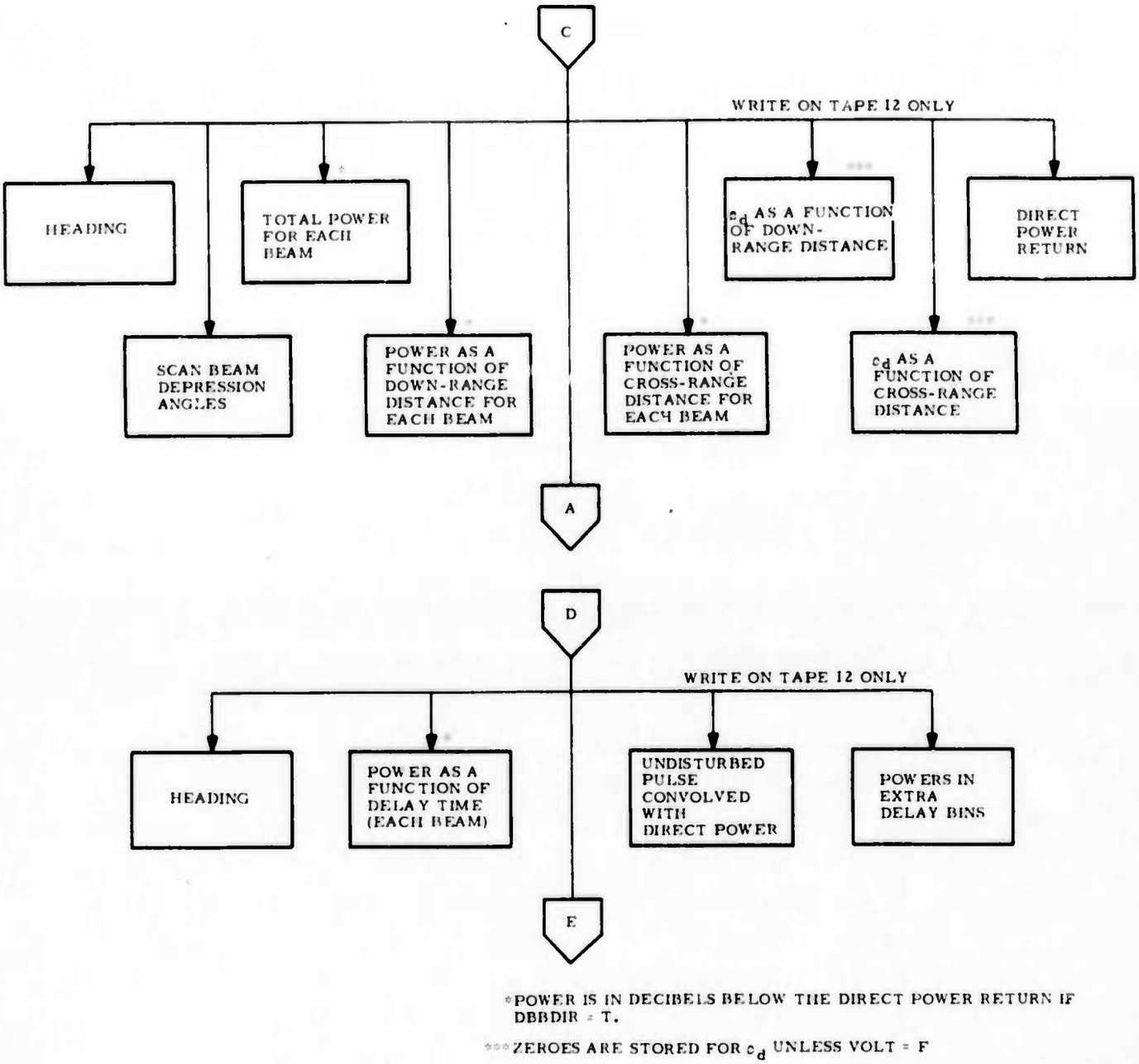

Figure 43d. Program Flowchart (Cont)

reference coordinate system through an angle θ equal to the angle between the positive x axis and the projection into the xy plane of the line segment through the foot of the receiver and the source (see Figure 44). In the measurements mode the source is always in the xz plane (i.e., y = o) and the receiver coordinate system is identical to the reference coordinate system. It is also assumed without loss of generality, that in the tracking mode the source is initially in the xz plane. Accordingly, in both modes of operation surface statistics are read in relative to the reference coordinate system.

Antenna Patterns

In the measurements mode there are provisions for up to ten different scan beams and one source beam. The scan beam depression angles are specified by input and each scan beam has the same beamwidth, also specified by input. The source beamwidth is variable (input) but in practice is set to a large value to simulate an isotropic source.

In the tracking mode the tracking beam is established as a four-beam amplitude sensing cluster to allow for monopulse tracking in all radar coordinates and for general target flight paths. Subroutines TBEAM, PATTERN, and B1POSTN initially establish and position the cluster about the antenna axis. It is assumed that the antenna axis is initially pointed at the true target. At later times the subroutine B1POSTN is all that is needed to reposition the cluster.

Currently all antenna patterns (both modes) are analytic and are modeled by Bessel functions of variable (input) orders. This allows flexibility in establishing the desired sidelobe levels. However, with regard to the computer examples that follow the Bessel function of order three is used to establish the patterns. In this case the sidelobe level is 30.6db down. Since the patterns are all established in subroutines (as opposed to the main program) they may be easily replaced by actual patterns during the experimental phase of the multipath measurements program.

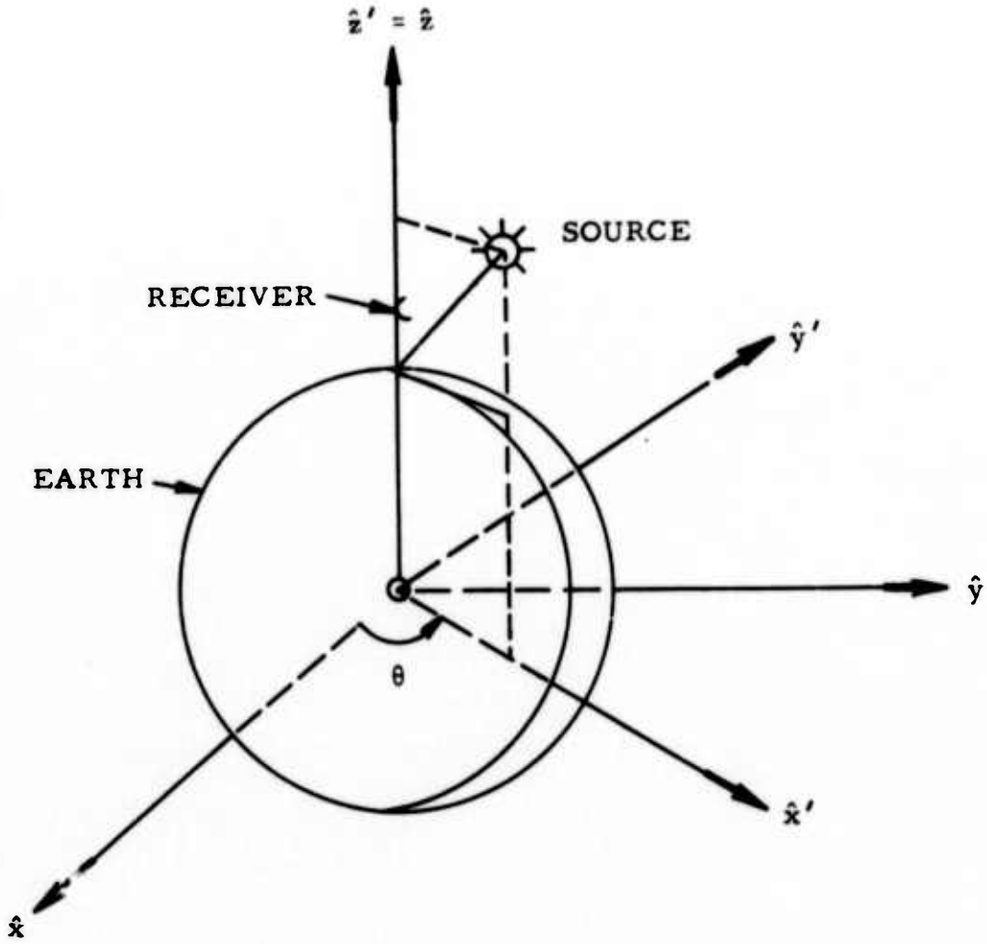

Figure 44. Receiver/Reference Coordinate System

Glistening Surface

The terrain between the receiver and the source is divided into down-range/cross-range ground patches, the dimensions of which are specified by input (Figure 45). Two criteria for a patch corner to be on the glistening surface are available depending on the sense of the logical switch UNIFORM:

o If UNIFORM = T, a uniform distribution of surface slopes is assumed with mean zero and standard deviation

$$\sigma = \frac{\beta_o}{\sqrt{3}} = \frac{2\sigma_h}{d_c\sqrt{3}} \quad .^{1} \tag{4.4.1}$$

Under this option a patch corner is on the glistening surface when

$$\beta \leq \beta_o \quad . \text{ (Figure 46)} \tag{4.4.2}$$

o If UNIFORM = F, a Gaussian distribution of surface slope is with zero mean and standard deviation $\sigma = \beta_o$. In this case a patch corner is on the glistening surface when

$$\beta \leq 3\beta_o \text{ (Figure 46)} \tag{4.4.3}$$

The subroutine Scan generates the glistening surface and stores the necessary data associated with its subpatches. The left half (positive y) of the glistening surface and its patch data are generated/stored first. The computer starts at the foot of the receiver and generates the subpatches for positive y in the sequence shown in Figure 45. For each down-range position, cross-range patches are constructed until any one of the following criteria are met:

- Both far patch corners (in y-direction) are off the glistening surface.
- The average of the two far corner (in y-direction) diffuse patch gains G_o (equation 3.4.7) is less than .01.

---

1. The notations used in this section are defined in Section 2.

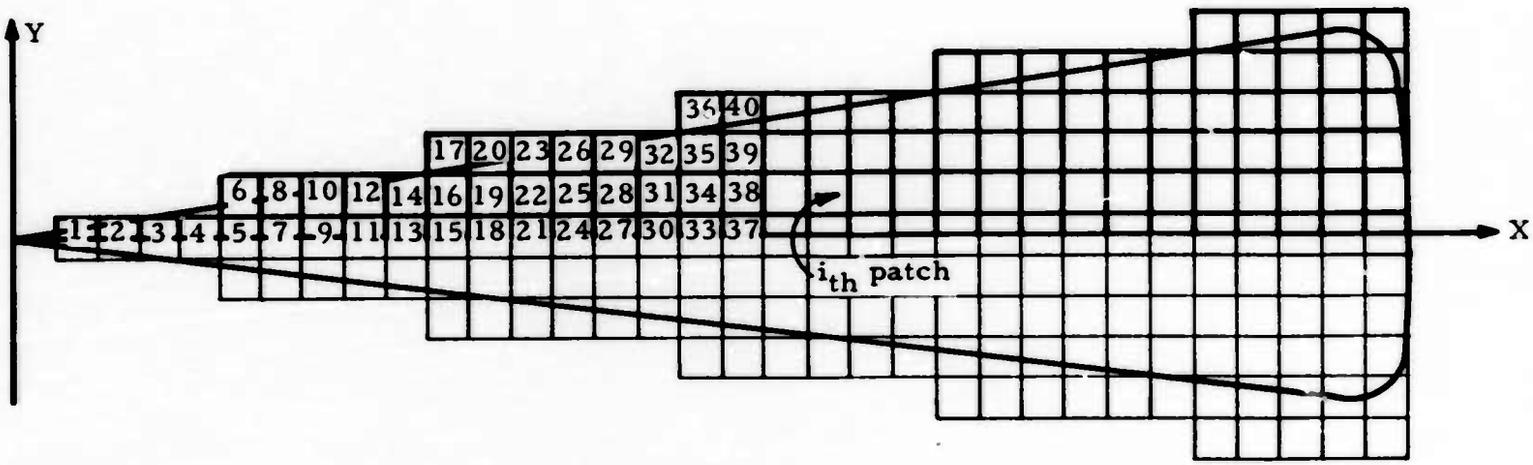

Figure 45. Glistening Surface (Projection on x, y Plane)

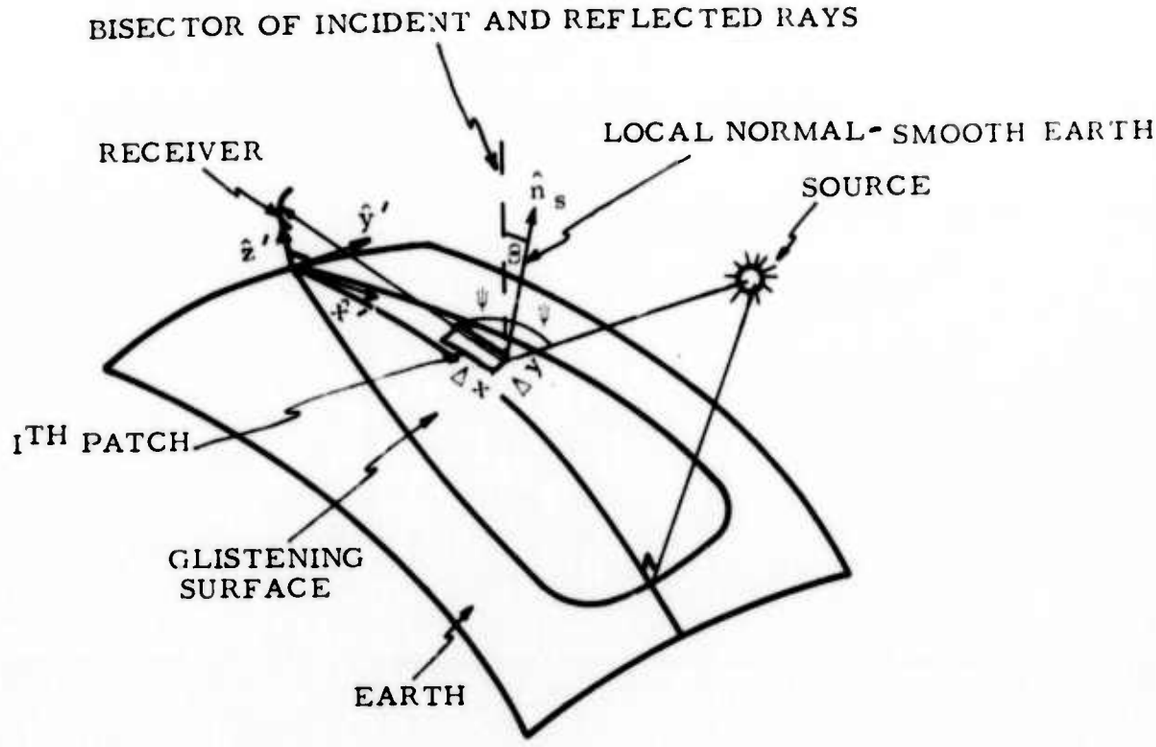

Uniform surface slope distribution: $\beta \leq \beta_0$

Gaussian surface slope distribution: $\beta \leq 3\beta_0$, $\sigma = \beta_0$

Figure 46. Glistening Surface Determination

- The number of cross-range patches is greater than or equal to NYMAX (input).

This process is continued for each down-range position until the far patch corners in the down-range (X) direction lie beyond the minimum of the ground range to the receiver horizon and the ground range GRMAX specified by input. When this happens the computer starts back at the foot of the receiver and generates the right half (negative y) of the glistening surface using the same procedures.

Although the initial patch dimensions (Δx, Δy) are specified by input, the computer will subdivide each patch into an appropriate number of subpatches according to the following scheme:

Let P_1, P_2, P_3, P_4 be the corners of a typical curved earth surface patch shown in Figure 47. The computer first determines the maximum differential change in diffuse patch gain across the patch in the x-direction according to the formula

$$\text{GRADX} = \max \left(|G_o(P_2) - G_o(P_1)|, |G_o(P_4) - G_o(P_3)| \right) \qquad (4.4.4)$$

where $G_o(P_i)$, $i = 1, 2, 3, 4$ is the diffuse patch gain (equation 3.4.7) at the i^{th} patch corner. If GRADX is greater than the maximum allowed patch gain differential (DGBALL) in the x-direction, the surface patch is subdivided into NXSD subpatches in the down-range direction, where NXSD is computed from the following

$$\left.\begin{aligned} N &= \text{INT (GRADX/DGBALL)} \\ \text{NXSD} &= \text{Min (N, NXSDMX)} \end{aligned}\right\} \qquad (4.4.5)$$

Here INT denotes conversion from decimal to integer constants (via truncation) and NXSDMX is the maximum number of down-range subdivisions specified by input.

Next, the gain differential across the patch in the y direction is calculated from the formula

$$GRADY = \max \left(\left| G_o(P_3) - G_o(P_1) \right|, \left| G_o(P_4) - G_o(P_2) \right| \right), \quad (4.4.6)$$

and if this value is greater than the maximum allowed gain differential (DGBALL1) in the y-direction, NYSD subpatches are established in the cross-range direction according to

$$\left.\begin{aligned} M &= INT\,(GRADY/DGBALL1) \\ NYSD &= \min\,(M,\ NYSDMX) \end{aligned}\right\} \quad (4.4.7)$$

where NYSDMX is the maximum number of subdivisions in the y direction.

A total of NXSD · NYSD subpatches are therefore generated. Also, patch data for each subpatch, in addition to that generated for the father patch, is computed and stored for each subpatch corner. The same patch information computed and stored for the father patch is also computed/stored for the subpatches and is given in Table VI.

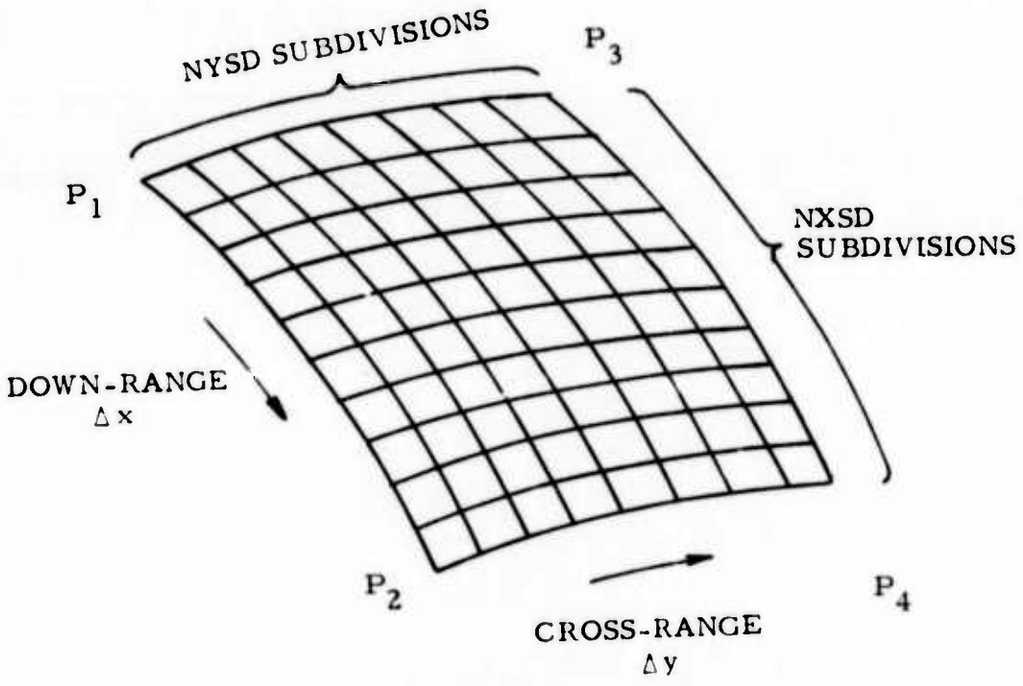

Figure 47. Glistening Patch Subdivision

Table VI

Variable	Definition
BETA	Angle between the local normal at the patch corner and the bisector of the angle between the source-to-patch corner and patch corner-to-receiver vectors. (Figure 46).
FUDGE	Roughness factor
GAINB (BETA, I)	Diffuse patch gain for the angle BETA and for the Ith set of surface statistics.
DELAY	Path difference between the direct and indirect paths at a corner.
ROZERO	Fresnel reflection coefficient
X	X-coordinate of rough-earth patch corner (Receiver coordinate system)
Y	Y-coordinate of rough-earth patch corner (Receiver coordinate system)
Z	Z-coordinate of rough-earth patch corner (Receiver coordinate system)
D	Divergence factor
UXLN	X-coordinate of local (unit) normal at patch corner (receiver coordinate system)
UYLN	Y-coordinate of local (unit) normal at patch corner (receiver coordinate system)
UZLN	Z-coordinate of local (unit) normal at patch corner (receiver coordinate system)
SLOPE (I, 7)	Vegetation factor at a corner associated with the Ith set of surface statistics
SLOPE (I, 8)	Rms, surface height of the small-scale surface irregularities at a corner associated with the Ith set of surface statistics
THET1	Angle between the source-to-patch corner vector and the local normal at the patch corner
THET2	Angle between the patch corner-to-receiver vector and the local normal at the patch corner.

As indicated in the preceding table, the father patch and subpatch corners are rough-earth corners, that is, for each patch the surface statistics are scanned to see if a patch corner lies on a gross terrain feature (hill). If so, the patch corner is located on the terrain feature.

Once Table VI has been generated for a particular patch/subpatch, the data are averaged over the four patch/subpatch corners and the resulting information is used to determine the field distribution associated with the patch/subpatch and the mean reflected power from the patch/subpatch.

Measurements Mode

The scan beams are first positioned in azimuth and elevation to look at various regions on the glistening surface. Sidelobe as well as main beam reflections are all accounted for in measuring surface reflections from a given patch.

Three Fortran variables PULSE, VOLT, and PASS TGT are introduced to denote, respectively, a pulse source as opposed to a CW source, a voltage option as opposed to a power option, and a passive target as opposed to an active transmitter. The voltage option implies that all signals from various portions of the glistening surface which enter the receiver simultaneously in time are summed at rf with amplitude and phase preserved during the summation. The power option assumes that only the powers are summed, phase information being ignored.

These variables are logical switches taking on the values T (true) or F (false) and the simulation is capable of running in any of the modes shown in Table VII.

Table VII

PULSE	VOLT	PASS TGT
F	T	F
T	T	F
F	F	F
T	F	F
F	T	T
T	T	T
F	F	T
T	F	T

Assume until stated otherwise that PASS TGT = F, then if Volt = T a reflected field distribution is estabi shed for each glistening surface patch/subpatch and each scan beam, and will vary from patch to patch for each beam as the patch data (Table VI) changes. A sample reflected field is then chosen for each patch/subpatch and each beam (see Section 2) from the appropriate distribution and summed. The result is a one-dimensional array of sample field representing the total fields reflected from the glistening surface, one sample for each scan beam. Although the direct field from the source enters only the sidelobes of each of the scan beams, it is never-the-less calculated and added to the sample reflected fields for each beam. The resulting array is then transformed to a power array, the components of which are the sample powers associated with the different beam positions. Carrying out this sampling process over all Monte Carlo members, and averaging for each beam position over the total number of samples yields the mean power seen by the receiver for each beam position.

If PULSE = F and VOLT = T, in addition to summing the sample fields over the total glistening surface, they are also stored in down-range and cross-range arrays for the graphing of the spatial distribution of power as a function of down-range or cross-range position.

In the event Pulse = T and Volt = T, delay bins (with delay measured with respect to the direct path) are created for each beam. Then for each of the beams, sample reflected fields from each patch/subpatch are apportioned (subroutine SPREAD) over the correct delay bins that fall between the minimum and maximum delays for the patch/subpatch. After scanning the whole glistening surface the fields collected in each of the delay bins are convolved with the pulse and transformed to power (in that order) to form a two-dimensional array, the elements of which denote sample power returns as a function of beam position and time delay. Such arrays are determined for each Monte Carlo sample and then averaged (element wise) to form a two-dimensional array of mean power returns as a function of beam position and delay time. For a fixed beam position the power for a given time delay is the mean power returned within a pulsewidth of the given delay time and is associated with a specific resolution cell on the ground.

When Volt = F a deterministic (as opposed to a Monte Carlo) approach is used to quantify the glistening surface reflections. In this case mean reflected powers are computed for each patch/subpatch (see Section 2) and each beam and added beamwise over the glistening surface to obtain the total mean reflected power for each scan beam. The direct power entering the sidelobes of the scan beams is then added to the total reflected power to yield the total apparent power at the receiver for each beam position. Now if Pulse = F, the mean patch powers are stored in down-range and cross-range arrays for graphing the spatial distribution of power as a function of down-range or cross-range position. If on the other hand Pulse = T, delay bins are created just as in the case when Volt = T, except now mean patch powers are stored in the bins in place of sample fields and the pulse is convolved with these bins for each beam to form mean power arrays as a function of delay for each scan beam.

Finally, in the event that a common antenna is used for both transmission and reception (PASS TGT = T), all the above options and associated procedures hold except that they are first carried out to determine the power at the target and the pulse shape (if Pulse = T) at the target. They are then repeated for the return paths. In this case the glistening surface is scanned twice, once for the forward paths and once for the return paths.

Tracking Mode

When operating in this mode the program sets Volts = T, PASSTGT = T, NSAMPLE = 1. Since NSAMPLE = 1, only one sample field is taken from each patch during a scan of the glistening surface. Accordingly, the output of this mode of operation represents typical tracking errors (as opposed to mean tracking errors) that may be encountered during any one pass of the target. This was done specifically to save computer time since tracking error determination at each data point along the target flight path requires scanning the glistening surface twice (approximately .46 cp minutes per scan). In the event mean tracking errors are preferred only slight program modifications are required.

At present tracking in the elevation coordinate only for in-plane (xz-plane) flight paths with constant target velocity is simulated. However, three-dimensional tracking geometry is used so that tracking in all radar coordinates for general target flight paths can be added at a later date without major changes to the main program coding.

Basically, this mode of operation simulates a closed loop tracker with GHK filtering. Initially the main beam (4 beam cluster - see Section 4.4, Antenna Patterns) axis is directed at the target but is subsequently allowed to wander from the true target direction as the multipath reflections are received at the radar. At each data point along the target flight path, the total voltage field returned to the radar is computed for each of the four beams in the tracking beam cluster according to the procedures described for the measurements mode when Volt = T, PASSTGT = T, NSAMPLE = 1, and either pulse = T or pulse = F.

In the event Pulse = T, the voltage field arrays established for each beam in the cluster are added in the correct way to determine two voltage arrays, one for the difference channel and one for the sum channel. Each of these arrays contains voltages as a function of delay time. These points in each array that fall within the range gate of the radar are then computed and averaged vectorially to give average voltages associated with the range gate for the sum and difference channels. If Pulse = F, corresponding to long pulses, the voltages in the sum and difference channels are not given as a function of time delay; the arrays for each channel contain only one element; and the averaging is not necessary.

Once the sum vector (Σ) and the difference vector (Δ) at the radar have been determined, the rough boresite error is computed as

$$\text{DELPHI} = \frac{\Delta \cdot \Sigma}{|\Sigma| \sqrt{|\Sigma|^2 + |\Delta|^2}} \qquad (4.4.8)$$

where the Dot ($\cdot$) denotes the classical dot product of two vectors and $||$ denotes the magnitude of a vector. Using (4.4.8) a rough estimate of the target elevation

is computed and then passed through a GHK filter to yield a smoothed estimate of the target's present elevation [1] and a prediction of its elevation at the next data point along the flight path. Based on this prediction the tracking beam is re-aimed and time is incremented to consider the next data point on the target flight path. Before moving to a new data point the estimate of the current target elevation is compared with the true target elevation to determine the tracking error in the elevation coordinate. These errors are stored as a function of slant range to the target for graphing purposes.

4.5 Computer Examples

Three receiver-source geometries that are typical of those to be used during the measurement phase of the multipath program are considered here. They are summarized below in Table VIII and depicted in Figure 48.

Table VIII

Geometry	RCVR Ht	Source Ht	RCVR-Source Gr Dist
1	4 m	200 m	3 km
2	4 m	300 m	5 km
3	4 m	500 m	10 km

Figures 49 through 55 depict mean power curves for each of these geometries and a 1 ns pulse beacon. The mean power reflected from the glistening surface together with the direct power return entering the sidelobes of the receive beams is graphed in each of these figures against time delay, measured with respect to the direct return, for each of the scan beams shown in the main beam coverage diagrams, Figure 42. Figures 49, 51, and 53 correspond to geometries 1, 2, and 3, respectively, with the terrain between the receiver and the source having an rms slope of .1 and $\sigma_h/\lambda = 5$ (moderately rough surface). Figures 50, 52, and 54 are for the same respective geometries except that a hill has

[1] Elevation is measured with respect to the local horizontal at the radar.

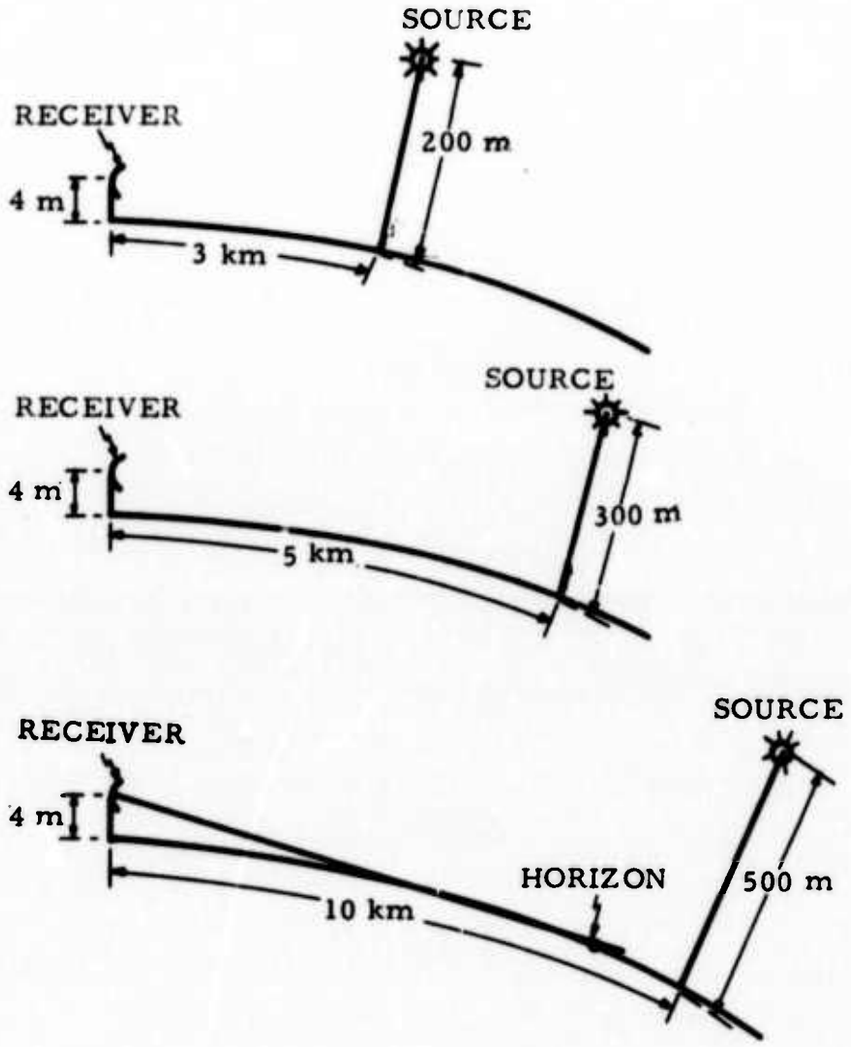

Figure 48. Receiver-Source Geometries

been added between the receiver and the source. The hill has a slope ±.04796 radians; a maximum height of 3 m; and extends from 989.6 m to 1114.4 m down-range. Figure 55 corresponds to geometry 1 over an ocean at sea state 3.

A comparison (geometry 1) between the power option (VOLT = F) and the VOLTAGE option (VOLT = T) is given in Figures 56 through 60 for each of the scan beams in Figure 42 and for a very rough surface ($\beta_o = .25$, $\sigma_n/\lambda = 10$).

4.6 Recommendations for Program Refinements

Although the computer simulation is detailed in its treatment of the current multipath theory, there are certain modifications which should be made that would add to its flexibility and usefulness as a model for practical measurements over ground and water. Some of the more important refinements are suggested below:

1. In the present version of the computer simulation the user may alter the surface statistics and allow for gross terrain features between the receiver and source. This is done however, as a function of down-range distance from the receiver, that is, the terrain features may be accounted for and the surface statistics altered on various down-range intervals between the receiver and the source. To bring this terrain model into closer agreement with what will be found at the measurement sites, provisions should be made for the input of terrain characteristics as a function of both down-range and cross-range position. This can be done by dividing the terrain (independent of the glistening surface sub-divisions) between the receiver and the source into patches and allowing for the input of a matrix of surface characteristics, with each row of the matrix containing the surface data for a patch. Then as the glistening surface is scanned, the matrix of surface data can also be scanned for the correct terrain statistics over a glistening surface patch.

2. Although the user may allow for gross terrain features between the receiver and the source, the shadowing of terrain features by others is not accounted for. If the model is to simulate actual test data, the inclusion of these shadowing effects should be added to the computer model.

3. The antenna patterns currently used in the simulation are analytic (Bessel functions). Although they served the purpose during the simulation construction, debugging, and testing, provisions should be made for the input of actual far field and near field antenna patterns. Since all analytic patterns are currently established by subroutines, this modification would require only the replacement of these routines by those appropriate for the input and interpolation of the actual patterns.

4. The simulation currently uses the equivalent 4/3 earth's radius which appplies only when the index of refraction decreases uniformly with increasing height. A normal profile of refractive index however, does not describe all propagation conditions. Provisions should therefore be made for computing the effect of the propagation medium (changes of atmospheric refraction) on radar coverage and to incorporate these effects in measuring the glistening surface and the reflections from this surface.

5. Finally, in-plane closed loop tracking is now available in the elevation coordinate only. Modifications should be made to allow tracking in all radar coordinates for targets on general flight paths.

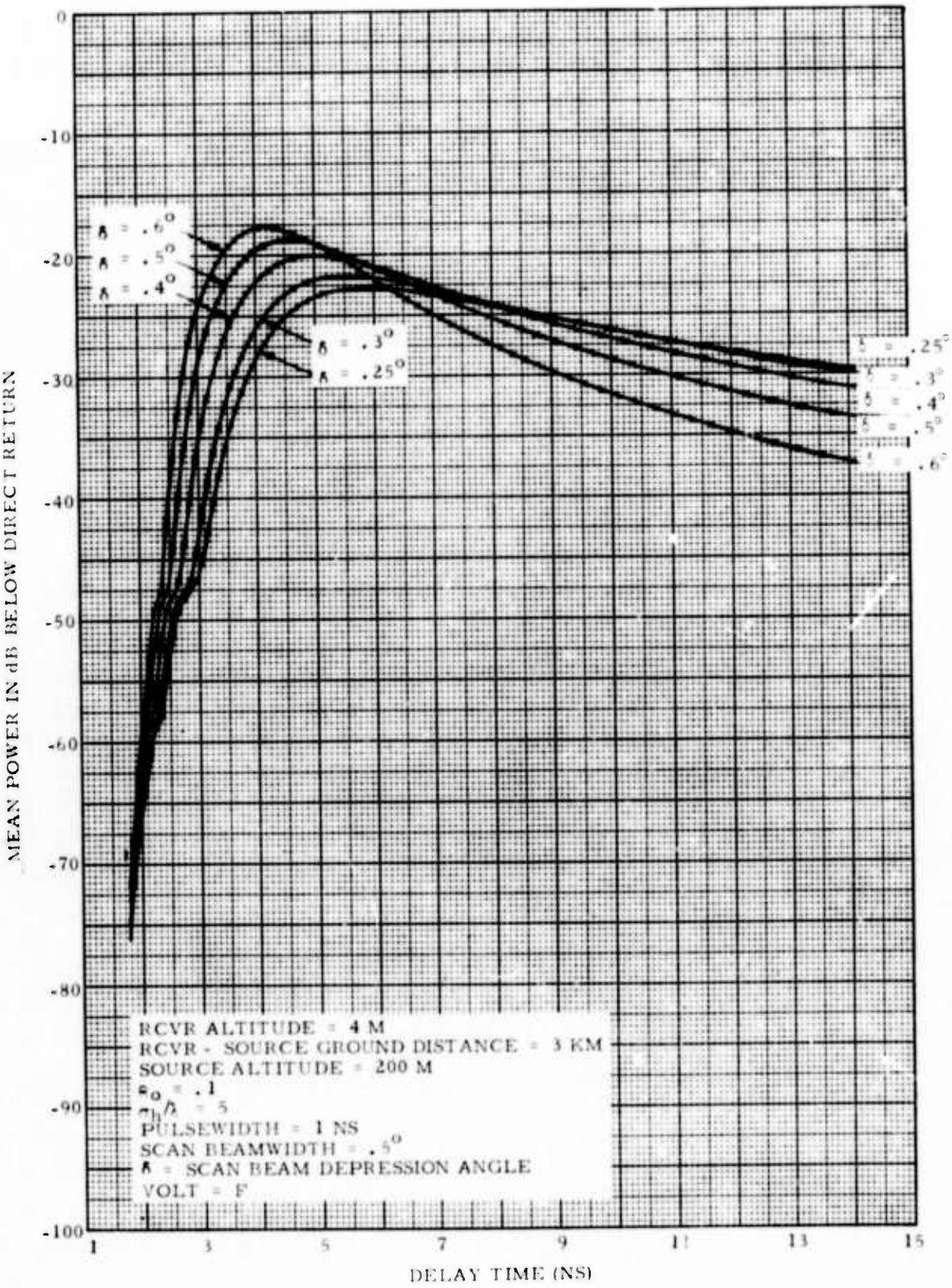

Figure 49. Multipath Power Curves. Mean Power vs Time Delay (ε_o = .1, σ_h/λ = 5, Geometry 1)

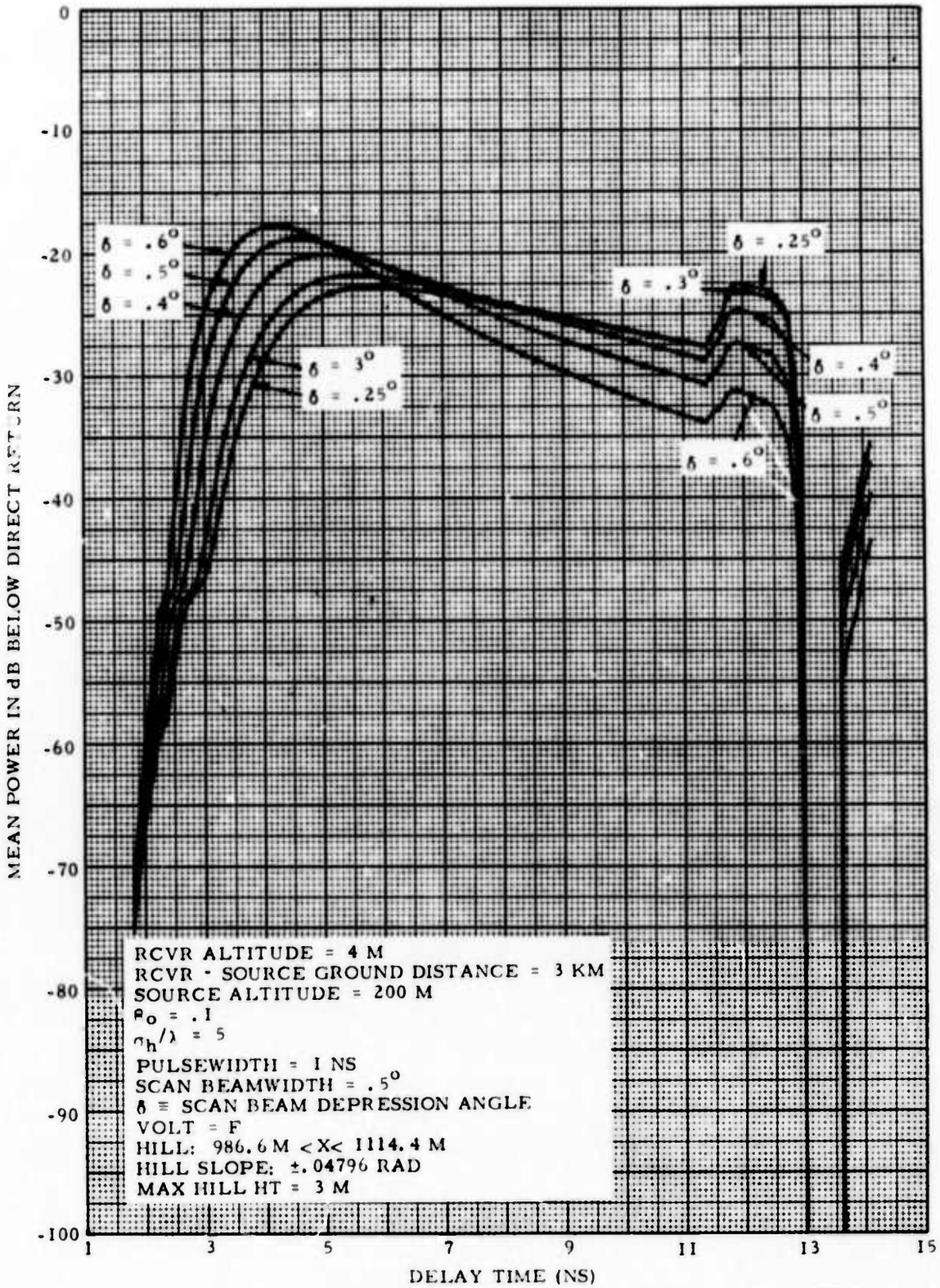

Figure 50. Multipath Power Curves, Mean Power vs Time Delay (β_o = .1, σ_h/λ = 5, Geometry 1, Hill)

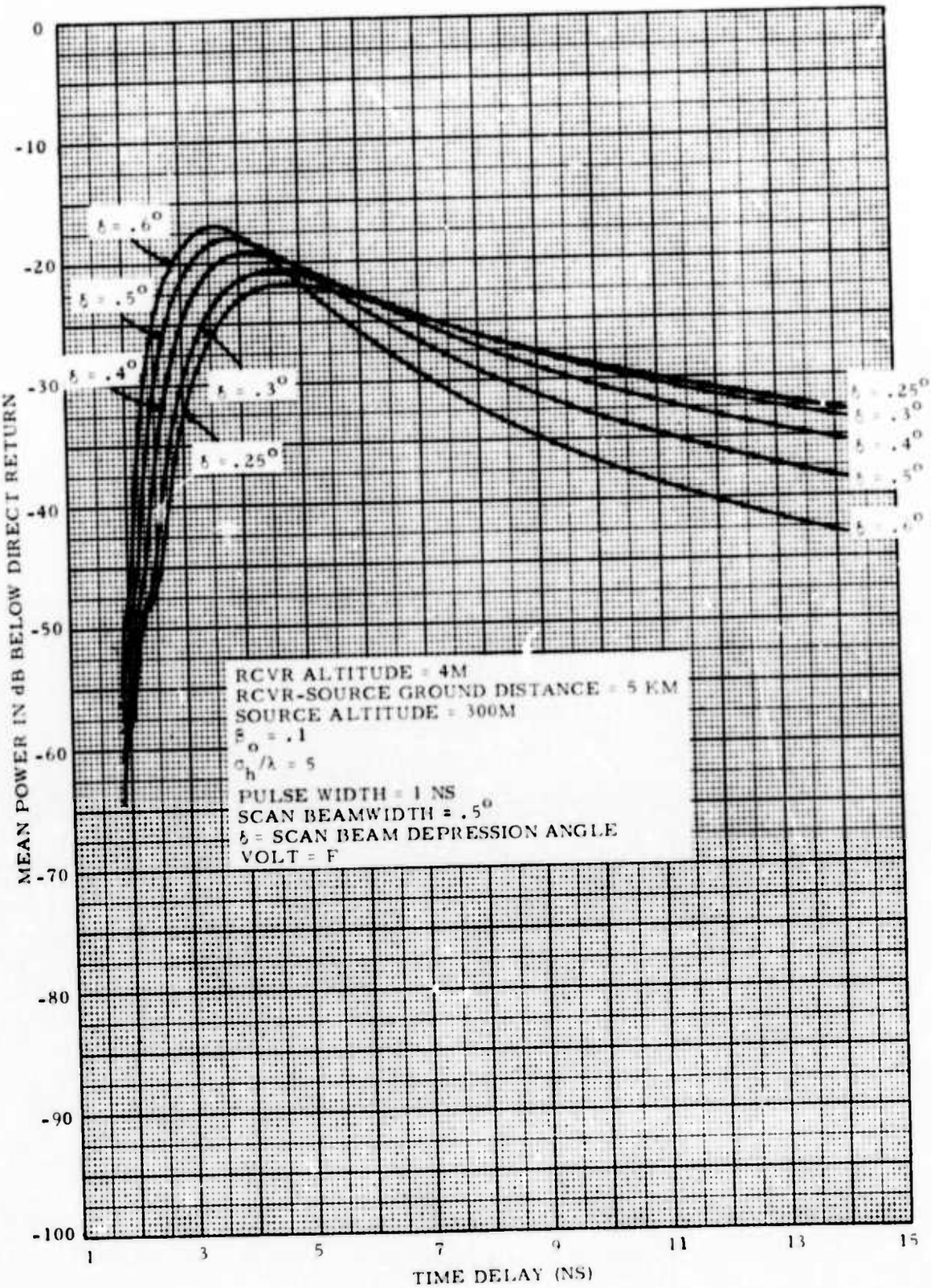

Figure 51. Multipath Power Curves, Mean Power vs Time Delay (θ_o = .1, σ_h/λ = 5, Geometry 2)

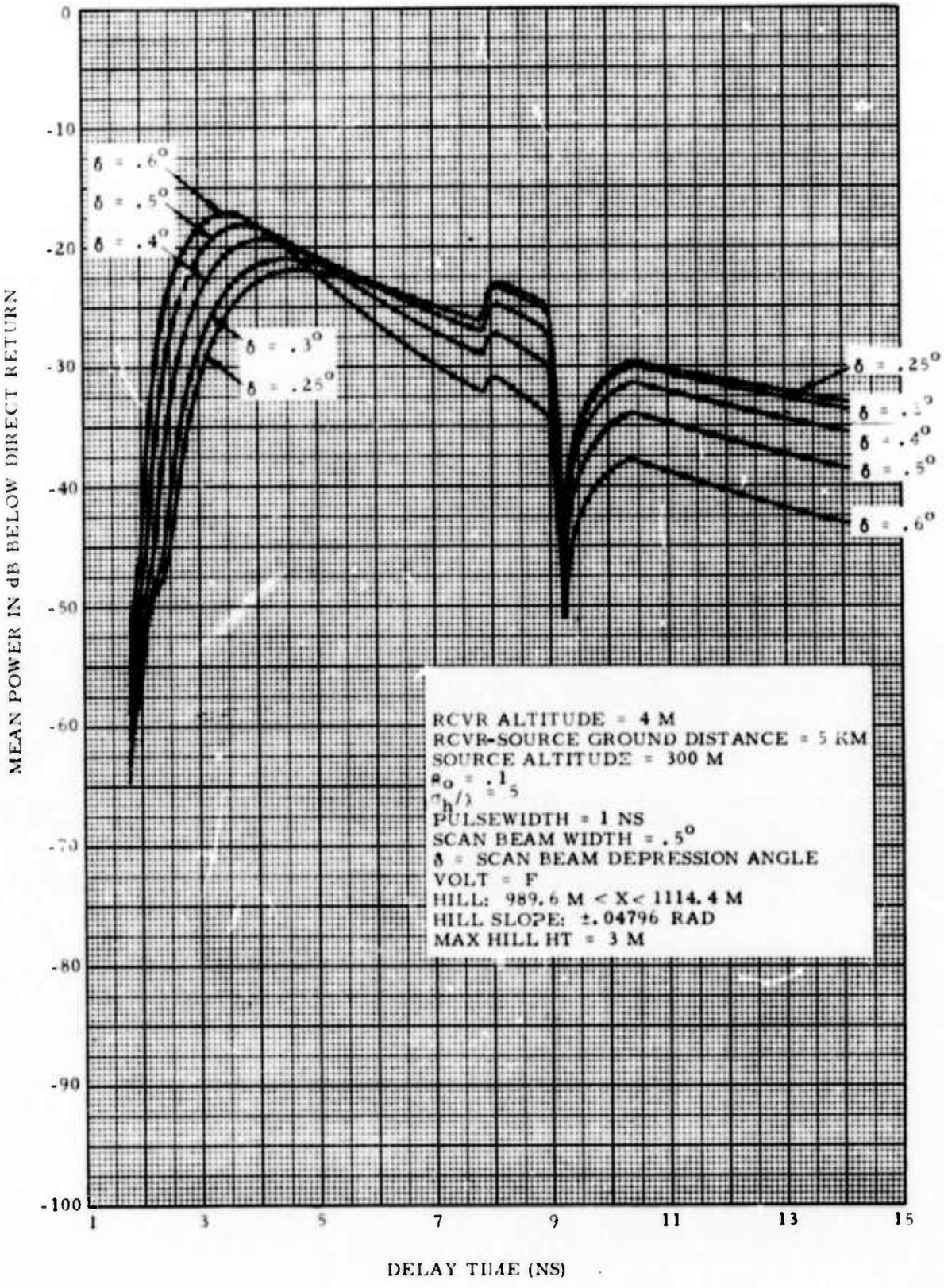

Figure 52. Multipath Power Curves, Mean Power vs Time Delay (β_o = .1, σ_h/λ = 5, Geometry 2, Hill)

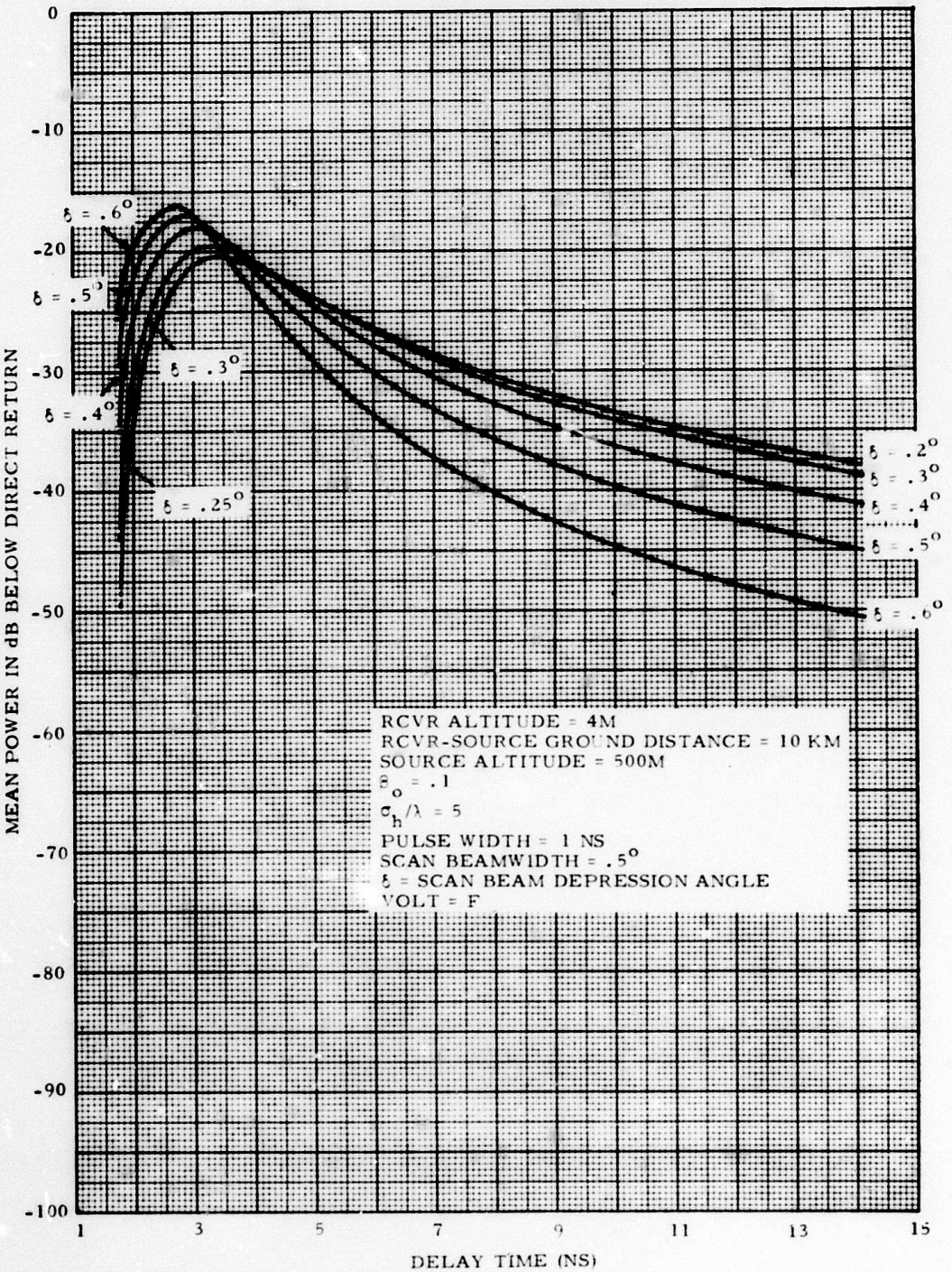

Figure 53. Multipath Power Curves, Mean Power vs Time Delay (β_o = .1, σ_h/λ = 5, Geometry 3)

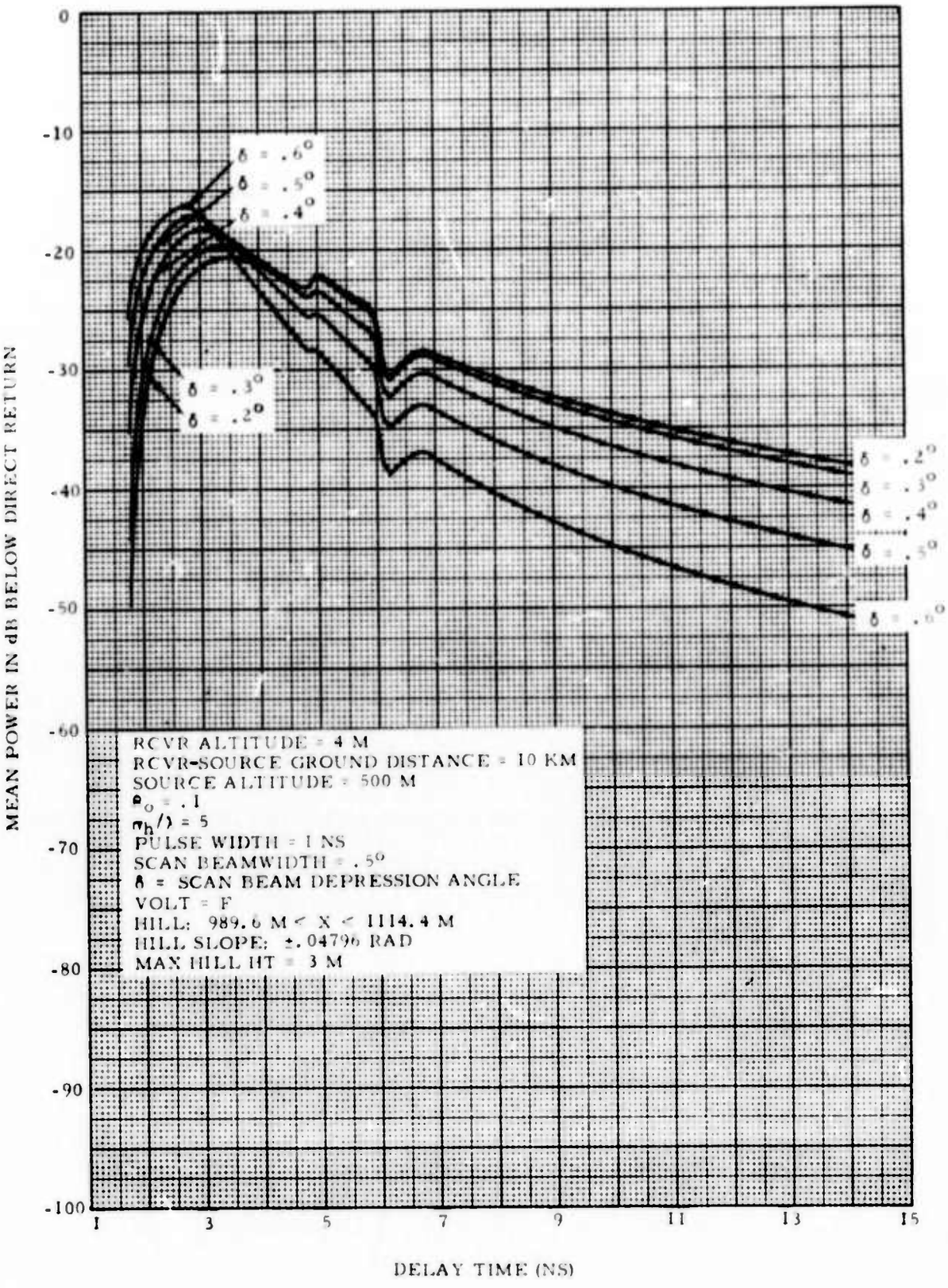

Figure 54. Multipath Power Curves, Mean Power vs Time Delay (θ_o = .1, σ_h/λ = 5, Geometry 3, Hill)

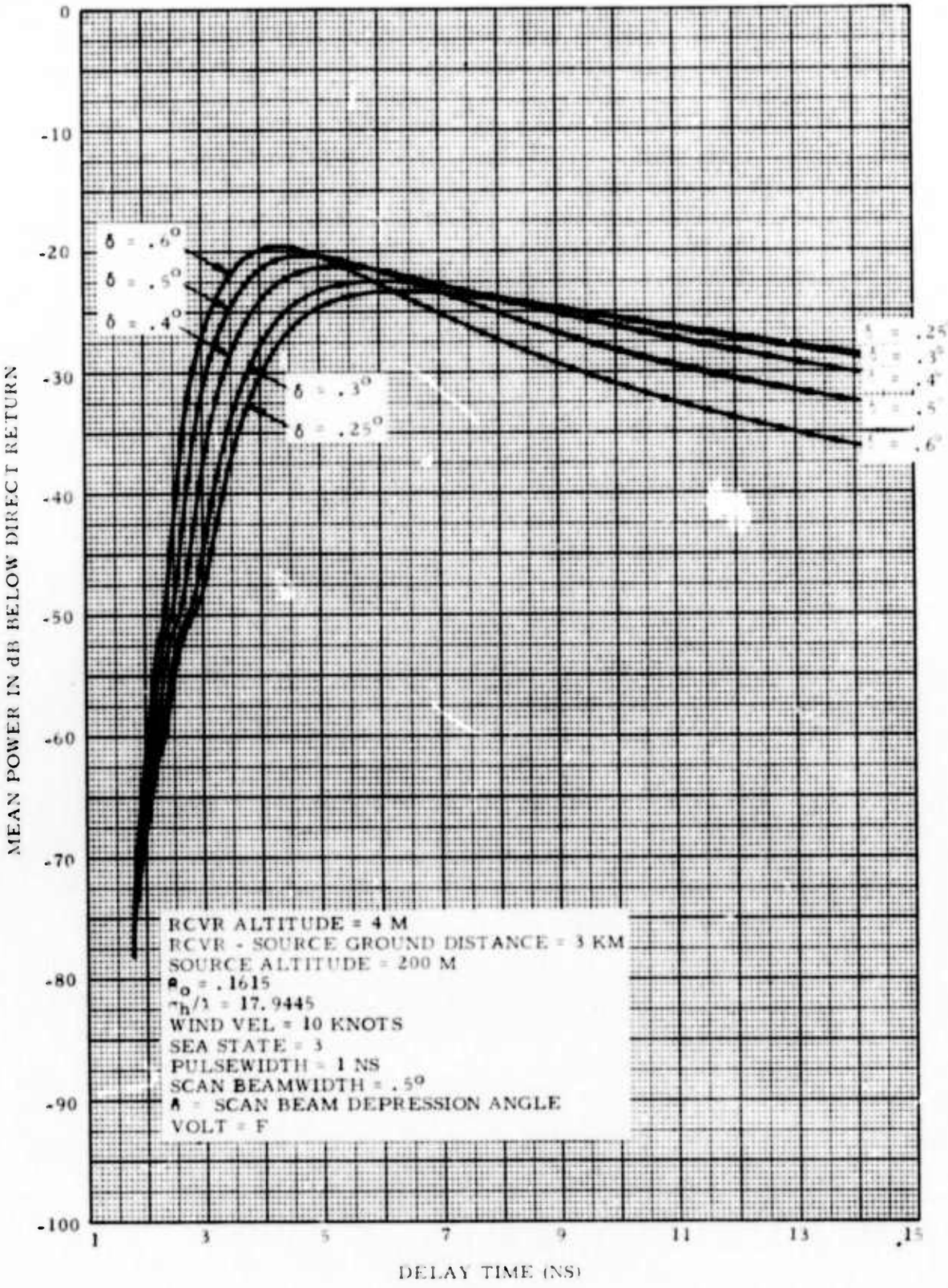

Figure 55. Multipath Power Curves, Mean Power vs Time Delay (over water-sea state 3)

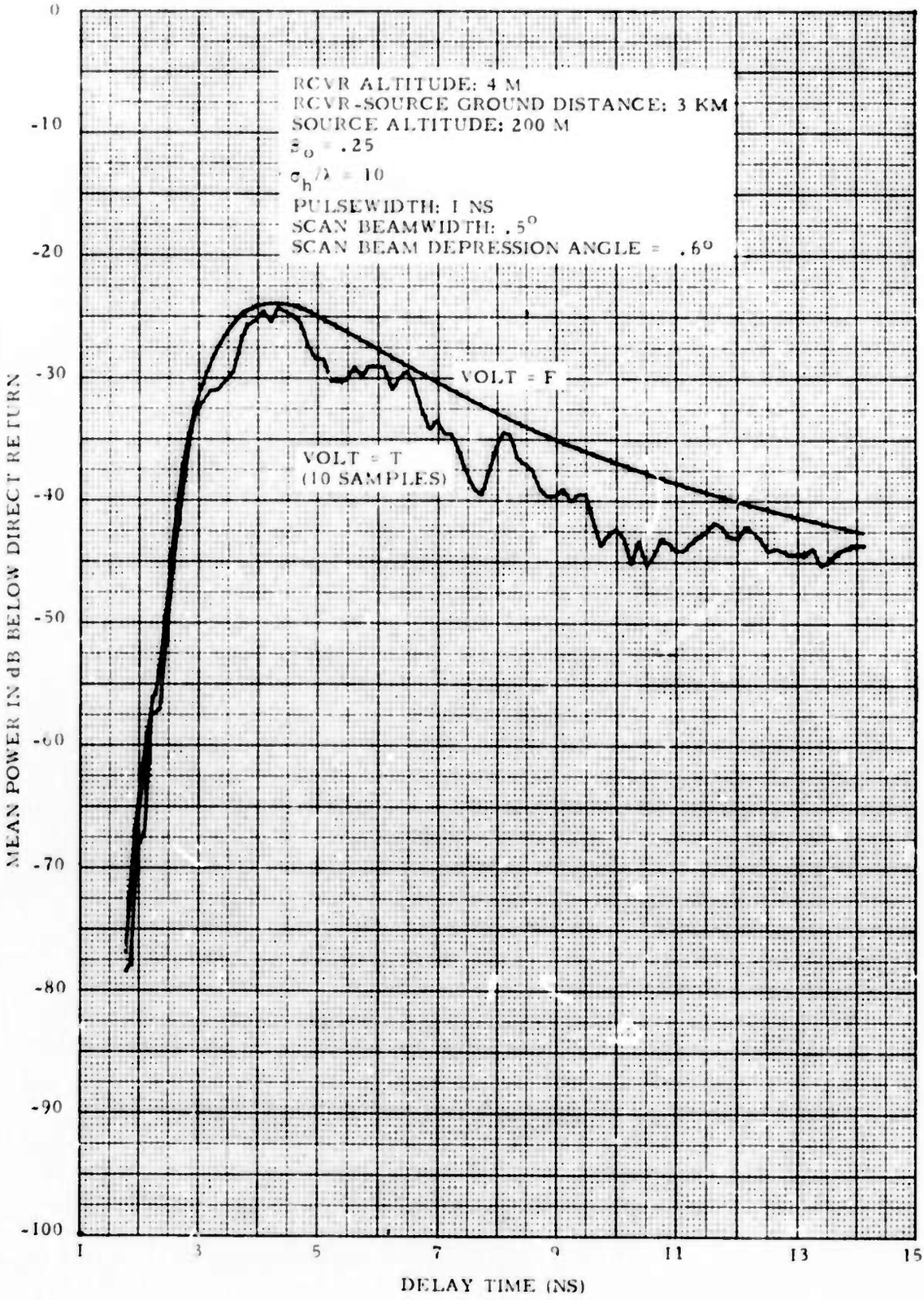

Figure 56. Multipath Power Curves, Mean Power vs Time Delay (ρ_o = .25, σ_h/λ = 10, Geometry 1, δ = .6°)

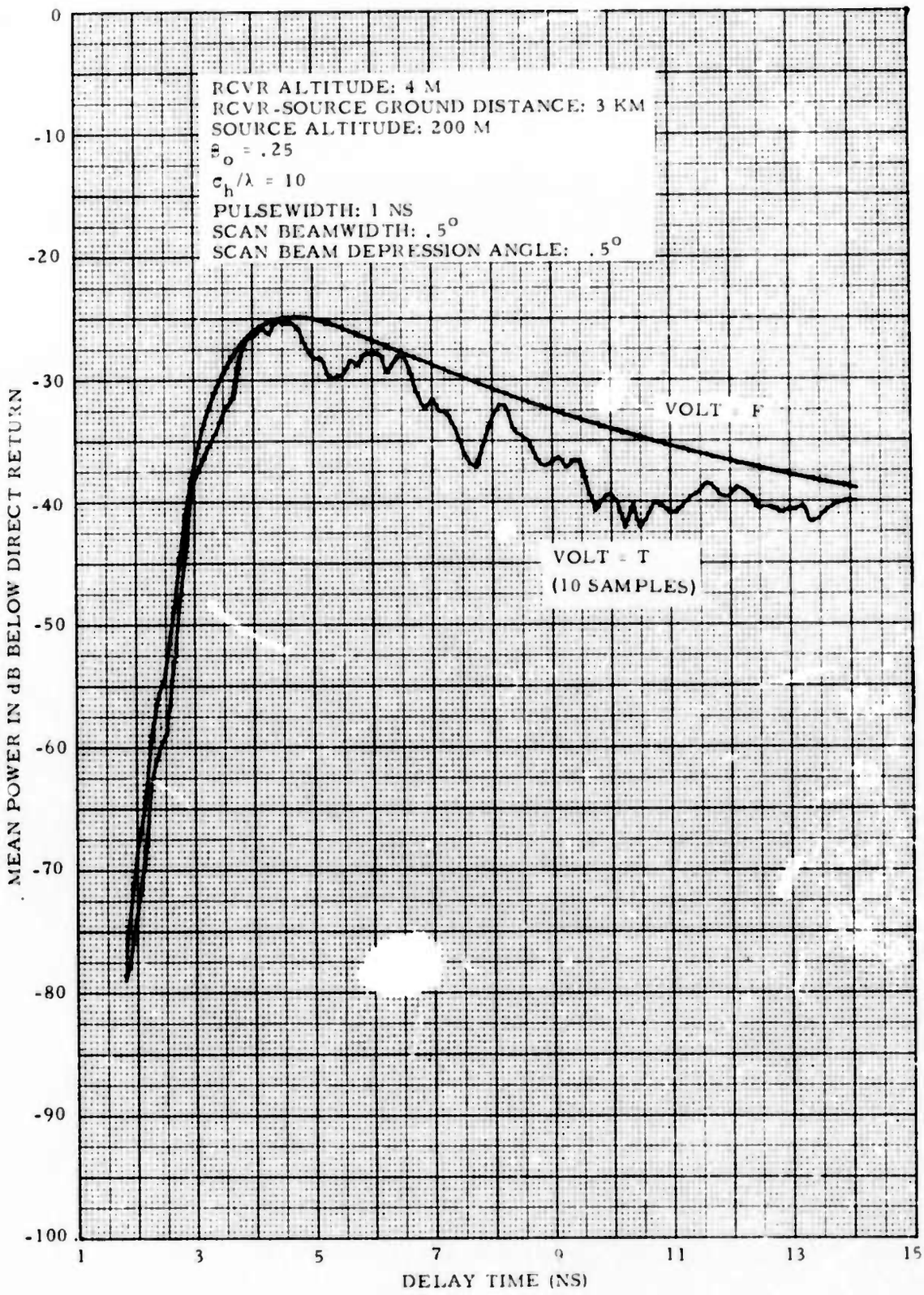

Figure 57. Multipath Power Curves, Mean Power vs Time Delay (β_o = .25, σ_h/λ = 10, Geometry 1, δ = .5°)

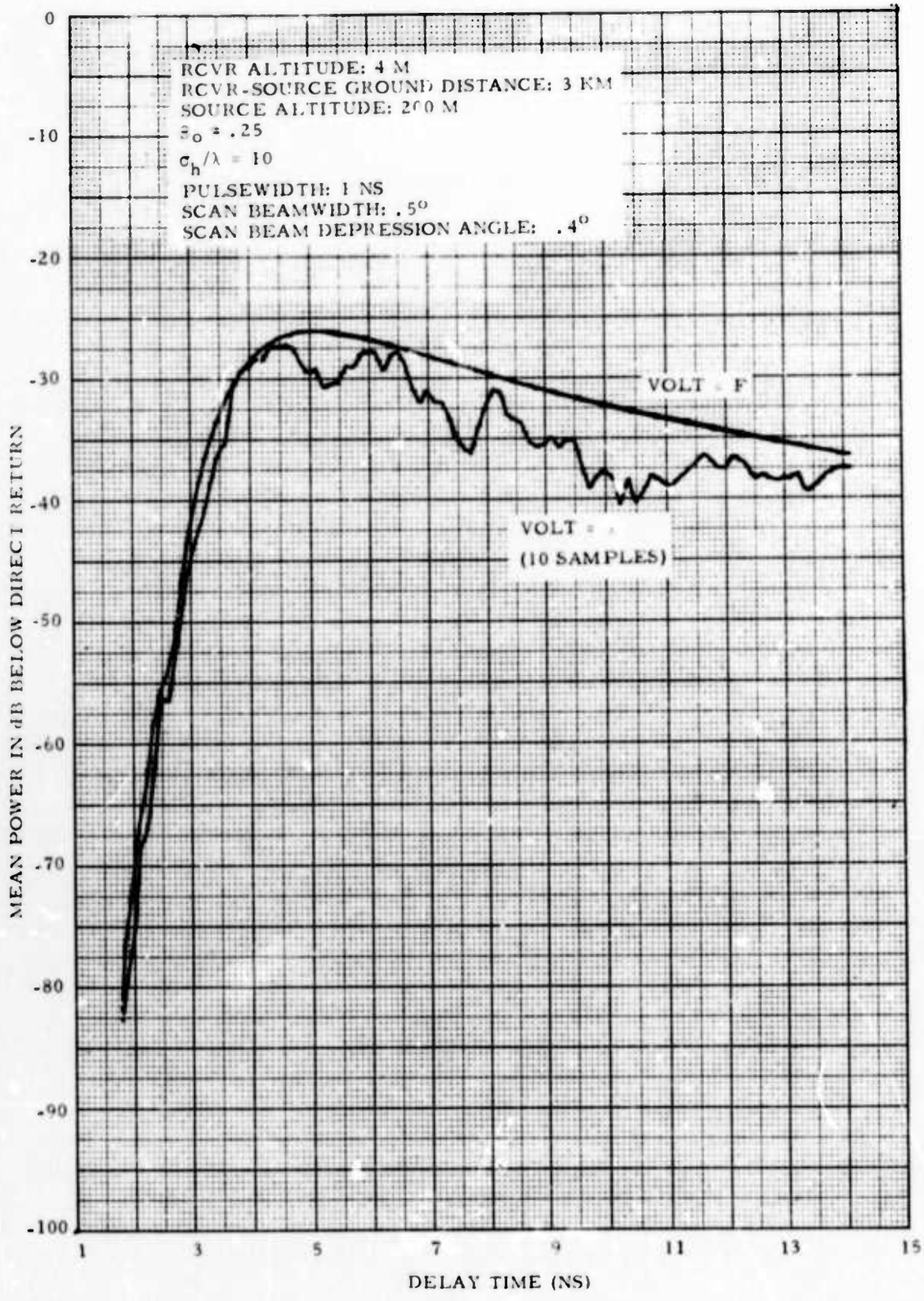

Figure 58. Multipath Power Curves, Mean Power vs Time Delay (β_o = .25, σ_h/λ = 10, Geometry 1, δ = .4°)

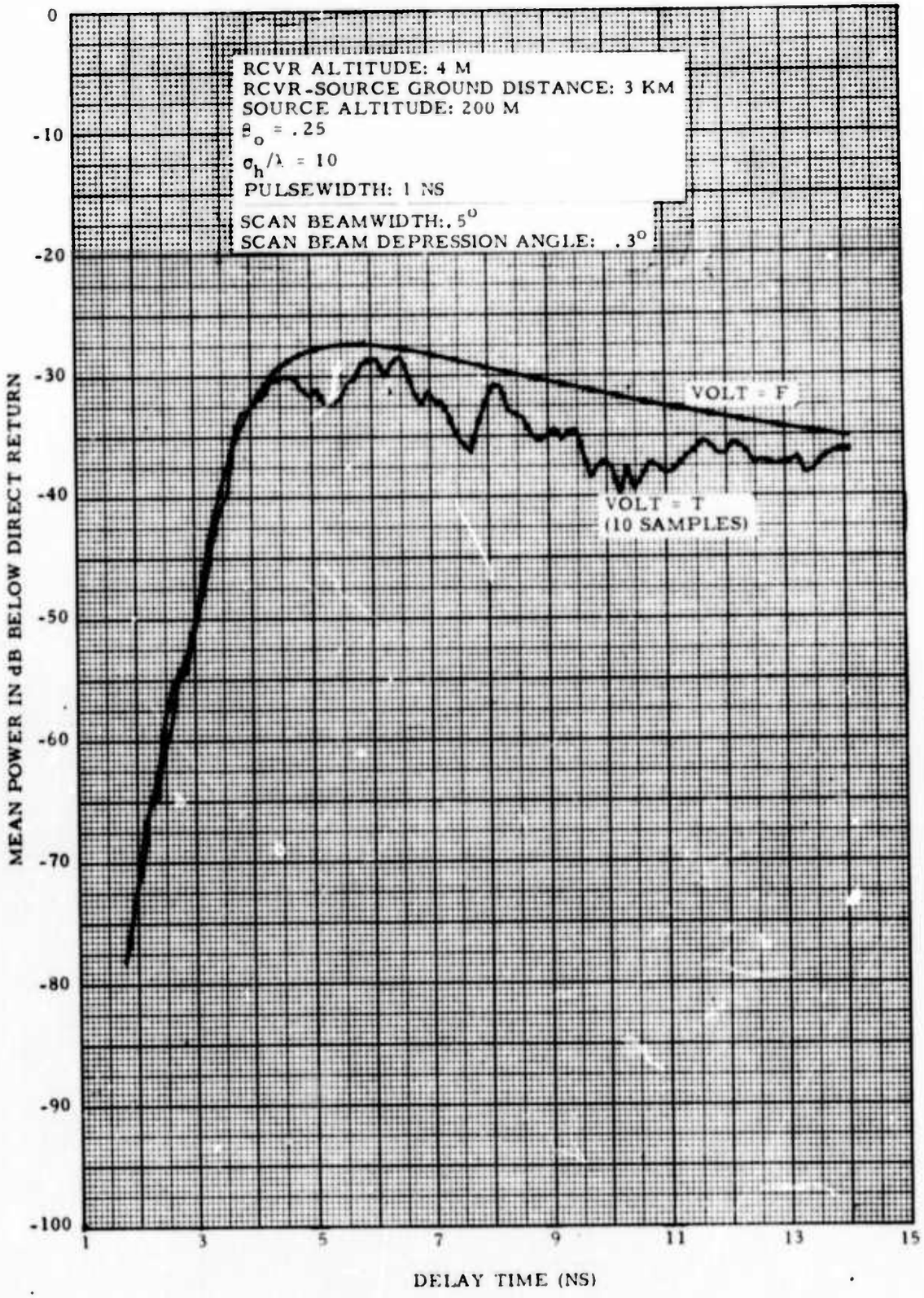

Figure 59. Multipath Power Curves, Mean Power vs Time Delay (B_o = .25, σ_h/λ = 10, Geometry 1, δ = .3°)

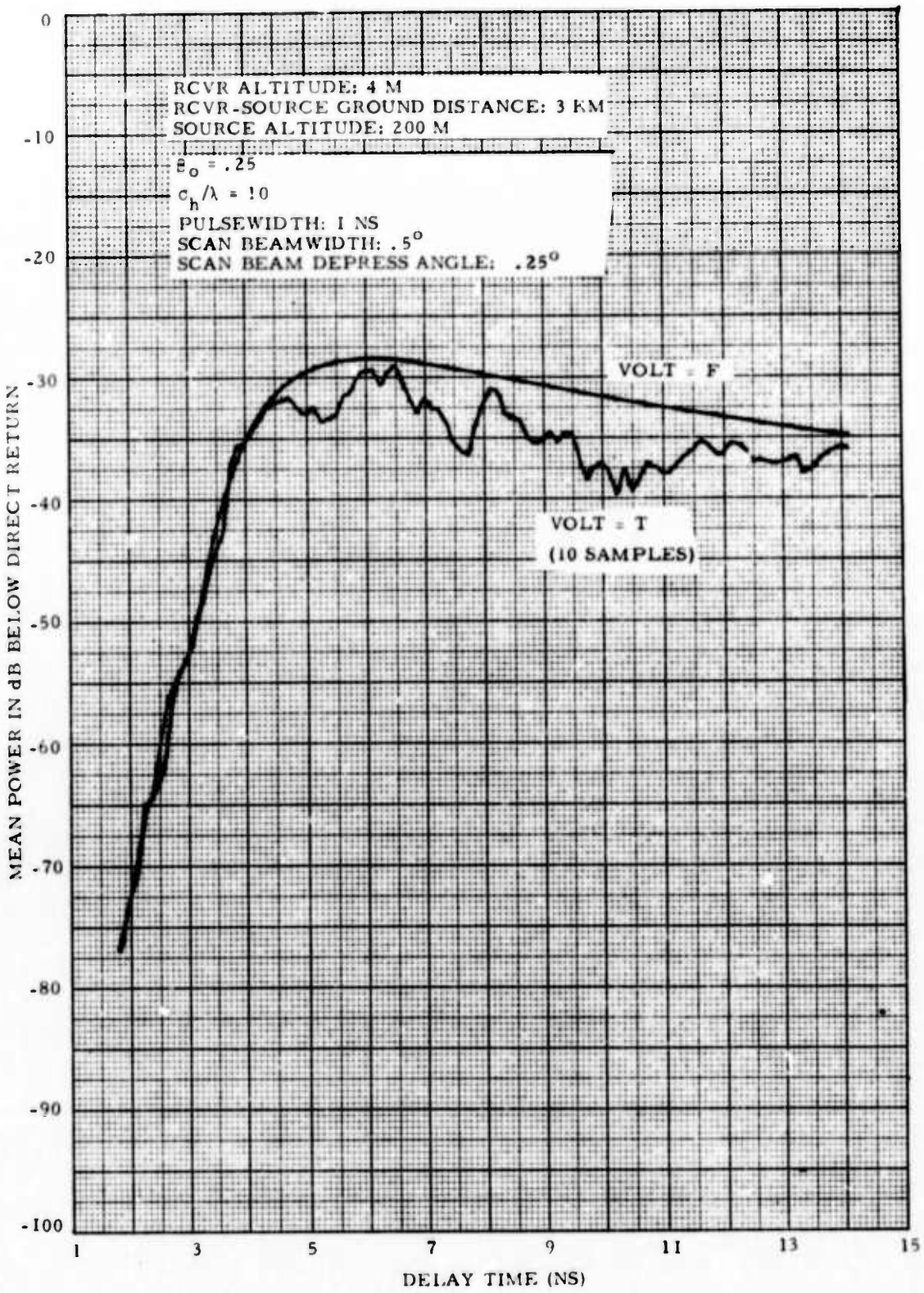

Figure 60. Multipath Power Curves, Mean Power vs Time Delay (β_o = .25, σ_h/λ = 10, Geometry 1, δ = .25°)

SECTION 5. RECOMMENDATIONS FOR PHASES II AND III

The material presented in the previous sections represents a comprehensive study of the feasibility of performing and carefully interpreting meaningful diffuse reflectivity measurements. The techniques developed appear promising and it is believed that the equipment can be assembled quickly so that measurements can begin early in the spring of 1975.

Figure 61. is a tentative recommended schedule for carrying out Phase II, Measurements and Data Reduction. Phase II would be performed over an 18 month period, terminating in April 1976. Phase III, Comprehensive Reporting, would follow directly, concluding after six months with the publication of a handbook of surface reflectivity incorporating all the latest information. The total effort would be completed over a two year period, which allows adequate time for gathering data over varying terrain/ocean sites during all seasons of the year.

It is recommended that the first three measurements sequences be performed at Otis AFB, Race Point Coast Guard Station, and Westover AFB in that order. Subsequent measurements will be made over more complex terrain to be selected after experience with initial measurement activity has been gathered. As the seasons change a few sites will be revisited to obtain comparative data. Analysis effort will be interspersed with measurement activity. This procedure will contribute to continual improvement of technique and it will also insure true availability of up-to-date reflectivity information.

Phase II would begin in November 1974 with a four month preparation period during the winter months during which equipments would be ordered, constructed, assembled and checked out. In addition, analysis software would be generated to permit accurate interpretation of measurements in terms of the current diffuse reflectivity theory. Final preparation would be made at the first site (Otis) and measurements would begin in March assuming that all snow had cleared away, which is normally the case at that time of year. Data analysis would be performed at Raytheon, Wayland immediately following the measurements.

The measurement, analysis pattern would recur a number of times through March 1976, with measurements in January and February constituting winter repeats at sites visited earlier. Consolidated data analysis would then be performed and issued in a Final Report early in May 1976.

The plan for Phase II will be provided in greater detail in a formal proposal soon after submittal of this report.

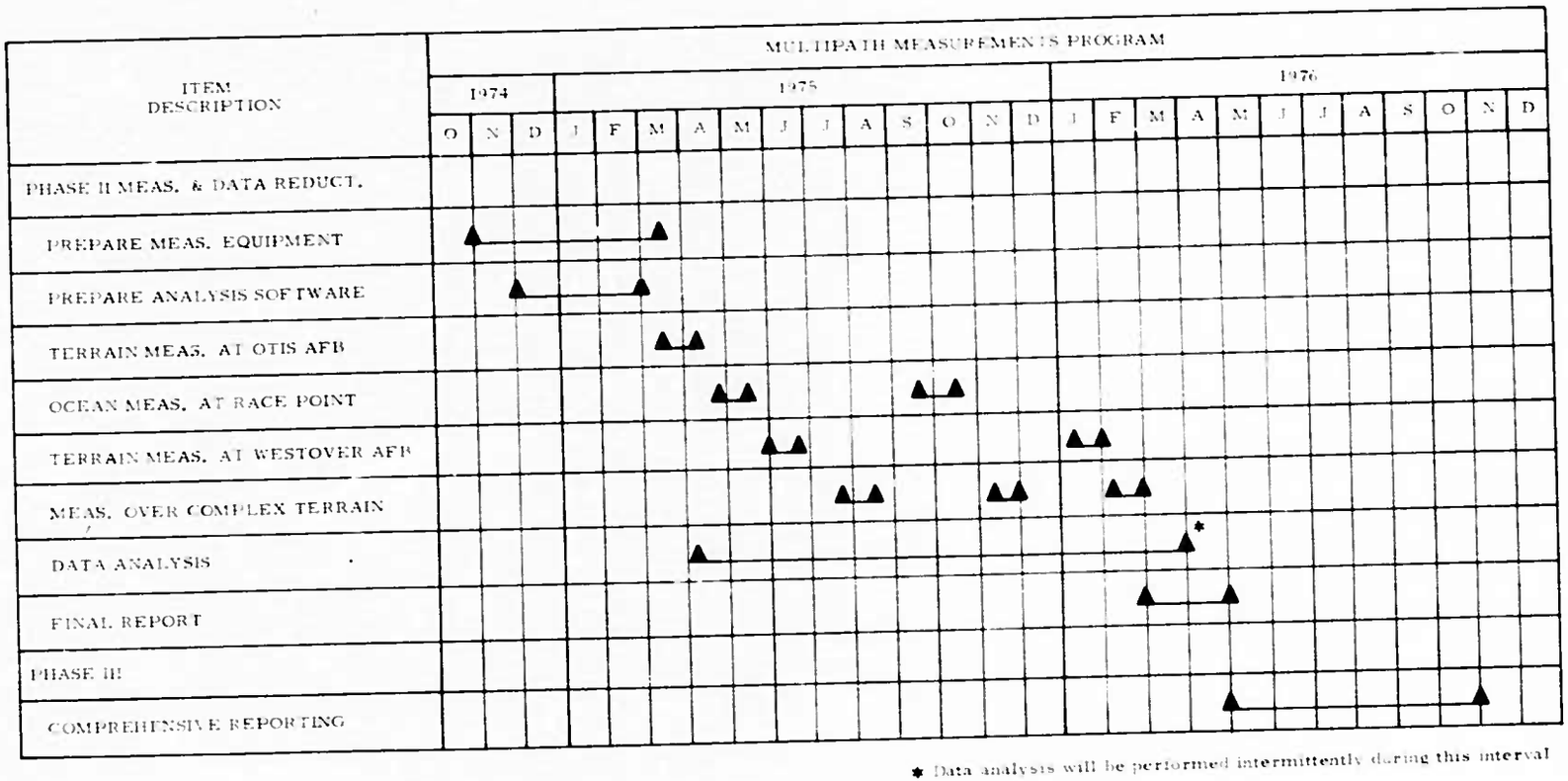

Figure 61. Recommended Schedule- Phases II and III

APPENDIX A
MULTIPATH COMPUTER SIMULATION FLOW CHART

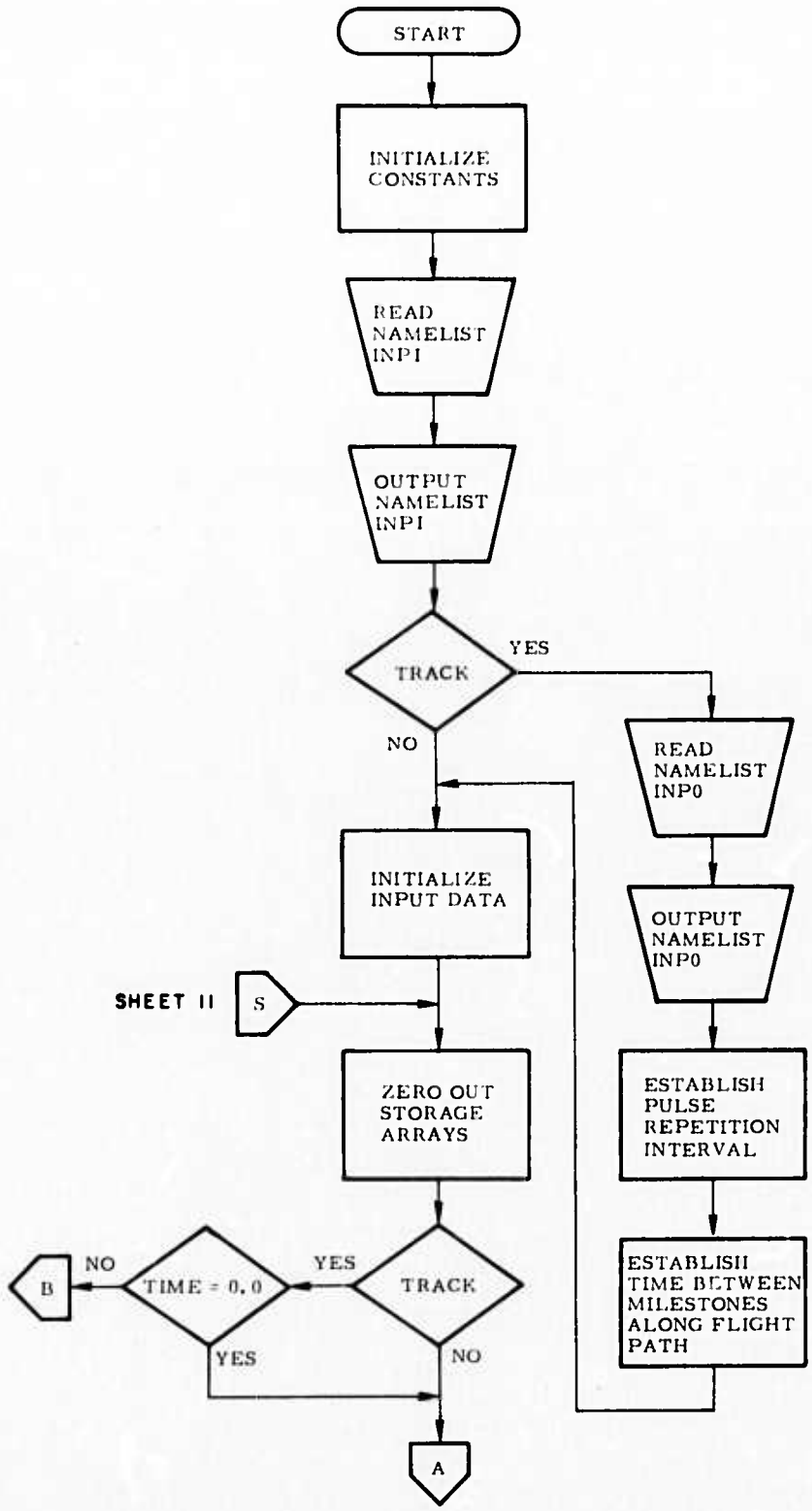

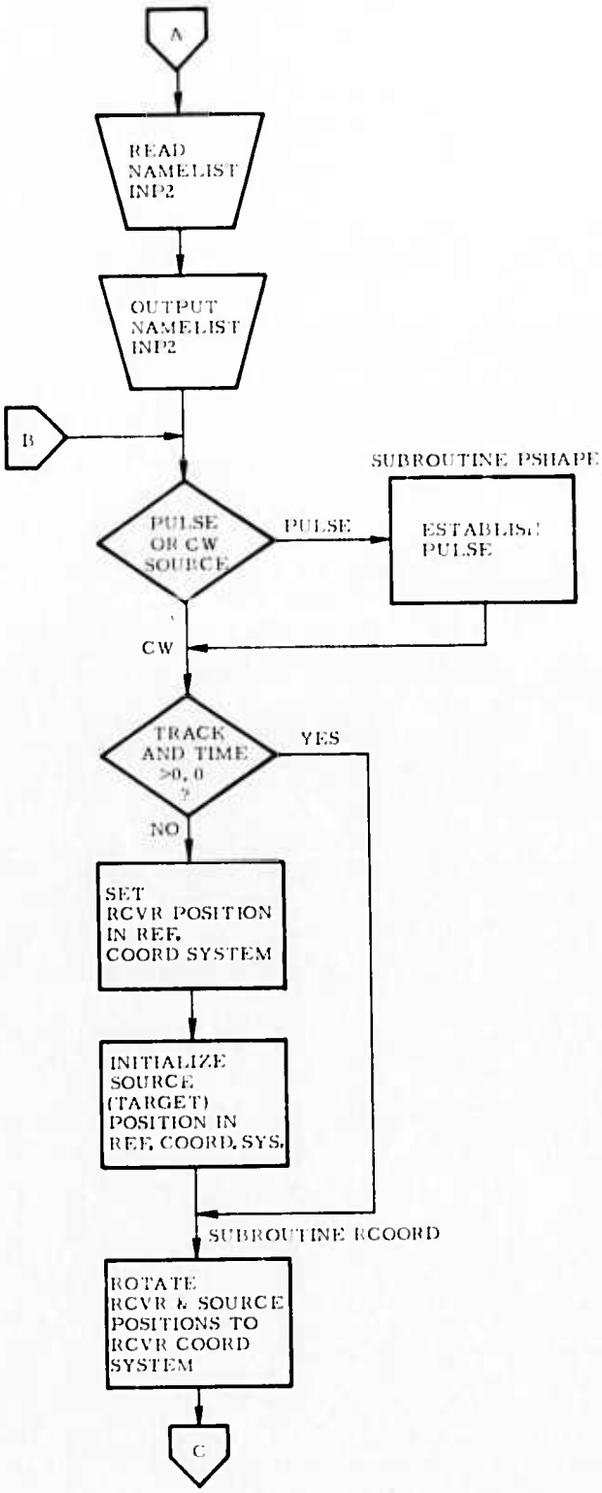
A
READ NAMELIST INP2
OUTPUT NAMELIST INP2
B
SUBROUTINE PSHAPE
PULSE OR CW SOURCE
PULSE
ESTABLISH PULSE
CW
TRACK AND TIME >0.0
YES
NO
SET RCVR POSITION IN REF. COORD SYSTEM
INITIALIZE SOURCE (TARGET) POSITION IN REF. COORD. SYS.
SUBROUTINE RCOORD
ROTATE RCVR & SOURCE POSITIONS TO RCVR COORD SYSTEM
C

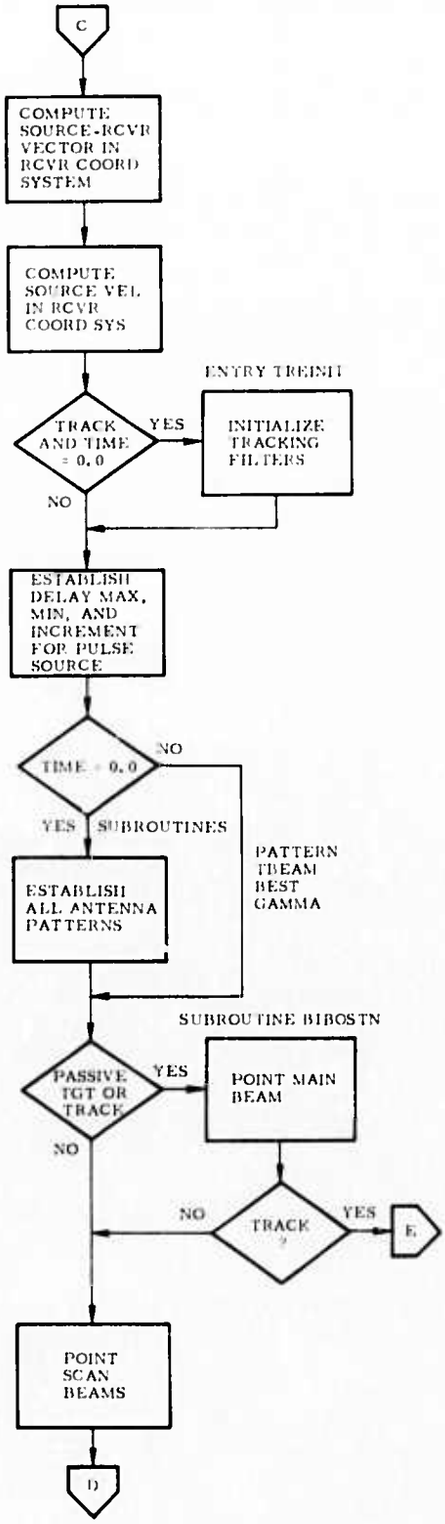
C
COMPUTE SOURCE-RCVR VECTOR IN RCVR COORD SYSTEM
COMPUTE SOURCE VEL IN RCVR COORD SYS
ENTRY TREINIT
TRACK AND TIME = 0.0
YES
INITIALIZE TRACKING FILTERS
NO
ESTABLISH DELAY MAX, MIN, AND INCREMENT FOR PULSE SOURCE
TIME = 0.0
NO
YES
SUBROUTINES
ESTABLISH ALL ANTENNA PATTERNS
PATTERN
TBEAM
BEST
GAMMA
SUBROUTINE BIBOSTN
PASSIVE TGT OR TRACK
YES
POINT MAIN BEAM
NO
NO
TRACK
YES
E
POINT SCAN BEAMS
D

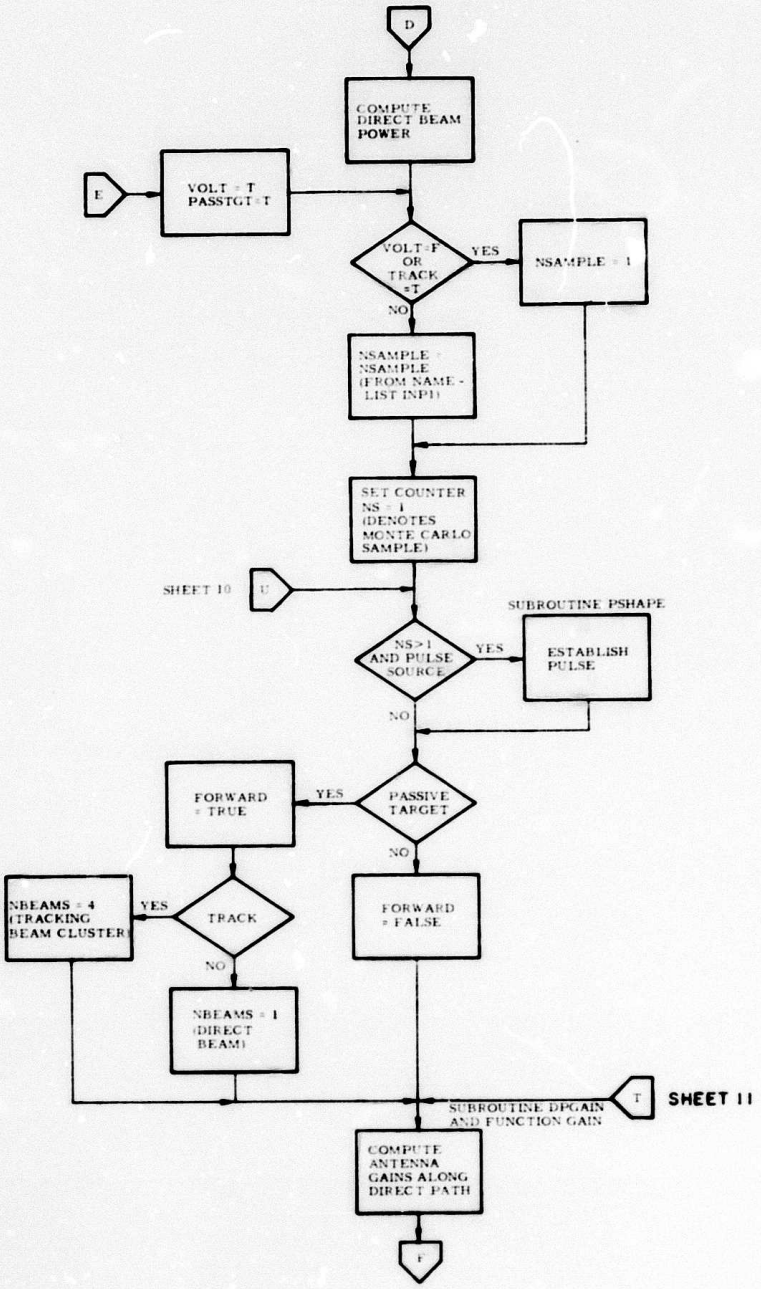
D
COMPUTE DIRECT BEAM POWER
E
VOLT = T PASSTGT=T
VOLT=F OR TRACK =T
YES
NSAMPLE = 1
NO
NSAMPLE = NSAMPLE (FROM NAME-LIST INPT)
SET COUNTER NS = 1 (DENOTES MONTE CARLO SAMPLE)
SHEET 10
U
SUBROUTINE PSHAPE
NS>1 AND PULSE SOURCE
YES
ESTABLISH PULSE
NO
FORWARD = TRUE
YES
PASSIVE TARGET
NO
NBEAMS = 4 (TRACKING BEAM CLUSTER)
YES
TRACK
FORWARD = FALSE
NO
NBEAMS = 1 (DIRECT BEAM)
T
SHEET 11
SUBROUTINE DFGAIN AND FUNCTION GAIN
COMPUTE ANTENNA GAINS ALONG DIRECT PATH
F

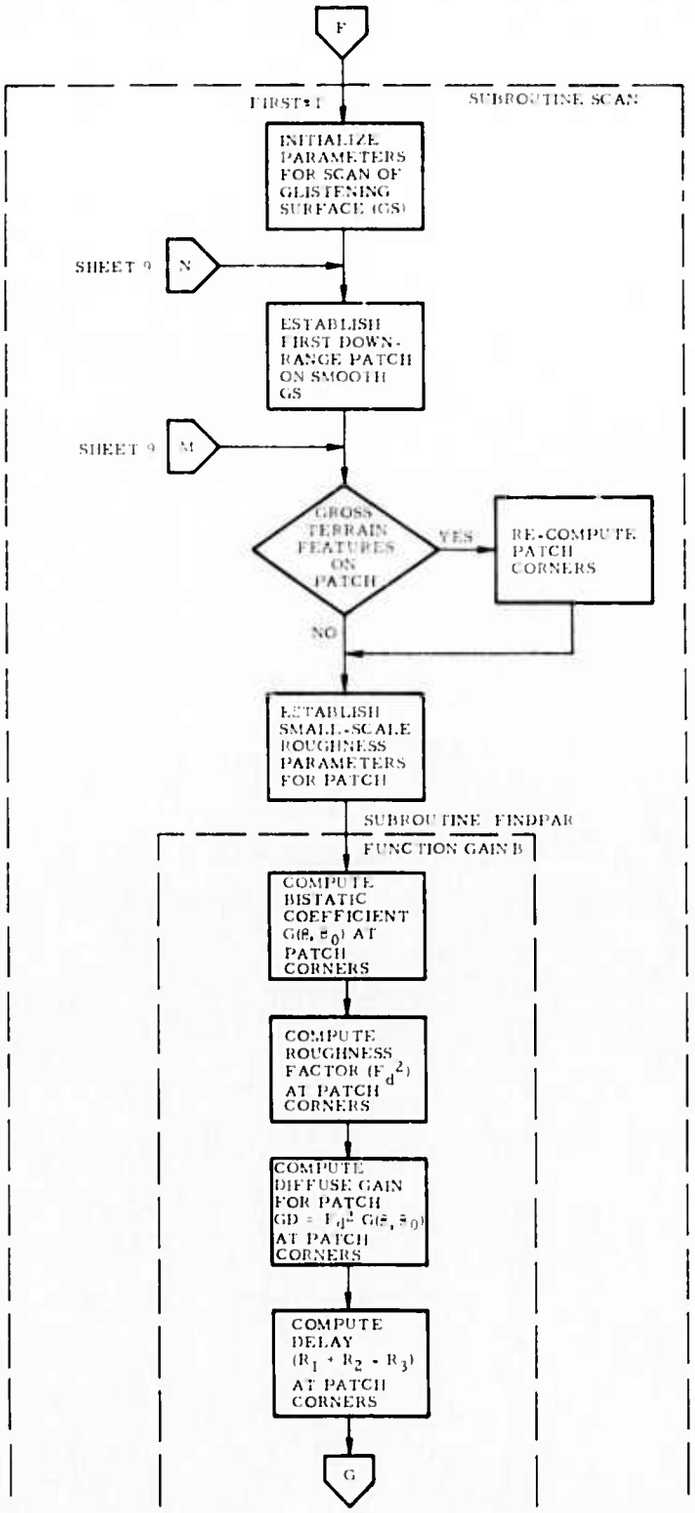
F
SUBROUTINE SCAN
FIRST=1
INITIALIZE PARAMETERS FOR SCAN OF GLISTENING SURFACE (GS)
SHEET 9
N
ESTABLISH FIRST DOWN-RANGE PATCH ON SMOOTH GS
SHEET 9
M
GROSS TERRAIN FEATURES ON PATCH
YES
RE-COMPUTE PATCH CORNERS
NO
ESTABLISH SMALL-SCALE ROUGHNESS PARAMETERS FOR PATCH
SUBROUTINE FINDPAR
FUNCTION GAINB
COMPUTE BISTATIC COEFFICIENT $G(\theta, \theta_0)$ AT PATCH CORNERS
COMPUTE ROUGHNESS FACTOR (F_d^2) AT PATCH CORNERS
COMPUTE DIFFUSE GAIN FOR PATCH $GD = F_d^2 G(\theta, \theta_0)$ AT PATCH CORNERS
COMPUTE DELAY $(R_1 + R_2 - R_3)$ AT PATCH CORNERS
G

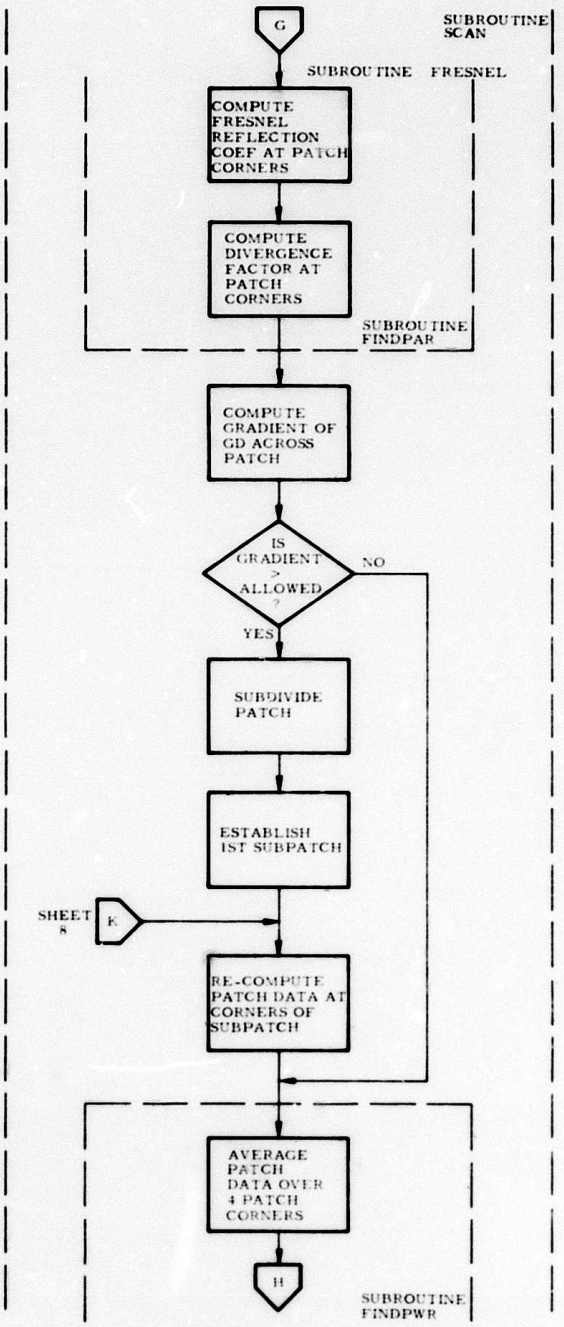
G
SUBROUTINE SCAN
SUBROUTINE FRESNEL
COMPUTE FRESNEL REFLECTION COEF AT PATCH CORNERS
COMPUTE DIVERGENCE FACTOR AT PATCH CORNERS
SUBROUTINE FINDPAR
COMPUTE GRADIENT OF GD ACROSS PATCH
IS GRADIENT > ALLOWED ?
NO
YES
SUBDIVIDE PATCH
ESTABLISH IST SUBPATCH
SHEET 8
K
RE-COMPUTE PATCH DATA AT CORNERS OF SUBPATCH
AVERAGE PATCH DATA OVER 4 PATCH CORNERS
H
SUBROUTINE FINDPWR

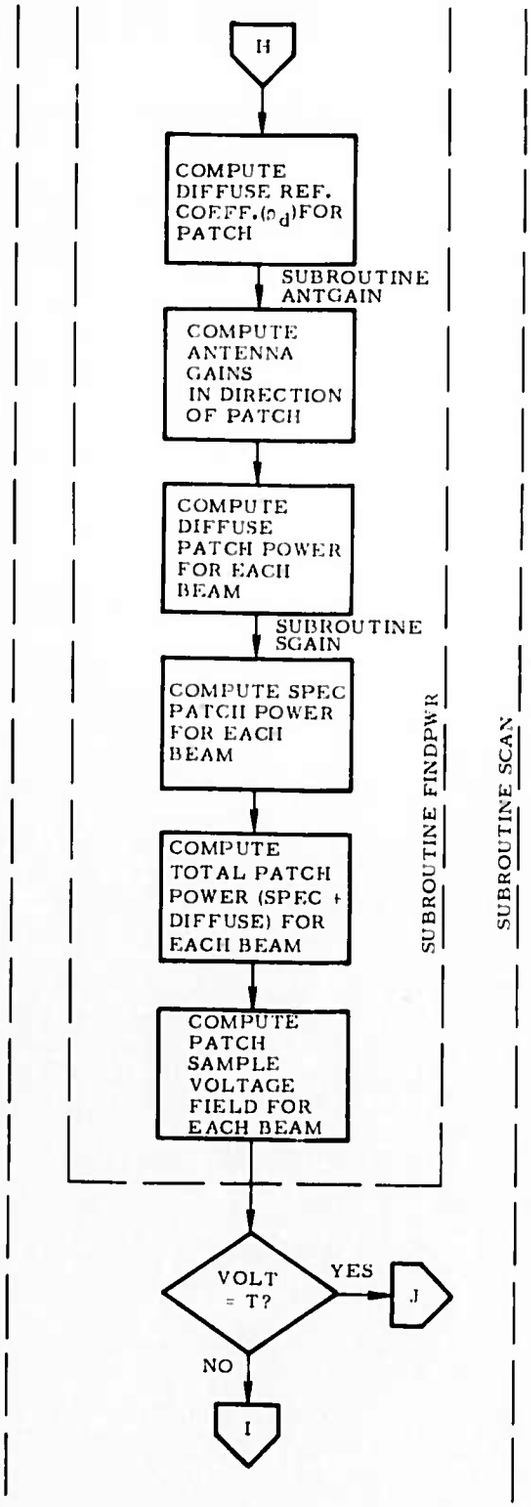
H
COMPUTE DIFFUSE REF. COEFF. (ρ_d) FOR PATCH
SUBROUTINE ANTGAIN
COMPUTE ANTENNA GAINS IN DIRECTION OF PATCH
COMPUTE DIFFUSE PATCH POWER FOR EACH BEAM
SUBROUTINE SGAIN
COMPUTE SPEC PATCH POWER FOR EACH BEAM
COMPUTE TOTAL PATCH POWER (SPEC + DIFFUSE) FOR EACH BEAM
COMPUTE PATCH SAMPLE VOLTAGE FIELD FOR EACH BEAM
SUBROUTINE FINDPWR
SUBROUTINE SCAN
VOLT = T?
YES
J
NO
I

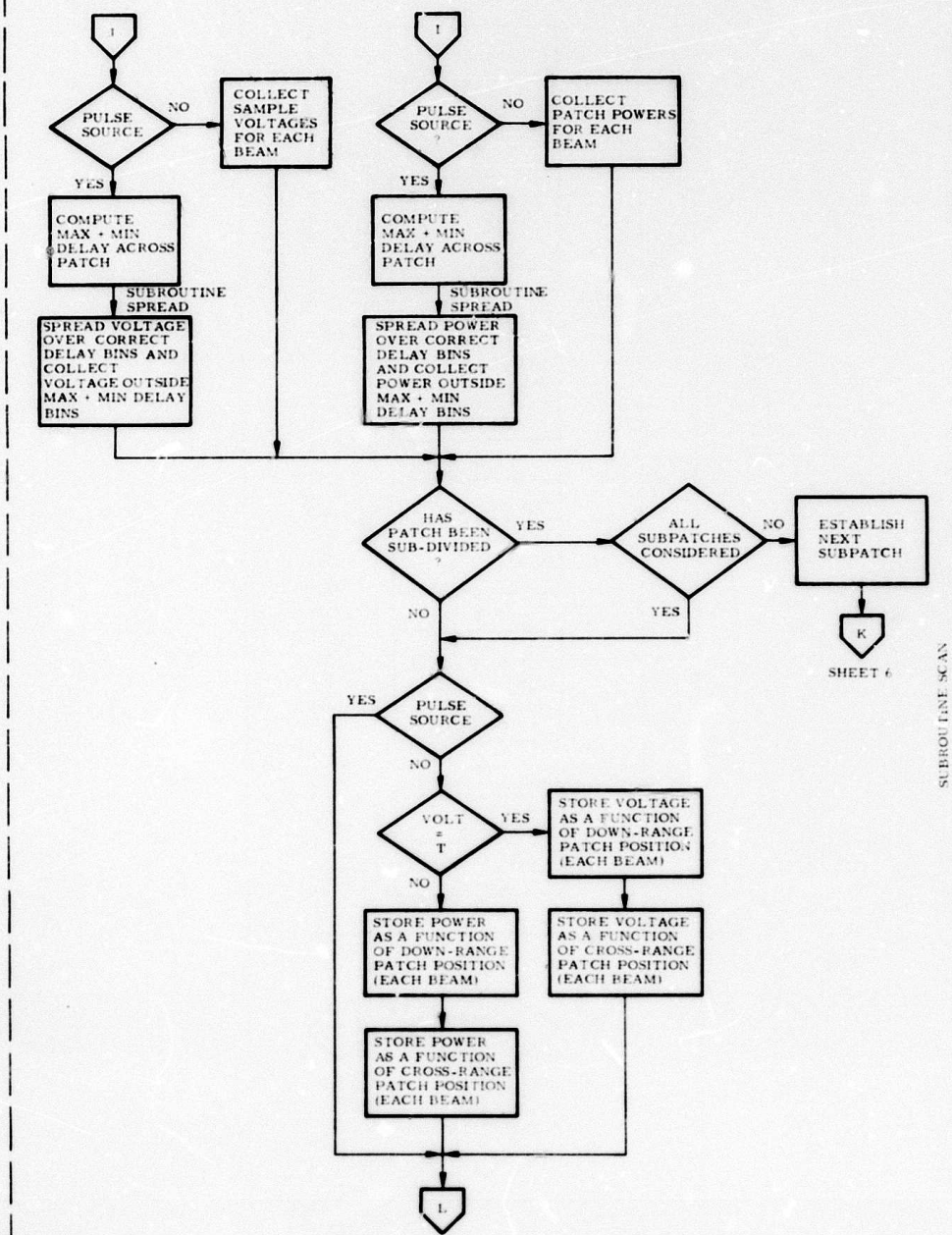
I
PULSE SOURCE ?
NO
COLLECT SAMPLE VOLTAGES FOR EACH BEAM
YES
COMPUTE MAX + MIN DELAY ACROSS PATCH
SUBROUTINE SPREAD
SPREAD VOLTAGE OVER CORRECT DELAY BINS AND COLLECT VOLTAGE OUTSIDE MAX + MIN DELAY BINS
I
PULSE SOURCE ?
NO
COLLECT PATCH POWERS FOR EACH BEAM
YES
COMPUTE MAX + MIN DELAY ACROSS PATCH
SUBROUTINE SPREAD
SPREAD POWER OVER CORRECT DELAY BINS AND COLLECT POWER OUTSIDE MAX + MIN DELAY BINS
HAS PATCH BEEN SUB-DIVIDED ?
YES
ALL SUBPATCHES CONSIDERED
NO
ESTABLISH NEXT SUBPATCH
K
SHEET 6
YES
NO
PULSE SOURCE ?
YES
NO
VOLT = T
YES
STORE VOLTAGE AS A FUNCTION OF DOWN-RANGE PATCH POSITION (EACH BEAM)
NO
STORE POWER AS A FUNCTION OF DOWN-RANGE PATCH POSITION (EACH BEAM)
STORE VOLTAGE AS A FUNCTION OF CROSS-RANGE PATCH POSITION (EACH BEAM)
STORE POWER AS A FUNCTION OF CROSS-RANGE PATCH POSITION (EACH BEAM)
L
SUBROUTINE SCAN

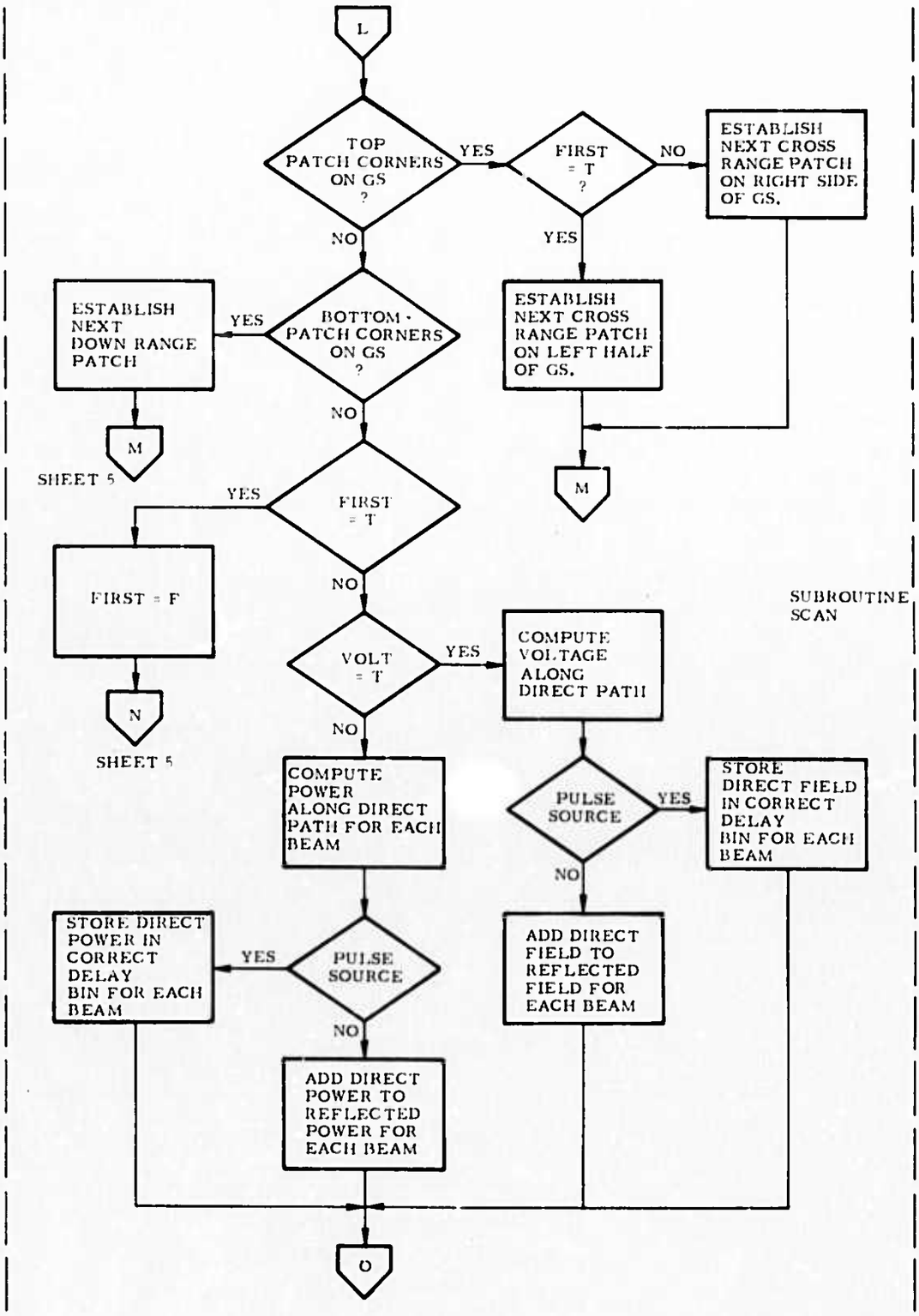
L
TOP PATCH CORNERS ON GS ?
YES
FIRST = T ?
NO
ESTABLISH NEXT CROSS RANGE PATCH ON RIGHT SIDE OF GS.
NO
YES
ESTABLISH NEXT DOWN RANGE PATCH
YES
BOTTOM PATCH CORNERS ON GS ?
ESTABLISH NEXT CROSS RANGE PATCH ON LEFT HALF OF GS.
NO
M
SHEET 5
M
YES
FIRST = T
FIRST = F
NO
SUBROUTINE SCAN
VOLT = T
YES
COMPUTE VOLTAGE ALONG DIRECT PATH
N
SHEET 5
NO
COMPUTE POWER ALONG DIRECT PATH FOR EACH BEAM
PULSE SOURCE
YES
STORE DIRECT FIELD IN CORRECT DELAY BIN FOR EACH BEAM
NO
STORE DIRECT POWER IN CORRECT DELAY BIN FOR EACH BEAM
YES
PULSE SOURCE
ADD DIRECT FIELD TO REFLECTED FIELD FOR EACH BEAM
NO
ADD DIRECT POWER TO REFLECTED POWER FOR EACH BEAM
O

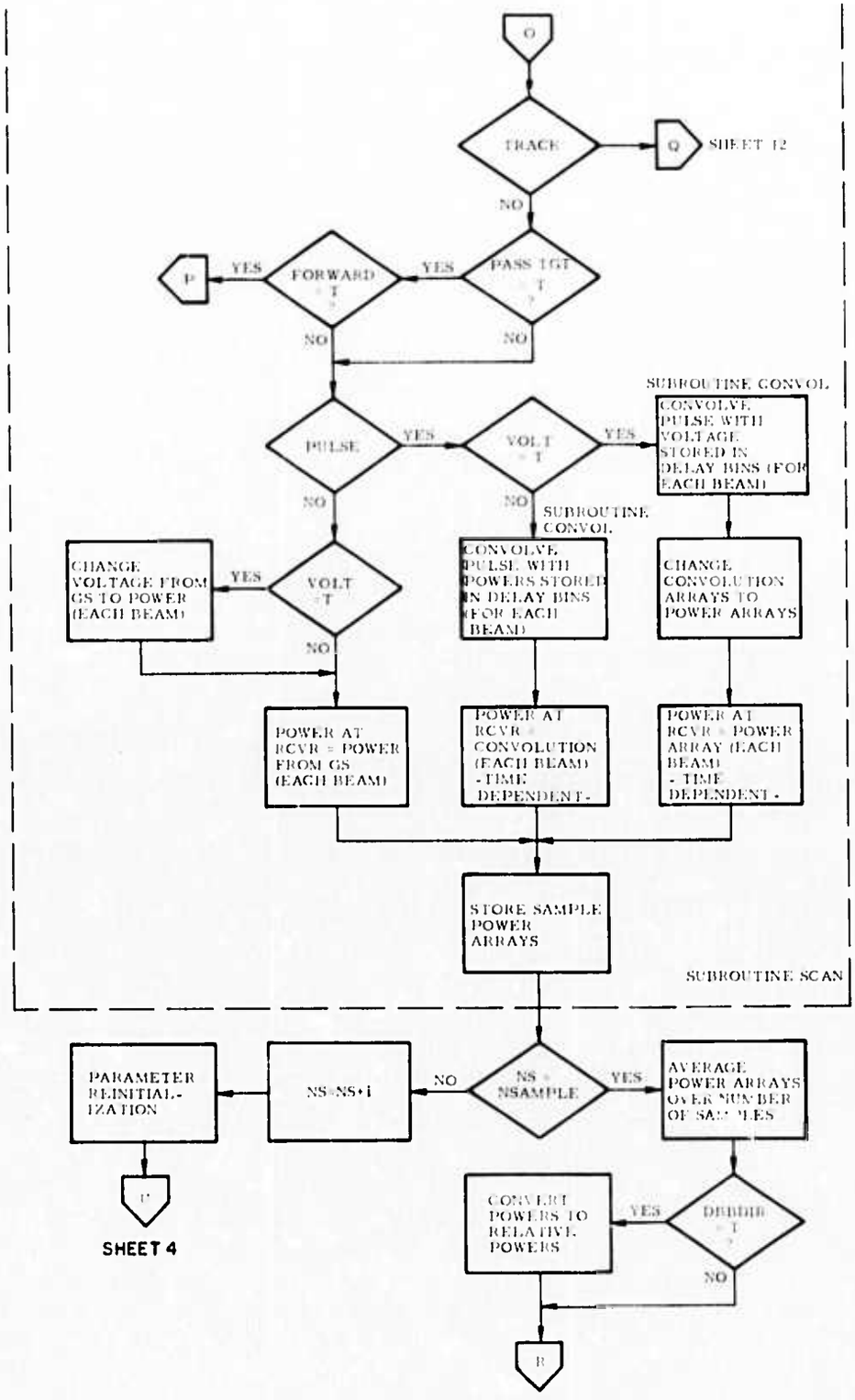
O
TRACK
Q
SHEET 12
NO
P
YES
FORWARD T
YES
PASS TGT T
NO
NO
SUBROUTINE CONVOL
CONVOLVE PULSE WITH VOLTAGE STORED IN DELAY BINS (FOR EACH BEAM)
PULSE
YES
VOLT T
YES
NO
NO
SUBROUTINE CONVOL
CONVOLVE PULSE WITH POWERS STORED IN DELAY BINS FOR EACH BEAM)
CHANGE CONVOLUTION ARRAYS TO POWER ARRAYS
CHANGE VOLTAGE FROM GS TO POWER (EACH BEAM)
YES
VOLT T
NO
POWER AT RCVR = POWER FROM GS (EACH BEAM)
POWER AT RCVR = CONVOLUTION (EACH BEAM) - TIME DEPENDENT -
POWER AT RCVR = POWER ARRAY (EACH BEAM) - TIME DEPENDENT -
STORE SAMPLE POWER ARRAYS
SUBROUTINE SCAN
PARAMETER REINITIAL-IZATION
NS=NS+1
NO
NS = NSAMPLE
YES
AVERAGE POWER ARRAYS OVER NUMBER OF SAMPLES
P
SHEET 4
CONVERT POWERS TO RELATIVE POWERS
YES
DBDDB T
NO
R

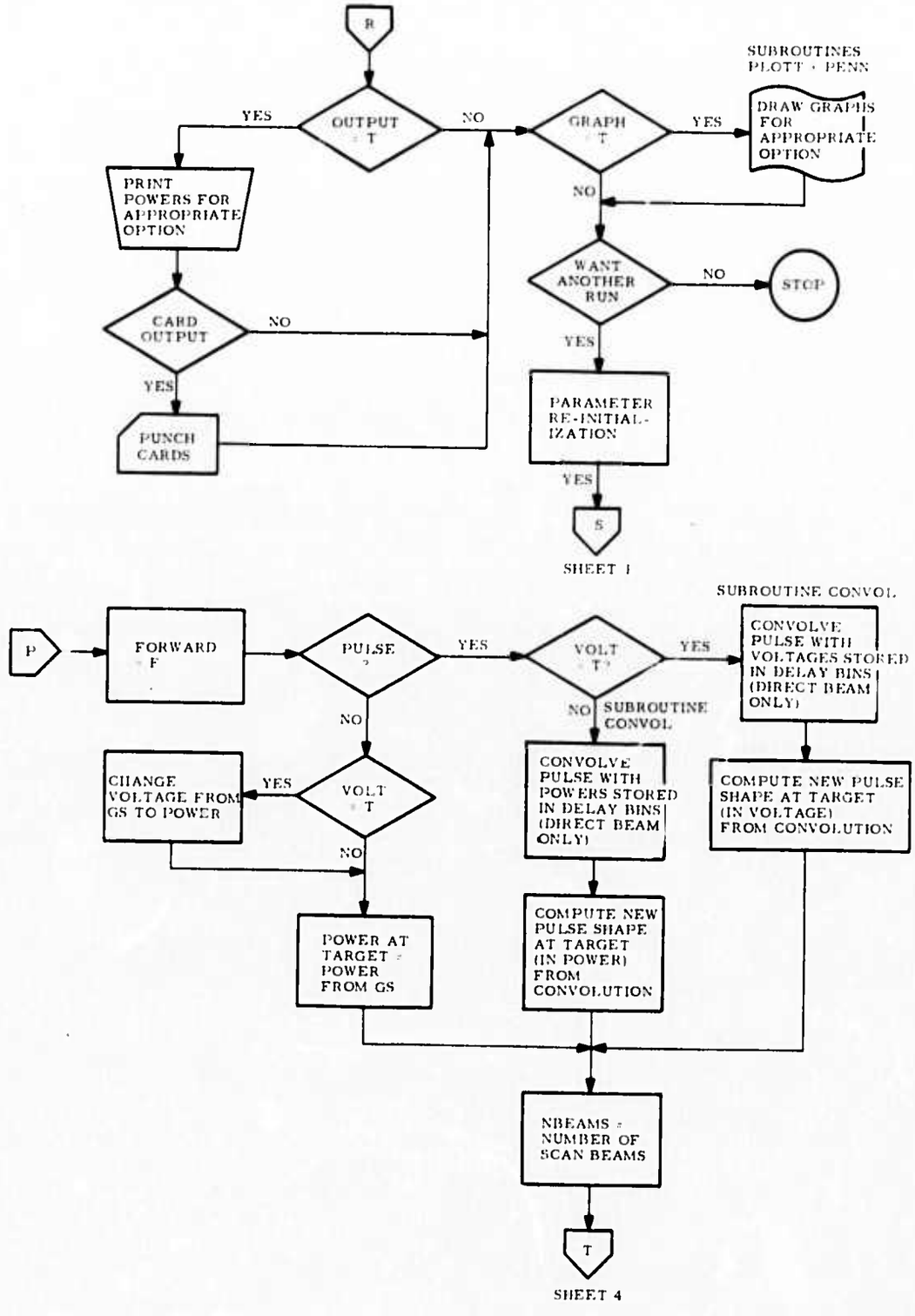
R
OUTPUT = T
YES
NO
PRINT POWERS FOR APPROPRIATE OPTION
CARD OUTPUT
NO
YES
PUNCH CARDS
GRAPH = T
YES
SUBROUTINES PLOTT + PENN
DRAW GRAPHS FOR APPROPRIATE OPTION
NO
WANT ANOTHER RUN
NO
STOP
YES
PARAMETER RE-INITIAL-IZATION
YES
S
SHEET 1
P
FORWARD = F
PULSE = ?
YES
VOLT = T?
YES
SUBROUTINE CONVOL
CONVOLVE PULSE WITH VOLTAGES STORED IN DELAY BINS (DIRECT BEAM ONLY)
NO
SUBROUTINE CONVOL
NO
CHANGE VOLTAGE FROM GS TO POWER
YES
VOLT = T
NO
CONVOLVE PULSE WITH POWERS STORED IN DELAY BINS (DIRECT BEAM ONLY)
COMPUTE NEW PULSE SHAPE AT TARGET (IN VOLTAGE) FROM CONVOLUTION
POWER AT TARGET = POWER FROM GS
COMPUTE NEW PULSE SHAPE AT TARGET (IN POWER) FROM CONVOLUTION
NBEAMS = NUMBER OF SCAN BEAMS
T
SHEET 4

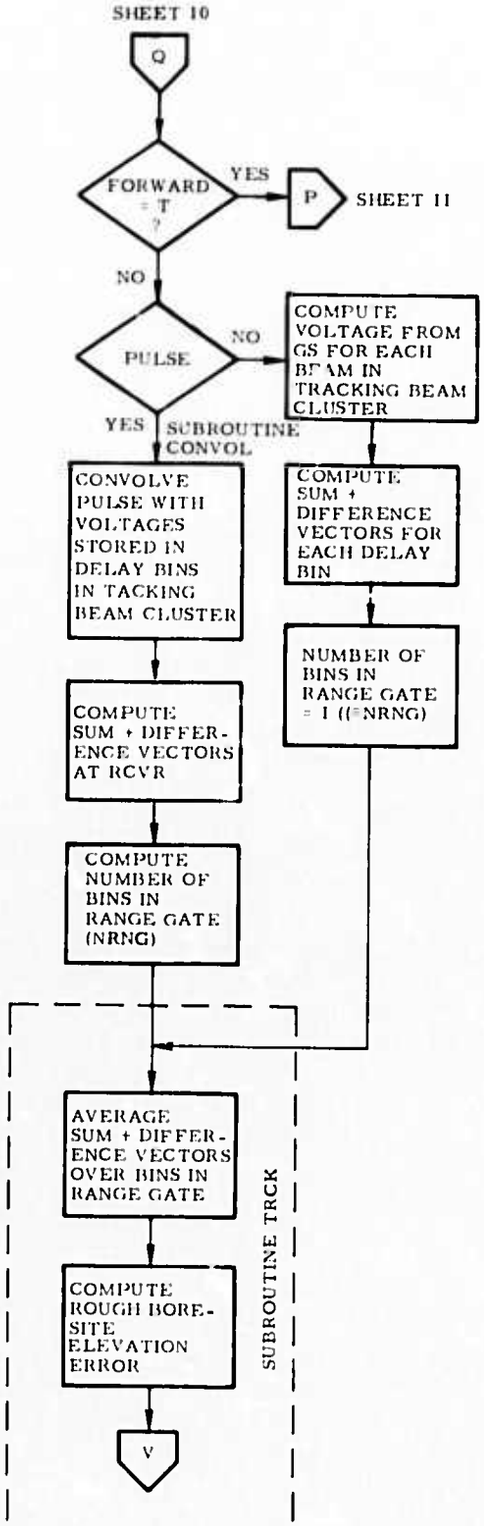
SHEET 10
Q
FORWARD = T ?
YES
P
SHEET 11
NO
PULSE
NO
COMPUTE VOLTAGE FROM GS FOR EACH BEAM IN TRACKING BEAM CLUSTER
YES
SUBROUTINE CONVOL
CONVOLVE PULSE WITH VOLTAGES STORED IN DELAY BINS IN TACKING BEAM CLUSTER
COMPUTE SUM + DIFFERENCE VECTORS FOR EACH DELAY BIN
NUMBER OF BINS IN RANGE GATE = I ((=NRNG)
COMPUTE SUM + DIFFERENCE VECTORS AT RCVR
COMPUTE NUMBER OF BINS IN RANGE GATE (NRNG)
AVERAGE SUM + DIFFERENCE VECTORS OVER BINS IN RANGE GATE
COMPUTE ROUGH BORESITE ELEVATION ERROR
V
SUBROUTINE TRCK

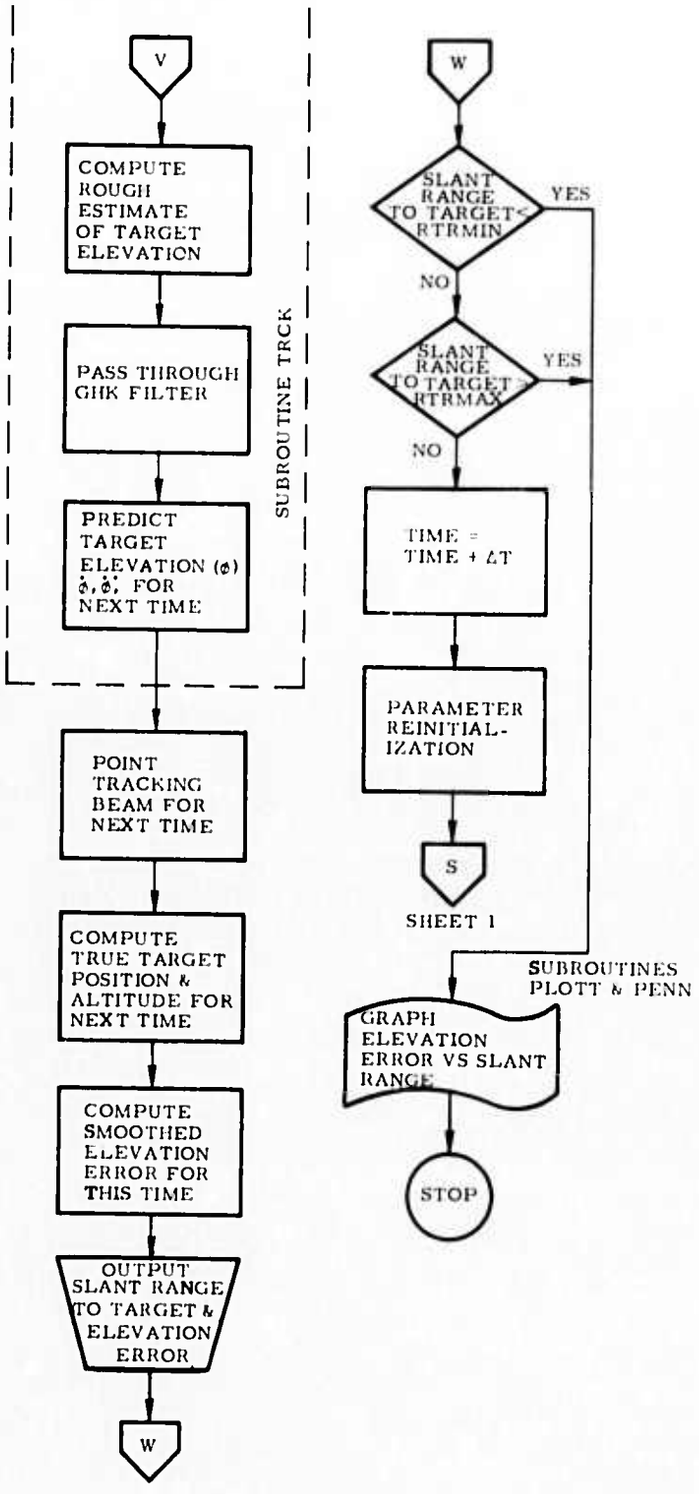
V
COMPUTE ROUGH ESTIMATE OF TARGET ELEVATION
PASS THROUGH GHK FILTER
PREDICT TARGET ELEVATION (φ) φ̇, φ̈ FOR NEXT TIME
SUBROUTINE TRCK
POINT TRACKING BEAM FOR NEXT TIME
COMPUTE TRUE TARGET POSITION & ALTITUDE FOR NEXT TIME
COMPUTE SMOOTHED ELEVATION ERROR FOR THIS TIME
OUTPUT SLANT RANGE TO TARGET & ELEVATION ERROR
W
W
SLANT RANGE TO TARGET < RTRMIN
YES
NO
SLANT RANGE TO TARGET > RTRMAX
YES
NO
TIME = TIME + ΔT
PARAMETER REINITIAL-IZATION
S
SHEET 1
SUBROUTINES PLOTT & PENN
GRAPH ELEVATION ERROR VS SLANT RANGE
STOP

APPENDIX B

MULTIPATH COMPUTER PROGRAM LISTING

PROGRAM MULTPTH

```
      PROGRAM MULTPTH(INPUT,OUTPUT,PUNCH,TAPE5=INPUT,TAPE6=OUTPUT,
     $ TAPE7=PUNCH,TAPE12)
C
C     WRITTEN BY P.E.CORNWELL AND S.POWERS MAY 1974
C
      COMMON YOUT2(102,10),RDYOUT2(102),RYOUT2(102,10)
      COMMON DELOUT(127,10),XOUT(102,10),YOUT(102,10),EXTRA(10,2),
     1       OUTC(127),DARRAY(127)
      COMMON RDELOUT(127,10),RXOUT(102,10),RYOUT(102,10),REXTRA(10,2),
     1       RRHOARY(10)
      COMMON/TRP/JCALL
      COMMON/BEAMS/SANGLE(10,2),UXS(10),UYS(10),UZS(10)
      COMMON/DERV/PARRAY(127),ARYPAR(5),GBETZ0(10),G10,G20(10),NP,
     1            DIRDOP,DFLT,UNIFORM,RANGLE,SIGZ0,ROZERO,NCC,
     2            FORPI,PID2,XTR,YTR,ZTR,RTR,RHOARY(10)
      COMMON/EXT/NYMAX
      COMMON/INC/DX,DY
      COMMON/INPUTS/XTP,YTP,ZTP,XTV,YTV,ZTV,XRP,YRP,ZRP,GRMAX,GRAPH,NG,
     $              NSAMPLE,VOLT,VPUL,NSLOPE,SLOPE(10,9),
     $              NXSDMX,NYSDMX,DGBALL,DGBALL1,TRACK,NOUT,
     $              PI,REARTH,XLAM,PASSTGT,FORWARD,PULSE,SQPULSE,PWIDTH
      COMMON/PATD/JD,BWD,CD,AD,SIOD,JS,BWS,CSCAN,ASCAN,SIOSCAN,
     $            JB,BWB,CR,AB,SIOB
      COMMON/PGAIN/GT,PT,GR,RADCON
      COMMON/PLTYPE/PENPLOT
      COMMON/POINT/UXPOINT,UYPOINT,UZPOINT,DSINE(10)
      COMMON/PROPT/PRINT1,PRINT2,PRINT3,PRINT4,PRINT5,IPRINT(20)
      COMMON/RTYPE/SPEC,DIFFUSE
      COMMON/XSTUFF/RDXOUT(102),RDYOUT(102)
      COMMON/TGAIND/G20P(4),G10P(4)
      COMMON/TGAINP/G1P(4),G2P(4)
      COMMON/TRK/PHITP,PHITPD,PHITPDD,ANTSLOP
      COMMON/SINFO/SCOUNT,SDATA1(100),SDATA2(100),SDATA3(100)
      COMMON/SPOINTS/ XSP(100),YSP(100),ZSP(100)
      COMMON/MULSPEC/SPCHECK
C
      DIMENSION ITITLE(5),TTITLE1(5)
      DIMENSION PHIERR(500),SRANGE(500)
      DIMENSION SUM(127),DELTA(127)
      LOGICAL VPOL,PULSE,PASSTGT,FORWARD,SQPULSE,TRACK,GRAPH,OUTPUT
      LOGICAL UNIFORM,VOLT,NEWSLOP,NEWBEAM
      LOGICAL PENPLOT
      COMPLEX ROZERO,DELOUT,OUTC,EXTRA,XOUT,YOUT,RHOARY
      COMPLEX YOUT2
      COMPLEX SUM,DELTA
      REAL MINDEL,MAXDEL
      LOGICAL SPEC,DIFFUSE,DBBDIR
      LOGICAL PRINT1,PRINT2,PRINT3,PRINT4,PRINT5
      REAL MINDELF,MAXDELF
```

```
      INTEGER SCOUNT
      INTEGER RUNN
C
C
      DATA ITITLE /10H POWER FOR,10H CW CASE  ,10H          ,
     1            10H           ,10H           /
      DATA ITITLE1/10H POWER FOR,10H PULSE CAS,10HE         ,
     1            10H           ,10H           /
      DATA RTCONV,REARTH,PI/.3048,6.5E6,3.1415926535898/
      DATA JD,JS,JB,XDB/2,2,2,3./
      DATA BWD,BWS,BWB /.5,.5,90./
      DATA IDIM /10/
      NAMELIST/OUT/UXS,UYS,UZS,UXPOINT,UYPOINT,UZPOINT
      NAMELIST/INP0/PRF,TIMEOUT,RTRMIN,RTRMAX
      NAMELIST/INP1/TRACK
      NAMELIST/INP2/DGBALL,DGBALL1,DX,DY,
     X  GR,GR0,GRMAX,GT,HR,
     1  HT,ICALC,MAXDEL,MINDEL,NBEAMS,NOUT,NP,NR,NSAMPLE,NSLOPE,
     2  NYMAX,OBBDIR,
     3  NXSDMX,NYSDMX,PT,PWIDTH,SIGZ0,XLAM,XV,YV,ZV,GRAPH,
     4 NEWBEAM,NEWSLOP,OUTPUT,PASSTGT,PULSE,SUPULSE,UNIFORM,
     5  VOLT,VPUL,SPEC,DIFFUSE,PRINT1,PRINT2,PRINT3,PRINT4,PRINT5
     6 ,PENPLOT,SANGLE,SLOPE,NPN
C
C     INITIAL CONSTANTS
C
      JCALL=0
      JTIME=0
      JJ=1
      JTT=0
      JT=0
      JJMAX=180
      RUNN=1
      DEGCONV=PI/180.
      A=1./SQRT(2.)
      FORPI=4.*PI
      PID2=PI/2.
      READ INP1
      PRINT INP1
      IF(.NOT.TRACK) GO TO 5
      READ INP0
      PRINT INP0
      PRI=1./PRF
      IF(PRI.GE.TIMEOUT) GO TO 6
      TLNTH=TIMEOUT/PRI
      KTLNTH=INT(TLNTH)
      TLNTHP=KTLNTH
      IF(TLNTHP.EQ.TLNTH) GO TO 5
```

```
      TIMEOUT=TLNTHP*PRI
    8 WRITE(6,3051)TIMEOUT
      GO TO 5
    6 TIMEOUT=PRI
      GO TO 8
C
C     INITILIZE INPUT DATA
C
    5 SIGZ0=1.0
      GT=1.0
      PT=1.0
      GR=1.0
      XLAM=.0164592
      GRMAX=10000.0
      NBEAMS=IDIM
      NG=1
      NP=5
      ICALC=0
      NSLOPE=2
      NOUT=20
      DX=100.0
      DY=10.0
      NXSDMX=10
      NYSDMX=10
      NSAMPLE=1
      DGBALL=.01
      DGBALL1=.01
      NR=1
      PENPLOT=.FALSE.
      DBBDIR=.FALSE.
      PWIDTH=1.0E-09
      NEWBEAM=.TRUE.
      NEWSLOP=.TRUE.
      VOLT=.FALSE.
      UNIFORM=.FALSE.
      SIGZ0=1.0
      OUTPUT=.TRUE.
      VPOL=.FALSE.
      GRAPH=.FALSE.
      PULSE=.TRUE.
      SQPULSE=.TRUE.
      PASSTGT=.FALSE.
      SPEC=.TRUE.
      DIFFUSE=.TRUE.
      HR=4.0
      HT=200.0
      GR0=10000.0
      NYMAX=10.0
```



```
      XV=-1000.0
      YV =0.0
      ZV =0.0
      MINDEL=0.0
      MAXDEL=2000
      PRINT1=.FALSE.
      PRINT2=.FALSE.
      PRINT3=.FALSE.
      PRINT4=.FALSE.
      PRINT5=.FALSE.
C
C     ZERO OUT STURAGE ARRAYS
C
      DO 7 J=1,IDIM
      UXS(J)=0.0
      UYS(J)=0.0
      UZS(J)=0.0
    7 CONTINUE
 1010 CONTINUE
      UXPOINT=0.
      UYPOINT=0.
      UZPOINT=0.
 1011 DO 10 J=1,127
      PARRAY(J)=0.0
   10 CONTINUE
      PT=1.
      DO 12 J=1,102
      DO 12 K=1,IDIM
      XOUT(J,K)=0.0
      YOUT(J,K)=0.0
      YOUT2(J,K)=0.0
      RXOUT(J,K)=0.0
      RYOUT(J,K)=0.0
      RYOUT2(J,K)=0.
   12 CONTINUE
      DO 14 J=1,127
      SUM(J)=0.0
      DELTA(J)=0.0
   14 CONTINUE
      DO 13 J=1,127
      DO 13 K=1,IDIM
      DELOUT(J,K)=0.0
      RDELOUT(J,K)=0.
   13 CONTINUE
      DO 15 I=1,20
   15 IPRINT(I)=0
      DO 20 J=1,IDIM
      G20(J)=0.
```

```
      RHOARY(J)=0.0
      RRHOARY(J)=0.0
      EXTRA(J,1)=0.0
      EXTRA(J,2)=0.0
      REXTRA(J,1)=0.0
 20   REXTRA(J,2)=0.0
      IF(TRACK.AND.JT.EQ.1) GO TO 16
C
C
      READ INP2
C*************************************************************
      PRINT INP2
      IF(.NOT.SPEC.AND..NOT.DIFFUSE)STOP10
      SPCHECK=SQRT(DX**2+DY**2)
C
C ESTABLISH PULSE SHAPE
   16 IF(PULSE)CALL PSHAPE(PWIDTH,NPN,PARRAY,DELT)
      IF(TRACK.AND.JT.EQ.1)GO TO 18
C
C     RECEIVER POSITION IN REFERENCE COORDINATE SYSTEM
C
      XR=0.0
      YR=0.0
      ZR=REARTH+HR
C
C     INITIAL TARGET POSITION IN REFERENCE COORDINATE SYSTEM
C
      XT=(REARTH+HT)*SIN(GRO/REARTH)
      YT=0.0
      ZT=(REARTH+HT)*COS(GRO/REARTH)
C
C     SET UP VECTOR FROM RECIEVER TO TARGET (REF. COORD. SYSTEM)
C
   18 XRT=XT-XR
      YRT=YT-YR
      ZRT=ZT-ZR
C
C     CHANGE TO A UNIT VECTOR
C
      RRT=SQRT(XRT**2+YRT**2+ZRT**2)
      UXRT=XRT/RRT
      UYRT=YRT/RRT
      UZRT=ZRT/RRT
C
C     RECIEVER POSITION IN RECIEVER COORDINATE SYSTEM
C
      RANGLE=ATAN(YT/XT)
      CALL RCOORD(RANGLE,XR,YR,ZR,XRP,YRP,ZRP)
```

```
C
C     VECTOR FROM TARGET TO RECEIVER
C
      CALL RCOORD(RANGLE,-XRT,-YRT,-ZRT,XTR,YTR,ZTR)
      RTR=RRT
C
C     TARGET POSITION IN RECIEVER COORDINATE SYSTEM
C
      CALL RCOORD(RANGLE,XT,YT,ZT,XTP,YTP,ZTP)
C
C     TARGET VELOCITY IN RECIEVER COORDINATE SYSTEM
C
      CALL RCOORD(RANGLE,XV,YV,ZV,XTV,YTV,ZTV)
C
C     INITIALIZE TRACKING FILTERS
C
      IF(.NOT.TRACK) GO TO 17
      IF(JTIME.GT.0) GO TO 17
      CALL TRKINIT(SUM,DELTA,1,PHITS,TIMEOUT)
C
C     COMPUTE HORIZON GROUND RANGE
C
   17 COEA=ACOS(REARTH/(REARTH+HR))
      HGR=REARTH*COEA
C
C     COMPUTE SLANT RANGE TO HORIZON
C
      HSL=REARTH*TAN(COEA)
C
C     ESTABLISH ARYPAR (GRAPHING LIMITS)
C
      IF(ICALC.EQ.0) GO TO 55
      ARYPAR(1)=MINDEL
      ARYPAR(2)=MAXDEL
      GO TO 70
   55 ARYPAR(1)=MINDEL
      IF(HR.LT.HT) GO TO 60
      AX=XTP
      AY=YTP
      AZ=ZTP-REARTH
      RAR=SQRT(AX**2+AY**2+AZ**2)
      ARYPAR(2)=RAR+HR-RRT
      GO TO 70
   60 IF(GRO.GE.HGR) GO TO 56
      AX=REARTH*SIN(GRO/REARTH)
      AY=0.0
      AZ=ZR-REARTH*COS(GRO/REARTH)
      RAR=SQRT(AX**2+AY**2+AZ**2)
```

```
      ARYPAR(2)=RAR+HT-RRT
      GO TO 70
   56 COEA1=GRO/REARTH
      DTHETAA=ABS(COEA1-COEA)
      TG1=REARTH**2+(REARTH+HT)**2-2.*REARTH*(REARTH+HT)*COS(DTHETAA)
      TG=SQRT(TG1)
      ARYPAR(2)=HSL+TG-RRT
   70 IF(PULSE) GO TO 75
      ARYPAR(3)=(ARYPAR(2)-ARYPAR(1))
      ARYPAR(3)=ARYPAR(3)/NOUT
      GOTO 76
   75 ARYPAR(3)=DELT*3.E8
   76 BOUT=(ARYPAR(2)-ARYPAR(1))
      BOUT=BOUT/ARYPAR(3)
      NOUT=INT(BOUT)
      IF(NOUT.EQ.0)GO TO 77
      IF(NOUT.GT.100)NOUT=100
      COUT=NOUT
      ARYPAR(2)=ARYPAR(3)*COUT
      ARYPAR(2)=ARYPAR(2)+ARYPAR(1)
      GO TO 78
   77 NPN=NPN+1
      NP=NPN
      DELT=PWIDTH/NPN
      ARYPAR(3)=DELT*3.E08
      IF(NPN.GT.100)GO TO 700
      CALL PSHAPE(PWIDTH,NPN,PARRAY,DELT)
      GO TO 76
  700 JJ=JJ-1
      WRITE(6,3055)
      GO TO 4999
C
C     CALCULATE THE DIRECT DOPPLER
C
   78 DIRDOP=XTV*UXRT+YTV*UYRT+ZTV*UZRT
      DIRDOP=-DIRDOP
      IF(JT.EQ.1) GO TO 6000
C
C     SURFACE SLOPE INFORMATION
C
C
   86 DO 85 J=1,NSLOPE
      GBETZ0(J)=(1./TAN(SLOPE(J,2)))**2
   85 CONTINUE
C
C     ESTABLISH ALL ANTENNA PATTERNS
C
   90 IF(TRACK) GO TO 100
```

```
      IF(RUNN.GT.1)GO TO 120
C
C     DIRECT BEAM
C
      CALL PATTERN(JD,BWD,CD,AD,SIOD,A)
C
C     SCAN BEAM
C
      CALL PATTERN(JS,BWS,CSCAN,ASCAN,SIOSCAN,A)
C
C     TARGET BEAM
C
  110 IF(.NOT.PASSTGT) CALL PATTERN(JB,BWB,CB,AB,SIOB,A)
      GO TO 120
C
C     TRACKING BEAM
C
  100 CALL TBEAM(BWD,JD,XDR,CD,AD,SIOD,SIID)
      JT=1
      GO TO 6000
C
C     IF PASSTGT ESTABLISH POINTING DIRECTION OF
C     TRANSMIT BEAM IN RECEIVER COORDINATE SYSTEM
C
  120 IF(.NOT.PASSTGT) GO TO 125
      UXPOINT=-XTR/RTR
      UYPOINT=-YTR/RTR
      UZPOINT=-ZTR/RTR
C
C     COMPUTE UNIT VECTORS OF SCAN ANGLES
C
  125 IF(.NOT.NEWBEAM)GOTO 131
      DO 130 J=1,NBEAMS
      SANGLE(J,1)=SANGLE(J,1)*DEGCONV
      SANGLE(J,2)=SANGLE(J,2)*DEGCONV
      XS=COS(SANGLE(J,2))*COS(SANGLE(J,1))
      YS=COS(SANGLE(J,2))*SIN(SANGLE(J,1))
      ZS=SIN(SANGLE(J,2))
      RS=SQRT(XS**2+YS**2+ZS**2)
      UXS(J)=XS/RS
      UYS(J)=YS/RS
      UZS(J)=ZS/RS
  130 CONTINUE
C
C     COMPUTE DIRECT BEAM POWER
C
  131 DPOWER=PT*GT*GR*(XLAM**2)/((FORPI*RRT)**2)
      IF(PASSTGT) DPOWER=DPOWER*SIGZO/(FORPI*RRT**2)
```

```
      GO TO 150
 6000 NBEAMP=4
      VOLT=.TRUE.
      PASSTGT=.TRUE.
      NBEAMS=4
      IF(JTT.EQ.1) GO TO 149
      UXPOINT=-XTR/RTR
      UYPOINT=-YTR/RTR
      UZPOINT=-ZTR/RTR
      JTT=1
  149 CALL BIPOSTN(UXS,UYS,UZS,SIID)
C
C     ESTABLISH SLOPE OF DELTA VECTOR AT ORIGIN
C     ASSUMING INPLANE MOTION AND ANALYTIC PATTERNS
C
      IF(JTIME.EQ.0)CALL DIFSLOP(JD,CD,AD,UXS,UYS,UZS,ANTSLOP,XRT,ZRT)
C
C     COMPUTE POWER AND PULSE SHAPE AT TARGT
C
  150 IF(.NOT.VOLT.OR.TRACK)NSAMPLE=1
      DO 2000 NS=1,NSAMPLE
      NP=NPN
C
C     ESTABLISH PULSE IF PULSE = .TRUE.  AND NS .NE. 1
C
      IF(NS.EQ.1)GOTO 199
      IF(PULSE)CALL PSHAPE(PWIDTH,NP,PARRAY,DELT)
  199 IF(TRACK) GO TO 6010
      IF(PASSTGT) GO TO 200
      FORWARD=.FALSE.
      CALL DPGAIN(NBEAMS)
      CALL SCAN(NBEAMS)
      GO TO 800
  200 NBEAMP=1
 6010 FORWARD=.TRUE.
      CALL DPGAIN(NBEAMP)
      CALL SCAN(NBEAMP)
      IF(PULSE) GO TO 210
      PT=RHOARY(1)
      IF(.NOT.TRACK)GO TO 209
      SUM(1)=.5*(RHOARY(1)+RHOARY(2)+RHOARY(3)+RHOARY(4))
      PT=SUM(1)*CONJG(SUM(1))
      GO TO 208
  209 CONTINUE
      IF(VOLT)PT=RHOARY(1)*CONJG(RHOARY(1))
  208 CONTINUE
      GT=1.0
      GO TO 220
```

```
  210 PT=1.0
      GT=1.0
      IF(.NOT.TRACK)GO TO 211
      DO 212 J=1,NBEAMS
      CALL CONVOL(J)
      DO 213 K=1,NCC
      DELOUT(K,J)=OUTC(K)
  213 CONTINUE
  212 CONTINUE
      DO 214 K=1,NCC
      NP=NCC
      SUM(K)=.5*(DELOUT(K,1)+DELOUT(K,2)+DELOUT(K,3)+DELOUT(K,4))
      S=SUM(K)*CONJG(SUM(K))
      PARRAY(K)=SQRT(S)
  214 CONTINUE
      GO TO 220
  211 CALL CONVOL(1)
      NP=NCC
      DO 240 J=1,NCC
      PARRAY(J)=OUTC(J)
      S=OUTC(J)*CONJG(OUTC(J))
      IF(VOLT)PARRAY(J)=SQRT(S)
  240 CONTINUE
  220 FORWARD=.FALSE.
C
C     CALCULATE POWER FOR RETURN TRIP
C
      CALL DPGAIN(NBEAMS)
      CALL SCAN(NBEAMS)
  800 IF(PULSE) GO TO 820
      IF(.NOT.TRACK) GO TO 801
      SUM(1)=.5*(RHOARY(1)+RHOARY(2)+RHOARY(3)+RHOARY(4))
      DELTA(1)=((RHOARY(1)+RHOARY(2))-(RHOARY(3)+RHOARY(4)))
      DELTA(1)=.5*DELTA(1)
      GO TO 8000
  801 DO 830 J=1,NBEAMS
      IF(VOLT)RHOARY(J)=RHOARY(J)*CONJG(RHOARY(J))
      RRHOARY(J)=RHOARY(J)+RRHOARY(J)
  830 CONTINUE
      DO 840 J=1,102
      DO 840 K=1,NBEAMS
      IF(VOLT)XOUT(J,K)=XOUT(J,K)*CONJG(XOUT(J,K))
      IF(VOLT)YOUT(J,K)=YOUT(J,K)*CONJG(YOUT(J,K))
      IF(VOLT)YOUT2(J,K)=YOUT2(J,K)*CONJG(YOUT2(J,K))
      RXOUT(J,K)=XOUT(J,K)+RXOUT(J,K)
      RYOUT(J,K)=RYOUT(J,K)+YOUT(J,K)
      RYOUT2(J,K)=RYOUT2(J,K)+YOUT2(J,K)
  840 CONTINUE
```

```
      GO TO 2000
  820 IF(.NOT.TRACK) GO TO 821
      DO 822 J=1,NBEAMS
      CALL CONVOL(J)
      DO 823 K=1,NCC
      DELOUT(K,J)=OUTC(K)
  823 CONTINUE
  822 CONTINUE
      DO 824 K=1,NCC
      SUM(K)=.5*(DELOUT(K,1)+DELOUT(K,2)+DELOUT(K,3)+DELOUT(K,4))
      DELTA(K)=DELOUT(K,1)+DELOUT(K,2)-DELOUT(K,3)-DELOUT(K,4)
      DELTA(K)=.5*DELTA(K)
  824 CONTINUE
C
C     CALCULATE NUMBER OF PTS. IN GATE(NRNG)
C
      RESOLTN=(3.E08)*PWIDTH
      XNRNG=RESOLTN/ARYPAR(3)
      NRNG=INT(XNRNG)
      YNRNG=NRNG
      IF(YNRNG.LT.XNRNG)NRNG=NRNG+1
      IF(RESOLTN.GT.ARYPAR(2))NRNG=NCC
      GO TO 9000
  821 DO 850 J=1,NBEAMS
      CALL CONVOL(J)
      DO 850 K=1,NCC
      DELOUT(K,J)=OUTC(K)
      IF(VOLT)DELOUT(K,J)=DELOUT(K,J)*CONJG(DELOUT(K,J))
      RDELOUT(K,J)=RDELOUT(K,J)+DELOUT(K,J)
  850 CONTINUE
      DO 880 J=1,NBEAMS
      DO 880 K=1,2
      IF(VOLT)EXTRA(J,K)=EXTRA(J,K)*CONJG(EXTRA(J,K))
      REXTRA(J,K)=REXTRA(J,K)+EXTRA(J,K)
  880 CONTINUE
      GO TO 2000
 8000 NRNG=1
 9000 CALL TRCK(SUM,DELTA,NRNG,PHITS,TIMEOUT)
C
C     COMPUTE TRUE TARGET ELEVATION
C
      T1=SQRT(XT**2+YT**2+ZT**2)
      T2=SQRT(XR**2+YR**2+ZR**2)
      T3=SQRT((XT-XR)**2+(YT-YR)**2+(ZT-ZR)**2)
      TELEV=ACOS((T3**2+T2**2-T1**2)/(2.*T3*T2))
      TELEV=TELEV-PI/2.
      TELEVD=180./PI*TELEV
C
```

```
C     POINT TRACKING BEAM(FOR INPLANE TARGET ONLY)
C
      PHIRAD=PHITP*PI/180.
      AZP=0.0
      UXPT=COS(PHIRAD)*COS(AZP)
      UYPT=COS(PHIRAD)*SIN(AZP)
      UZPT=SIN(PHIRAD)
C
C     ROTATE POINTING DIRECTION TO RECEIVER COORD. SYSTEM
C
      CALL RCOORD(AZP,UXPT,UYPT,UZPT,UXPOINT,UYPOINT,UZPOINT)
C
C     SET POSITION OF TARGET FOR NEXT TIME
C
C     CONSTANT VELOCITY ASSUMED
C
      XT=XT+XV*TIMEOUT
      YT=YT+YV*TIMEOUT
      ZT=ZT+ZV*TIMEOUT
C
C     COMPUTE NEW TARGET HEIGHT
C
      HT=SQRT(XT**2+YT**2+ZT**2)
      HT=HT-REARTH
C
C     COMPUTE GROUND RANGE TO TARGET FOR NEXT TIME
C
      XYL=SQRT(XT**2+YT**2)
      STH=ATAN(XYL/ZT)
      GRO=REARTH*STH
C
C     COMPUTE ERROR
C
      PHIERRP=PHITS-TELEVD
 9010 PHIERR(JJ)=PHIERRP
      SRANGE(JJ)=RTR
      WRITE(6,3052)SRANGE(JJ),PHIERR(JJ)
 3052 FORMAT(6X7HSRANGE=E20.8,7HPHIERR=E20.8)
      IF(RTR.LE.RTRMIN.OR.RTR.GT.RTRMAX) GO TO 4999
      IF(JJ.GE.JJMAX) GO TO 4999
      JJ=JJ+1
      JTIME=1
      GO TO 1011
 4999 DO 5999J=1,JJ
      IN=JJ+1
      INN=IN-J
      SRANGE(J)=SRANGE(INN)
      PHIERR(J)=PHIERR(INN)
```

```
5999 CONTINUE
     CALL PICTUR(SRANGE,PHIERR,JJ)
     IF(PENPLOT) CALL PENN(SRANGE,PHIERR,JJ,1,6)
     GO TO 5000
2000 CONTINUE
     DO 890 J=1,100
     DO 890 K=1,NBEAMS
     RXOUT(J,K)=RXOUT(J,K)/NSAMPLE*(1./(120.*PI))
     RYOUT(J,K)=RYOUT(J,K)/NSAMPLE*(1./(120.*PI))
     RYOUT2(J,K)=RYOUT2(J,K)/NSAMPLE*(1./(120.*PI))
     IF(.NOT.DBBDIR)GOTO 890
     IF(RXOUT(J,K).LT.1.E-40)RXOUT(J,K)=1.E-40
     IF(RYOUT(J,K).LT.1.E-40)RYOUT(J,K)=1.E-40
     IF(RYOUT2(J,K).LT.1.E-40)RYOUT2(J,K)=1.E-40
     RXOUT(J,K)=10.*ALOG10(RXOUT(J,K)/DPOWER)
     RYOUT(J,K)=10.*ALOG10(RYOUT(J,K)/DPOWER)
     RYOUT2(J,K)=10.*ALOG10(RYOUT2(J,K)/DPOWER)
     IF(RXOUT(J,K).LT.-200.)RXOUT(J,K)=-200.
     IF(RYOUT(J,K).LT.-200.)RYOUT(J,K)=-200.
     IF(RYOUT2(J,K).LT.-200.)RYOUT2(J,K)=-200.
 890 CONTINUE
     DO 891 J=1,NBEAMS
     RRHOARY(J)=RRHOARY(J)/NSAMPLE*(1./(120.*PI))
 891 CONTINUE
     DO 892 J=1,NCC
     DO 892 K=1,NBEAMS
     RDELOUT(J,K)=RDELOUT(J,K)/NSAMPLE*(1./(120.*PI))
     IF(.NOT.DBBDIR)GO TO 892
     IF(RDELOUT(J,K).LT.1.E-40)RDELOUT(J,K)=1.E-40
 892 CONTINUE
C
C    IF A PULSE RADAR IS USED, ESTABLISH DPOWER AS A FUNCTION OF TIME
C
     DPOWER=DPOWER/(120.*PI)
     DPDB=10.*ALOG10(DPOWER)
     DELOUT(1,1)=DPOWER
     DO 895 J=2,NOUT
     DELOUT(J,1)=0.0
 895 CONTINUE
     CALL CONVOL(1)
     DO 896 J=1,NCC
     DARRAY(J)=OUTC(J)
 896 CONTINUE
     IF(.NOT.DBBDIR) GO TO 897
     DO 898 J=1,NBEAMS
     DO 898 K=1,NCC
     RDELOUT(K,J)=10.*ALOG10(RDELOUT(K,J)/DPOWER)
     IF(RDELOUT(K,J).LT.-200.)RDELOUT(K,J)=-200.
```

```
  898 CONTINUE
  897 DO 893 J=1,NBEAMS
      DO 893 K=1,2
      REXTRA(J,K)=REXTRA(J,K)/NSAMPLE*(1./(120.*PI))
      IF(.NOT.DBBDIR)GO TO 893
      IF(REXTRA(J,K).LT.1.E-40)REXTRA(J,K)=1.E-40
      REXTRA(J,K)=10.*ALOG10(REXTRA(J,K)/DPOWER)
      IF(REXTRA(J,K).LT.-200.)REXTRA(J,K)=-200.
  893 CONTINUE
C
C     OUTPUT
C
  900 WRITE(6,3000)SCOUNT
      DO 3010 J=1,SCOUNT
      WRITE(6,3020)
      WRITE(6,3030)XSP(J),YSP(J),ZSP(J)
      WRITE(6,3040)
 3010 WRITE(6,3050)SDATA1(J),SDATA2(J),SDATA3(J)
      IF(PULSE) GO TO 910
      WRITE(12,995)(ITITLE(J),J=1,5)
      WRITE(12,920)(SANGLE(I,1),SANGLE(I,2),RRHOARY(I),I=1,NBEAMS),
     $((RXOUT(J,K),J=1,102),K=1,NBEAMS),((RYOUT(J,K),J=1,102),K=1,
     $NBEAMS),(RDXOUT(J),J=1,102),(RDYOUT(J),J=1,102),
     $((RYOUT2(J,K),J=1,102),K=1,NBEAMS),(RDYOUT2(J),J=1,102),DPOWER
      IF(.NOT. OUTPUT) GO TO 1000
      WRITE(6,930)
      WRITE(6,925)(SANGLE(I,1),SANGLE(I,2),RRHOARY(I),I=1,NBEAMS)
      WRITE(6,940)DPOWER
      PRINT 1001,(RDXOUT(J),J=1,102)
      PRINT 1002,(RDYOUT(J),J=1,102)
      PRINT 1003,(RDYOUT2(J),J=1,102)
      PRINT 1004,((RXOUT (J,K),J=1,102 ),K=1,NBEAMS)
      PRINT 1005,((RYOUT (J,K),J=1,102 ),K=1,NBEAMS)
      PRINT 1006,((RYOUT2(J,K),J=1,102 ),K=1,NBEAMS)
      GO TO 1000
  910 WRITE(12,995)(ITITLE1(J),J=1,5)
      WRITE(12,950)((RDELOUT(J,K),J=1,NCC),K=1,NBEAMS),
     $(DARRAY(J),J=1,NOUT),((REXTRA(J,K),J=1,NBEAMS),K=1,2)
      IF(.NOT.OUTPUT) GO TO 1000
      WRITE(6,960)
      WRITE(6,970)ARYPAR(1),ARYPAR(2),ARYPAR(3)
      DO 980 J=1,NBEAMS
      WRITE(6,985)J,SANGLE(J,1),J,SANGLE(J,2)
      WRITE(6,990)(K,J,RDELOUT(K,J),K=1,NCC)
  980 CONTINUE
      WRITE(6,999)
      WRITE(6,996)(DARRAY(J),J=1,NOUT)
      WRITE(6,940)DPDB
```

```
      WRITE(6,997)
      WRITE(6,996)((REXTRA(J,K),K=1,2),J=1,NBEAMS)
 1000 IF(GRAPH) CALL PLOTT(NBEAMS)
C
C     CHECK TO SEE IF ANOTHER RUN IS TO BE MADE
C
      IF(RUNN .GE. NR) GO TO 5000
      RUNN=RUNN+1
      GO TO 1010
C
C     FORMATS
C
  920 FORMAT(6X,3E15.6)
  925 FORMAT(E18.6,2E24.6)
  930 FORMAT(/9X,7HAZIMUTH,16X9HELEVATION,16X5HPOWER/)
  950 FORMAT(6X,6E15.6)
  940 FORMAT(/22X,*DPOWER=* E12.6)
  960 FORMAT(/9X,3HMIN,21X,3HMAX,20X,4HDELR/)
  970 FORMAT(E16.6,2E24.6)
  985 FORMAT(21X,*SANGLE(*I2*,1)=*F15.6,*SANGLE(*I2*,2)=*E15.6)
  990 FORMAT(25X,*RDELOUT(*I3,*,*I2,*)=*E15.6)
  991 FORMAT(//9X,*RDXOUT AND RDYOUT ARRAYS*)
  992 FORMAT(//9X,*RYOUT AND RYOUT2 ARRAYS*)
  995 FORMAT(6X,5A10)
  996 FORMAT(5X,5E15.6)
  997 FORMAT(///14X *EXTRA POWER RETURN*)
  999 FORMAT(/// 14X* DIRECT POWER RETURN*)
 1001 FORMAT(//* RDXOUT* /(10E12.4))
 1002 FORMAT(//* RDYOUT* /(10E12.4))
 1003 FORMAT(//* RDYOUT2*/(10E12.4))
 1004 FORMAT( //* RXOUT*/(10E12.4))
 1005 FORMAT( //* RYOUT*/(10E12.4))
 1006 FORMAT(//* RYOUT2*/(10E12.4))
 3000 FORMAT(27HNUMBER OF SPECULAR POINTS =I4)
 3020 FORMAT(32X,14HSPECULAR POINT)
 3030 FORMAT(6X,1H(,E20.8,1H,E20.8,1H,E20.8,1H))
 3040 FORMAT(12X5HSDELR,13X4HRHS2,12X5HGAINS)
 3050 FORMAT(6X,3E20.8)
 3051 FORMAT(1X54HTIMESTEP BETWEEN OUTPUTPOINTS HAS BEEN ADJUSTED TO EQU
     $,2HAL,E20.8)
 3053 FORMAT(23HADJUSTMENT IN NP NEEDED)
 5000 STOP
      END
```

```
      SUBROUTINE ANTGAIN(PDATA,G1,G2,NBEAMS,SINE)
      EXTERNAL GAIN
C
      COMMON YOUT2(102,10),RDYOUT2(102),RYOUT2(102,10)
      COMMON DELOUT(127,10),XOUT(102,10),YOUT(102,10),EXTRA(10,2),
     1       OUTC(127),DARRAY(127)
      COMMON RDELOUT(127,10),RXOUT(102,10),RYOUT(102,10),REXTRA(10,2),
     1       RRHOARY(10)
      COMMON/TGAINP/G1P(4),G2P(4)
      COMMON/TGAIND/G20P(4),G10P(4)
      COMMON/BEAMS/SANGLE(10,2),UXS(10),UYS(10),UZS(10)
      COMMON/DERV/PARRAY(127),ARYPAR(5),GBETZ0(10),G10,G20(10),NP,
     1            DIRDOP,DFLT,UNIFORM,RANGLE,SIGZ0,R0ZERO,NCC,
     2            FURPI,PID2,XTR,YTR,ZTR,RTR,RHOARY(10)
      COMMON/INC/DX,DY
      COMMON/INPUTS/XTP,YTP,ZTP,XTV,YTV,ZTV,XRP,YRP,ZRP,GRMAX,GRAPH,NG,
     $              NSAMPLE,VOLT,VPOL,NSLOPE,SLOPE(10,9),
     $              NXSDMX,NYSDMX,DGBALL,DGBALL1,TRACK,NOUT,
     $              PI,REARTH,XLAM,PASSTGT,FORWARD,PULSE,SQPULSE,PWIDTH
      COMMON/PATD/JD,BWD,CD,AD,SI0D,JS,BWS,CSCAN,ASCAN,SI0SCAN,
     $            JB,BWB,CB,AB,SI0B
      COMMON/PGAIN/GT,PT,GR,RADCON
      COMMON/POINT/UXPOINT,UYPOINT,UZPOINT,DSINE(10)
      COMMON/SPOINTS/ XSP(100),YSP(100),ZSP(100)
      COMMON/SINFO/SCOUNT,SDATA1(100),SDATA2(100),SDATA3(100)
      COMMON/PROPT/PRINT1,PRINT2,PRINT3,PRINT4,PRINT5,IPRINT(20)
C
      DIMENSION PDATA(9),G2(10),SINE(10)
      LOGICAL VPOL,PULSE,PASSTGT,FORWARD,SQPULSE,TRACK,GRAPH
      LOGICAL PRINT1,PRINT2,PRINT3,PRINT4,PRINT5
      LOGICAL UNIFORM,VOLT
      COMPLEX ROZERO,DELOUT,OUTC,EXTRA,XOUT,YOUT,RHOARY
      COMPLEX YOUT2
      INTEGER SCOUNT
C
      IPRINT(1)=IPRINT(1)+1
      IF(PRINT5)PRINT 7777
 7777 FORMAT(* ANTGAIN*)
C
C     ZERO OUT ARRAYS
C
      DO 5 J=1,10
      G2(J)=0.0
    5 CONTINUE
      G1=0.0
      DO 6 J=1,4
      G1P(J)=0.0
      G2P(J)=0.0
    6 CONTINUE
```

```
C
C     COMPUTE VECTOR FROM TARGET TO PATCH
C
      XTG=PDATA(1)-XTP
      YTG=PDATA(2)-YTP
      ZTG=PDATA(2)-ZTP
C
C     COMPUTE VECTOR FROM RECEIVER TO PATCH
C
      XRG=PDATA(1)-XRP
      YRG=PDATA(2)-YRP
      ZRG=PDATA(3)-ZRP
C
C     CHANGE TO UNIT VECTORS
C
      RTG=SQRT(XTG**2+YTG**2+ZTG**2)
      RRG=SQRT(XRG**2+YRG**2+ZRG**2)
      RTGI=1./RTG
      RTRI=1./RTR
      RRGI=1./RRG
      UXTG=XTG*RTGI
      UYTG=YTG*RTGI
      UZTG=ZTG*RTGI
      UXTR=XTR*RTRI
      UYTR=YTR*RTRI
      UZTR=ZTR*RTRI
      UXRG=XRG*RRGI
      UYRG=YRG*RRGI
      UZRG=ZRG*RRGI
      IF(PASSTGT) GO TO 10
C
C     COMPUTE GAIN ANGLE FOR TARGET TO PATCH DIRECTION
C
      ALPHA=ACOS(UXTR*UXTG+UYTR*UYTG+UZTR*UZTG)
C
C     COMPUTE VOLTAGE GAIN G1
C
      G1=GAIN(ALPHA,JB,CB,ASB)
C
C     COMPUTE GAINS FOR EACH SCAN BEAM POSITION
C
   40 DO 20 J=1,NBEAMS
      ALPHA=UXS(J)*UXRG+UYS(J)*UYRG+UZS(J)*UZRG
      ALPHA=ACOS(ALPHA)
      G2(J)=GAIN(ALPHA,JS,CSCAN,ASCAN)
      SINE(J)=G1*G2(J)
      SINE(J)=SIGN(1.,SINE(J))
      G2(J)=G2(J)**2
```

```
   20 CONTINUE
C
C     CHANGE G1 TO POWER
C
      G1=G1**2
      RETURN
   10 IF(TRACK) GO TO 50
      IF(.NOT.FORWARD) GO TO 30
C
C     COMPUTE VGAIN AT RADAR FOR DIRECTION OF PATCH
      ALPHA=ACOS(UXRG*UXPOINT+UYRG*UYPOINT+UZRG*UZPOINT)
      G1=GAIN(ALPHA,JD,CD,AD)
      G2(1)=1
      SINE(1)=G1*G2(1)
      SINE(1)=SIGN(1.,SINE(1))
      G1=G1**2
      RETURN
   30 G1=1
      GO TO 40
   50 DO 60 J=1,4
      ALPHA=ACOS(UXRG*UXS(J)+UYRG*UYS(J)+UZRG*UZS(J))
      G1P(J)=GAIN(ALPHA,JD,CD,AD)
      G2P(J)=1.
      SINE(J)=G1P(J)*G2P(J)
      SINE(J)=SIGN(1.,SINE(J))
      G1P(J)=G1P(J)**2
   60 CONTINUE
      IF(FORWARD)RETURN
      DO 70 J=1,4
      G2P(J)=G1P(J)
      G1P(J)=1.
   70 CONTINUE
      RETURN
      END
```



```
      SUBROUTINE B1POSTN(UXS,UYS,UZS,SI1D)
      COMMON/POINT/UXPOINT,UYPOINT,UZPOINT,DSINE(10)
      DIMENSION UXS(10),UYS(10),UZS(10)
      THETA=ATAN(UYPOINT/UXPOINT)
      SI=ATAN(UZPOINT/SQRT(UXPOINT**2+UYPOINT**2))
      RAD=SI1D*3.1415926535898/180.
      X1=COS(SI)*COS(THETA)*COS(RAD)**2
      X2=COS(RAD)*SIN(RAD)*SIN(THETA)
      X3=SIN(RAD)*SIN(SI)*COS(THETA)
      Y1=COS(SI)*SIN(THETA)*COS(RAD)**2
      Y2=COS(RAD)*SIN(RAD)*COS(THETA)
      Y3=SIN(RAD)*SIN(SI)*SIN(THETA)
      Z1=SIN(SI)*COS(RAD)**2
      Z2=SIN(RAD)*COS(SI)
      UXS(1)=X1+X2-X3
      UYS(1)=Y1-Y2-Y3
      UZS(1)=Z1+Z2
      UXS(2)=X1-X2-X3
      UYS(2)=Y1+Y2-Y3
      UZS(2)=Z1+Z2
      UXS(3)=X1-X2+X3
      UYS(3)=Y1+Y2+Y3
      UZS(3)=Z1-Z2
      UXS(4)=X1+X2+X3
      UYS(4)=Y1-Y2+Y3
      UZS(4)=Z1-Z2
      RETURN
      END
```

```
      SUBROUTINE  BESJ(X,FNU,N,F)
C-----------------------------------------------------------------------
C     REGULAR BESSEL FUNCTIONS OF REAL ARGUMENT.
C-----------------------------------------------------------------------
C     ARGUMENT DEFINITION
C        X     IS THE ARGUMENT OF THE BESSEL FUNCTION.
C        FNU   IS THE FRACTIONAL PART OF THE ORDER.
C        N     IS THE INTEGRAL PART OF THE HIGHEST ORDER TO BE
C              COMPUTED.
C        F     IS THE OUTPUT ARRAY OF BESSEL FUNCTIONS.
C-----------------------------------------------------------------------
C     REFERENCES
C        M. GOLDSTEIN AND R.M. THALER, RECURRENCE TECHNIQUES FOR THE
C             CALCULATION OF BESSEL FUNCTIONS, MTAC, 1959.
C        M. GOLDSTEIN AND R. M. THALER, BESSEL FUNCTIONS FOR LARGE
C             ARGUMENTS, MTAC, 1958.
C        G.N. WATSON, A TREATISE ON THE THEORY OF BESSEL FUNCTIONS,
C             CAMBRIDGE UNIVERSITY PRESS, 1948.
C-----------------------------------------------------------------------
      DIMENSION   F(1),C(5)
      DATA  PI2/1.57079632/
      F(1)=1.0
      DO 100 I=1,N
100   F(I+1)=0
      NN=IABS(N)
      CX=2./X
      IF(FNU.GT.1.5)GO TO 1
      IY=1
      GO TO 2
1     FNU=FNU-2.
      IY=2
2     CXNU=CX*FNU
      IF(X.GT.50.)GO TO 12
      KK=X+20.
      M=MAX0(KK,NN+10)
      IF(X.LT.1.)GO TO 3
      KK=39.*X**.333333333
      GO TO 4
3     KK=172.69388/(3.6888795-ALOG(X))
4     M=MIN0(M,KK)/2
      K=M+M+1
      F(K+1)=1.E-37
      F(K+2)=0.
      KK=K+1
      TT=FNU+KK
      DO 5 I=1,K
      J=KK-I
      TT=TT-1.
5     F(J)=CX*TT*F(J+1)-F(J+2)
```

```
      IF(X.GT.10.)GO TO 12
      PHI=FNU+2.
      ALFA=F(1)+F(3)*PHI
      T1=FNU-1.
      T2=T1-1.
      TT=1.
      DO 6 I=2,M
      TT=TT+1.
      PHI=PHI*(FNU+TT+TT)*(T1+TT)/(TT*(T2+TT+TT))
6     ALFA=PHI*F(2*I+1)+ALFA
      CALL GAMMA(1.+FNU,TT,IXXX,JXXX)
      IF(IXXX.EQ.1)GO TO 50
      IF(JXXX.EQ.1)GO TO 50
      ALFA=CX**FNU*ALFA*TT
      I1=1
7     DO 8 I=I1,K
8     F(I)=F(I)/ALFA
      IF(N.GE.0)GO TO 11
9     IF(IY.EQ.2) GO TO 49
      F(2)=CXNU*F(1)-F(2)
      IF(NN.LE.1)RETURN
      TT=FNU
      DO 10 I=2,NN
      TT=TT-1.
10    F(I+1)=CX*TT*F(I)-F(I-1)
11    IF(IY.EQ.1)RETURN
49    N=M
      X=Y1
      FNU=Y2
50    RETURN
C.....ASYMPTOTIC EXPANSION......
12    KK=1
      FU=FNU
      XXX=1./X
      XX=XXX*XXX
      TT=1./SQRT(PI2*X)
13    A=FU**2-.25
      C(5)=.25
      C(4)=.15625*A-.375
      C(3)=(.1171875*A-1.15625)*A+1.875
      C(2)=((.09521484375*A-2.38671875)*A+14.2265625)*A-19.6875
      C(1)=(((.08093261719*A-4.100585937)*A+58.224609375)*A-277.875)*A+3
     *54.375
      P=C(1)
      DO 14 I=2,5
14    P=P*XX+C(I)
      BT=(P*A*XX+1.)*TT
      C(5)=.5
```

```
      C(4)=.041666666*A-.25
      C(3)=(.0125*A-.35)*A+.75
      C(2)=((.000558035718*A-.4241071428)*A+3.60267857)*A-5.625
      C(1)=(((.0030381944*A-.486111)*A+10.28645833)*A-58.)*A+78.75
      P=C(1)
      DO 15 I=2,5
15    P=P*XX+C(I)
      PHI=X+XXX*P*A-(FU+.5)*PI2
      IF(KK.EQ.2)GO TO 16
      F1=BT*COS(PHI)
      Y1=BT*SIN(PHI)
      FU=FNU+1.
      KK=2
      GO TO 13
16    F2=BT*COS(PHI)
      Y2=BT*SIN(PHI)
      IF(X.GT.50.)GO TO 17
      IF(ABS(F1).LT.ABS(F2))GO TO 20
      ALFA=F(1)/F1
      GO TO 22
17    F(1)=F1
      F(2)=F2
      IF(N)9,11,18
18    IF(N.LE.1)GO TO 11
      TT=FNU
      DO 19 I=2,NN
      TT=TT+1.
19    F(I+1)=CX*TT*F(I)-F(I-1)
      GO TO 11
20    ALFA=F(2)/F2
22    F(1)=F1
      F(2)=F2
      I1=3
      GO TO 7
      END
```

```
      SUBROUTINE CONVOL (NBEAMC)
C
      COMMON YOUT2(102,10),RDYOUT2(102),RYOUT2(102,10)
      COMMON DELOUT(127,10),XOUT(102,10),YOUT(102,10),EXTRA(10,2),
     1       OUTC(127),DARRAY(127)
      COMMON RDELOUT(127,10),RXOUT(102,10),RYOUT(102,10),REXTRA(10,2),
     1       RRHOARY(10)
      COMMON/TGAINP/G1P(4),G2P(4)
      COMMON/TGAIND/G20P(4),G10P(4)
      COMMON/DERV/PARRAY(127),ARYPAR(5),GBETZ0(10),G10,G20(10),NP,
     1            DIRDOP,DFLT,UNIFORM,RANGLE,SIGZ0,RDZERO,NCC,
     2            FORPI,PI02,XTR,YTR,ZTR,RTR,RHOARY(10)
      COMMON/INPUTS/XTP,YTP,ZTP,XTV,YTV,ZTV,XRP,YRP,ZRP,GRMAX,GRAPH,NG,
     $              NSAMPLF,VOLT,VPUL,NSLOPE,SLOPE(10,9),
     $              NXSDMX,NYSDMX,DGBALL,DGBALL1,TRACK,NOUT,
     $              PI,REARTH,XLAM,PASSTGT,FORWARD,PULSE,SGPULSE,PWIDTH
      COMMON/SPOINTS/ XSP(100),YSP(100),ZSP(100)
      COMMON/SINFO/SCOUNT,SDATA1(100),SDATA2(100),SDATA3(100)
      COMMON/PROPT/PRINT1,PRINT2,PRINT3,PRINT4,PRINT5,IPRINT(20)
      LOGICAL PRINT1,PRINT2,PRINT3,PRINT4,PRINT5
      LOGICAL VPOL,PULSE,PASSTGT,FORWARD,SGPULSE,TRACK,GRAPH
      LOGICAL UNIFORM,VOLT
      COMPLEX RDZERO,DELOUT,OUTC,EXTRA,XOUT,YOUT,RHOARY
      COMPLEX YOUT2
      INTEGER SCOUNT
C
C
C     PROGRAM TO CONVOLVE RANGE(TIME) DELAY WITH THE
C           TRANSMITTED PULSE SHAPE.
C
C     DONE FOR ANTENNA BEAM(NBEAMC)
C
C     RESULT PLACED IN OUTC FOR OUTPUT
C
C
C     WRITTEN BY STAN POWERS MAY 1974
C
C
C
      IF(PRINT5)PRINT 7777
 7777 FORMAT(* CONVOL*)
      IPRINT(2)=IPRINT(2)+1
C
C     FIND NUMBER OF OUTPUT POINTS
C
      NCC=MIN0(125,NOUT+NP-1)
C
C     ZERO OUT ARRAY
C
```

```
      DO 100 I=1,NCC
      OUTC(I)=0.0
  100 CONTINUE
C
C     DO CONVOLUTION
C
      DO 200 N=1,NCC
C
C     FIND LOWER AND UPPER BOUND
C
      NL=AMAX0(1,N-NOUT+1)
      NU=MIN0(N,NP)
C
C
      DO 300 J=NL,NU
      KK=N-J+1
      OUTC(N)=OUTC(N)+PARRAY(J)*DELOUT(KK,NBEAMC)
  300 CONTINUE
  200 CONTINUE
      RETURN
      END
```



```
      SUBROUTINE DIFSLOP(JD,CD,AD,UXS,UYS,UZS,ANTSLOP,XRT,ZRT)
      DIMENSION UXS(1),UYS(1),UZS(1),DER(4)
      PHI=.1E-10
      ELEV=PHI+ATAN(ZRT/XRT)
      XDER=COS(ELEV)
      ZDER=SIN(ELEV)
      YDER=0.0
      DO 10 J=1,4
      ANGLE=XDER*UXS(J)+YDER*UYS(J)+ZDER*UZS(J)
      ANGLE=ACOS(ANGLE)
      DER(J)=GAIN(ANGLE,JD,CD,AD)
   10 CONTINUE
      ANTSLOP=.5*(DER(1)+DER(2)-DER(3)-DER(4))
      ANTSLOP=ANTSLOP/PHI
      WRITE(6,20)ANTSLOP
   20 FORMAT(6X8HANTSLOP=E20.8)
      RETURN
      END
```

```
      SUBROUTINE DPGAIN(NBEAMS)
C
      COMMON/TGAINP/G1P(4),G2P(4)
      COMMON/TGAIND/G20P(4),G10P(4)
      COMMON/BEAMS/SANGLE(10,2),UXS(10),UYS(10),UZS(10)
      COMMON/DERV/PARRAY(127),ARYPAR(5),GBETZ0(10),G10,G20(10),NP,
     1            DIRDOP,DELT,UNIFORM,RANGLE,SIGZ0,ROZERO,NCC,
     2            FORPI,PID2,XTR,YTR,ZTR,RTR,RHOARY(10)
      COMMON/INPUTS/XTP,YTP,ZTP,XTV,YTV,ZTV,XRP,YRP,ZRP,GRMAX,GRAPH,NG,
     $              NSAMPLE,VOLT,VPOL,NSLOPE,SLOPE(10,9),
     $              NXSDMX,NYSDMX,DGBALL,DGBALL1,TRACK,NOUT,
     $              PI,REARTH,XLAM,PASSTGT,FORWARD,PULSE,SQPULSE,PWIDTH
      COMMON/PATD/JD,BWD,CD,AD,SIOD,JS,BWS,CSCAN,ASCAN,SIOSCAN,
     $            JB,BWB,CB,AB,SIOB
      COMMON/POINT/UXPOINT,UYPOINT,UZPOINT,DSINE(10)
      COMMON/PROPT/PRINT1,PRINT2,PRINT3,PRINT4,PRINT5,IPRINT(20)
      COMMON/SPOINTS/ XSP(100),YSP(100),ZSP(100)
      COMMON/SINFO/SCOUNT,SDATA1(100),SDATA2(100),SDATA3(100)
C
      LOGICAL PRINT1,PRINT2,PRINT3,PRINT4,PRINT5
      LOGICAL VPOL,PULSE,PASSTGT,FORWARD,SQPULSE,TRACK,GRAPH,OUTPUT
      LOGICAL UNIFORM,VOLT,NEWSLOP
      COMPLEX ROZERO,RHOARY
      INTEGER SCOUNT
C
      IF(PRINT5)PRINT 7777
 7777 FORMAT(* DPGAIN*)
      IPRINT(3)=IPRINT(3)+1
C
      UXRT=-XTR/RTR
      UYRT=-YTR/RTR
      UZRT=-ZTR/RTR
      IF(PASSTGT)GOTO 10
   30 G10=1.
      DO 20 J=1,NBEAMS
      ALPHA=UXS(J)*UXRT+UYS(J)*UYRT+UZS(J)*UZRT
      ALPHA=ACOS(ALPHA)
      G20(J)=GAIN(ALPHA,JS,CSCAN,ASCAN)
      DSINE(J)=SIGN(1.,G20(J))
      G20(J)=G20(J)**2
   20 CONTINUE
      RETURN
   10 IF(TRACK) GO TO 40
      IF(.NOT.FORWARD)GOTO 30
      ALPHA=UXRT*UXPOINT+UYRT*UYPOINT+UZRT*UZPOINT
      ALPHA=ACOS(ALPHA)
      G10=GAIN(ALPHA,JD,CD,AD)
      G20(1)=1.
      DSINE(1)=SIGN(1.,G10)
```

```
      G10=G10**2
      RETURN
   40 DO 50 J=1,4
      ALPHA=UXRT*UXS(J)+UYRT*UYS(J)+UZRT*UZS(J)
      ALPHA=ACOS(ALPHA)
      G10P(J)=GAIN(ALPHA,JD,CD,AD)
      G20P(J)=1.
      DSINE(J)=SIGN(1.,G10P(J))
      G10P(J)=G10P(J)**2
   50 CONTINUE
      IF(FORWARD)RETURN
      DO 60 J=1,4
      G20P(J)=G10P(J)
      G10P(J)=1.
   60 CONTINUE
      RETURN
      END
```



```
      SUBROUTINE FIELD(VOLTAGE,GAINS,PDATA,G1,G2,NBEAMS,PHOZERO,GD,
     $FRPHASE,FR,DX,DY,ANG1,ANG2,RGR,RGT,SINE)
      COMMON/GRAZE/PARPP(2,2,2)
      COMMON/TGAINP/G1P(4),G2P(4)
      COMMON/PGAIN/GT,PT,GR,RADCON
      COMMON/TGAIND/G20P(4),G10P(4)
      COMMON/INPUTS/XTP,YTP,ZTP,XTV,YTV,ZTV,XRP,YRP,ZRP,GRMAX,GRAPH,NG,
     $              NSAMPLE,VOLT,VPOL,NSLOPE,SLOPE(10,9),
     $              NXSDMX,NYSDMX,DGBALL,DGBALL1,TRACK,NOUT,
     $              PI,REARTH,XLAM,PASSTGT,FORWARD,PULSE,SQPULSE,PWIDTH
      COMMON/DERV/PARRAY(127),ARYPAR(5),GBETZ0(10),G10,G20(10),NP,
     1            DIRDOP,DELT,UNIFORM,RANGLE,SIGZ0,ROZERO,NCC,
     2            FORPI,PID2,XTR,YTR,ZTR,RTR,RHOARY(10)
      DIMENSION FIELDM(10),G2(10),SINE(10),VAR(10),S1(10),S2(10)
      DIMENSION FIZERO(10),X(10),Y(10),S1P(10),S2P(10),VOLTAGE(10)
      DIMENSION PDATA(9)
      LOGICAL UNIFORM,GRAPH,VOLT,VPOL,TRACK,PASSTGT,FORWARD
      LOGICAL PULSE,SQPULSE
      COMPLEX ROZERO,RHOARY,VOLTAGE,FR,E2,AVG,EXPON,FIELDM
      SIFUN(X)=EXP(-(PDATA(9)*X)**2/2.)
      E2=0.
      DO 1 J=1,10
      FIELDM(J)=0.
      VAR(J)=0.
      S1(J)=0.
      S2(J)=0.
      FIZERO(J)=0.
      X(J)=0.
      Y(J)=0.
      S1P(J)=0.
      S2P(J)=0.
    1 CONTINUE
      EXPON=0.
      AVG=0.
C
C     COMPUTE MEAN VOLTAGE FIELD FOR PATCH
C
      IF(GAINS.GT.0.0) GO TO 10
      GO TO 20
   10 CONST1=SQRT(GAINS)
      CONST1=CONST1/FORPI
      CONST2=-PDATA(4)*XLAM*SQRT(PT)*CONST1
      CONST3=FORPI/(2.*XLAM)
      CONST4=CONST3*(RGR+RGT)
      EXPON=CMPLX(COS(CONST4),SIN(CONST4))
      AVG=CONST2*EXPON*FR
      DO 30 J=1,NBEAMS
      FIELDM(J)=SINE(J)*SQRT(G1P(J)*G2P(J))*AVG
      IF(.NOT.TRACK)FIELDM(J)=SINE(J)*SQRT(G1*G2(J))*AVG
```

```
   30 CONTINUE
C
C      FIND VARIANCES OF VOLTAGE FIELDS
C
   20 CON1=PT*(PDATA(4)**2)*(PHOZERO**2)*GD
      CON1=CON1*DX*DY*(XLAM**2)
      CON1=CON1/((FORPI**3)*(RGR*RGT)**2)
      DO 40 J=1,NBEAMS
      VAR(J)=G1P(J)*G2P(J)*CON1
      IF(.NOT.TRACK)VAR(J)=G1*G2(J)*CON1
   40 CONTINUE
C
C      COMPUTE CORRELATION COEFFICIENT
C
      IF(GAINS.GT.0.0) GO TO 50
      C=0.
      GO TO 60
   50 VZ=-FORPI/(2.*XLAM)
      VZ=VZ*(COS(ANG1)+COS(ANG2))
      ANG3=FORPI/(2.*XLAM)
      ANG3=2.*(ANG3*RGR+FRPHASE)
      XNUM1=SIFUN(VZ)**2-SIFUN(2.*VZ)
      XNUM1=XNUM1*SIN(ANG3)
      XDEN1=(1.-SIFUN(VZ)**2)**2
      XDEN1=XDEN1-((SIFUN(VZ)**2-SIFUN(2.*VZ))*COS(ANG3))**2
      XDEN1=SQRT(XDEN1)
      C=XNUM1/XDEN1
C
C      COMPUTE S1 AND S2
C
   60 IF(GAINS.GT.0.) GO TO 70
      XK=1.
      GO TO 80
   70 XNUM2=1.-SIFUN(VZ)**2
      XNUM2=XNUM2+(SIFUN(VZ)**2-SIFUN(2.*VZ))*COS(ANG3)
      XDEN2=1.-SIFUN(VZ)**2
      XDEN2=XDEN2-(SIFUN(VZ)**2-SIFUN(2.*VZ))*COS(ANG3)
      XK=XNUM2/XDEN2
      XK=SQRT(XK)
   80 DO 90 J=1,NBEAMS
      S1(J)=VAR(J)/(XK**2+1.)
      S2(J)=(XK**2)*S1(J)
   90 CONTINUE
C
C      COMPUTE ROTATION ANGLE FOR INDEPENDENCE
C
      DO 100 J=1,NBEAMS
      IF(S1(J).EQ.S2(J)) GO TO 110
```

```
      FIZERO(J)=2.*C*SQRT(S1(J)*S2(J))
      FIZERO(J)=.5*ATAN(FIZERO(J)/(S1(J)-S2(J)))
      GO TO 100
  110 IF(C.LT.0.)FIZERO(J)=-PI/4.
      IF(C.GT.0.)FIZERO(J)=PI/4.
      IF(C.EQ.0.)FIZERO(J)=0.0
  100 CONTINUE
C
C     COMPUTE COMPONENTS OF MEAN FIELDS
C
      DO 120 J=1,NBEAMS
      X(J)=REAL(FIELDM(J))
      Y(J)=AIMAG(FIELDM(J))
  120 CONTINUE
C
C     COMPUTE ROTATED STANDARD DEVIATIONS
C
      DO 130 J=1,NBEAMS
      S1P(J)=S1(J)*(COS(FIZERO(J))**2)
      S1P(J)=S1P(J)+S2(J)*(SIN(FIZERO(J))**2)
      S1P(J)=SQRT(S1P(J))
      S2P(J)=S2(J)*(COS(FIZERO(J))**2)
      S2P(J)=S2P(J)+S1(J)*(SIN(FIZERO(J))**2)
      S2P(J)=SQRT(S2P(J))
  130 CONTINUE
C
C     COMPUTE RANDOM FIELDS
C
      CALL GAUSS(1,,0,0,V)
      DO 150 J=1,NBEAMS
      SSI=X(J)*COS(FIZERO(J))+Y(J)*SIN(FIZERO(J))
      SSI=SSI+V*S1P(J)
      ATA=Y(J)*COS(FIZERO(J))-X(J)*SIN(FIZERO(J))
      ATA=ATA+V*S2P(J)
      XPR=SSI*COS(FIZERO(J))-ATA*SIN(FIZERO(J))
      YPR=SSI*SIN(FIZERO(J))+ATA*COS(FIZERO(J))
      E2=CMPLX(XPR,YPR)
      VOLTAGE(J)=E2
  150 CONTINUE
      RETURN
      END
```

```
      SUBROUTINE FINDPAR(YF,XF,NR,NC,PAR,PARP)
C
      COMMON YOUT2(102,10),RDYOUT2(102),RYOUT2(102,10)
      COMMON DELOUT(127,10),XOUT(102,10),YOUT(102,10),EXTRA(10,2),
     1       OUTC(127),DARRAY(127)
      COMMON RDELOUT(127,10),RXOUT(102,10),RYOUT(102,10),REXTRA(10,2),
     1       RRHOARY(10)
      COMMON/GRAZE/PARPP(2,2,2)
      COMMON/TGAINP/G1P(4),G2P(4)
      COMMON/TGAIND/G20P(4),G10P(4)
      COMMON/BEAMS/SANGLE(10,2),UXS(10),UYS(10),UZS(10)
      COMMON/DERV/PARRAY(127),ARYPAR(5),GBETZ0(10),G10,G20(10),NP,
     1            DIRDOP,DELT,UNIFORM,RANGLE,SIGZ0,ROZERO,NCC,
     2            FORPI,PID2,XTR,YTR,ZTR,RTR,RHOARY(10)
      COMMON/INPUTS/XTP,YTP,ZTP,XTV,YTV,ZTV,XRP,YRP,ZRP,GRMAX,GRAPH,NG,
     $              NSAMPLE,VOLT,VPOL,NSLOPE,SLOPE(10,9),
     $              NXSDMX,NYSDMX,DGBALL,DGBALL1,TRACK,NOUT,
     $              PI,REARTH,XLAM,PASSTGT,FORWARD,PULSE,SQPULSE,PWIDTH
      COMMON/PATD/JD,BWD,CD,AD,SIOD,JS,BWS,CSCAN,ASCAN,SIOSCAN,
     $            JB,BWB,CB,AB,SIOB
      COMMON/PGAIN/GT,PT,GR,RADCON
      COMMON/PROPT/PRINT1,PRINT2,PRINT3,PRINT4,PRINT5,IPRINT(20)
      COMMON/RCOEF/FRES(2,2)
      COMMON/RTYPE/SPEC,DIFFUSE
      COMMON/SPOINTS/ XSP(100),YSP(100),ZSP(100)
      COMMON/SINFO/SCOUNT,SDATA1(100),SDATA2(100),SDATA3(100)
      COMMON/RANGE/RGR,RGT
      COMMON/MULSPEC/SPCHECK
C
      DIMENSION PAR(2,2,6),PARP(2,2,9)
      LOGICAL VPOL,PULSE,PASSTGT,FORWARD,SQPULSE,TRACK,GRAPH
      LOGICAL UNIFORM,VOLT
      LOGICAL SPEC,DIFFUSE
      LOGICAL PRINT1,PRINT2,PRINT3,PRINT4,PRINT5
      COMPLEX ROZERO,DELOUT,OUTC,EXTRA,XOUT,YOUT,RHOARY
      COMPLEX YOUT2
      COMPLEX FRES
      INTEGER SCOUNT
C
      F(A,B,C)=EXP(-(4.*PI*A*SIN(B)/C)**2)
      IF(PRINT5)PRINT 7777
 7777 FORMAT(* FINDPAR*)
      IPRINT(4)=IPRINT(4)+1
C
C     SMOOTH EARTH PATCH CORNER (RECEIVER COORDS.)
C
      ANGX=XF/REARTH
      ANGY=YF/REARTH
      ANGXY=SQRT(XF**2+YF**2)/REARTH
```

```
      X=REARTH*SIN(ANGX)
      Y=REARTH*SIN(ANGY)
      Z=REARTH*COS(ANGXY)
      GRR=XF
C
C     SURFACE SLOPE DETERMINATION
C
      IF(.NOT. TRACK) GO TO 24
      RANGLEP=-RANGLE
      CALL RCOORD(RANGLEP,X,Y,Z,XREF,YREF,ZREF)
      ANGLE=ASIN(XREF/REARTH)
      GRR=REARTH*(ANGLE)
   24 DO 20 I=1,NSLOPE
      RDIFF=SLOPE(I,1)-GRR
      IF(RDIFF .GE. 0.) GO TO 10
   20 CONTINUE
      STOP103
   10 XPSLOPE=SLOPE(I,3)
      YPSLOPE=SLOPE(I,4)
      HILLHT=SLOPE(I,9)
      IF(.NOT.TRACK) GO TO 11
      CALL RCOORD(RANGLE,SLOPE(I,3),SLOPE(I,4),SLOPE(I,9),XPSLOPE,
     $            YPSLOPE,HILLHT)
C
C     MEAN ROUGH EARTH PATCH CORNER (RECIEVER COORDS.)
C
   11 RR=SQRT(X**2+Y**2+Z**2)
      UX=X/RR
      UY=Y/RR
      UZ=Z/RR
      X=(REARTH+HILLHT)*UX
      Y=(REARTH+HILLHT)*UY
      Z=(REARTH+HILLHT)*UZ
C
C     VECTOR FROM PATCH CORNER TO TARGET
C
      XGT=XTP-X
      YGT=-Y
      ZGT=ZTP-Z
      RGT=SQRT(XGT**2+YGT**2+ZGT**2)
      RGTI=1.0/RGT
C
C     VECTOR FROM PATCH CORNER TO RECEIVER
C
      XGR=XRP-X
      YGR=-Y
      ZGR=ZRP-Z
      RGR=SQRT(XGR**2+YGR**2+ZGR**2)
```

```
      RGRI=1.0/RGR
C
C     FIND EQUATION OF THE BISECTING VECTOR
C
      XBI=XGT*RGTI+XGR*RGRI
      YBI=YGT*RGTI+YGR*RGRI
      ZBI=ZGT*RGTI+ZGR*RGRI

      RBI=SQRT(XBI**2+YBI**2+ZBI**2)
C
C       FIND UNIT  VECTORS
C
      UXGT=XGT*RGTI
      UYGT=YGT*RGTI
      UZGT=ZGT*RGTI
      UXGR=XGR*RGRI
      UYGR=YGR*RGRI
      UZGR=ZGR*RGRI
C
C       FIND BETA
C
      PROJ1=SQRT(X**2+Z**2)
      PROJ2=SQRT(Y**2+Z**2)
      ANGXP=ACOS(Z/PROJ1)
      ANGYP=ACOS(Z/PROJ2)
      GAM1=ANGXP-ATAN(XPSLOPE)
      GAM2=ANGYP-ATAN(YPSLOPE)
C
C     LOCAL NORMAL
C
      XLN=SIN(GAM1)
      YLN=COS(GAM1)*TAN(GAM2)
      ZLN=COS(GAM1)
C
C     UNIT VECTOR
C
      RLN=SQRT(XLN**2+YLN**2+ZLN**2)
      RLNI=1./RLN
      UXLN=XLN*RLNI
      UYLN=YLN*RLNI
      UZLN=ZLN*RLNI
      CBETA=(XBI*UXLN+YBI*UYLN+ZBI*UZLN)/RBI
      BETA=ACOS(CBETA)
C
C     REFLECTION ANGLES
C
      THET1=ACOS(UXGT*UXLN+UYGT*UYLN+UZGT*UZLN)
      THET2=ACOS(UXGR*UXLN+UYGR*UYLN+UZGR*UZLN)
```

```
      ACHANGE=THET2
      IF(.NOT.FORWARD)GOTO 25
      THET2=THET1
      THET1=ACHANGE
   25 GAMA1=PID2-THET1
      GAMA2=PID2-THET2
C
C     CALCULATE ROUGHNESS FACTOR
C
      A1=SLOPE(I,8)*SIN(GAMA1)/XLAM
      A2=SLOPE(I,8)*SIN(GAMA2)/XLAM
      IF(A1.LE..2.OR.A2.LE..2)GOTO 12
      FUDGE=1.
      GOTO 13
   12 FUDGE=SQRT((1.-F(SLOPE(I,8),GAMA1,XLAM))*(1.-F(SLOPE(I,8),GAMA2,
     $XLAM)))
   13 IF(GAMA1 .LT. 0.0 .OR. GAMA2 .LT. 0.0) FUDGE=0.0
C
C     ESTABLISH PAR (PATCH CORNER DATA)
C
      PAR(NR,NC,5)=BETA
      PAR(NR,NC,3)=FUDGE
      PAR(NR,NC,6)=FUDGE*GAINB(BETA,I)
      IF(SPEC.AND..NOT.DIFFUSE)PAR(NR,NC,6)=0.
      DELAY =RGT+RGR+RTR
      PAR(NR,NC,2)=DELAY
      DUP=-(XTV*UXGT+YTV*UYGT+ZTV*UZGT)
      PAR(NR,NC,1)=DIRDUP+DUP
C
      CALL FRESNEL(I,GAMA1,PHUZERO,D)
      PAR(NR,NC,4)=0.0
      FRES(NR,NC)=RUZERO
      PARP(NR,NC,1)=X
      PARP(NR,NC,2)=Y
      PARP(NR,NC,3)=Z
      PARP(NR,NC,4)=D
      PARP(NR,NC,5)=UXLN
      PARP(NR,NC,6)=UYLN
      PARP(NR,NC,7)=UZLN
      PARP(NR,NC,8)=SLOPE(I,7)
      PARP(NR,NC,9)=SLOPE(I,8)
      PARPP(NR,NC,1)=THET1
      PARPP(NR,NC,2)=THET2
      RETURN
         END
```

```
      SUBROUTINE FINDPWR(PARP,PAR,DX,DY,DPOWER,SPOWER,VOLTAGE,NBEAMS)
C
      COMMON YOUT2(102,10),RDYOUT2(102),RYOUT2(102,10)
      COMMON DELOUT(127,10),XOUT(102,10),YOUT(102,10),EXTRA(10,2),
     1       OUTC(127),DARRAY(127)
      COMMON RDELOUT(127,10),RXOUT(102,10),RYOUT(102,10),REXTRA(10,2),
     1       RRHOARY(10)
      COMMON/GRAZE/PARPP(2,2,2)
      COMMON/TGAIND/G20P(4),G10P(4)
      COMMON/TGAINP/G1P(4),G2P(4)
      COMMON/BEAMS/BANGLE(10,2),UXS(10),UYS(10),UZS(10)
      COMMON/DERV/PARRAY(127),ARYPAR(5),GBETZ0(10),G10,G20(10),NP,
     1            DIRDOP,DFLT,UNIFORM,RANGLE,SIGZ0,ROZERO,NCC,
     2            FORPI,PIN2,XTR,YTR,ZTR,HTR,RHOARY(10)
      COMMON/INPUTS/XTP,YTP,ZTP,XTV,YTV,ZTV,XRP,YRP,ZRP,GRMAX,GRAPH,NG,
     $              NSAMPLE,VOLT,VPOL,NSLOPE,SLOPE(10,9),
     $              NX3DMX,NYSDMX,DGBALL,DGBALL1,TRACK,NOUT,
     $              PI,REARTH,XLAM,PASSTGT,FORWARD,PULSE,SOPULSE,PWIDTH
      COMMON/PATD/JD,BWD,CD,AD,SIOD,JS,BWS,CSCAN,ASCAN,SIOSCAN,
     $            JB,BWB,CB,AB,SIOB
      COMMON/PGAIN/GT,PT,GR,RADCON
      COMMON/PROPT/PRINT1,PRINT2,PRINT3,PRINT4,PRINT5,IPRINT(20)
      COMMON/RCOEF/FRES(2,2)
      COMMON/RODD/ROD
      COMMON/RTYPE/SPEC,DIFFUSE
      COMMON/PATCH/XGR,YGR,ZGR,XGT,YGT,ZGT
      COMMON/SPOINTS/ XSP(100),YSP(100),ZSP(100)
      COMMON/SINFO/SCOUNT,SDATA1(100),SDATA2(100),SDATA3(100)
      COMMON/MULSPEC/SPCHECK
C
      REAL IPART
      LOGICAL PRINT1,PRINT2,PRINT3,PRINT4,PRINT5
      LOGICAL SPEC,DIFFUSE
      DIMENSION PAR(2,2,6),PARP(2,2,9)
      DIMENSION PDATA(9),G2(10),SINE(10)
      DIMENSION DPOWER(10),SPOWER(10)
      DIMENSION VOLTAGE(10)
      LOGICAL VPOL,PULSE,PASSTGT,FORWARD,SOPULSE,TRACK,GRAPH
      LOGICAL UNIFORM,VOLT
      COMPLEX DDELR
      COMPLEX ROZERO,DELOUT,OUTC,EXTRA,XOUT,YOUT,RHOARY
      COMPLEX VOLTAGE,CDELR,CPHI
      COMPLEX YOUT2
      COMPLEX FRES,FR
      INTEGER SCOUNT
      NAMELIST/INFO1/RTR,RGR,RGT,GS,GD,ROD
      NAMELIST/INFO2/DELRMIN,DELRMAX
      NAMELIST/INFO3/PHASE
      NAMELIST/INFO4/DPOWER,SPOWER,VOLTAGE
```

```
C
      IF(PRINT5)PRINT 7777
 7777 FORMAT(* FINDPRW*)
      IPRINT(5)=IPRINT(5)+1
C
C     ZERO OUT PATCH DATA ARRAY
C
      DO 10 J=1,9
 10   PDATA(J)=0.0
C
C     FIND AVERAGE PATCH DATA
C
      DO 20 J=1,9
      DO 30 K=1,2
      DO 30 L=1,2
 30   PDATA(J)=PDATA(J)+PARP(K,L,J)
 20   PDATA(J)=PDATA(J)*.25
C
C     FIND AVERGE PATCH GAIN AND AVG. FRESNEL REFL. COEFF.
C
      ANG1=0.
      ANG2=0.
      FR=0.
      GD=0.0
      DO 40 J=1,2
      DO 40 K=1,2
      FR=FR+FRES(J,K)
   40 GD=GD+PAR(J,K,6)
      FR=FR*.25
      GD=GD*.25
      DO 41 J=1,2
      DO 41 K=1,2
      ANG1=ANG1+PARPP(J,K,1)
   41 ANG2=ANG2+PARPP(J,K,2)
      ANG1=ANG1*.25
      ANG2=ANG2*.25
      IPART=AIMAG(FR)
      RPART=REAL(FR)
      PHOZERO=SQRT(RPART**2+IPART**2)
      CPHI=FR/PHOZERO
      FRPHASE=ACOS(RPART)
      IF(IPART.LT.0.0)FRPHASE=2.*PI-FRPHASE
C
C     FIND APPROXIMATE PATCH AREA
C
      PAREA=ABS(DX*DY)
C
C     FIND VECTOR FROM PATCH TO RECEIVER
```

```
C
      XGR=-PDATA(1)
      YGR=-PDATA(2)
      ZGR=ZRP-PDATA(3)
C
C     FIND VECTOR FROM PATCH TO TRANSMITTER (TARGET INCASE OF PASSTGT)
C
      XGT=XTP-PDATA(1)
      YGT=PDATA(2)
      ZGT=ZTP-PDATA(3)
C
C     FIND VECTOR LENGTHS
C
      RGRS=XGR**2+YGR**2+ZGR**2
      RGTS=XGT**2+YGT**2+ZGT**2
      RGR=SQRT(RGRS)
      RGT=SQRT(RGTS)
C
C     COMPUTE DIFFUSE REFLECTION COEFFICIENT FOR PATCH
C     ASSUMING OMNIDIRECTIONAL ANTENNA
C
      ROD=(1./FORPI)*(RTR/(RGR*RGT))**2
      ROD=ROD*GD*PAREA
C
C     FIND ANTENNA GAINS
C
      CALL ANTGAIN(PDATA,G1,G2,NBEAMS,SINE)
      IF(TRACK)GO TO 100
C
C     FIND DIFFUSE PATCH POWERS
C
      DO 50 J=1,NBEAMS
      DPOWER(J)=RADCON*G1*G2(J)*GD*PAREA*(PHOZERO*PDATA(8))**2
 50   DPOWER(J)=DPOWER(J)/(RGTS*RGRS)
C
C     FIND SPECULAR GAIN FOR PATCH
C
   51 CALL SGAIN(PARP,PDATA,GAINS,SDELR)
C
C     COMPUTE SPECULAR PATCH POWER
C
   71 DO 70 J=1,NBEAMS
   70 SPOWER(J)=RADCON*G1*G2(J)*GAINS*(PHOZERO*PDATA(8)*PDATA(4))**2
  100 IF(TRACK)CALL SGAIN(PARP,PDATA,GAINS,SDELR)
      CALL FIELD(VOLTAGE,GAINS,PDATA,G1,G2,NBEAMS,PHOZERO,GD
     $FRPHASE,FR,DX,DY,ANG1,ANG2,RGR,RGT,SINE)
      IF(PRINT2)PRINT 94,(DPOWER(J),J=1,NBEAMS)                    PRINT2
      IF(PRINT2)PRINT 95,(SPOWER(J),J=1,NBEAMS)                    PRINT2
```

```
      IF(PRINT2)PRINT 96,(VOLTAGE(J),J=1,NBEAMS)
   90 FORMAT(* RTR,RGR,RGT,GS,GD,ROD,DELRMIN,DELRMAX* 8E12.4)
   93 FORMAT(//* PHASE* E12.4)
   94 FORMAT(//* DPOWER*/(5E12.4))
   95 FORMAT(//* SPOWER*/(5E12.4))
   96 FORMAT(//* VOLTAGE*/(10E12.4))
      RETURN
      END
```



```
      SUBROUTINE FRESNEL(I,GAMA1,PHOZERO,D)
C
      COMMON YOUT2(102,10),RDYOUT2(102),RYOUT2(102,10)
      COMMON DELOUT(127,10),XOUT(102,10),YOUT(102,10),EXTRA(10,2),
     1       OUTC(127),DARRAY(127)
      COMMON RDELOUT(127,10),RXOUT(102,10),RYOUT(102,10),RFXTRA(10,2),
     1       RRHOARY(10)
      COMMON/BEAMS/SANGLE(10,2),UXS(10),UYS(10),UZS(10)
      COMMON/TGAINP/G1P(4),G2P(4)
      COMMON/TGAIND/G2DP(4),G1DP(4)
      COMMON/DERV/PARRAY(127),ARYPAR(5),GBEIZO(10),G10,G20(10),NP,
     1            DIRDOP,DELT,UNIFORM,RANGLE,SIGZO,ROZERO,NCC,
     2            FORPI,PID2,XTR,YTR,ZTR,RTR,RHOARY(10)
      COMMON/INC/DX,DY
      COMMON/INPUTS/XTP,YTP,ZTP,XTV,YTV,ZTV,XRP,YRP,ZRP,GRMAX,GRAPH,NG,
     $              NSAMPLE,VOLT,VPOL,NSLOPE,SLOPE(10,9),
     $              NXSDMX,NYSDMX,DGBALL,DGBALL1,TRACK,NOUT,
     $              PI,REARTH,XLAM,PASSTGT,FORWARD,PULSE,SOPULSE,PWIDTH
      COMMON/PATD/JD,BWD,CD,AD,SIOD,JS,BWS,CSCAN,ASCAN,SIOSCAN,
     $            JB,BWB,CB,AB,SIOB
      COMMON/PGAIN/GT,PT,GR,RADCON
      COMMON/PROPT/PRINT1,PRINT2,PRINT3,PRINT4,PRINT5,IPRINT(20)
      COMMON/SINFO/SCOUNT,SDATA1(100),SDATA2(100),SDATA3(100)
      COMMON/SPOINTS/ XSP(100),YSP(100),ZSP(100)
      COMMON/RANGE/RGR,RGT
C
      REAL IPART
      LOGICAL PRINT1,PRINT2,PRINT3,PRINT4,PRINT5
      LOGICAL VPOL,PULSE,PASSTGT,FORWARD,SOPULSE,TRACK,GRAPH
      LOGICAL UNIFORM,VOLT
      COMPLEX ROZERO,DELOUT,OUTC,EXTRA,XOUT,YOUT,RHOARY
      COMPLEX YOUT2
      COMPLEX EP,A,B,C
      INTEGER SCOUNT
C
      IF(PRINT5)PRINT 7777
 7777 FORMAT(* FRESNEL*)
      IPRINT(6)=IPRINT(6)+1
C
      EPR=SLOPE(I,5)
      EPI=-60.0*XLAM*SLOPE(I,6)
      EP=CMPLX(EPR,EPI)
      A=1.
      IF(VPOL) A=EP
      B=A*SIN(GAMA1)-CSQRT(EP-COS(GAMA1)**2)
      C=A*SIN(GAMA1)+CSQRT(EP-COS(GAMA1)**2)
      ROZERO =B/C
C
C     COMPUTE DIVERGENCE FACTOR
```

```
C
   36 C=SIN(GAMA1)
      D1=1.+2.*RGR*RGT/(REARTH*(RGR+RGT)*C)
      D1=1./SQRT(D1)
      D2=1.+2.*RGR*RGT/(REARTH*(RGR+RGT))
      D2=1./SQRT(D2)
      D=D1*D2
      IPART=AIMAG(RUZERO)
      RPART=REAL(RUZERO)
      PH. ERO=SQRT(IPART**2+RPART**2)
      RE' RN
      END
      FUNCTION GAIN(A,K,R,C)
      COMMON/TGAINP/G1P(4),G2P(4)
      COMMON/TGAIND/G20P(4),G10P(4)
      COMMON/PROPI/PRINT1,PRINT2,PRINT3,PRINT4,PRINT5,IPRINT(20)
      LOGICAL PRINT1,PRINT2,PRINT3,PRINT4,PRINT5
      DIMENSION F(100)
      DO 10 J=1,100
      F(J)=0.0
   10 CONTINUE
C
      IF(PRINT5)PRINT 7777
 7777 FORMAT(* GAIN*)
      IPRINT(7)=IPRINT(7)+1
C
      N=K+1
      BETA=180./3.1415926535898*A
      SI=C*BETA
      CALL BESJ(SI,0.,N,F)
      GAIN=B*F(N)/(SI**N)
      RETURN
      END
      FUNCTION GAINB(BETA,T)
C
      COMMON YOUT2(102,10),RDYOUT2(102),RYOUT2(102,10)
      COMMON DELOUT(127,10),XOUT(102,10),YOUT(102,10),EXTRA(10,2),
     1       OUTC(127),DARRAY(127)
      COMMON RDELOUT(127,10),RXOUT(102,10),RYOUT(102,10),REXTRA(10,2),
     1       RRHOARY(10)
      COMMON/TGAIND/G20P(4),G10P(4)
      COMMON/TGAINP/G1P(4),G2P(4)
      COMMON/DERV/PARRAY(127),ARYPAR(5),GBETZ0(10),G10,G20(10),NP,
     1            DIRDOP,DELT,UNIFORM,RANGLE,SIGZ0,RUZERO,NCC,
     2            FURPI,PI02,XTR,YTR,ZTR,RTR,RHOARY(10)
      COMMON/INC/DX,DY
      COMMON/INPUTS/XTP,YTP,ZTP,XTV,YTV,ZTV,XRP,YRP,ZRP,GRMAX,GRAPH,NG,
     3              NSAMPLE,VOLT,VPOL,NSLOPE,SLOPE(10,9),
```

```
     $               NXSDMX,NYSDMX,DGBALL,DGBALL1,TRACK,NOUT,
     $               PI,REARTH,XLAM,PASSTGT,FORWARD,PULSE,SQPULSE,PWIDTH
      COMMON/PATD/JB,BWD,CR,AD,SIOD,JS,BWS,CSCAN,ASCAN,SIOSCAN,
     $             JB,BWB,CR,AB,SIOB
      COMMON/PGAIN/GT,PT,GR,RADCON
      COMMON/PROPT/PRINT1,PRINT2,PRINT3,PRINT4,PRINT5,IPRINT(20)
      COMMON/SINFO/SCOUNT,SDATA1(100),SDATA2(100),SDATA3(100)
      COMMON/SPOINTS/ XSP(100),YSP(100),ZSP(100)
C
      LOGICAL PRINT1,PRINT2,PRINT3,PRINT4,PRINT5
      LOGICAL VPOL,PULSE,PASSTGT,FORWARD,SQPULSE,TRACK,GRAPH
      LOGICAL UNIFORM,VOLT
      COMPLEX RUZERO,DELOUT,OUTC,EXTRA,XOUT,YOUT,RHOARY
      COMPLEX YOUT2
      INTEGER SCOUNT
C
      IF(PRINT5)PRINT 7777
 7777 FORMAT(* GAINB*)
      IPRINT(8)=IPRINT(8)+1
C
      IF(.NOT. UNIFORM) GO TO 10
      GAINB=GBETZ0(I)
      IF(BETA .GT. SLOPE(I,2)) GAINB=0.0
      RETURN
   10 GAINB=GBETZ0(I)*EXP(-TAN(BETA)**2/(TAN(SLOPE(I,2))**2))
      IF(BETA .GT. 3.*SLOPE(I,2)) GAINB=0.0
      RETURN
      END
```

```
      SUBROUTINE  GAMMA(X,GAMMAX,IRTN3,IRTN4)
C-----------------------------------------------------------------------
C     CALCULATION OF THE GAMMA FUNCTION OF X.
C-----------------------------------------------------------------------
      DIMENSION   A(8)
      DATA  (A(I),I=1,8)/-.577191652,.988205891,-.897056937,.918206857,-
     *.756704078,.482199394,-.193527818,.035868343/
      DATA  CV/.434294482/
      IRTN3=0
      IRTN4=0
      IF(ABS(X).LT.33.) GO TO 1
C-----------------------------------------------------------------------
C     THE MAGNITUDE OF X IS GREATER THAN 33.
C     THE BRIGGSIAN LOGARITHM OF THE GAMMA FUNCTION OF X  IS CALCULATED.
C-----------------------------------------------------------------------
      GAMMAX=(X-.5)*CV*ALOG(ABS(X))-CV*X+.39908995+CV*ALOG(1.+1./(12.*X)
     *+1./(288.*X*X)-139./(51840.*X*X*X*X))
      GO TO 7310
C-----------------------------------------------------------------------
C     INITIALIZATION OF FACTOR (FACTORIAL X) AND XFACT (X-1).
C-----------------------------------------------------------------------
1     FACTOR=1.
      XFACT=X-1.
      IF(XFACT.LT.0.) GO TO 3
C-----------------------------------------------------------------------
C     POSITIVE X
C-----------------------------------------------------------------------
2     IF(XFACT.LT.1.) GO TO 5
      FACTOR=FACTOR*XFACT
      XFACT=XFACT-1.
      GO TO 2
C-----------------------------------------------------------------------
C     NEGATIVE X
C-----------------------------------------------------------------------
3     XFACT=XFACT+1.
      FACTOR=FACTOR*XFACT
      IF(XFACT)3,7,4
4     FACTOR=1./FACTOR
C-----------------------------------------------------------------------
C     CALCULATION OF THE GAMMA FUNCTION OF X
C     THIS IS EQUAL TO THE GAMMA FUNCTION OF XFACT+1.
C-----------------------------------------------------------------------
5     GAMMAX=0.
      L1=(IABS(1-(8))+1)/1
      DO 6 L2=1,L1
      I=8+(L2-1)*(-1)
6     GAMMAX=(GAMMAX+A(I))*XFACT
      GAMMAX=(1.+GAMMAX)*FACTOR
      RETURN
```



```
C-----------------------------------------------------------------------
C     ERROR RETURN FOR X NEGATIVE INTEGER.
C-----------------------------------------------------------------------
7     GO TO 7311
7310  IRTN3=1
      RETURN
7311  IRTN4=1
      RETURN
      END
```

```
      SUBROUTINE GAUSS(S,AM,V)
      A=0.0
      DO 50 I=1,12
      Y=RANF(0)
   50 A=A+Y
      V=(A-6.)*S+AM
      RETURN
      END
```



```
      SUBROUTINE PATTERN(N,THETA,CP,AP,SI0,A)
      DIMENSION F(100)
      COMMON/TRP/JCALL
      COMMON/PROPT/PRINT1,PRINT2,PRINT3,PRINT4,PRINT5,IPRINT(20)
      LOGICAL PRINT1,PRINT2,PRINT3,PRINT4,PRINT5
C
      IF(PRINT5)PRINT 7777
 7777 FORMAT(* PATTERN*)
      IPRINT(9)=IPRINT(9)+1
C
C     INITIALIZATION
C
      K=0
      SIINC=.01
      KK=1
      SI=.1E-08
      C=2.**(N+1)
      X=N+2
      CALL GAMMA(X,GAMMAX,IRET1,IRET2)
      C=C*GAMMAX
      M=N+1
C
C     CALCULATE VALUE OF ST FOR WHICH BESSEL FUNCTION EQUALS A
C
   40 CALL BESJ(SI,0.,M,F)
      IF(JCALL.EQ.1)CALL BFSJ(SI*AP,0.,M,F)
      IF(JCALL.EQ.1)C=CP
      Y=C*F(M)/(SI**M)
      IF(Y .GT. A) GO TO 10
      IF(K .EQ. 1) GO TO 20
      KK=1
      SI2=SI
      SI1=SI-SIINC
      K=1
   70 SI=SI1
   60 DIFF= ABS(Y-A)
      IF(DIFF .LT. .001) GO TO 30
      SIINC=(SI2-SI1)*.5
   50 SI=SI+SIINC
      IF(KK .GT. 1000) STOP500
      KK=KK+1
      GO TO 40
   10 IF(K .EQ. 0) GO TO 50
      SI1=SI
      GO TO 60
   20 SI2=SI
      GO TO 70
   30 SI0=SI2
      IF(JCALL.EQ.1)RETURN
```



```
      CP=C*(THETA/(2.*SI0))**M
      AP=2.*SI0/THETA
      RETURN
      END
```

```
      SUBROUTINE PENN(X,Y,N,K,J)
      DIMENSION X(1),Y(1)
      PUNCH 100,N,K
      GO TO(10,20,30,40,50,60),J
   10 PUNCH 200
      PUNCH 210
      GO TO 500
   20 PUNCH 250
      PUNCH 260
      GO TO 500
   30 PUNCH 300
      PUNCH 310
      GO TO 500
   40 PUNCH 350
      PUNCH 360
      GO TO 500
   50 PUNCH 400
      PUNCH 410
      GO TO 500
   60 PUNCH 700
      PUNCH 710
  500 PUNCH 600,(X(I),Y(I),I=1,N)
      RETURN
  100 FORMAT(2I5)
  200 FORMAT(10X,45HPLOT OF REFLECTED POWER VS DOWNRANGE DISTANCE)
  210 FORMAT(18HDOWNRANGE DISTANCE,2X5HPOWER)
  250 FORMAT(10X,52HPLOT OF REFLECTION COEFFICIENT VS DOWNRANGE DISTANCE
     $)
  260 FORMAT(18HDOWNRANGE DISTANCE,2X4HRHOD)
  300 FORMAT(10X53HPLOT OF REFLECTION COEFFICIENT VS CROSSRANGE DISTANCE
     $)
  310 FORMAT(19HCROSSRANGE DISTANCE,1X4HRHOD)
  350 FORMAT(10X46HPLOT OF REFLECTED POWER VS CROSSRANGE DISTANCE)
  360 FORMAT(19HCROSSRANGE DISTANCE,1X5HPOWER)
  400 FORMAT(10X21HPLOT OF POWER VS TIME)
  410 FORMAT(4HTIME,16X,5HPOWER)
  600 FORMAT(4E20.7)
  700 FORMAT(10X28HPLOT OF ERROR VS SLANT RANGE)
  710 FORMAT(5HRANGE,15X,9HELEVATION)
      END
```

```
      SUBROUTINE  PICTUR (X,Y,N)
C
C     CRAIG*S PLOTTING ROUTINE
C
      INTEGER S,SX,SD,SI
      DIMENSION X(1),Y(1),L(101)
      DATA SD/1H./,SX/1HX/,SI/1HI/,S/1H /
C
      YU=Y(1)
      YL=Y(1)
      DO 9900 I=2,N
      Z=Y(I)
      IF (Z .GT. YU) YU=Z
      IF (Z .LT. YL) YL=Z
 9900 CONTINUE
      YD=YU-YL
      IF(YD)8950,8999,8950
 8950 CONTINUE
      YM= (YU+YL)/2.
      DO 9902 I=1,101
 9902 L(I)=SD
      WRITE(6,9912)
      WRITE(6,9913)
      WRITE (6, 9915) YL,YM,YU
      WRITE(6,9914)
      WRITE(6,9911) L
      DO 9903 I=1,101
 9903 L(I)=S
      L(1)=SD
      L(51)=SD
      L(101)=SD
      DO 9904 I=1,N
      KN=IFIX(((Y(I)-YL)/YD)*100.0+.5)+1
      LSAVE=L(KN)
      L(KN)=SX
C     WRITE(6,9910) X(I),Y(I)
      WRITE(6,9910)X(I),L,Y(I)
C     WRITE(6,9911) L
C     L(KN)=S
      L(KN)=LSAVE
 9904 CONTINUE
      RETURN
 8999   WRITE(6,9800)YD
      RETURN
 9800  FORMAT(1X,///,* VALUE OF GRAPH IS CONSTANT = *,E20.8,///)
 9912 FORMAT(1H1)
 9913 FORMAT(3H X=,112X,3H Y=)
 9915 FORMAT (5X,1E20.8,30X,1E20.8,30X,1E20.8)
 9914 FORMAT(1H0)
```



```
 9911 FORMAT (1H+,14X,101A1)
C9910 FORMAT(1H ,E14.7,1H.,49X1H.,49X1H.,E14.7)
 9910 FORMAT(1H ,E14.7,101A1,E14.7)
        END
```

```
      SUBROUTINE PLOTT(NBEAMS)
C
      COMMON YOUT2(102,10),RDYOUT2(102),RYOUT2(102,10)
      COMMON DELOUT(127,10),XOUT(102,10),YOUT(102,10),EXTRA(10,2),
     1       OUTC(127),DARRAY(127)
      COMMON RDELOUT(127,10),RXOUT(102,10),RYOUT(102,10),REXTRA(10,2),
     1       RRHOARY(10)
      COMMON/INC/DX,DY
      COMMON/DERV/PARRAY(127),ARYPAR(5),GBETZ0(10),G10,G20(10),NP,
     1            DIRDOP,DELT,UNIFORM,RANGLE,SIGZC,ROZERO,NCC,
     2            FORPI,PID2,XTR,YTR,ZTR,RTR,RHOARY(10)
      COMMON/INPUTS/XTP,YTP,ZTP,XTV,YTV,ZTV,XRP,YRP,ZRP,GRMAX,GRAPH,NG,
     $              NSAMPLE,VOLT,VPOL,NSLOPE,SLOPE(10,9),
     $              NXSDMX,NYSDMX,DGBALL,DGBALL1,TRACK,NOUT,
     $              PI,REARTH,XLAM,PASSTGT,FORWARD,PULSE,SQPULSE,PWIDTH
      COMMON/PROPT/PRINT1,PRINT2,PRINT3,PRINT4,PRINT5,IPRINT(20)
      COMMON/PLTYPE/PENPLOT
      COMMON/XSTUFF/RDXOUT(102),RDYOUT(102)
      DIMENSION X(102),Y(102),YP(102),YPP(204),POWER(204),T(127)
      LOGICAL PRINT1,PRINT2,PRINT3,PRINT4,PRINT5
      LOGICAL VPOL,PULSE,PASSTGT,FORWARD,SQPULSE,TRACK,GRAPH
      LOGICAL PENPLOT,VOLT
      COMPLEX ROZERO,DELOUT,OUTC,EXTRA,XOUT,YOUT,RHOARY
      COMPLEX YOUT2
C
      IF(PULSE)GOTO 1000
      YP(1)=0.
      Y(1)=0.
      X(1)=1.E-10
      DO 10 J=2,102
      X(J)=X(J-1)+DX
      Y(J)=Y(J-1)+DY
      YP(J)=YP(J-1)+DY
   10 CONTINUE
C
C     PLOT OF REFLECTED POWER VS DOWNRANGE DISTANCE
C
      DO 20 K=1,NBEAMS
      WRITE(6,6000)
      DO 30 J=1,102
      POWER(J)=RXOUT(J,K)
   30 CONTINUE
      IF(PENPLOT)CALL PENN(X,POWER,102,K,1)
      CALL PICTUR(X,POWER,102)
   20 CONTINUE
C
C     PLOT OF REFLECTION COEFFICIENT VS DOWNRANGE DISTANCE
C
      IF(VOLT.OR.PULSE)GOTO 40
```

```
      WRITE(6,6010)
      IF(PENPLOT)CALL PENN(X,RDXOUT,102,1,2)
      CALL PICTUR(X,RDXOUT,102)
C
C     PLOT OF REFLECTION COEFFICIENT VS CROSS RANGE
C
   40 DO 50 J=1,102
      K=J-1
      KK=102-K
      YPP(J)=YP(KK)
   50 CONTINUE
      DO 60 J=103,203
      YPP(J)=Y(J-101)
   60 CONTINUE
      IF(VOLT.OR.PULSE)GOTO 70
      WRITE(6,6020)
      DO 80 J=1,102
      K=J-1
      KK=102-K
      POWER(J)=RDYOUT(KK)
   80 CONTINUE
      DO 90 J=103,203
      POWER(J)=RDYOUT(J-101)
   90 CONTINUE
      IF(PENPLOT)CALL PENN(YPP,POWER,203,1,3)
      CALL PICTUR(YPP,POWER,203)
C
C     PLOT OF REFLECTED POWER VS CROSS RANGE
   70 DO 100 L=1,NBEAMS
      WRITE(6,6030)
      DO 110 J=1,102
      K=J-1
      KK=102-K
      POWER(J)=RYOUT2(KK,L)
  110 CONTINUE
      DO 120 J=103,203
      POWER(J)=RYOUT(J-101,L)
  120 CONTINUE
      IF(PENPLOT)CALL PENN(YPP,POWER,203,L,4)
      CALL PICTUR(YPP,POWER,203)
  100 CONTINUE
      GOTO 5000
C
C     PLOT OF POWER VS TIME
C
 1000 WRITE(6,6040)
      DO 1010 K=1,NBEAMS
      T(1)=ARYPAR(1)

      T(1)=T(1)/(3.E08)
      POWER(1)=RDELOUT(1,K)
      DO 1020 J=2,NCC
      T(J)=T(J-1)+DELT
      POWER(J)=RDELOUT(J,K)
 1020 CONTINUE
      IF(PENPLOT)CALL PENN(T,POWER,NCC,K,5)
      CALL PICTUR(T,POWER,NCC)
 1010 CONTINUE
 5000 RETURN
 6000 FORMAT'10X,45HPLOT OF REFLECTED POWER VS DOWNRANGE DISTANCE///)
 6010 FORMAT(10X,52HPLOT OF REFLECTION COEFFICIENT VS DOWNRANGE DISTANCE
     $///)
 6020 FORMAT(10X53HPLOT OF REFLECTION COEFFICIENT VS CROSSRANGE DISTANCE
     $///)
 6030 FORMAT(10X46HPLOT OF REFLECTED POWER VS CROSSRANGE DISTANCE///)
 6040 FORMAT(10X21HPLOT OF POWER VS TIME)
      END
```

```
      SUBROUTINE PSHAPF(PWIDTH,NP,PARRAY,DELT)
C
      COMMON/INPUTS/XTP,YTP,ZTP,XTV,YTV,ZTV,XRP,YRP,ZRP,GRMAX,GRAPH,NG,
     $              NSAMPLF,VOLT,VPOL,NSLOPE,SLOPE(10,9),
     $              NXSDMX,NYSDMX,DGBALL,DGBALL1,TRACK,NOUT,
     $              PI,REARTH,XLAM,PASSTGT,FORWARD,PULSE,SQPULSE,PWIDDUM
      COMMON/PROPT/PRINT1,PRINT2,PRINT3,PRINT4,PRINT5,IPRINT(20)
      COMMON/SINFO/SCOUNT,SDATA1(100),SDATA2(100),SDATA3(100)
      COMMON/SPOINTS/ XSP(100),YSP(100),ZSP(100)
      LOGICAL PRINT1,PRINT2,PRINT3,PRINT4,PRINT5
C
      DIMENSION PARRAY(1)
      LOGICAL SQPULSE,VOLT
      INTEGER SCOUNT
C
      IF(PRINT5)PRINT 7777
 7777 FORMAT(* PSHAPE*)
      IPRINT(10)=IPRINT(10)+1
C
      XNP=NP
      PID2=PI/2.
C
C     IF A SQUARE PULSE IS NOT CHOSEN, A COSINE PULSE IS USED
C
      IF(.NOT. SQPULSE) GO TO 10
      DELT = PWIDTH/(XNP-1.)
      DO 20 J=1,NP
      PARRAY(J)=1.0
   20 CONTINUE
      RETURN
   10 T0=PWIDTH*.5
      OMEGA=PID2/T0
      IF(VOLT)OMEGA=ACOS(.41421356)/T0
      DELT=2.*PI/(OMEGA*(XNP-1.))
      T=-PI/OMEGA
      DO 30 J=1,NP
      PARRAY(J)=(1.0 + COS(OMEGA*T))*.5
      T=T+DELT
   30 CONTINUE
      RETURN
      END
```



```
      SUBROUTINE RCOORD(THETA,X,Y,Z,XP,YP,ZP)
      COMMON/PROPT/PRINT1,PRINT2,PRINT3,PRINT4,PRINT5,IPRINT(20)
      LOGICAL PRINT1,PRINT2,PRINT3,PRINT4,PRINT5
C
C
      IF(PRINT5)PRINT 7777
 7777 FORMAT(* RCOORD*)
      IPRINT(11)=IPRINT(11)+1
C
      XP=X*COS(THETA)+Y*SIN(THETA)
      YP=Y*COS(THETA)-X*SIN(THETA)
      ZP=Z
      RETURN
      END
```

```
      SUBROUTINE  SCAN(NBEAMS)
C
      COMMON YOUT2(102,10),RDYOUT2(102),RYOUT2(102,10)
      COMMON DELOUT(127,10),XOUT(102,10),YOUT(102,10),FXTRA(10,2),
     1       OUTC(127),DARRAY(127)
      COMMON RDELOUT(127,10),RXOUT(102,10),RYOUT(102,10),REXTRA(10,2),
     1       RRHOARY(10)
      COMMON/GRAZE/PARPP(2,2,2)
      COMMON/TGAINP/G2OP(4),G1OP(4)
      COMMON/TGAINP/G1P(4),G2P(4)
      COMMON/BEAMS/SANGLE(10,2),UXS(10),UYS(10),UZS(10)
      COMMON/DERV/PARRAY(127),ARYPAR(5),GBETZO(10),G10,G20(10),NP,
     1            DIRDOP,DELT,UNIFORM,RANGLE,SIGZO,ROZERO,NCC,
     2            FORPI,PID2,XTR,YTR,ZTR,RTR,RHOARY(10)
      COMMON/EXT/NYMAX
      COMMON/INC/DX,DY
      COMMON/INPUTS/XTP,YTP,ZTP,XTV,YTV,ZTV,XRP,YRP,ZRP,GRMAX,GRAPH,NG,
     $              NSAMPLE,VOLT,VPOL,NSLOPE,SLOPE(10,9),
     $              NXSDMX,NYSDMX,DGBALL,DGBALL1,TRACK,NOUT,
     $              PI,REARTH,YLAM,PASSTGT,FORWARD,PULSE,SOPULSE,PWIDTH
      COMMON/PATD/JD,BWD,CD,AD,STOD,JS,BWS,CSCAN,ASCAN,STOSCAN,
     $            JB,BWB,CB,AB,STOB
      COMMON/PGAIN/GT,PT,GR,RADCON
      COMMON/POINT/UXPOINT,UYPOINT,UZPOINT,DSINE(10)
      COMMON/PROPT/PRINT1,PRINT2,PRINT3,PRINT4,PRINT5,IPRINT(20)
      COMMON/RCOEF/FRES(2,2)
      COMMON/ROOD/ROD
      COMMON/XSTUFF/RDXOUT(102),RDYOUT(102)
      COMMON/SINFO/SCOUNT,SDATA1(100),SDATA2(100),SDATA3(100)
      COMMON/SPOINTS/ XSP(100),YSP(100),ZSP(100)
      COMMON/MULSPEC/SPCHECK
C
      DIMENSION PWRDIS(10)
      DIMENSION X(2),Y(2),XS(2),YS(2),GBETA(2,2)
      DIMENSION PAR(2,2,6),PARP(2,2,9)
      DIMENSION PARS(2,2,6),PARPS(2,2,9)
      DIMENSION DPOWER(10),DPOWERS(10),SPOWER(10),SPOWERS(10)
      DIMENSION VOLTAGE(10)
      LOGICAL VPOL,PULSE,PASSTGT,FORWARD,SOPULSE,TRACK,GRAPH
      LOGICAL PRINT1,PRINT2,PRINT3,PRINT4,PRINT5
      LOGICAL UNIFORM,VOLT,FIRST
      COMPLEX ROZERO,DELOUT,OUTC,EXTRA,XOUT,YOUT,RHOARY
      COMPLEX VOLTAGE,PWRDTS
      COMPLEX YOUT2,FRES
      INTEGER SCOUNT
      EQUIVALENCE(GBETA(1),PAR(1,1,6))
      NAMELIST/OUT1/VOLTAGE
C
      IF(PRINT5)PRINT 7777
```

```
 7777 FORMAT(* SCAN*)
      IPRINT(12)=IPRINT(12)+1
C
C     COMPUTE RADAR RANGE CONSTANT
C
      RADCON=PT*GT*GR*(XLAM**2)/(FORPI**3)
      IF(PASSTGT .AND.FORWARD)RADCON=PT*GT*SIGZ0/(FORPI**2)
C
C     ZERO OUT POWER ARRAYS
C
      DO 100 J=1,2
      DO 100 K=1,2
      DO 99 L=1,6
      PAR(J,K,L)=0.0
      PARS(J,K,L)=0.0
      PARP(J,K,L)=0.0
      PARPS(J,K,L)=0.0
   99 CONTINUE
      DO 98 L=7,9
      PARP(J,K,L)=0.0
      PARPS(J,K,L)=0.0
   98 CONTINUE
  100 CONTINUE
      DO 200 J=1,NBEAMS
      VOLTAGE(J)=0.0
      DPOWER(J)=0.0
      DPOWERS(J)=0.0
      SPOWER(J)=0.0
      SPOWERS(J)=0.0
      RHOARY(J)=0.0
      DO 210 K=1,102
      XOUT(K,J)=0.0
      YOUT(K,J)=0.0
      YOUT2(K,J)=0.
      DELOUT(K,J)=0.0
  210 CONTINUE
      DO 211 K=103,127
      DELOUT(K,J)=0.0
  211 CONTINUE
      EXTRA(J,1)=0.0
      EXTRA(J,2)=0.0
  200 CONTINUE
      DO 250 J=1,102
      RDXOUT(J)=0.
      RDYOUT(J)=0.
      RDYOUT2(J)=0.
  250 CONTINUE
      DO 212 J=1,127
```

```
      OUTC(J)=0.0
  212 CONTINUE
C
C     INITIAL CONSTANTS
C
      X(1)=XRP+1.0E-10
      Y(2)=0.0
      NX=1
      NY=1
      SCOUNT=0.0
C
C     MINIMUM OF GROUND RANGE TO HORIZON AND INPUT GROUND RANGE
C
      THETA=ACOS(REARTH/ZRP)
      RHOR=REARTH*THETA
      RHOR=AMIN1(RHOR,GRMAX)
      FIRST=.TRUE.
      EPS1=.01
      EPS2=.01
C
C       LOOP FOR NEXT X
C
101   CONTINUE
      X(2)=X(1)+DX
      IF(X(2).GT.RHOR)X(2)=RHOR
C
C     FIND PARAMETERS FOR THE BOTTOM PATCH CORNERS
C
      CALL FINDPAR(Y(2),X(2),2,2,PAR,PARP)
      CALL FINDPAR(Y(2),X(1),2,1,PAR,PARP)
C
C      FIND NEXT Y
C
102   CONTINUE
      Y(1)=Y(2)+DY
C
C     FIND PARAMETERS FOR THE TOP PATCH CORNERS
C
      CALL FINDPAR(Y(1),X(2),1,2,PAR,PARP)
      CALL FINDPAR(Y(1),X(1),1,1,PAR,PARP)
C
C     CHECK GRADIENT IN THE X DIRECTION
C
      GRADX=AMAX1(ABS(PAR(2,1,6)-PAR(2,2,6)),ABS(PAR(1,1,6)-PAR(1,2,6)))
C
C       DIVIDE X INTO REQUIRED INTERVALS
C
      TV1=GRADX/DGRALL
```

```
      IF(TV1.GT.1000.) TV1=1000.
      NXSD=INT(TV1)+1
      NXSD=MIN0(NXSD,NXSDMX)
C
C        CHECK GRADIENT IN Y DIRECTION
C
      GRADY=AMAX1(ABS(PAR(1,1,6)-PAR(2,1,6)),ABS(PAR(1,2,6)-PAR(2,2,6)))
C
C     DIVIDE Y INTO REQUIRED INTERVALS
C
      TV2=GRADY/DGBALL1
      IF(TV2.GT.1000.) TV2=1000.
      NYSD=INT(TV2)+1
      NYSD=MIN0(NYSD,NYSDMX)
C
C     ZERO OUT PWRDIS ARRAY
C
      RHOD=0.
      DO 20 J=1,10
      PWRDIS(J)=0.
   20 CONTINUE
C
C        CHECK TO SEE IF THE PATCH HAS BEEN DIVIDED
C
      IF(NYSD.EQ.1 .AND. NXSD.EQ.1)  GO TO 103
      DDX=DX/NXSD
      DDY=DY/NYSD
      XS(2)=X(1)
      DO 10 JJ=1,NXSD
      XS(1)=XS(2)
      XS(2)=XS(1)+DDX
      YS(2)=Y(2)
C
C     FIND PARAMETERS FOR BOTTOM OF THE SQUARE
C
      CALL FINDPAR(YS(2),XS(2),2,2,PARS,PARPS)
      CALL FINDPAR(YS(2),XS(1),2,1,PARS,PARPS)
      DO 30 K=1,NYSD
      YS(1)=YS(2)+DDY
C
C     FIND PARAMETERS OF THE TOP OF THE SQUARE
C
      CALL FINDPAR(YS(1),XS(1),1,1,PARS,PARPS)
      CALL FINDPAR(YS(1),XS(2),1,2,PARS,PARPS)
C
C     FIND POWER FOR A SMALL PATCH
C
      CALL FINDPWR(PARPS,PARS,DDX,DDY,DPOWERS,SPOWERS,VOLTAGE,
```

```
     $NBEAMS)
      IF(VOLT.OR.PULSE)GOTO 27
      RHOD=RHOD+ROD
   27 DO 25 J=1,NBEAMS
      IF(VOLT) GO TO 600
      PWRDIS(J)=DPOWERS(J)+SPOWERS(J)+PWRDIS(J)
      RHOARY(J)=RHOARY(J)+DPOWERS(J)+SPOWERS(J)
      IF(PULSE) RHOARY(J)=DPOWERS(J)+SPOWERS(J)
      GO TO 25
  600 RHOARY(J)=RHOARY(J)+VOLTAGE(J)
      PWRDIS(J)=PWRDIS(J)+VOLTAGE(J)
      IF(PULSE)RHOARY(J)=VOLTAGE(J)
   25 CONTINUE
      CALL SPREAD(PARS,NBEAMS)
C
C       PREPARE TO GO TO THE NEXT PATCH
C
      CALL SHIFT(PARS,PARPS)
      YS(2)=YS(1)
30    CONTINUE
   10  CONTINUE
      IF(VOLT.OR.PULSE)GOTO 104
      RDXOUT(NX)=RDXOUT(NX)+RHOD
      IF(FIRST)GOTO 11
      RDYOUT2(NY)=RDYOUT2(NY)+RHOD
      GOTO 104
   11 RDYOUT(NY)=RDYOUT(NY)+RHOD
      GO TO 104
103   CONTINUE
C
C     FIND POWER FOR A LARGE PATCH
C
      CALL FINDPWR(PARP,PAR,DX,DY,DPOWER,SPOWER,VOLTAGE,NBEAMS)
      IF(VOLT.OR.PULSE)GOTO 28
      RHOD=ROD
      RDXOUT(NX)=RDXOUT(NX)+RHOD
      IF(FIRST)GOTO 29
      RDYOUT2(NY)=RDYOUT2(NY)+RHOD
      GOTO 28
   29 RDYOUT(NY)=RDYOUT(NY)+RHOD
   28 DO 26 J=1,NBEAMS
      IF(VOLT) GO TO 610
      PWRDIS(J)=DPOWER(J)+SPOWER(J)
      RHOARY(J)=RHOARY(J)+DPOWER(J)+SPOWER(J)
      IF(PULSE)RHOARY(J)=DPOWER(J)+SPOWER(J)
      GO TO 26
  610 RHOARY(J)=RHOARY(J)+VOLTAGE(J)
      PWRDIS(J)=VOLTAGE(J)
```

```
      IF(PULSE) RHOARY(J)=VOLTAGE(J)
   26 CONTINUE
      CALL SPREAD(PAR,NBEAMS)
104   CONTINUE
C
C     RANGE DISTRIBUTIONS
C
      IF(PULSE) GO TO 22
      DO 230 J=1,NBEAMS
      XOUT(NX,J)=XOUT(NX,J)+PWRDIS(J)
      IF(FIRST)GOTO 230
      YOUT2(NY,J)=YOUT2(NY,J)+PWRDIS(J)
      GOTO 220
  230 YOUT(NY,J)=YOUT(NY,J)+PWRDIS(J)
  220 SCHECK1=(PAR(1,2,6)+PAR(1,1,6))/2.
      IF(NY.GE.NYMAX)GO TO 221
      IF(SCHECK1 .GT. EPS1) GO TO 105
  221 IF(X(2).GE.RHOR)GOTO 106
      X(1)=X(2)
      Y(2)=0.0
      NY=1
      NX=NX+1
      GO TO 101
  105 CONTINUE
      NY=NY+1
C
C     PREPARE TO GO TO NEXT PATCH
C
      CALL SHIFT(PAR,PARP)
      Y(2)=Y(1)
      GO TO 102
  106 DY=-DY
      Y(2)=0.0
      X(1)=XRP+1.E-10
      IF(.NOT.FIRST) GO TO 900
      FIRST=.FALSE.
      NX=1
      NY=1
      GO TO 101
  900 IF(PASSTGT.AND.FORWARD)GOTO 300
      IF(VOLT)GOTO 310
      DO 320 J=1,NBEAMS
      DPOWER(J)=PT*GT*G20(J)*(XLAM**2)/((FORPI*RTR)**2)
      RHOARY(J)=RHOARY(J)+DPOWER(J)
      IF(PULSE)DELOUT(1,J)=DELOUT(1,J)+DPOWER(J)
  320 CONTINUE
      RETURN
  310 DO 330 J=1,NBEAMS
```

```
      IF(.NOT.TRACK)GO TO 311
      VOLTAGE(J)=DSINE(J)*SQRT(PT*GT*G20P(J)*(XLAM**2)/((FORPI*RTR)**2))
      GO TO 312
  311 VOLTAGE(J)=DSINE(J)*SQRT(PT*GT*G20(J)*(XLAM**2)/((FORPI*RTR)**2))
  312 RHOARY(J)=RHOARY(J)+VOLTAGE(J)
      IF(PULSE)DELOUT(1,J)=DELOUT(1,J)+VOLTAGE(J)
  330 CONTINUE
      RETURN
  300 IF(VOLT)GOTO 910
      DPOWER(1)=PT*GT*SIGZ0*G10/(FORPI*(RTR**2))
      RHOARY(1)=RHOARY(1)+DPOWER(1)
      IF(PULSE)DELOUT(1,1)=DELOUT(1,1)+DPOWER(1)
      RETURN
  910 IF(.NOT.TRACK)GO TO 920
      DO 930 J=1,4
      VOLTAGE(J)=DSINE(J)*SQRT(PT*GT*SIGZ0*G10P(J)/(FORPI*(RTR**2)))
      RHOARY(J)=RHOARY(J)+VOLTAGE(J)
      IF(PULSE)DELOUT(1,J)=DELOUT(1,J)+VOLTAGE(J)
  930 CONTINUE
      RETURN
  920 VOLTAGE(1)=DSINE(1)*SQRT(PT*GT*SIGZ0*G10/(FORPI*(RTR**2)))
      RHOARY(1)=RHOARY(1)+VOLTAGE(1)
      IF(PULSE)DELOUT(1,1)=DELOUT(1,1)+VOLTAGE(1)
      RETURN
         END
```

```
      SUBROUTINE SGAIN(PARP,PDATA,GAINS,SDELR)
C
      COMMON YOUT2(102,10),RDYOUT2(102),RYOUT2(102,10)
      COMMON DELOUT(127,10),XOUT(102,10),YOUT(102,10),EXTRA(10,2),
     1       OUTC(127),DARRAY(127)
      COMMON RDELOUT(127,10),RXOUT(102,10),RYOUT(102,10),REXTRA(10,2),
     1       RRHOARY(10)
      COMMON/BEAMS/SANGLE(10,2),UXS(10),UYS(10),UZS(10)
      COMMON/TGAINP/G1P(4),G2P(4)
      COMMON/TGAIND/G2DP(4),G1DP(4)
      COMMON/DERV/PARRAY(127),ARYPAR(5),GBETZ0(10),G10,G20(10),NP,
     1            DIRDOP,DFLT,UNIFORM,RANGLE,SIGZ0,ROZERO,NCC,
     2            FORPI,PI02,XTR,YTR,ZTR,RTR,RHOARY(10)
      COMMON/INPUTS/XTP,YTP,ZTP,XTV,YTV,ZTV,XRP,YRP,ZRP,GRMAX,GRAPH,NG,
     $              NSAMPLE,VOLT,VPOL,NSLOPE,SLOPE(10,9),
     $              NXSDMX,NYSDMX,DGBALL,DGBALL1,TRACK,NOUT,
     $              PI,REARTH,XLAM,PASSTGT,FORWARD,PULSE,SQPULSE,PWIDTH
      COMMON/PATD/JD,BWD,CD,AD,SIGD,JS,BWS,CSCAN,ASCAN,SIGSCAN,
     $            JB,BWB,CB,AB,SIGB
      COMMON/PGAIN/GT,PT,GR,RADCON
      COMMON/PROPT/PRINT1,PRINT2,PRINT3,PRINT4,PRINT5,IPRINT(20)
      COMMON/PATCH/XGR,YGR,ZGR,XGT,YGT,ZGT
      COMMON/RTYPE/SPEC,DIFFUSE
      COMMON/SINFO/SCOUNT,SDATA1(100),SDATA2(100),SDATA3(100)
      COMMON/SPOINTS/ XSP(100),YSP(100),ZSP(100)
      COMMON/MULSPEC/SPCHECK
      DIMENSION PARP(2,2,9),PDATA(9)
C
      LOGICAL VPOL,PULSE,PASSTGT,FORWARD,SQPULSE,TRACK,GRAPH
      LOGICAL PRINT1,PRINT2,PRINT3,PRINT4,PRINT5
      LOGICAL UNIFORM,VOLT
      LOGICAL SPEC,DIFFUSE
      COMPLEX ROZERO,DELOUT,OUTC,EXTRA,XOUT,YOUT,RHOARY
      COMPLEX YOUT2
      INTEGER SCOUNT
C
      IF(PRINT5)PRINT 7777
 7777 FORMAT(* SGAIN*)
      IPRINT(13)=IPRINT(13)+1
C
      SDELR=0.0
      GAINS=0.0
      IF(.NOT.SPEC)RETURN
C
C     FIND UNIT NORMAL TO PATCH
C
      RLNTH=SQRT(PDATA(5)**2+PDATA(6)**2+PDATA(7)**2)
      RLNTHI=1./RLNTH
      UXLN=PDATA(5)*RLNTHI
```

```
      UYLN=PDATA(6)*RLNTHI
      UZLN=PDATA(7)*RLNTHI
      HRP=XGR*UXLN+YGR*UYLN+ZGR*UZLN
      HTP=XGT*UXLN+YGT*UYLN+ZGT*UZLN
      IF(HRP.LT.0.0.OR.HTP.LT.0.0)RETURN
      RCOEFF=PDATA(1)*UXLN+PDATA(2)*UYLN+(PDATA(3)-ZRP)*UZLN
      XR=RCOEFF*UXLN
      YR=RCOEFF*UYLN
      ZR=RCOEFF*UZLN+ZRP
      TCOEFF=UXLN*(PDATA(1)-XTP)+UYLN*PDATA(2)+UZLN*(PDATA(3)-ZTP)
      XT=TCOEFF*UXLN+XTP
      YT=TCOEFF*UYLN
      ZT=TCOEFF*UZLN+ZTP
C
C     CALCULATE VECTOR IN TANGENT PLANE FROM RECEIVER TO TARGET
C
      PX=XT-XR
      PY=YT-YR
      PZ=ZT-ZR
C
C     COMPUTE UNIT VECTOR
C
      RPR=SQRT(PX**2+PY**2+PZ**2)
      RPRI=1./RPR
      UPX=PX*RPRI
      UPY=PY*RPRI
      UPZ=PZ*RPRI
C
C     COMPUTE SPECULAR POINT IN TANGENT PLANE
C
      RL=RPR*HRP/(HRP+HTP)
      XSPEC=RL*UPX
      YSPEC=RL*UPY
      ZSPEC=RL*UPZ
      XSPEC=XR+XSPEC
      YSPEC=YR+YSPEC
      ZSPEC=ZR+ZSPEC
      XMIN=AMIN1(PARP(1,1,1),PARP(1,2,1),PARP(2,1,1),PARP(2,2,1))
      XMAX=AMAX1(PARP(1,1,1),PARP(1,2,1),PARP(2,1,1),PARP(2,2,1))
      YMIN=AMIN1(PARP(1,1,2),PARP(1,2,2),PARP(2,1,2),PARP(2,2,2))
      YMAX=AMAX1(PARP(1,1,2),PARP(1,2,2),PARP(2,1,2),PARP(2,2,2))
      IF(XMIN.GT.XSPEC.OR.XSPEC.GT.XMAX)RETURN
      IF(YMIN.GT.YSPEC.OR.YSPEC.GT.YMAX)RETURN
C
C     SPECULAR POINT IS IN PATCH
C
      IF(SCOUNT.EQ.0) GO TO 200
C
```

```
C     CHECK TO SEE IF SPECULAR POINT IS BEING COUNTED TWICE
C
      DO 90 J=1,SCOUNT
      A=ABS(XSP(J)-XSPEC)
      B=ABS(YSP(J)-YSPEC)
      C=ABS(ZSP(J)-ZSPEC)
      SUM=A+B+C
      IF(SUM.LT.SPCHECK)RETURN
   90 CONTINUE
C
C     STORE SPECULAR POINT AND COMPUTE SPECULAR GAIN
C
  200 SCOUNT=SCOUNT+1
      XSP(SCOUNT)=XSPEC
      YSP(SCOUNT)=YSPEC
      ZSP(SCOUNT)=ZSPEC
      GAMA=ATAN(HRP/RL)
      G=FORPI*PDATA(9)*SIN(GAMA)/XLAM
      G=G**2
      IF(G.GT.220)RETURN
      GAINS=EXP(-G)
      SDATA2(SCOUNT)=GAINS
C
C     COMPUTE DISTANCE FROM SPECULAR POINT TO TARGET
C
      DT=SQRT((XTP-XSPEC)**2+(YTP-YSPEC)**2+(ZTP-ZSPEC)**2)
C
C     COMPUTE DISTANCE FROM SPECULAR POINT TO RECEIVER
C
      DR=SQRT((XRP-XSPEC)**2+(YRP-YSPEC)**2+(ZRP-ZSPEC)**2)
C
C     COMPUTE SPECULAR PATH DIFFERENCE
C
      SDELR=DT+DR-RTR
      GAINS=GAINS/((DT+DR)**2)
      SDATA1(SCOUNT)=SDELR
      SDATA3(SCOUNT)=GAINS
      RETURN
      END
```



```
      SUBROUTINE SHIFT(PAR,PARP)
C
      COMMON/PROPI/PRINT1,PRINT2,PRINT3,PRINT4,PRINT5,IPRINT(20)
      LOGICAL PRINT1,PRINT2,PRINT3,PRINT4,PRINT5
      DIMENSION PAR(2,2,6),PARP(2,2,9)
C
      IF(PRINT5)PRINT 7777
 7777 FORMAT(* SHIFT*)
      IPRINT(14)=IPRINT(14)+1
C
      DO 10 J=1,6
      DO 10 K=1,2
      PAR(2,K,J)=PAR(1,K,J)
      PARP(2,K,J)=PARP(1,K,J)
 10   CONTINUE
      DO 20 J=7,9
      DO 20 K=1,2
      PARP(2,K,J)=PARP(1,K,J)
   20 CONTINUE
      RETURN
         END
```

```
      SUBROUTINE SPREAD(PAR,NBEAM)
C
      COMMON YOUT2(102,10),RDYOUT2(102),RYOUT2(102,10)
      COMMON DELOUT(127,10),XOUT(102,10),YOUT(102,10),EXTRA(10,2),
     1       OUTC(127),DARRAY(127)
      COMMON RDELOUT(127,10),RXOUT(102,10),RYOUT(102,10),REXTRA(10,2),
     1       RRHOARY(10)
      COMMON/TGAIND/G20P(4),G10P(4)
      COMMON/TGAINP/G1P(4),G2P(4)
      COMMON/BEAMS/SANGLE(10,2),UXS(10),UYS(10),UZS(10)
      COMMON/DERV/PARRAY(127),ARYPAR(5),GBETZ0(10),G10,G20(10),NP,
     1            DIRDOP,DFLT,UNIFORM,RANGLE,SIGZ0,ROZERO,NCC,
     2            PORPI,PIH2,XTR,YTR,ZTR,RTR,RHOARY(10)
      COMMON/INC/DX,DY
      COMMON/INPUTS/XTP,YTP,ZTP,XTV,YTV,ZTV,XRP,YRP,ZRP,GRMAX,GRAPH,NG,
     $              NSAMPLE,VOLT,VPOL,NSLOPE,SLOPE(10,9),
     $              NXSDMX,NYSDMX,DGBALL,DGBALL1,TRACK,NOUT,
     $              PI,REARTH,XLAM,PASSTGT,FORWARD,PULSE,SQPULSE,PWIDTH
      COMMON/PATD/JD,BWD,CD,AD,SIOD,JS,BWS,CSCAN,ASCAN,SIOSCAN,
     $            JB,BWB,CB,AB,SIOB
      COMMON/PGAIN/GT,PT,GR,RADCON
      COMMON/PROPT/PRINT1,PRINT2,PRINT3,PRINT4,PRINT5,IPRINT(20)
      LOGICAL PRINT1,PRINT2,PRINT3,PRINT4,PRINT5
C
      DIMENSION PAR(2,2,6)
      DIMENSION PPB(30)
      LOGICAL VPOL,PULSE,PASSTGT,FORWARD,SQPULSE,TRACK,GRAPH
      LOGICAL UNIFORM,VOLT
      COMPLEX ROZERO,DELOUT,OUTC,EXTRA,XOUT,YOUT,RHOARY
      COMPLEX YOUT2
C
      IF(PRINT5)PRINT 7777
 7777 FORMAT(* SPREAD*)
      IPRINT(15)=IPRINT(15)+1
C
C     IF CW CASE PARAMETERS ARE NOT STORED
C
      IF(.NOT.PULSE)RETURN
      AMNVAL=AMIN1(PAR(1,1,2),PAR(1,2,2),PAR(2,1,2),PAR(2,2,2))
      AMXVAL=AMAX1(PAR(1,1,2),PAR(1,2,2),PAR(2,1,2),PAR(2,2,2))
      IF(ARYPAR(3).GT.0.)GOTO 11
      DUM=AMNVAL
      AMNVAL=AMXVAL
      AMXVAL=DUM
   11 CONTINUE
      DVAL=ABS((AMXVAL-AMNVAL)/ARYPAR(3))
      DO 101 I=1,NBEAM
      PPB(I)=RHOARY(I)/DVAL
  101 CONTINUE
```

```
      BINMN=(AMNVAL-ARYPAR(1))/ARYPAR(3)+1.
      BINMX=(AMXVAL-ARYPAR(1))/ARYPAR(3)+1.
      IF(BINMN.GT.FLOAT(NOUT+1)) GO TO 12
      IF(BINMX.LT.1.) GO TO 13
      NBINMN=INT(BINMN)
      NBINMX=INT(BINMX)
      IF(NBINMX-NBINMN-1)14,15,16
   14 CONTINUE
      DO 102 I=1,NBEAM
      DELOUT(NBINMN,I)=DELOUT(NBINMN,I)+RHOARY(I)
  102 CONTINUE
      GO TO 10
   16 CONTINUE
      KK=NBINMN+1
      KKK=NBINMX-1
      DO 17 K=KK,KKK
      IF(K.LT.1) GO TO 170
      IF(K.GT.NOUT) GO TO 171
      DO 172 I=1,NBEAM
  172 DELOUT(K,I)=DELOUT(K,I)+PPB(I)
      GO TO 17
C
C     HERE IF WITHIN DISPLAY RANGE
  170 CONTINUE
C
C     HERE IF BELOW DISPLAY
C
      DO 173 I=1,NBEAM
      EXTRA(I,1)=EXTRA(I,1)+PPB(I)
  173 CONTINUE
      GO TO 17
  171 CONTINUE
C
C     HERE IF ABOVE DISPLAY
C
      DO 174 I=1,NBEAM
      EXTRA(I,2)=EXTRA(I,2)+PPB(I)
  174 CONTINUE
   17 CONTINUE
   15 CONTINUE
      P=NBINMN+1-BINMN
      IF(NBINMN .LT.1) GO TO 151
      DO 152 I=1,NBEAM
      DELOUT(NBINMN,I)=DELOUT(NBINMN,I)+P*PPB(I)
  152 CONTINUE
      GO TO 153
  151 CONTINUE
      DO 154 I=1,NBEAM
```

```
      EXTRA(I,1)=EXTRA(I,1)+P*PPB(I)
  154 CONTINUE
  153 CONTINUE
C
C     DO UPPER PARTIAL BIN
C
      P=BINMX-NBINMX
      IF(NBINMX .GT. NOUT) GO TO 155
      DO 156 I=1,NBEAM
      DELOUT(NBINMX,I)=DELOUT(NBINMX,I)+P*PPB(I)
  156 CONTINUE
      GO TO 157
  155 CONTINUE
      DO 158 I=1,NBEAM
      EXTRA(I,2)=EXTRA(I,2)+P*PPB(I)
  158 CONTINUE
  157 CONTINUE
      GO TO 10
   12 CONTINUE
C
C     HERE IF ALL VALUES ARE BELOW ARRAY
C
      DO 121 I=1,NBEAM
      EXTRA(I,1)=EXTRA(I,1)+RHOARY(1)
  121 CONTINUE
      GO TO 10
C
C     HERE IF ALL VALUES ARE ABOVE ARRAY
C
   13 CONTINUE
      DO 131 I=1,NBEAM
      EXTRA(I,2)=EXTRA(I,2)+RHOARY(I)
  131 CONTINUE
   10 CONTINUE
      RETURN
         END
```

```
      SUBROUTINE TBEAM(THETA,N,XDB,C,A,SI0,SI1)
      COMMON/TRP/JCALL
      COMMON/PROPI/PRINT1,PRINT2,PRINT3,PRINT4,PRINT5,IPRINT(20)
      LOGICAL PRINT1,PRINT2,PRINT3,PRINT4,PRINT5
C
      IF(PRINT5)PRINT 7777
 7777 FORMAT(* TBEAM*)
      IPRINT(16)=IPRINT(16)+1
C
      JCALL=0
      AA=1./SQRT(2.)
      CALL PATTERN(N,THETA,C,A,SI0,AA)
      DBLEVEL=XDB/20.
      DBLEVEL=1./(10.0**DBLEVEL)
      JCALL=1
      CALL PATTERN(N,THETA,C,A,SI1,DBLEVEL)
      JCALL=0
      RETURN
      END
```



```
      SUBROUTINE TRCK(SUM,DELTA,NRNG,PHITS,PRI)
      COMMON/TRK/PHITP,PHITPD,PHITPDD,ANTSLOP
      COMMON/DERV/PARRAY(127),ARYPAR(5),GBETZ0(10),G10,G20(10),NP,
     1            DIRDOP,DELT,UNIFORM,RANGLE,SIGZ0,ROZERO,NCC,
     2            FORPI,PID2,XTR,YTR,ZTR,RTR,RHOARY(10)
      COMMON/INPUTS/XTP,YTP,ZTP,XTV,YTV,ZTV,XRP,YRP,ZRP,GRMAX,GRAPH,NG,
     $              NSAMPLE,VOLT,VPOL,NSLOPE,SLOPE(10,9),
     $              NXSDMX,NYSDMX,DGBALL,DGBALL1,TRACK,NOUT,
     $              PI,REARTH,XLAM,PASSTGT,FORWARD,PULSE,SQPULSE,PWIDTH
      DIMENSION SUM(127),DELTA(127)
      COMPLEX ROZERO,RHOARY
      COMPLEX SUM,DELTA
      COMPLEX SUM1,DELTA1
      REAL KT
      LOGICAL UNIFORM,VPOL,VOLT,GRAPH,TRACK
      LOGICAL PASSTGT,FORWARD,PULSE,SQPULSE
      DATA GT,HT,KT/.5,.09,0.0/
      NAMELIST/INP1/SUM1,DELTA1,TSUM,TDELTA
      NAMELIST/FILTER/DELPHI,PHITR,PHITS,PHITSD,PHITSDD,PHITP,PHITPD,
     $                PHITPDD
C
```

```
C     SUBROUTINE TO GENERATE BORESITE ERRORS
C     TRACK TARGET AND POINT TRACKING ANTENNA
C
C
C     CURRENT TRACKER IS AN AVERAGE POWER UNIFORM WEIGHTING TRACKER
C
C
C
C     FIND AVGE SUM AND DIFFERENCE VECTORS
C
      DELTA1=0.
      SUM1=0.
      DO 10 J=1,NRNG
      SUM1=SUM1+SUM(J)
      DELTA1=DELTA1+DELTA(J)
   10 CONTINUE
      SUM1=SUM1/NRNG
      DELTA1=DELTA1/NRNG
      TSUM=SUM1*CONJG(SUM1)
      TDELTA=DELTA1*CONJG(DELTA1)
C
C     FIND ROUGH BORESITE ERROR
C
      DDOTSX=REAL(SUM1)*REAL(DELTA1)
      DDOTSY=AIMAG(SUM1)*AIMAG(DELTA1)
      DDOTS=DDOTSX+DDOTSY
      DELPHI=DDOTS/((SQRT(TSUM*TDELTA))*SQRT(TSUM))
      PHITR=PHITP+DELPHI
C
C     PASS THROUGH GHK FILTERS
C
      PHITS=PHITP+GT*(PHITR-PHITP)
      PHITSD=PHITPD+HT/PRI*(PHITR-PHITP)
      PHITSDD=PHITPDD+2.*KT/(PRI**2)*(PHITR-PHITP)
C
C     PREDICTED VALUES
C
      PHITP=PHITS+PHITSD*PRI+PHITSDD*PRI**2*.5
      PHITPD=PHITSD+PHITSDD*PRI
      PHITPDD=PHITSDD
      RETURN
      ENTRY TRKINIT
C
C     CALL ONCE AT START OF TRACK TO INITIALIZE FILTERS
C
      PHITP=180./PI*ATAN(ZTR/XTR)
      PHITPD=180./PI*(((XTR*ZTV-ZTR*XTV)/(RTR**2)))
      PHITPD=-PHITPD
      PHITPDD=0.0
```



```
      RETURN
      END
```

APPENDIX C
DETAILED MULTIPATH THEORY

Kirchhoff Solution for the Scattered Field

Let P be an observation point and R' the distance of P from a point $(x, y, \zeta(x,y))$ on the surface element S (Figure 6[1]). The scattered field E_2 at P satisfies the reduced wave equation

$$\nabla^2 E + R^2 E = 0 \tag{1}$$

together with appropriate boundary conditions on S. The solution of (1) in terms of values of E and its normal derivative on S is given by the Helmholtz integral

$$E_2(P) = \frac{1}{4\pi} \iint_S \left(E \frac{\partial \Psi}{\partial n} - \Psi \frac{\partial E}{\partial n}\right) dS \tag{2}$$

where

$$\Psi = \frac{e^{ikR'}}{R'} \tag{3}$$

is a well known fundamental solution (in 3-dimensions) of (1).

Assumption 1: Let the surface element S be small enough so that the reflected rays reaching P may be considered parallel (or equivalently, let $R' \to \infty$, that is to say, remove P to the Fraunhofer zone of diffraction).

Under assumption 1, (3) may be replaced by the approximation

$$\Psi \approx \frac{e^{i\left(kR_2 - \vec{k}_2 \cdot \vec{r}\right)}}{R_2} \tag{4}$$

[1] All notation and assumptions throughout this Appendix are consistent with those introduced in sections 2.1 through 2.3 of this final report.

where R_2 is the distance of P from the origin of the selected coordinate system (see Figure 6).

Assumption 2: Assume the surface does not contain a large number of sharp edges or other irregularities with small radii of curvature, i.e., assume the radius of curvature of the irregularities is large compared with the wavelength λ.[1]

Within assumption 2, the field and its normal derivative on S may be approximated by

$$(E)_S = (1 + R^{\pm})\, E_1 \qquad (2)$$

$$\left(\frac{\partial E}{\partial n}\right)_S = j\,(1 - R^{\pm})\, E_1\, (\vec{k}_1 \cdot \hat{n}) \qquad (5)$$

where $\hat{n}$ denotes the unit normal to S (see Figure 9).

Substitution of (4) and (5) into (2) now leads to the equivalent integral representation of the scattered field at P

$$E_2(P) = \frac{ike^{ikR_2}}{4\pi R_2} A_1 \iint_A (a\,\zeta_x + c\zeta_y - b)\, e^{i\vec{v}\cdot\vec{r}}\, dA \qquad (3)(6)$$

where

$$a = (1 - R)\sin\theta_1 + (1 + R)\sin\theta_2 \cos\theta_3$$
$$b = (1 + R)\cos\theta_2 - (1 - R)\cos\theta_1$$
$$c = (1 + R)\sin\theta_2 \sin\theta_3$$
$$\vec{v} = k\,[(\sin\theta_1 - \sin\theta_2\cos\theta_3)\,\hat{x}_o - \sin\theta_2\sin\theta_3\,\hat{y}_o - (\cos\theta_1 + \cos\theta_2)\,\hat{z}_o].$$

---

[1] Brekhovskikh (Ref 4) suggests the criterion $4\pi r_c \cos(\mathcal{A}) >> \tau$ where r_c is the radius of curvature of the surface irregularities and $\mathcal{A}$ is the local angle of incidence.

[2] Henceforth the superscript $\pm$ on R will be dropped for notational convenience.

[3] Imbedded in A_1 are the peak transmitter power and the antenna gains for non-isotropic antennas.

and the integration is now over the rectangular projection of S onto the xy-plane. Also ζ_x and ζ_y denote partial derivatives of $\zeta(x, y)$ with respect to x and y, respectively.

Mean Scattered Power

The mean scattered power from the surface patch S is given by

$$\langle \delta P_2 \rangle = 1/2\, Y_o\, E_2 E_2^* \qquad (1) \qquad (7)$$

where the asterisk (*) denotes the complex conjugate, and Y_o is the admittance of free space.

To facilitate the determination of $\langle E_2 E_2^* \rangle$, set

$$\rho = \frac{E_2}{E_{20}} \qquad (8)$$

where E_{20} is the field at P reflected from a smooth, perfectly conducting plane element in the direction of specular reflection. In addition, the plane element has the same area as the surface element S, and is under the same angle of incidence and at the same distance from P. Finally, the incident wave is assumed horizontally polarized. Under these restrictions, the integrations in (6) can be carried out to yield

$$E_{20} = \frac{ikA_1}{2\pi R_2}\, e^{ikR_2}\, \cos\theta_1\, \delta A \quad . \qquad (9)$$

With the above normalization the mean scattered patch power is

$$\langle \delta P_2 \rangle = 1/2\, Y_o\, |E_{20}|^2\, \rho\rho^* \qquad (10)$$

and it remains only to determine $\langle \rho\rho^* \rangle$ from the expression for ρ:

$$\rho = \frac{1}{2 \cos\theta_1\, \delta A} \iint_A (a\zeta_x + c\zeta_y - b)\, e^{i\vec{v} \cdot \vec{r}}\, dA \qquad (11)$$

---

1. Here E_2 has been time reduced and denotes the field at the peak of a sine wave (in t). The 1/2 has been included to account for averaging over time.

From this expression

$$\left\langle \rho\rho^* \right\rangle = \frac{1}{4\cos^2\theta_1 (\delta A)^2} \int_{-Y}^{Y}\int_{-X}^{X}\int_{-Y}^{Y}\int_{-X}^{X} \left\langle (a\zeta_{x_1} + c\zeta_{y_1} - b) \times \right.$$

$$\left. (\bar{a}\zeta_{x_2} + \bar{c}\zeta_{y_2} - \bar{b})\, e^{i\vec{v}\cdot(\vec{r}_1 - \vec{r}_2)} \right\rangle dx_1\, dy_1\, dx_2\, dy_2 \qquad (12)$$

where $\vec{r}_1$ and $\vec{r}_2$ denote vectors from the origin to the variable points (x_1, y_1, ζ_1) and (x_2, y_2, ζ_2), respectively.

Assumption 3: Assume the covariance between a, b, c, $\bar{a}$, $\bar{b}$, $\bar{c}$ and the partials of ζ may be neglected. In addition let $\left\langle R(\zeta_x) \right\rangle \approx R(\zeta_x = \left\langle \zeta_x \right\rangle) = R(\psi = \psi_1)$ and the reflection angles θ_1, θ_2, θ_3 remain essentially constant over S.

Assumption 4: $A >> \lambda$.

Assumption 5: Let the surface element S be very rough, that is to say,

$$\sqrt{g} = \frac{2\pi\sigma_h}{\lambda}(\cos\theta_1 + \cos\theta_2) >> 1. \qquad (13)$$

Within the assumptions 3 and 4, (12) may be replaced by

$$\left\langle \rho\rho^* \right\rangle = \frac{BB^*}{4\cos^2\theta_1 (\delta A)^2} \int_{-Y}^{Y}\int_{-X}^{X}\int_{-Y}^{Y}\int_{-X}^{X} \left\langle e^{i[v_x(x_1 - x_2) + v_y(y_1 - y_2)} \right.$$

$$\left. \times\, e^{i v_z (\zeta_1 - \zeta_2)} \right\rangle dx_1\, dy_1\, dx_2\, dy_2 \qquad (14)$$

where

$$BB^* = |R(\psi_1)|^2 \frac{|\vec{v}|^4}{(kv_z)^2} \qquad (15)$$

and v_x, v_y, v_z denote the x, y, z components, respectively of $\vec{v}$ (see (6)). It should be noted here that (14) follows by expanding (12) and integrating by parts term by term taking, at the same time, the term BB* out from under the

integrals (assumption 3). Boundary terms that arise during the integrations by parts are also neglected in arriving at (14) as they remain small (by assumption 4) in comparison to other remaining terms.

The term $\left\langle e^{iv_z(\zeta_1-\zeta_2)} \right\rangle$ in the integrand of (14) is the two-dimensional characteristic function of the distribution

$$W(z_1, z_2) = \frac{1}{2\pi\sigma_h^2\sqrt{1-C^2}} \exp\left[-\frac{z_1^2 - 2Cz_1z_2 + z_2^2}{2\sigma_h^2(1-C^2)}\right] \tag{16}$$

and is equal to

$$\left\langle e^{iv_z(\zeta_1-\zeta_2)} \right\rangle = \exp\left[-g(1-C)\right] \tag{17}$$

where g is defined in (13) and the C appearing in both (16) and (17) is the normalized correlation function

$$C(\tau) = e^{-\tau^2/d_c^2} \tag{18}$$

Here τ is a separation parameter equal to the distance between the variable points (x_1, y_1) and (x_2, y_2) in A, and d_c is the correlation distance equal to the distance in which $c(\tau)$ drops to the value e^{-1}. This value of d_c should be small compared with A, for in the contrary case the surface element S, in contrast to being rough, would contain just a few irregularities.

To proceed with the determination of $\langle \rho\rho^* \rangle$, first approximate the integral on the right-hand side of (14) by an integral over the smallest circle, containing the rectangular region A. With the radius of this circle equal to L, and with the introduction of the polar coordinate transformation

$$\left.\begin{aligned} x_1 - x_2 &= \tau \cos\varphi \\ y_1 - y_2 &= \tau \sin\varphi \end{aligned}\right\} , \tag{19}$$

$$\langle \rho o^* \rangle \approx \frac{BB^*}{4 \cos^2 \theta_1 (\delta A)} \int_o^L \int_o^{2\pi} e^{i v_x \tau \cos\varphi + i v_y \tau \sin\varphi}$$

$$x \exp [-g (1-C)] \tau d\tau d\varphi \tag{20}$$

The integral over φ in the above expression may be evaluated and leads to a Bessel function of order zero so that $\langle \rho\rho^* \rangle$ may be taken as

$$\langle \rho\rho^* \rangle = \frac{\pi BB^*}{2 \cos^2 \theta_1 (\delta A)} \int_o^L J_o (v_{xy}\tau) \exp [-g (1 - C] \tau d\tau \tag{21}$$

where

$$v_{xy} = \sqrt{v_x^2 + v_y^2} \quad . \tag{22}$$

Now it may be shown (using the assumption 5) that the integral in (21) receives significant contributions only from the neighborhood of $\tau = 0$, whence $\langle \rho\rho^* \rangle$ is set equal to

$$\langle \rho\rho^* \rangle = \frac{\pi BB^*}{2 \cos^2 \theta_1 (\delta A)} \int_o^\infty J_o (v_{xy}\tau) \exp [-g (1 - C)] \tau d\tau \tag{23}$$

In addition the approximation $\exp (\tau^2/d_c^2) = C(\tau) \approx 1 - \tau^2/d_c^2$ may also be used to yield

$$\langle \rho\rho^* \rangle = \frac{\pi BB^*}{2 \cos^2 \theta_1 (\delta A)} \int_o^\infty J_o (v_{xy}\tau) \exp \left(\frac{-g\tau^2}{d_c^2}\right) \tau d\tau \tag{24}$$

Now the integral in (24) is well known and can be evaluated with the result

$$\langle \rho\rho^* \rangle = \frac{\pi B B^*}{4 \cos^2 \theta_1 \, (\delta A)} \frac{d_c^2}{g} \exp\left(- v_{xy}^2 d_c^2 / 4g \right) \tag{25}$$

The quantities β_o, β defined by

$$\left.\begin{aligned} \tan \beta_o &= 2\sigma_h / d_c \\ \tan \beta &= v_{xy} / v_z \end{aligned}\right\} \tag{26}$$

are now introduced to further simplify the expression for $\langle \rho\rho^* \rangle$. Note here that β_o may be considered as a measure of the rms slope of the surface irregularities and β is the angle between the bisector of the incident and reflected waves and the local normal to S (see Figure 8). Equation (15) together with (26) leads to the final expression for $\langle \rho\rho^* \rangle$:

$$\langle pp^* \rangle = \frac{\pi \, |R(\psi_1)|^2 \cot^2 \beta_o}{(\delta A) \, k^2 \cos^2 \theta_1 \cos^4 \beta} \exp\left(\frac{-\tan^2 \beta}{\tan^2 \beta} \right) \tag{27}$$

Accordingly, within the assumptions of this section

$$\langle \delta P_2 \rangle = 1/2 \, Y_o \left[\frac{A_i^2 \, |R(\psi_1)|^2 \cot^2 \beta_o}{4\pi R_2^2} \exp\left(\frac{-\tan^2 \beta}{\tan^2 \beta_o} \right) \right] \delta A \tag{28}$$

where the $\cos^4 \beta$ in the denominator of (27) has been dropped, since in general β is small.

Theoretical Modifications

Unfortunately (28) is quite restrictive in view of assumption 5, that is, it was derived on the assumption that the surface element is very rough. Now in general the glistening surface contains many surface elements S, and even if the total glistening surface is uniform with respect to the roughness

parameters β_o, σ_h, d_c, some patches may be classified as rough and others as smooth since by (13) the parameter g is not only a function of these roughness parameters, but is also a function of the reflection angles to the patch. It is therefore clear that before the total power from the glistening surface can be determined, (27) must be altered appropriately and the assumption 5 relaxed.

In general, the variance $D\{\rho\}$ is given by

$$D\{\rho\} = \langle \rho \rho^* \rangle - \langle \rho \rangle \langle \rho \rangle^* \tag{29}$$

where

$$\langle \rho \rangle = \frac{-B}{2 \cos \theta_1 \, (\delta A)} \int_{-Y}^{Y} \int_{-X}^{X} e^{i(v_x x + v_y y)} \langle e^{i v_z \zeta} \rangle \, dx dy \tag{30}$$

and

$$B = \langle b \rangle + \frac{\langle a \rangle v_x + \langle c \rangle v_y}{v_z} \tag{31}$$

[1]

Now with $\langle e^{i v_z \zeta} \rangle$ given by

$$\langle e^{i v_z \zeta} \rangle = \exp\left(-\frac{1}{2} \sigma_h^2 v_z^2\right) \tag{32}$$

the integrations in (30) can be carried out and

$$\left.\begin{aligned} \langle \rho \rangle &= -R(\psi_1) f(\theta_1, \theta_2, \theta_3) \rho_o \langle e^{i v_z \zeta} \rangle \\ &= -R(\psi_1) f(\theta_1, \theta_2, \theta_3) \rho_o \exp\left(-\frac{1}{2} \sigma_h^2 v_z^2\right) \end{aligned}\right\} \tag{33}$$

[1] (30) and (31) were obtained in the same manner as (14) and (15).

where

$$f(\theta_1, \theta_2, \theta_3) = \frac{1 + \cos\theta_1 \cos\theta_2 - \sin\theta_1 \sin\theta_2 \cos\theta_3}{\cos\theta_1 (\cos\theta_1 + \cos\theta_2)} \tag{34}$$

$$\rho_o = \text{sinc}\ (v_x X)\ \text{sinc}\ (v_y V)^{1} \quad . \tag{35}$$

Under assumption 4, ρ_o is ≈ 0 except very near the direction of specular reflection ($\theta_1 = \theta_2$, $\theta_3 = 0$). It is therefore customary to set in practice

$$\rho_o = \begin{cases} 1 & \text{at the specular point} \\ 0 & \text{otherwise.} \end{cases} \tag{36}$$

Along with this replacement goes a re-interpretation of (33):

$$\langle \rho \rangle = \begin{cases} -R(\psi_1)\ \exp\left[-\frac{1}{2}\left(\frac{4\pi\sigma_h \cos\theta_1}{\lambda}\right)^2\right] & \text{if the specular point is on patch} \\ 0 & \text{otherwise} \end{cases} \tag{37}$$

and thus

$$\langle \rho \rangle \langle \rho \rangle^* = \begin{cases} |R(\psi_1)|^2\ \exp\left[-\left(\frac{4\pi\sigma_h \cos\theta_1}{\lambda}\right)^2\right] & \text{if the specular point is on patch} \\ 0 & \text{otherwise} \end{cases} \tag{38}$$

In the case of a rough surface ($g >> 1$) $\langle \rho \rangle \langle \rho \rangle^* \approx 0$ and

$$D\{\rho\} \approx \langle \rho\rho^* \rangle = \frac{\pi |R(\psi_1)|^2 \cot^2\beta_o}{k^2 \cos^2\theta_1} \exp\left(\frac{-\tan^2\beta}{\tan^2\beta_o}\right) \tag{39}$$

Recent developments (Ref 3) suggest an approach for the determination of $D\{\rho\}$ for arbitrary roughness. This approach involves multiplying (39) by

---

[1] $\text{sinc}\ (x) = \frac{\sin x}{x}$

an approprate roughness factor F_d^2 so that for arbitrary roughness

$$D\{\rho\} = F_d^2 \frac{\pi |R(\psi_1)|^2 \cot^2 \beta_o}{k^2 \cos^2 \theta_1} \exp\left(-\frac{\tan^2 \beta}{\tan^2 \beta_o}\right) \tag{40}$$

and

$$\langle \rho\rho^* \rangle = \frac{F_d^2 \pi |R(\psi_1)|^2 \cot^2 \beta_o}{k^2 \cos^2 \theta_1} \exp\left(-\frac{\tan^2 \beta}{\tan^2 \beta_o}\right) \delta A$$

$$+ \begin{cases} |R(\psi_1)|^2 \exp\left[-\left(\frac{4\pi\sigma_h \cos\theta_1}{\lambda}\right)^2\right] & \text{if the specular point is on the patch} \\ 0 & \text{otherwise} \end{cases} \tag{41}$$

At this point of this discussion, a few remarks about the replacement of (33) by (37) and about F_d^2 are in order. Consider the geometry in Figure 3 for the case of an isotropic source (beacon) and receiver. The expression (33) is a continuous representation of the mean normalized scattered field from the surface S and was derived from a continuously distributed field over S. The implication of this expression for $\langle \rho \rangle$ is that the most significant contribution to the mean scattered field arrives from a region concentrated about the specular point and is due to a point source located at the image source. The replacement of (33) by the discontinuous expression (37) is a bit artificial. On the other hand, it is considered only as an approximation to (33) for practical determinations in typical applications, and should be valid provided it is used within the assumptions leading to its derivation, of which a major assumption is that the patch size is large in comparison to the wave length λ. Along with the approximation (37) goes a re-interpretation of E_{20}. It should now be considered as the free space voltage field at the receiver (or the point P in the previous analysis) reflected or transmitted by the image source. As such, it should be taken as

$$E_{20} = \tilde{A}_1 \frac{e^{ik\,(R_1 + R_2)}}{R_1 + R_2} \quad [1] \tag{42}$$

where R_1 and R_2 are defined in Figure 3, and $\tilde{A}_1$ is associated with the power of the transmitting beacon. In light of the above remarks, the mean scattered field from S (for isotropic transmitting and receiving antennas) is taken as

$$\langle E_2 \rangle = \begin{cases} \dfrac{-R(\psi_1)\,\tilde{A}_1\, e^{iK\,(R_1 + R_2)}}{(R_1 + R_2)} \exp\left[-\frac{1}{2}\left(\dfrac{4\pi\sigma_h \cos\theta_1}{\lambda}\right)^2\right] & \text{if specular point is on patch} \\ 0 & \text{otherwise} \end{cases} \tag{43}$$

In reference to the roughness factor F_d^2 introduced in (40) to scale the diffuse surface reflections, its value, given in the literature as

$$F_d^2 = \sqrt{(1 - \rho_{s1}^2)\,(1 - \rho_{s2})^2} \tag{44}$$

where

$$\rho_{si}^2 = \exp\left[-\left(\frac{4\pi\sigma_h \sin(\psi_i)}{\lambda}\right)^2\right] \qquad i = 1, 2$$

is theoretically unproven. This however, should not in itself preclude its use, as it was logically determined in an effort to correlate the rough surface scattering theory with experimental data and in addition accounts for both the horizon effect for a curved earth and the energy reflected specularly at low grazing angles from tops of rounded irregularities. On the other hand, very little experimental data exists to support a general use of this specific roughness factor. The experimental measurements program developed under this contract is therefore designed in part to validate and improve (if necessary) this choice of F_d^2.

contrary

[1] This modification of E_{20} applies only in the determination of $\langle E_2 \rangle$ and not in the previous determination of $\langle E_2 E_2^* \rangle$ for a very rough surface.

In view of the above, for the case of isotropic antennas the mean-scattered power from S at the receiver is given as

$$\langle \delta P_2 \rangle = \frac{P_t \left| R(\psi_1) \right|^2 \cot^2 \beta_o F_d^2}{(4\pi (R_1 R_2)^2} \exp\left(\frac{-\tan^2 \beta}{\tan^2 \beta_o} \right) \delta A \tag{45}$$

$$+ \begin{cases} \dfrac{P_t \left| R(\psi_1) \right|^2}{4\pi (R_1 + R_2)^2} \exp\left[-\left(\dfrac{4\pi \sigma_h}{\lambda} \cos\theta_1 \right)^2 \right] & \text{if the specular point is on the Patch} \\ 0 & \text{otherwise} \end{cases}$$

where P_t is the peak power of the transmitting antenna. To obtain equation (45) from the previous analysis, replace A_1 in (9) and $\tilde{A}_1$ in (42) by their values $A_1 = \left(\dfrac{P_t}{2\pi Y_o R_1^2} \right)^{\frac{1}{2}}$, $\tilde{A}_1 = \left(\dfrac{P_t}{2\pi Y_o} \right)^{\frac{1}{2}}$, respectively. Then using the resulting expressions for E_{20}, together with equation (41), the mean scattered power from the surface patch S is calculated in accordance with equation (10).

If the transmitting and receiving antennas have different power gains, g_1 and g_2, respectively, in the direction of the surface patch S, the mean scattered patch power is determined by multiplying (45) by $\dfrac{\lambda^2}{4\pi} g_1 g_2$. Finally, since the Fresnel reflection coefficient $R(\psi_1)$ is theoretically valid only for a planar surface, it should be replaced wherever it appears in the above discussions by $DR(\psi_1)$ where D is the divergence factor introduced in Section 2.2 to account for the earth's curvature. The final expression for the mean scattered patch power is then

$$\langle \delta P_2 \rangle = \frac{P_t g_1 g_2 \lambda^2 D^2 |R(\psi_1)|^2 \cot^2 \theta_o F_d^2}{(4\pi)^3 (R_1 R_2)^2} \exp\left(-\frac{\tan^2 \theta}{\tan^2 \theta_o}\right) \delta A \tag{46}$$

$$+ \begin{cases} \dfrac{P_t g_1 g_2 \lambda^2 D^2 |R(\psi_1)|^2}{[4\pi (R_1 + R_2)]^2} \exp\left[-\left(\dfrac{4\pi \sigma_h}{\lambda} \cos \theta_1\right)^2\right] & \text{if the specular point is on the Patch} \\ 0 & \text{otherwise} \end{cases}$$

APPENDIX D

PHOTOGRAMMETRIC SURVEY

Orthophoto maps will be prepared for a strip of approximately 15,000 feet long by 1500 feet wide at a scale of 1" = 100' showing contours at a vertical interval of one foot. The orthophoto map enables a photographic image to replace the planimetric information contained in a conventional line and symbol map without loss of accuracy on all ground level detail. The maps will be prepared as follows:

1. Aerial Photography

Aerial photography will be acquired along the proposed strip to be mapped at a scale of 1" = 280' using a precision six inch focal length mapping camera. It is estimated that approximately twenty exposures will be required with a nominal 60% forward overlap.

2. Horizontal Control

Sufficient horizontal control will be established on the ground to provide two points of known position within each stereo pair (note - a stereo-pair consists of the overlapping portion of two consecutive exposures).

3. Vertical Points

Two lines of vertical control will be established - one line along each side of the strip to provide four points of known elevation within each stereo pair.

4. Photogrammetric Compilation

a. Hypsography (elevation data)

Using a Wild A-10 precision stereo-compilation instrument, contours at 1.0 ft vertical intervals will be plotted. Where contours are in excess of 100 ft apart spot elevations will be plotted.

b. Planimetry

Concurrently with the preparation of hypsographic data, a limited amount of planimetric information will be plotted. The photography will be enlarged from 1" = 280' to 1" = 100' and rectified to fit the planimetric detail plotted on the A-10 instrument. This produces a photographic image where all ground level is true to scale.

c. Map Sheets

The hypsographic data will be drafted and combined with the photographic image so that the contours appear as black lines superimposed on the photo base. Approximately 10 sheets, 18" x 24" will be produced for each mapping area.

Accuracy

Horizontal

90% of the planimetric detail at ground level will be within $\pm$1/40" of its true position at map scale relative to any other point of detail, and no point pair shall be in error by more than 1/20".

Vertical

90% of all contours will be accurate to within 0.5 ft of their elevation with respect to map datum and no contour will be in error by more than 1.0 ft.

90% of spot elevations will be accurate to within 0.25 ft of their elevation with respect to map datum and no spot elevation shall be in error by more than 0.5 ft.

Map Datum

Arbitrary vertical and horizontal datums will be used.

APPENDIX E

EFFECTS OF TROPOSPHERIC DISTURBANCES

In order to obtain some idea of the order of magnitude of the effects of tropospheric disturbances, a Ratheon developed computer program, Raytrace (developed for another project)* was run using an actual measured vertical profile of varying refractive index. This profile was chosen from a large number of such profiles to represent a rather severe deviation from the normal, such as might occur near the ocean no more than a third of the time. This test profile is shown in Figure E-1, together with the standard profile normalized to the same ground point value. The N_s numbers along the horizontal axis represent the amount by which the index of refraction (n) exceeds that of a vacuum: $N_s = (n - 1) \times 10^6$ (e.g., if the index of refraction is 1.000250, $N_s = 250$). Notice that at A there is an inversion in the slope of the measured curve as compared with the normal curve and that at B the slope is in the normal direction but very much steeper than normal (i.e., N_s changes more for a given small change in altitude). An inversion causes generally horizontal propagation paths to be concave upward and so brings the horizon (tangent point) closer than the geometric (straight-line propagation) horizon, as shown by curve A in Figure E-2 . Gradients in the normal direction (index of refraction decreasing with increasing altitude) result in propagation paths that are convex upward. If their radius of curvature is greater than the earth's radius (plus one-half the antenna height) then the horizon (tangent point) is further away than the geometric horizon, as shown by curve B in Figure E-2 . If their radius of curvature becomes less than the earth's radius, there is no tangent point, and the definition of "horizon" becomes questionable. Long before that, however, the theoretical horizon would have moved so far away that the disturbed tropospheric gradient which gave rise to the assumed curvature could no longer be expected to prevail.

For the Raytrace runs, it was assumed that the transmitter and receiver heights were 300 and 4 meters, respectively, and that the baseline distance was such that the elevation angle of the transmitter, from the receiver, would be 2 1/2°, looking along the curved path corresponding to the chosen tropospheric conditions. Two conditions were chosen:

* See Reference 13.

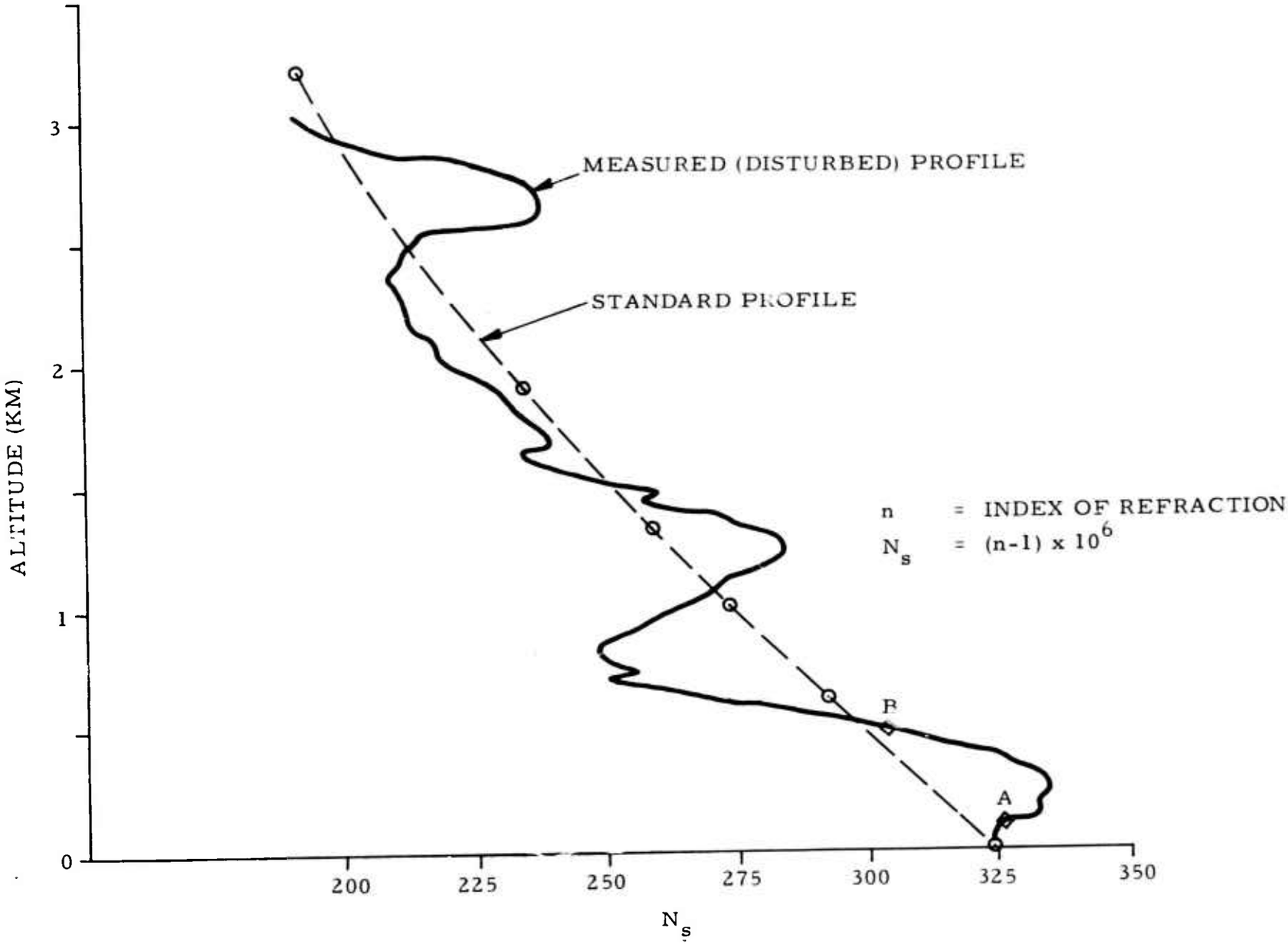

Figure E-1. Index of Refraction Profiles

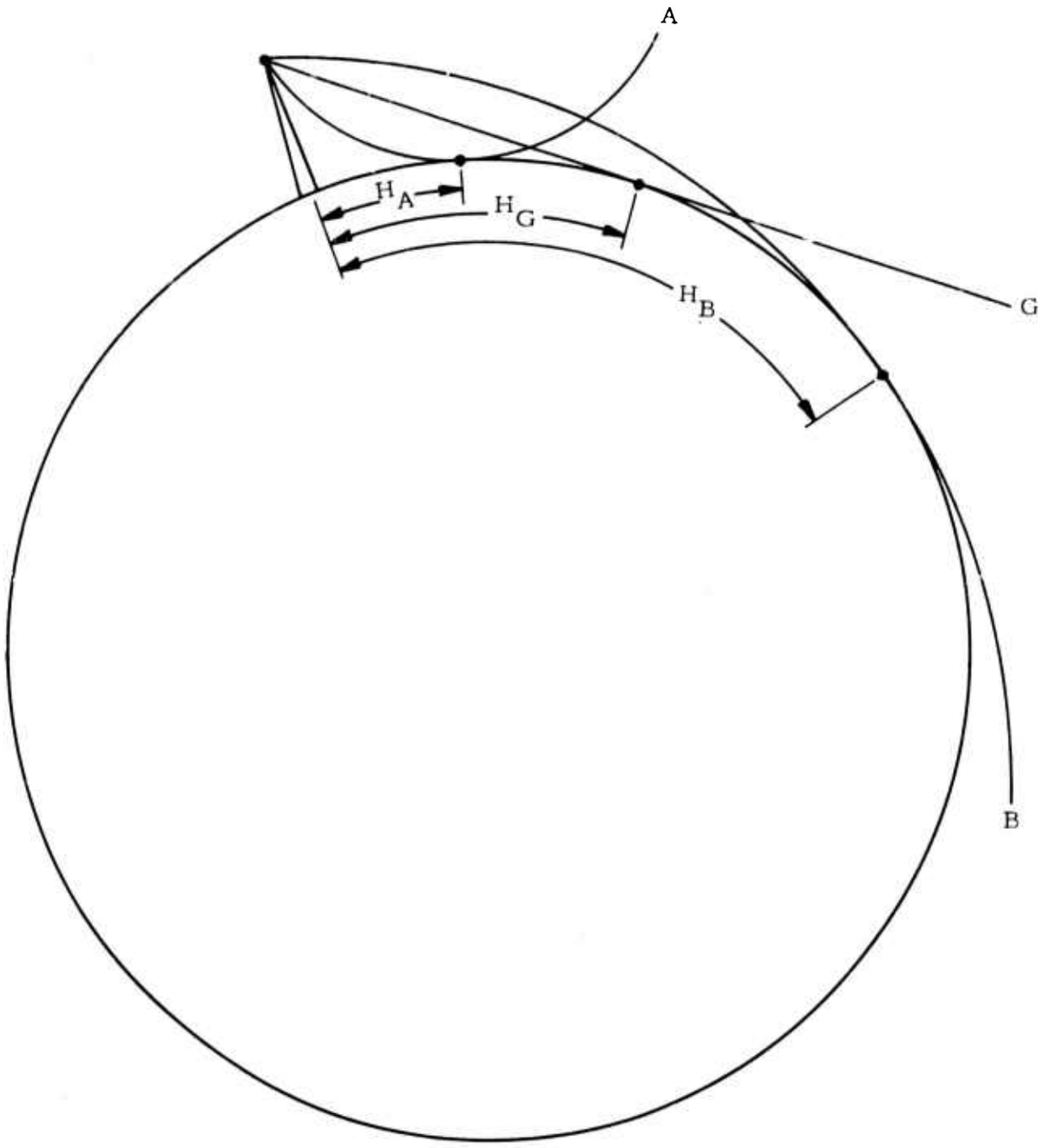

H_A = DISTANCE TO HORIZON FOR CONDITION A

H_G = DISTANCE TO GEOMETRIC (STRAIGHT-LINE) HORIZON

H_B = DISTANCE TO HORIZON FOR CONDITION B

Figure E-2. Effect of Ray Curvature on Horizon Distance

Condition A: The disturbed profile of Figure E - 1 was used as shown, so that the direct and reflected propagation paths were mostly confined to the region of the inversion, around point A.

Condition B: The disturbed profile of Figure E - 1 was assumed to have drifted downward so that the propagation paths were confined to the region of steep slope, around point B.

Condition A resulted in a horizon distance of about 5.6 kilometers from the receiver as compared with a geometric horizon at 7.15 kilometers or a "four-thirds earth" standard profile horizon at 8.25 kilometers. The receiver-to-transmitter baseline distance was 6.7 kilometers. Condition B resulted in a no-tangent curvature and a baseline distance of 6.8 kilometers.

The geometry of the simulation is shown in the inset at the top of Figure E - 3 . A number of reflection points were chosen and the path lengths, r_D, r_1, and r_2, with the assumed disturbed gradient profile were computed, as well as the corresponding straight-line path lengths. The differences, Δr_D, Δr_1, and Δr_2, were used to calculate the error in the difference between the times of arrival of the direct and reflected pulses:

$$\text{ERROR}_{\text{time}} = \frac{\Delta r_1 + \Delta r_2 - \Delta r_D}{0.3} \quad \text{(in nanoseconds)}$$

The resolution curves of Figure 16, corrected for baseline distance, provided the approximate sensitivity of range to time difference, as a function of ground distance, D_1. The sensitivity at each range multiplied by the time error gave the corresponding range error. These errors are plotted in Figure E - 3 .

Note that the errors as plotted are those that would result from assuming straight-line signal paths instead of the curved paths which actually result from conditions A and B. The data reduction procedure, however, assumes the curvature associated with a four-thirds earth model corresponding to the standard gradient profile which is in the direction of condition B. Hence, for condition A the errors would be somewhat larger, and for condition B they would be somewhat smaller, than those shown in Figure E-3. Overall, the maximum absolute error for both conditions would be well under 50 meters.

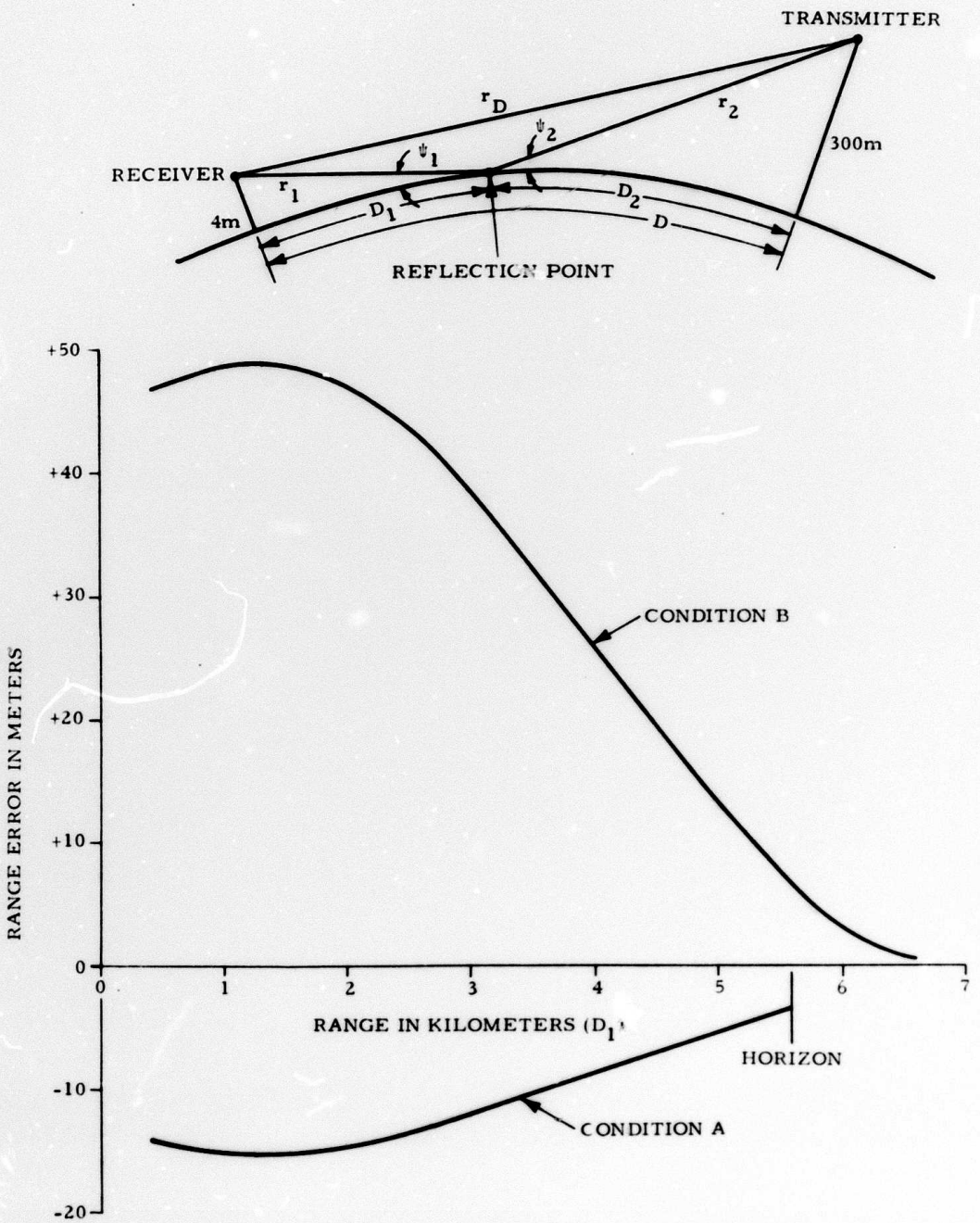

Figure E-3. Range Errors Due To Tropospheric Disturbance

APPENDIX F

THE STILWELL PROCESS

1. Optical Fourier Transform Photography

A photograph of the sea surface may be utilized to obtain a quantitative measure of the two-dimensional wave slope power spectrum density. If the skylight incident on the sea surface is a slowly varying function of zenith and azimuth angles, then the light reflected from the surface to an aerial camera will be intensity modulated by the sea surface slope structure. To the first order the reflected light intensity, which is a function of the water reflectivity, will be proportional to the local value of sea slope. The fundamental principle of wave to photographic image transfer is illustrated in Figure F-1. In A is shown the functional relationship between the local slope angle α and the corresponding image point in the film emulsion given by θ. Curve B is the water reflectivity $\Gamma(\alpha)$ and dictates the point value of reflected light intensity for a given α (or θ). If the incident skylight is of uniform value I_o over the camera field of view, then the light exposing the film is $I_o \Gamma(\alpha)$. Curve C is the film characteristic curve (Hurter-Driffield curve) which relates photographic density D to the log of exposure. Exposure is proportional to $I_o\Gamma(\alpha)$. The outcome relationship between density and θ is illustrated in D. Here, the density as measured by a scanning microdensitometer is functionally related to the slope angle. Treating the developed film negative as a diffraction grating and applying coherent optical signal processing methods will yield a two-dimensional power density spectrum. Alternatively, the sea negative density record may be digitized and the spectrum computed by FFT.

2. Experimental Procedure

The technique requires no special camera system. Conventional camera and optics such as a 35 mm Nikon with 50 mm lens for wavelengths in the range of 3 cm to 1 meter and at a stationary camera height of 19 meters above the surface have been used for the study of spectral trends. [1] A K-17 aerial camera

---

[1] D. Stilwell, "Optical Analysis for the 1971 ARPA Tower Experiment," Naval Research Laboratory," Report 7445, May 12, 1972.

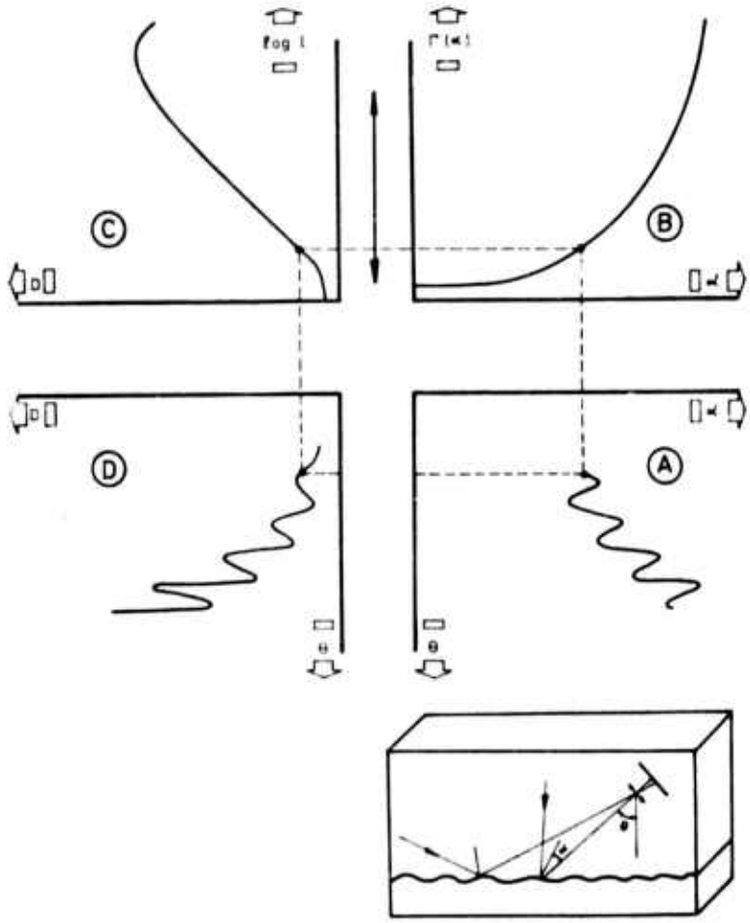

Figure F-1. Principle of Wave - Image Transfer

with 12" focal length lens has been used to study long wavelength spectra. The camera was at an altitude of 1500 feet mounted in a DC-3 and was not image motion compensated.[2] Ocean swell wavelengths of 366 meters and propagation direction have been measured from Apollo 7 space photography. A 70 mm Hasselblad camera with an 80 mm planar le s and loaded with SO - 368 film was used.[3] Measurement of very short waves of the order of 1 cm and less, called capillary waves, involves special considerations. This is because of their excessive slopes and propagation characteristics. Slopes are greater than 14^{o} and may be nearly vertical, and propagation occurs at about 25 cm/sec in all directions. Effective very low altitude photography of capillary waves requires an exposure time approximately 1/500 sec[3] and a skylight luminance rapidly varying with zenith angle.[4] Exposure latitude is now more critical and consequently depth of field must be carefully considered if the gravity wave heights exceed about 1 meter. Vertical photographs of the sky using a fisheye lens for skylight luminance calibration are now required.

For wind speeds in excess of 12 meters/second, fractional whitecap coverage becomes sufficiently great to preclude useful photographs for optical analysis. Significant haze level may also preclude useful photography.

3. Information Content of Sea Photographs

Optical analysis of the sea photograph negative or diffracting grating yields the power spectral density (or Fourier transform) of the normal angle of the surface (local normal zenith angle) as a function of directional wave numbers. The wave height spectrum and wave slope spectrum may be derived from the normal angle spectrum.

---

[2] "Space Geodesy Aircraft Experiment," Raytheon Company Equipment Div., Wayland, Mass., NASA Contract NASW 1932 Final Report.

[3] V. E. Noble, "Ocean Swell Measurements from Satellite Photographs," Remote Sensing of Environment 1 (1970), p. 151-154.

[4] Directional Wave Spectra From Daylight Scattering (Ref 8)

The mean-square wave height is determined by integrating the two-dimensional wave height spectrum over all wave number space. The mean-square slope spectrum for radar analysis is found by integrating the two-dimensional wave to slope spectrum over all wave number space. The slope of the sea has been found to be much more sensitive and instantaneously responsive to the wind speed than is the wave height.

4. JONSWAP 2

Raytheon is presently involved with capillary wave spectrum measurements in the North Sea using the optical Fourier transform technique. These measurements are part of the Joint North Sea Wave Project (JONSWAP) to study the energy balance of the overall wind wave spectrum which is characterized by a strong energy transfer from long waves to short waves. Results of this study will provide a unique opportunity to evaluate the technique against a number of alternative measuring techniques including laser instruments and capacitance probes. JONSWAP is an international joint air-sea interaction program sponsored by the Scientific Affairs Division of NATO.

Raytheon has been under contract with NATO, NOAA and NASA for support in JONSWAP.

APPENDIX G. DATA PROCESSING

Introduction

A system is described here for processing, displaying, and recording the received signal due to reflection from a glistening surface as described in Section 3. Provision will be made for displaying and recording the average signal within a time resolution cell of 1 nanosecond. Circuitry is included within the system to present the data as a function of time or as a function of ground range between receiver and transmitter.

The basic measurement is made by sampling the video-detected received signal with a sampling gate that has an extremely narrow acquisition time. One sample will be taken each pulse period. The beginning of each pulse period is to be indicated (initiated) by the reception of a direct path signal. Samples will be taken at times measured from the occurrence of the direct path pulse. In order to obtain video integration, as may be required, a predetermined number of samples will be made during each time slot. The time will then be incremented in a predetermined fashion and an equal number of samples will be taken at this new time. This process will be continued until the entire video signal has been sampled.

A sampling oscilloscope will be used to perform the sampling function and to provide a display. It will be modified to permit video integration as described. In addition, the time base (X-axis) will be modified so that the display can indicate average signal versus either time or distance. Circuitry will be included to record magnetically the sampled signal data as well as the receiver antenna beam pointing information, transmitter location data, and verbal comments.

Sampling Technique

Sampling oscilloscopes produce a point-by-point replica of fast repetitive waveforms. The basic procedure is to sample the repetitive waveform once each pulse period and hold or store each sample until the next sample is taken. Successive samples are made slightly later in time until the entire waveform has

been sampled at least once. The technique requires that the time between samples be equal to the pulse period augmented by a time increment small enough to permit observation of the most rapid variations in the waveform to be measured. This technique permits the use of comparatively low frequency methods to observe high frequency phenomena.

The timing of the sampling strobe is accomplished as depicted in Figure G-1. A trigger is established at the PRF from the detected direct signal. This trigger causes a linear ramp to run up. The linear ramp is compared to a reference signal. When the two are equal, the sampling strobe is initiated, the reference signal is increased a predetermined amount and the ramp is reset. The next trigger starts the ramp again, the comparison initiates the strobe, again the reference signal is increased and the ramp is reset. As this continues the reference voltage increases in steps, each step being used for ramp comparison and for horizontal displacement on the oscilloscope display. When the reference reaches maximum horizontal displacement, it is set to zero and the whole process is repeated.

Modification to Sampling Oscilloscope

Figure G-2 is a block diagram of the Hewlett-Packard sampling oscilloscope. The two blocks connected by dotted lines are those which will be modified or added for the multipath equipment (Scan Generator and Integrator).

Scan Generator

It was shown above that the time between the trigger and the strobe is determined by comparing a linear ramp with a staircase reference, the height of each staircase step determining the position of the corresponding strobe. By keeping the reference constant, the strobe can be made to occur at the same time after a number of triggers. By linearly incrementing the reference, successive strobes can be made to occur at linearly increasing times. In general, by suitably shaping the staircase it is possible to vary the strobe positioning as desired. Therefore, by properly modifying the staircase, it will be possible to provide video integration as required, as well as to sample in any predetermined sequence (e.g., equal increments of ground range).

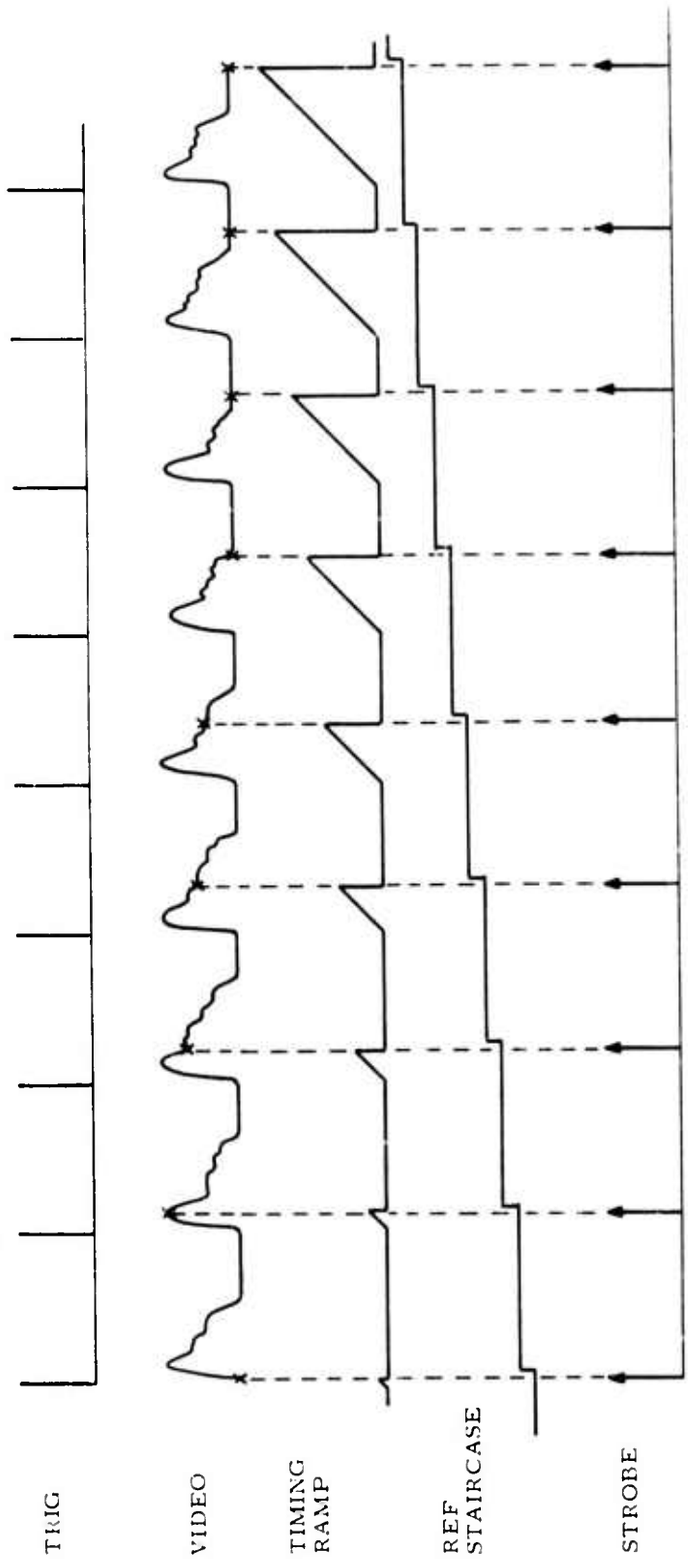

Figure G-1. Strobe Advance Mechanism

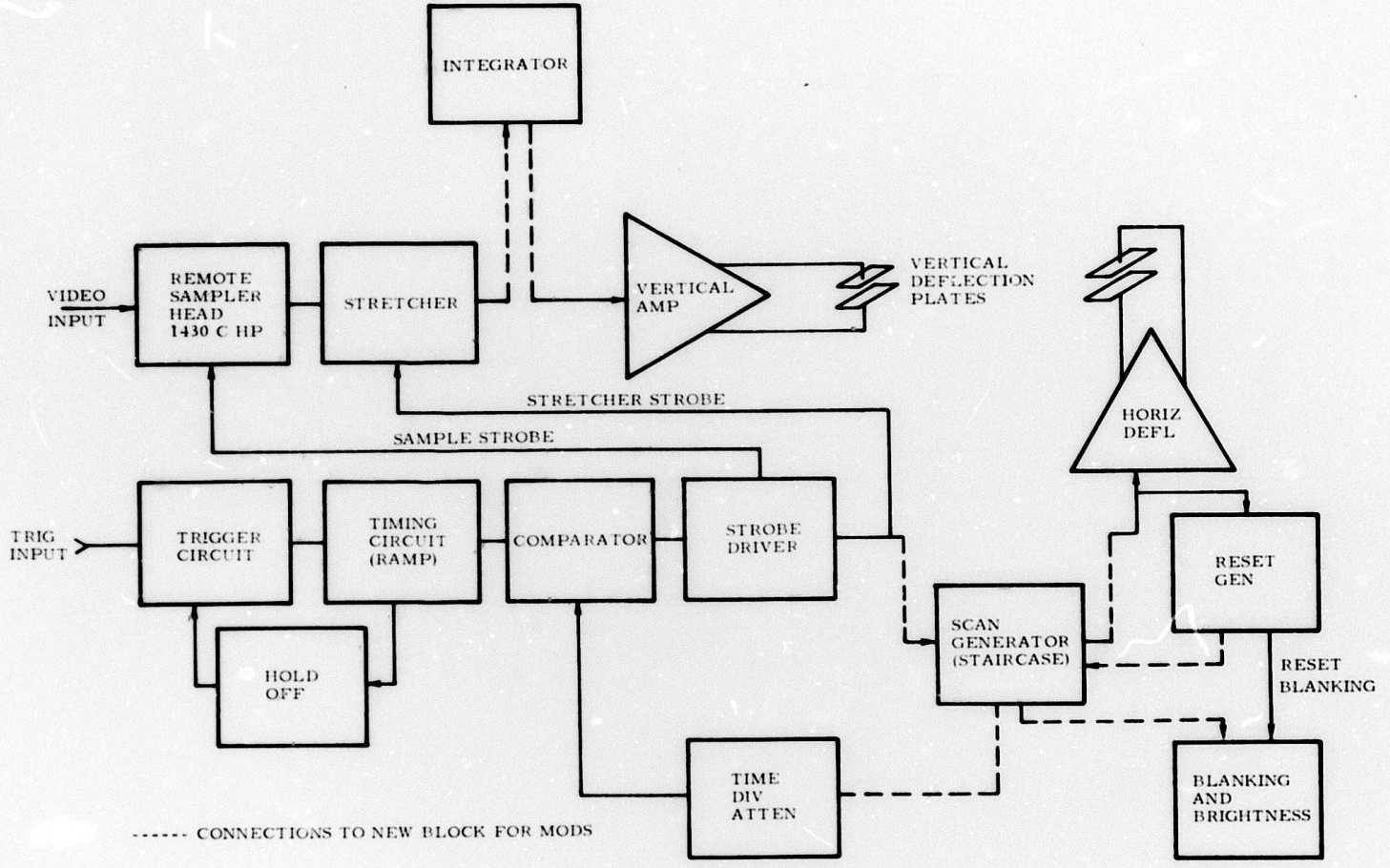

Figure G-2. Modified HP 1811A

Figure G-3 shows, in block diagram form, one possible way of doing this. The strobe from the comparator will be fed to a "divide by N" circuit, the value of N determined by the number of samples to be integrated, as selected by a front panel selector switch. The output pulses from the divider will then be counted. The count thus obtained will be used to address a programmed read-only-memory (PROM) which will in turn produce a sequence of binary words which when fed to the D/A converter will give the proper levels for the reference voltages used in the comparator to produce successive strobe pulses. As many PROM's may be used as staircase shapes desired. The particular PROM to be used will be selected by a front panel selector switch.

Integrator

The integrator (Figure G-4) will take its input from the stretched sample (held voltage). Since it is necessary to convert the analog signal to a digital word for recording this can be done at once, thus simplifying the integrator circuitry. When the proper number of pulses have been summed, the shift register delay is connected to the ENCODING circuit for recording and D/A converted for use as the vertical signal on the oscilloscope display.

Recording, Timing, etc. (Figure G-5)

It is suggested that a digital magnetic tape recorder be used to record the data obtained in this experiment. The advantage of having the data recorded in a form that can be used directly by a computer should prove beneficial in the data-analysis phase of the program.

The data to be recorded includes receiving antenna position, transmitting antenna location, and the reflected signal strength information obtained as previously described. In addition, file and/or record keeping words must be introduced for identification as needed in the analysis and it may be desirable to provide for recording verbal comments. Start and stop recorder commands must also be generated.

To accomplish this with no loss of data, the following sequence will be used:

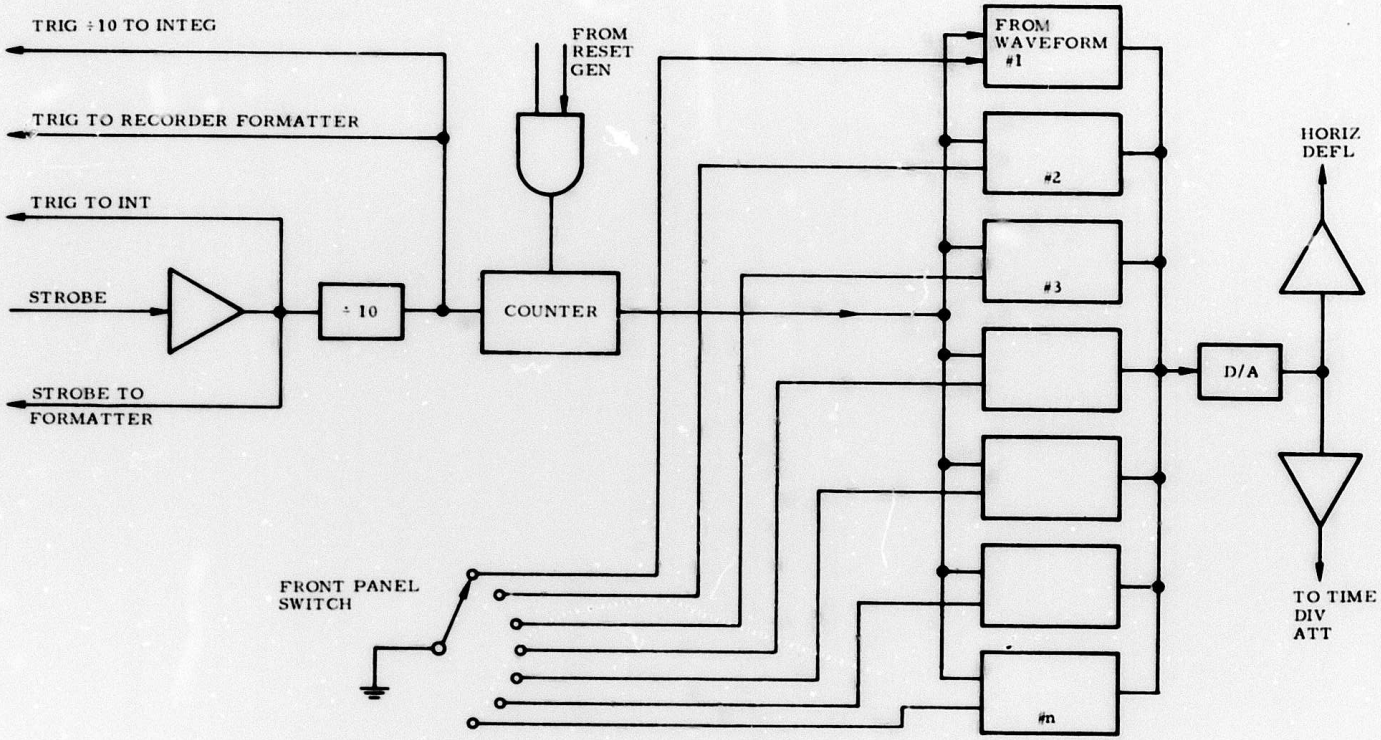

Figure G-3. Scan Generator Block Diagram

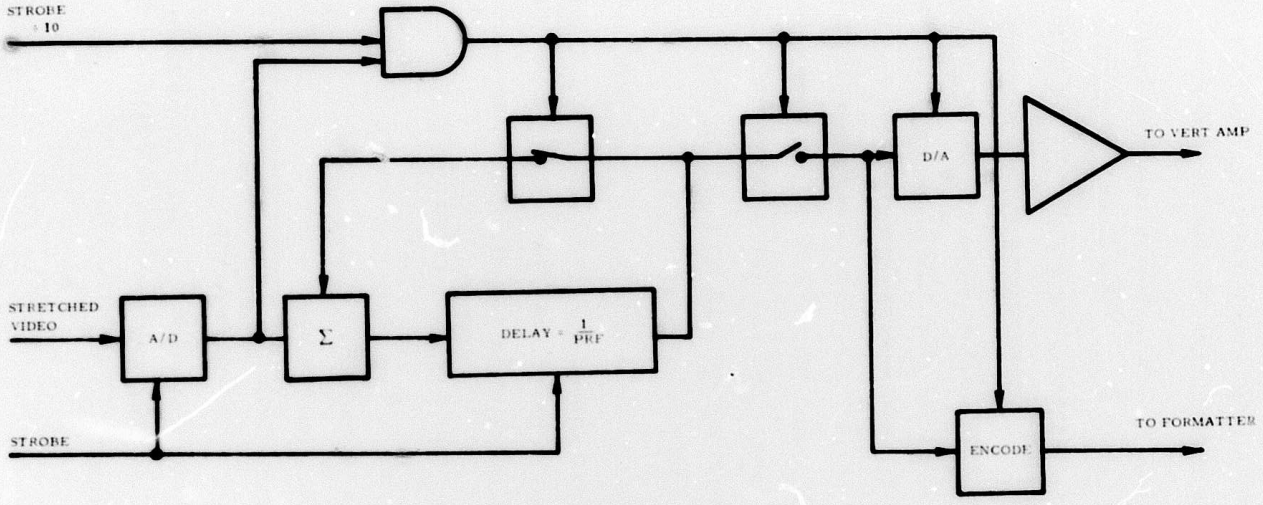

Figure G-4. Integrator Block Diagram

First, the receiver and transmitter antenna positions, file number, and record number will be stored in a register. The detected PRF (trigger) will be used to clock this information into the register.

The completion of this task will be indicated by counting, whereupon the sampling of data will take place. The sampled data will be stored in the same register. However, the sampling strobe will be used to clock the register during this time.

When all samples for a complete scan in range have been taken, the counter will indicate a predetermined number, and a sequence to empty the full or nearly full register will begin. The recorder will be started and the sampling counter reset to zero. When the recorder is up to speed, it will so indicate and a register read-out clock will be initiated. This clock will transfer the data stored in the register to the tape recorder. The counter will keep track of the clock and when the register is empty, the recorder will be stopped, the counter reset, and the logic prepared for a new cycle.

If verbal comments are to be entered, a front panel selector switch will be set accordingly, and the up-to-speed indication will then cause a COMMENT indicator light to be lit. At the end of the verbal comment input, a manual pushbutton will initiate the register read-out clock.

A typical format for one complete record will appear as follows:

1. Verbal Comment
2. File Identification Number
3. Record Identification Number
4. Receiver Antenna Azimuth Angle
5. Receiver Antenna Elevation Angle
6. Transmitter Azimuth Angle } as seen from the receiver or from an observation post of known location
7. Transmitter Elevation Angle }
8. Transmitter Range
9. Spare
10. Spare
11. Sampled Data

    ⋮

1000. Sampled Data

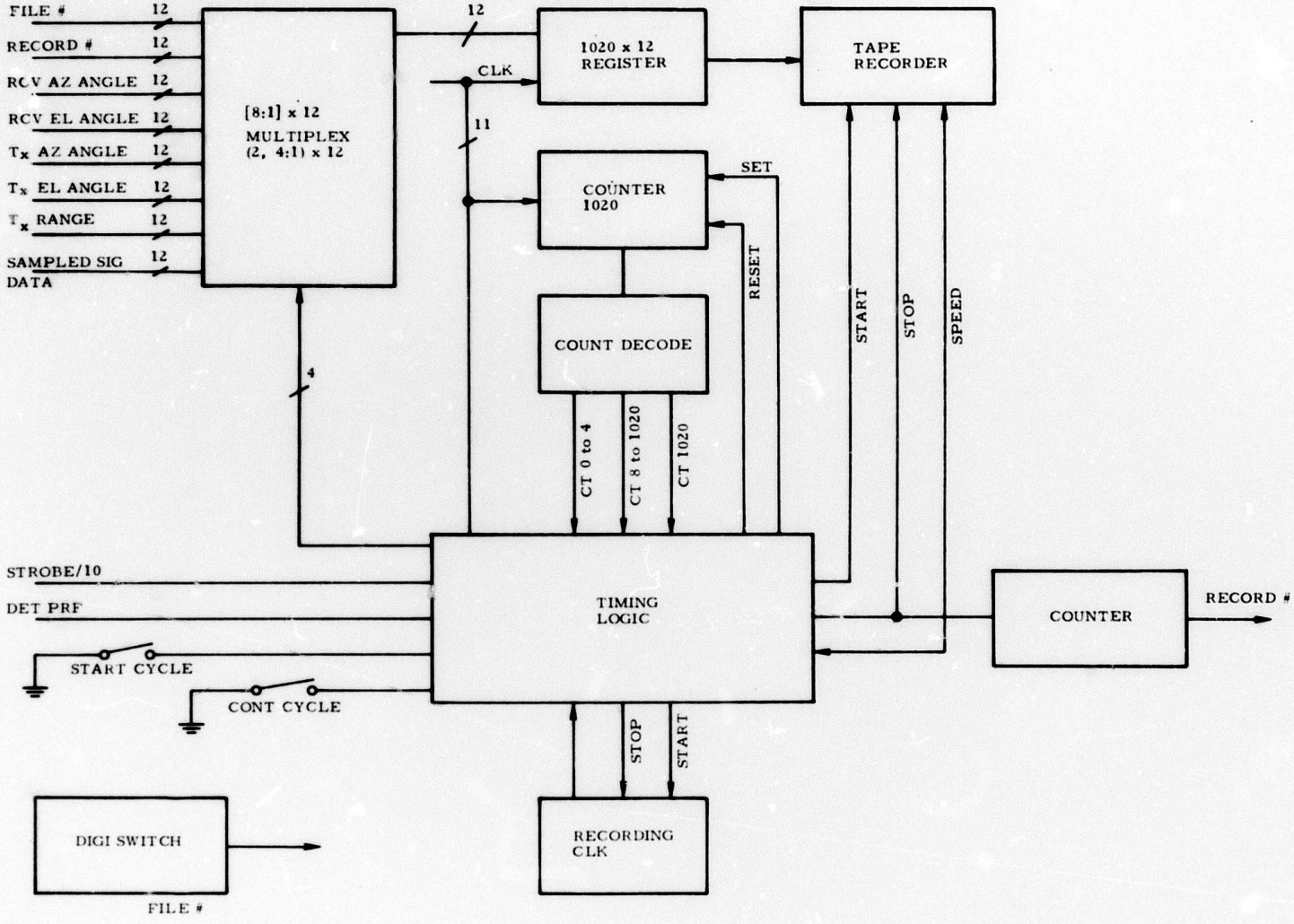

Figure G-5. Recorder Formatting and Timing

References

1. Beckmann, P. and Spizzichino, A., The Scattering of EM Waves from Rough Surfaces, New York: Pergamon, 1963.

2. Barton, D. K. and Ward, H. R., Handbook of Radar Measurement, Englewood Cliffs, New Jersey: Prentice-Hall, 1969, pp 147-154.

3. Barton, D, K., Low-Angle Radar Tracking, Proceedings IEEE, Volume 62, #6, June 1974.

4. Brekhovskikh, L. M., The Diffraction of Waves by a Rough Surface; Part I (in Russian). 2h. Eksper. i Teor. Fiz. 23, 275-289 (1952a)

5. Guthart, H. and Krishman, H. S., "Measurement of Surface-Wave Statistics", AIAA Enper No. 74-66 given at the American Institute of Aeronautics and Astronautics' 12th Aerospace Sciences Meeting, Washington, D. C. January 30, February 1, 1974.

6. Kasevich, R. S., Tang, C. H., and Henriksen, S. W., "Analysis and Optical Processing of Sea Photographs for Energy Spectra", IEEE Transactions on Geoscience Electronics, Vol GE-10, No. 1, January 1972, pp. 51-58.

7. Ross, Duncan B. and Cardone, V., "Observations of Oceanic White-caps and Their Relation to Remote Measurements of Surface Wind Speed", Journal of Geophysical Research, Vol. 79, No. 3 January 20, 1974, p. 444.

8. Kasevich, R. S., "Directional Wave Spectra from Daylight Scattering", paper presented at Fifty-fifth Annual Meeting of the American Geophysical Union, Oceanography Session, Washington, D. C., April 12, 1974.

9. Brookner, E., "Tropospheric Low Elevation Angle Fading", EB-73-14, EM-73-1100, Raytheon Company, Wayland, Mass. 01778, December 11, 1973.

10. Ruthroff, C. L., "Multiple-Path Fading on Line-of-Sight Microwave Radio Systems as a Function of Path Length and Frequency", The Bell System Technical Journal, Vol. 50, pp. 2375-2398, Sept. 1971.

11. Thompson, M. C., Jr., Wood, L. E. and Janes, H. B., "Phase and Fading Characteristics on the 10 to 40 GHz Band", Office of Telecommunications Sciences, Boulder, Colorado 80302, Oct. 5, 1972.

12. McCormick, K. S. and Maynard, L. A., "Measurements of Tropospheric Fading on Satellite-Earth Paths Using Spaced Receivers", Communications Research Center, Department of Communications, Ottawa, Ontario; presented at ACARD Symposium which was published in: "Statistical Methods and Instrumentation in Geophysics", Ed. Anton G. Kjelans, Norwegian Defense Research Establishment, Kjeller, Norway, Teknologisk Fonlag, Oslo, Norway, 1971.

13. Odom, D. B., et al, "Effects Simulation Program, Phase II", Raytheon Company, Wayland, Mass. Final report, submitted to Advanced Research Projects Agency, June 30, 1970.